ADDITIVE MANUFACTURING OF NON PLASTIC PORCELAIN MATERIAL BY DIRECT WRITING AND FREEZE CASTING

Magali Noemi Peña del Olmo

BSc Industrial Design (Hons)

MSc Design and Manufacture

A Doctoral Thesis

Submitted in partial fulfilment of the requirements of

De Montfort University for the degree of Doctor of Philosophy

2011

Abstract

Two direct consolidation methods usually used for advanced ceramics have been combined in this project in order to develop a novel fabrication route for traditional ceramics. Specifically the method used is based on the Additive Manufacturing extrusion process using direct writing of high solid loading ceramic pastes and then freeze-casting to solidify the deposited material. This novel fabrication method, for which a patent has been granted, has been christened "Direct Writing Freeze-Casting" (***DWFC***).

Although the ***DWFC*** process is the subject of investigation by other researchers for a range of different applications, including the production of medical implants with alumina, the research presented in this thesis focuses on its use in the manufacture of white wares, giftware, and applied arts and crafts in general. This new system will provide designers, potters, artists, craft makers and manufacturers with a flexible and automated way of manufacturing porcelain objects.

One of the major challenges to be overcome to exploit the ***DWFC*** process is the development of suitable slurry material formulations. Initial trials demonstrated that it is not possible to use conventional clay based porcelain materials with a platelet shaped microstructure which inhibits freeze casting. In this thesis the development and characterisation of non plastic porcelain slurry, based on substitution of kaolin (clay) with a calcined clay material (molochite), which can be processed using this new method is presented. The new non plastic porcelain formulation, which has a high solid load of 75.47% wt., has been subjected to detailed analysis to assess its suitability at each stage of the process; extrusion, freeze-casting (solidification) and firing.

The next stage of the trials was to characterise the performance of the new slurry formulation in every stage of the ***DWFC*** process. The initial formulation was adapted to optimise its performance in the extrusion process.

Extrusions trials were performed using a range of nozzle tip diameters and extrusions rates and it was found that it was not possible to successfully extrude using the smallest nozzle and highest extrusion rate. In addition other important extrusion parameters were examined, such as the stand-off distance between the substrate and the nozzle tip, extrusion rate and the velocity of the deposition head. It was found that when the stand-off distance is too small or too big flattening or curling of

the deposited bead respectively occurs. A polynomial equation was used to determine the optimum stand-off distance for a particular nozzle diameter.

The material was then subjected to two different (slow and fast) freeze casting regimes and fired at different temperatures. The water absorption, bulk density, apparent porosity and linear shrinkage were measured and the structure of the porosity assessed using both optical and Electron Scanning microscopy. Both raw powders and fired samples were characterized by means of X-ray diffraction (XRD). Interconnected porosity, with a dendritic shape is formed, which is a characteristic of freeze casting. Moreover, although the apparent porosity remains the same, the size of the pores reduces as the freezing rate increases.

Rheological testing was performed on the optimised slurry material using a range of methods, including cone & disc and concentric cylinder tests. In addition, a test rig was devised and manufactured which enabled rudimentary rheological testing of the slurry during actual extrusion to be undertaken. The trials showed that the material has a pseudoplastic, thixotropic behaviour. In addition it was found that there is a clear increase in the viscosity of the material as the plunger is displaced in the extrusion trials. This phenomenon is likely to be the result of “locking” of the angular particles in the slurry as pressure is applied to it. This was not observed in the other rheological trials highlighting the importance of testing materials in the mode of actual use.

In this research it proved possible to develop a non plastic porcelain material which can be successfully processed using the ***DWFC*** process. Unfortunately, the level of porosity in the final samples produced was higher than the 0.5% porosity level usually associated with conventional porcelain. However, it was possible to match the level of porosity encountered with other whiteware pastes, such as stone ware, or any other whiteware with talc as a component within the formulation.

Acknowledgment

I would like to acknowledge and thank Prof. Wimpenny not only for his technical supervision but also for his support, patience and encouragement during all these years of my research on this subject.

I would like to genuinely thank my supervisors Dr. Khalil and Dr. Gibbons for their guidance and setting an example for myself.

I would also thank Roy Carter for his help and advice in resolving the technical difficulties faced in this research. My sincerest appreciation to all members of the Additive Manufacturing Technology Group at De Montfort University, Leicester for their help and collaboration.

A special thanks to the Department of Geology, University of Leicester for their help and advice and also to the Glass and Ceramic Workshop, De Montfort University for their help and use of facilities.

Special thanks to the National Council of Science and Technology of Mexico, (CONACYT) for its support in my professional career.

My earnest thanks go to my parents, sisters, family and friends for their love and moral support throughout all my studies.

Table of Contents

List of Acronyms

AM	Additive Manufacturing
APA	Ammonium Polyacrylate
ASTM	American Standard Testing Methods
CAD	Computer Aided Design
CAM	Computer Aided Manufacturing
CAM-LEM	Computer-Aided Manufacturing of Laminated Engineering
CC	Contour Crafting
DW	Direct Writing
DWFC	Direct Writing Freeze-casting Method
DCIJP	Direct Ceramic Injection Printing
EFF	Extrusion Freeform Fabrication
FC	Freeze Casting
FCP	Fast Ceramic Production Process
FDC	Fused Disposition of Ceramics
FDM	Fused Disposition Modelling
FDMM	Fused Disposition of Multimaterials
FEF	Freeze-Form Extrusion Fabrication
FOC	Freedom of Creation
HFP	High Fired Porcelain
LENS	Laser Engineering Net Shaping
LOI	Loss On Ignition
LFP	Low Fired Porcelain
LFS	Linear Firing Shrinkage
3DP	Three Dimensional Printing
MJS	Multiphase Jet Solidification
PS	Particle Size
PSD	Particle Size Distribution
PAA	Poly(acrylic acid)
PVA	Polyvinyl Alcohol
Rep Rap	Replicating Rapid Prototyper
RP	Rapid Prototyping
RM	Rapid Manufacturing
SDM	Shape Deposition Modelling
SEM	Scanning Electron Microscope
SLS	Selective Laser Sintering
SLA	Stereolithography
TP	Traditional Porcelain
WA	Water Absorption
XRF	X-Ray Fluorescence
XRD	X-Ray Diffraction
YSZ	Yttria-stabilized zirconia

Table of Figures

List of Tables

1. INTRODUCTION

1.1 THESIS OUTLINE

Chapter One presents an overview of the thesis, followed by a brief introduction to the project, its context, aims and the methodology adopted.

Chapter Two addresses the literature review. This chapter presents the relevant background information for the research in the following order: i) a brief introduction to the concept of Additive Manufacturing (AM) of ceramics, ii) a detailed classification of the AM technology available in the ceramics field and its applications, iii) previous work done based on AM extrusion methods. This chapter contains discussion regarding the merits and limitations of these methods.

Chapter Three presents the methodology adopted, which is divided into three major phases: i) development and preparation of the ceramic material, ii) freeze-casting trials iii) and finally extrusion trials. A full description of materials and methods are also discussed in this chapter.

Chapter Four concentrates on the first phase of the experimental work, which involves the development of the material. The factors that make the characteristics of the powder desirable for the process are discussed in terms of particle size,

particle distribution, particle shape and degree of agglomeration. The chemical composition of the powder, its preparation and the additives involved are mentioned. Nozzle size and the critical nozzle height (distance between nozzle tip and previous layer) are established. This chapter also covers the extrusion properties of 2-dimensional and 3-dimensional parts.

Chapter Five addresses the second phase of the experimental work, which is the freeze-casting of the developed material. Issues such as the preparation of the slurry, sol composition and additives are examined. Relevant subjects such as agglomeration, solid load content, packing of particles, shrinkage, density and porosity are also discussed in this chapter.

Chapter Six presents the last phase of the experimental work, the extrusion trials of the slurries. Additionally the significance of the extrusion parameters are set out in this chapter as follows: i) physical properties of the fluid, such as density and viscosity, ii) nozzle travel speed (mm/s) (pressure, velocity and flow rate measurements).

Chapter Seven presents the results and final discussions; the final material formulation, freeze-casting and extrusion parameters are reviewed and the mechanical and chemical properties of the final body formed by the new process are described. The advantages and limitations of the use of conventional porcelain-type material on the new process are set out and an assessment of the progress made

towards achieving the original objectives defined at the beginning of the project. It also lists a brief summary of the project and the possibilities for further work based on the outcomes of this research.

1.2 RESEARCH BACKGROUND

In a world of constant change and innovation for consumer products, the need to provide products that meet the personal requirements of the user has become a challenge to design and manufacturing techniques. This suits the vital criteria of quality, high performance and competitive cost. Looking forward in time towards the possibilities of producing customised products for consumers on a major scale, the new goal for product developers is to bridge the gap between consumers, designers and manufacturers.

The simple idea that products can be totally adjusted to the customers' needs opens the gateway to exclusive and personalised design, giving the potential for much greater consumer satisfaction. AM techniques can be used for the manufacture of end-use products as well as prototypes and this provides the opportunity to change the paradigm from mass production to mass customisation; this last term refers to the manufacturing of customised products or components on a limited, yet cost-effective, scale [1] . These methods are unique in the way they perform, as they add and bond materials in layers to form objects without the application of traditional forming tools such as dies or moulds. This layer-wise deposition of material only

where it is required provides significant flexibility for the production of small, complex-shaped parts with unique structural features that are not achievable with other forming methods.

AM technology was not originally devised for the manufacturing of end-user products, and some problems remain such as geometry capture, poor surface finish, low-speed manufacturing speed and the use of a limited range of materials. Significant research is being conducted at present in order to overcome these limitations. However, much of this research has focused on plastic and metal products whereas ceramics have been relatively poorly studied. However, AM methods have developed sufficiently to suggest their applicability for the forming of ceramics parts.

Most recently, Additive Manufacturing of ceramics has benefited from techniques based on extrusion combined with conventional ceramic-forming methods: the “so called” direct casting processes [2], (sol-gel techniques, gel casting, starch consolidation, freeze-casting etc.). In these processes, the ceramic slurry is transformed into a solid state without the removal of its water content. This allows the use of a non-porous mould, which has considerable economic advantages as well as an improvement in the homogeneity of the green body. This approach gives improved dimensional control of the fired component and the potential to produce parts with complex geometry. One very successful approach is to extrude layers of

ceramic slurry with a fluid binder system that can be gelled by selective addition of a chemical agent to form the desired pattern for each layer. Whilst this route has been demonstrated only with alginate binders (Gel Casting Process), it should be possible to use other gelling systems, possibly including sols.[3]

It is in this scenario that the freeze-casting technique becomes a potential AM method. Different author[4] have described the possibility where a suspension deposited by a computer-controlled nozzle could be frozen layer-by-layer to form the desired shape and the green body can be obtained after freeze-drying. Unlike gel casting, in freeze-casting the solidification mechanism results from rapid cooling of the slurry, (typically a silica-based sol together with another ceramic material, such as alumina), which causes the concentration and the interaction of the particles of the sol at the boundaries of the ice crystals to produce irreversible bonding. Other particles in the mixture become locked in this solid framework and when the slurry returns to room temperature, it remains a brittle solid.

At first sight, the combination of freeze-casting with extrusion offers the following advantages: the elimination of capillary drying stress, (which could cause hard agglomerates or cracks and usually occurs due to drying and shrinkage), and the ease of debinding due to the small amount of organic additives used in the process.

1.3 PROJECT AIM AND OBJECTIVES

Aim: The aim of this PhD study is to develop a material (based on a triaxial whiteware formulation) which can be successfully processed using the new AM approach of combining direct writing and freeze casting to enable customised ceramic products to be formed.

Objectives:

- Investigate the suitability of conventional triaxial whiteware ceramic formulations for the DWFC process.
- Develop and fine tune a material that can be successfully extruded, freeze cast and fired.
- Investigate the properties of the new material formulation and compare with conventional porcelain materials.
- Develop improved processing conditions for the new material.

This project aims to explore the possibility of a new process that will combine freeze-casting and the basic principles of AM based on extrusion methods, to produce a route for the manufacture of high-integrity, ceramic end-products utilising so-called conventional, ceramic, porcelain materials (clay-based systems). This new method will be capable of producing new ceramic products without the cost and restrictions

associated with a conventional manufacturing porcelain process that requires tooling.

It is expected that this new AM method will give designers the opportunity to develop high-quality customized ceramics and allow unrivalled freedom of creation. It may open previously unimagined possibilities, as manufacturers will realise that they can reproduce any structure created using CAD. The limitations that this new system might possibly present will be monitored, discussed and compared with the available AM techniques which have been used for ceramics.

Conventional porcelain or similar ceramic materials were chosen as a starting material for fabrication in the new system due to their potential for high visual design impact, including high-quality surface finish, translucent properties and a large range of possible different commercial applications of the material itself. The biggest challenge in this research was the optimisation of non-technical porcelain paste in order to formulate a freeze-castable material whilst having the necessary qualities to be extruded through a fine nozzle.

1.4 OVERALL PROJECT

The primary phase of the project started with a review of the literature, which provides the essential foundation for the subsequent programme of this research. The literature review key topics are;

i) Study of state-of-the-art of AM for the production of ceramic objects.

ii) Ceramic materials and processes based on AM using extrusion methods and their characteristics (particle size, sintering temperatures etc).

iii) Investigation of previous work on freeze-casting and AM for the processing of ceramics, including descriptions of the process characteristics and parameters.

The next phase of the project was the experimental work where the information gathered in the literature review is used to devise an experimental plan for conducting the appropriate scoping trials to determine the system parameters to be used as a starting point for the subsequent, more detailed, tests. A test programme for the main experimental work, to explore the effects of the machine parameters, material composition factors, extrusion behaviour and quality of the ceramic parts produced was devised and conducted.

The final stage of the project involved the analysis and discussion of the results. Conclusions from the work were drawn and suggestions for further work laid out in the thesis.

2. THEORETICAL BACKGROUND

2.1 ADDITIVE LAYER MANUFACTURING

2.1.1 Introduction

Compared with other materials, ceramics offer a wide range of properties in terms of mechanical strength, thermal stability, hardness, thermal conductivity, chemical stability, oxidation resistance and good aesthetic appearance. Ceramics are inorganic, non-metallic materials that normally achieve their desirable properties when submitted to high temperatures during the fabrication process. [5]

In the last 20 years, a range of Rapid Prototyping (RP) processes, which build parts by the precise addition of material in layers, has been introduced into ceramic technology. All these RP approaches use processing technologies that allow the production of parts with the required geometrical complexities directly from a computer aided design (CAD) file without the use of traditional tools, such as moulds or dies [6].

Most recently, RP methods are being adopted for the production or end-user parts and, to reflect this important change, the term Additive Manufacturing (AM) has been formally adopted[7].

The majority of AM processes to produce polymeric objects have been extended for the production of metal and ceramic parts. Hitherto, the more mature techniques which have been used to process ceramics are: Stereolithography (SLA), Laminated Object Manufacturing (LOM), Fused Deposition Modelling (FDM), Selective Laser Sintering (SLS) and other techniques based on inkjet printing.

Initially, significant interest was focused on the development of ceramic powders for use in 3D printing and SLS, [8]however, recent interest has moved towards the processing of ceramic materials in aqueous or resin suspensions e.g. the direct writing extrusion approach, [9]stereolithography [10] etc.

Although there is a wide range of AM methods for processing ceramics, most of them follow the same basic process chain as shown in Figure. 2.1.

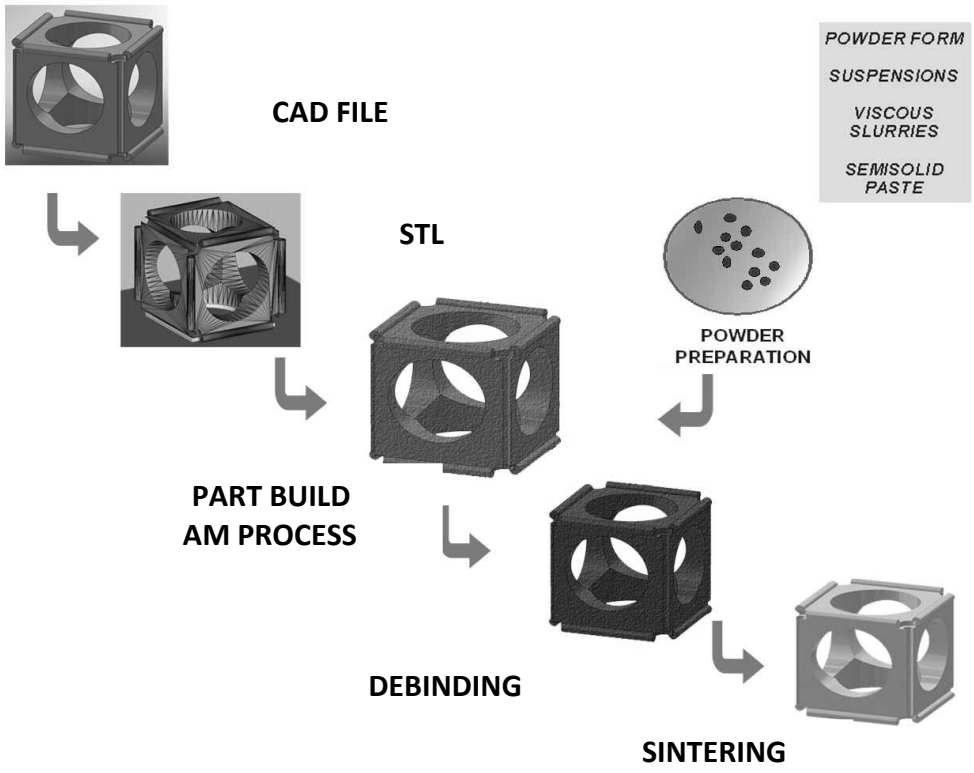

Figure 2.1: Basic Principle of Layer Manufacturing of Ceramics

The first step involves the creation a 3D CAD model of the desired object. This CAD data is then converted into a suitable format for processing (in the vast majority of processes this is an STL -standard triangulation language- file). This is a simplified representation of surfaces of the part by means of triangular facets. This data is then sliced to represent the layers which will be generated sequentially in the AM process.

Once the STL file is ready, the next step is the preparation of the ceramic material. AM of ceramics generally uses common starting materials in the form of powders, either to be used directly (e.g. SLS, 3D printing) or formed into suspensions of

different concentrations which can range from low viscosity liquids (for deposition by inkjet printing), through higher viscosity liquids (filled resin systems for SLA), viscous slurries for extrusion and, finally, semisolid paste materials (LOM).

In the vast majority of AM processes, a green part is produced which must then undergo a debinding operation before being fired at high temperature to achieve the required properties. Many of the processing issues (e.g. particle packing, polymeric additives, colloidal interactions, rheological behaviour, drying and binder removal etc.) used for common forming methods, such as slip casting, tape casting, extrusion or injection of ceramics, are applicable to these methods[6]. For example, a binder removal phase is required for most of the AM ceramic methods, which involves conveying ceramic particles in an organic medium such an oligomer or polymer that has to be removed before sintering. This follows the same procedure as with other common ceramic forming methods such as injection moulding of ceramics, gel casting etc.

Since the aim of the AM of ceramics is to produce high quality near net-shaped structural and/or functional ceramic parts, the main quality issues to consider are dimensional control, geometry of vertical walls, surface finish, microstructure and integrity (e.g. Porosity).

A brief recompilation and description of the most important AM techniques used for ceramics is presented in the next section. In addition to direct forming of parts using

AM methods, there is a wide range of indirect methods which employ a pattern or tool made by AM to form the ceramic objects. These techniques will only be mentioned briefly in this thesis.

2.2 AM OF CERAMICS METHODS: AN OVERVIEW

The numerous AM systems implemented in the market can be classified and described in various ways, but the most suitable way to categorize these systems is by their forming methods.

Therefore, in the present research study, these technologies are divided into four fundamental approaches: 1) polymerisation, 2) sintering or bonding of powders, 3) lamination and 4) extrusion or printing of ceramic loads. Table 2.1 shows the most representative technologies according to this classification.

Commercial processes for the Additive Manufacturing of Ceramics	
Mechanism	**Method**
Polymerisation	Stereolithography of ceramic-filled resin Paste Polymerisation Direct Photo Shaping (DPS) Indirect Stereolithography
Sintered or bonding of powders	Laser Sintering (LS) Laser Engineering Net Shaping (LENS) Bonding 3-Dimensional Printing Direct Ceramic Ink-jet Printing (DCIJP)
Lamination	Laminated Object Manufacturing (LOM) Computer-Aided Manufacturing of Laminated Engineering (CAM-LEM)
Extrusion or printed of slurries.	Fused Deposition Modelling of Ceramics Robocasting Contour Crafting (CC) Multiphase Jet Solidification (MJS)

Table 2.1: Additive Manufacturing Technologies of ceramics

2.2.1 Polymerization

2.2.1.1 Stereolithography of ceramic-filled resin

Stereolithography (SLA), invented by Chuck Hull [11], is one of the first AM technologies. In this method, a vat of liquid, UV-curable, photopolymer resin is selectively cured by a UV laser to form a multitude of solid layers which form the final part. For each layer, the laser beam traces a part cross-section pattern on the surface of the resin, which cures to a solid and bonds to the layer below. Figure 2.2 shows the basic principles of this process.

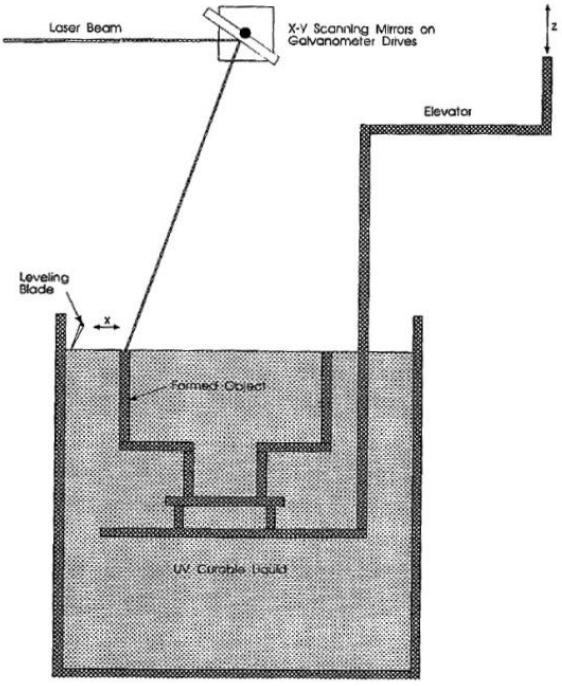

Figure 2.2: Stereolithography Process [12]

To form ceramics using this approach, the ceramic particles are mixed with the UV-curable photopolymer. The amount of the filler material is limited due to the

defined optical penetration depth which is required in the process[13], too much filler prevents a layer of the required thickness from being formed. Some UV-curable solutions used in the Stereolithography of ceramics are similar to gel casting solutions but with the thermal initiators replaced by photoinitiators.

Once the object has been created in layers in the Stereolithography process, it undergoes post-treatment to produce the final ceramic part. This post-treatment consists of debinding (removal of resin) by subjecting the part to around 160^{o}C for several hours to guarantee complete resin polymerization followed by pyrolisis at 500^{o}C to eliminate the organic component (resin) from the green ceramic. This is followed by a sintering phase, which leads to full densification by increasing the temperature from 500 to 1550^{o}C[14]. There is 15 to 25% shrinkage from the green part to the final component.

Preparation of the suspensions

The ceramic powder is dispersed in the photopolymer with the help of various additives. The additives act as dispersants, preventing the agglomeration and settling of the ceramic particles, and they also play the role of a thickening agent[15]. Obtaining effective dispersion for sub-micrometer powders requires careful design of the colloidal dispersant system.

A ceramic Stereolithography suspension must satisfy several, often conflicting, requirements. To obtain a dense green body, which is subject to lower shrinkage and has higher strength, a high-solid loading should be used. However, this creates two important problems, firstly the solid loading interferes with the curing of the resin and secondly, the high viscosity of this suspension makes it very difficult to process on conventional Stereolithography machines. Ideally, the ceramic suspension should have a viscosity less than 3Pa.s to enable effective recoating (deposition and levelling of resin layers)[10].

In recent years, a number of Stereolithography ceramics and glasses-filled resins [16] (Protool resin family) DSM SOMOS, Protocomposites, Envisiotec Nanocure RC 25 (87% ceramic filler) have been developed to produce improved properties, such as higher temperature resistance [13]. These materials, however, have a low volume fraction of filler material and are not subjected to secondary debinding and firing. Current applications include automotive components, light reflectors, pump impellers, injection moulds etc. Figure 2.3 shows a printed example of nanocure resin.

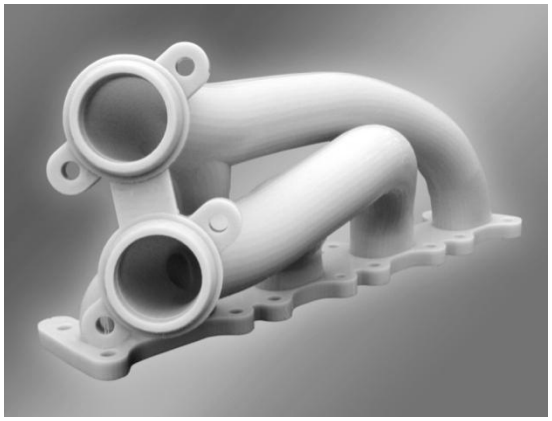

Figure 2.3: Automotive component, SOMOS Nanoform15120.

Courtesy: Alphaform [17]

2.2.1.2 Paste Polymerization

Unlike conventional Stereolithography equipment where a fluid monomer is required, an approach using a high-viscosity paste was first introduced by the French company Optoform[18]. In the Optoform process, the ceramic/photopolymer paste is introduced into a piston, which delivers a controlled quantity of the paste onto the working area. This enables homogeneous layers to be deposited. The layers have a smooth surface and can be selectively cured with a UV laser. Figure 2.4 shows the basic principles of this process for the fabrication of ceramic materials. Figure 2.5 shows the printing of the ceramic paste, and the laser solidification respectively.

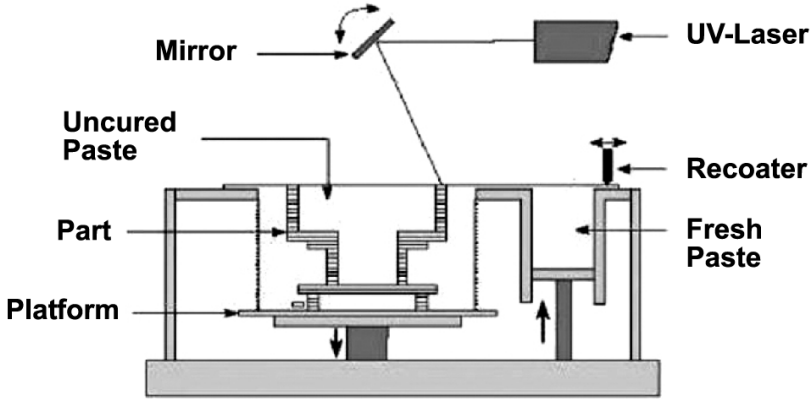

Figure 2.4: Paste Polymerization for the fabrication of ceramics[19]

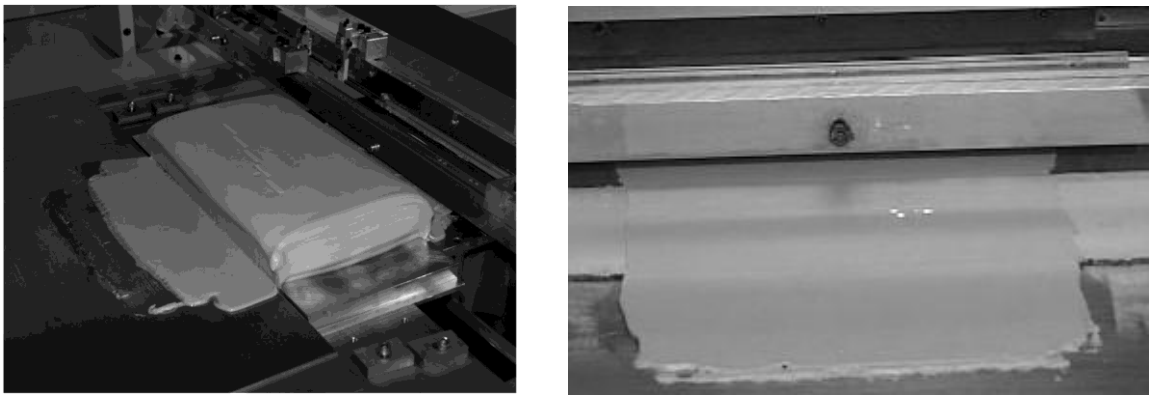

Figure 2.5: Laser printing of ceramic paste
Courtesy: Cerampilot [19]

After photo-polymerisation, debinding and sintering of the green state part takes place. Trials have demonstrated that the parts produced have similar properties to ceramic objects produced by conventional processes. This opens up the possibility of using the process for direct manufacturing of end-use parts rather than prototypes[20]. A clear example of a non-sintered ceramic part can be seen in Figure. 2.6. A step forward for this technology into direct manufacturing involves the

company Cerampilot and the Fast Ceramic Production Process (FCP), not only in rapid manufacturing of industrial, electronics and biomedical applications but very recently in the fabrication of luxury products like jewellery or translucid lamps, Materials used by this company include Alumina, Zirconia, Hydroxyapatite, Aluminium Nitrate, Mullite and Cordierite. An example of their applications is shown in Figure. 2.7 and 2.8.

Figure 2.6: Non-sintered ceramic part obtained using the Optoform process Courtesy: Sirris

Figure 2.7: AM of Jewellery, Zirconia Courtesy: Cerampilot France
After post-processing polishing in different colours. [21]

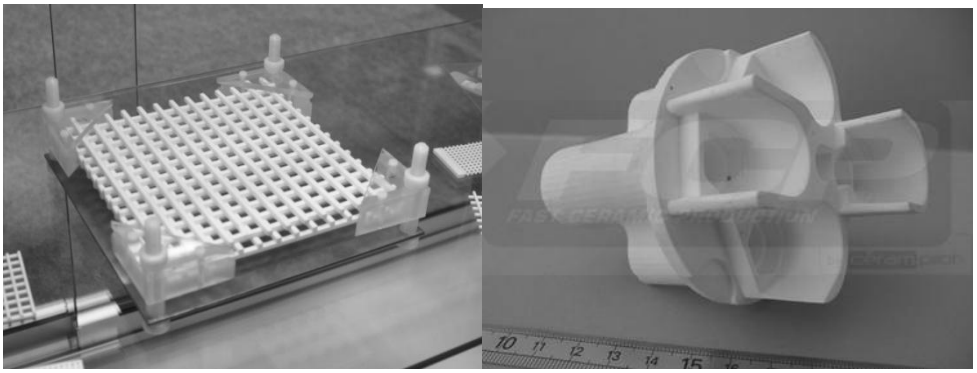

Figure 2.8: Honeycomb (left) and solid structure in Alumina (right).
Courtesy: Cerampilot France[21]

2.2.1.3 Direct Photo Shaping (DPS)

This process builds 3D objects from liquid photosensitive resin, as in Stereolithography, but in this case, the material is selectively hardened by a DLP (Digital Light Processing) projector unit. The DLP projector uses a series of micro mirrors which can be individually manipulated to project an image - the light section of which corresponds to the desired slice with the rest of the area remaining dark - which can cure an entire layer of resin simultaneously[22]. This process has been utilized for the production of ceramic parts by curing ceramic/photopolymer suspensions [23]. Figures 2.9 and 2.10 show the basic principles of the process.

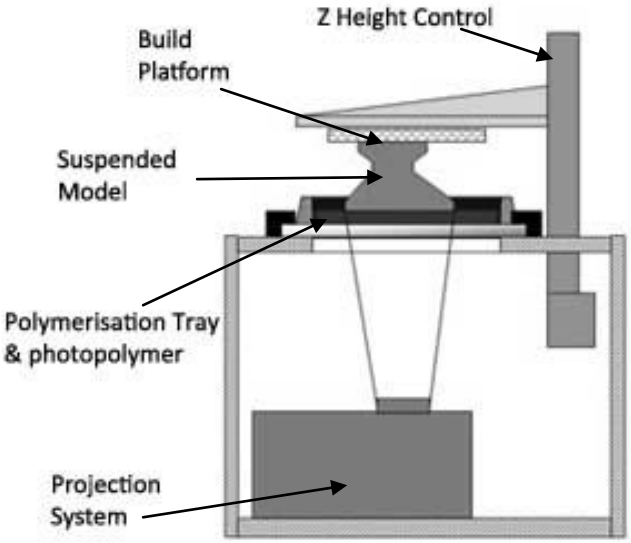

Figure 2.9: Direct Photo Shaping (DPS) [24]

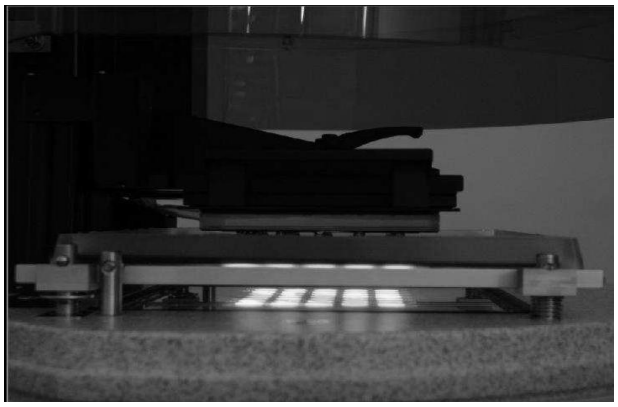

Figure 2.10: Image projection DPS process
Courtesy: ASERM (Rapid Manufacturing Spanish Association)

2.2.1.4 Indirect Stereolithography

There are two principal routes for the fabrication of ceramics by AM methods: **indirect** and **direct**. Indirect routes rely on an additional moulding step after fabricating the master pattern using AM. One example of the indirect AM method is the use of a sacrificial epoxy resin mould made by SLA process which is then filled with a thermally-curable HA-acrylate and cured at 85^{o}C. The cured part is then placed in a furnace at high temperature to burn away the mould and the acrylate binder within the suspension[25] .

2.2.2 Sintering or Bonding of Ceramic Powders

2.2.2.1 Laser Sintering

Laser Sintering (LS) was developed at the University of Texas by Deckard and Beaman[26]**.** In LS, the components are built layer-by-layer by scanning a laser beam over a thin layer of powdered material. The LS is quite a flexible technique as compared to other AM methods when it comes to processing a wide range of materials. The major benefit of the LS technique is that additional support structures are not usually necessary to provide supports for overhanging sections as infused powder fulfils this function. A graphic describing the process is shown in Figure. 2.11.

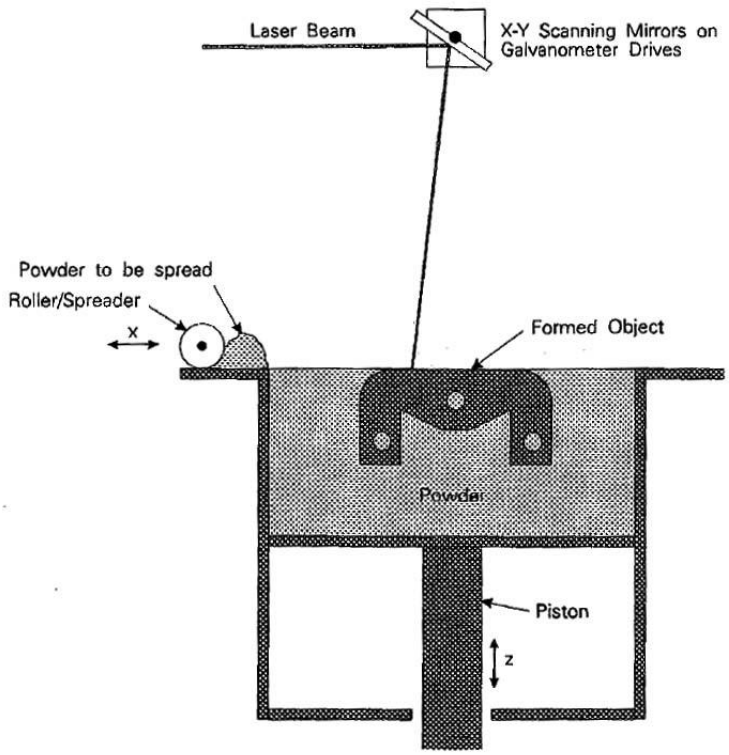

Figure 2.11: Schematic of the LS process[12]

LS can be used for both direct and indirect processing of ceramics. In the indirect route a polymer coated ceramic material is employed. The laser beam actually melts the polymer binder, which bonds the particles together (bonding-forming phase)[27].

The rest of the layer remains as a loose powder, the layer is lowered and a further powder layer is applied. The laser then bonds the next layer to the previous one. The procedure is repeated until a green ceramic part is completed. The polymer binder is then thermally removed before the part is sintered at a higher temperature to become fully consolidated.

On other hand, if a higher power laser system is employed, it is possible to dispense with the resin binder and fuse the ceramic powder directly in the laser sintering machine (direct process)[28]. The fusion of the ceramic particles together and bonding with the previous layer is the result of temperatures of 900°C (their melting point). Although ceramic objects created through this route still require thermal post processing (sintering) to produce the fully dense part, the debinding process is not required. The production of ceramic parts in this way can achieve savings in cost and time. It also allows the manufacturing of end-user parts see Figure 1.12.

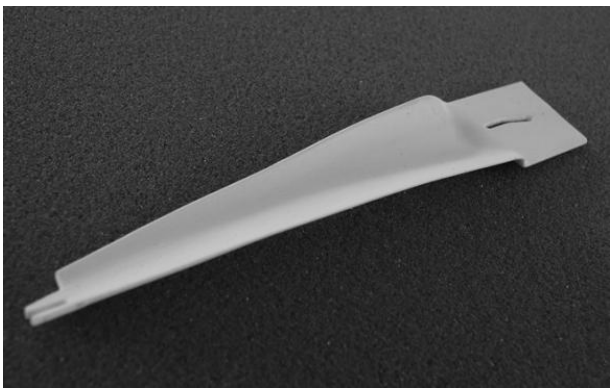

Figure 2.12: Manufacture of an end-use part in Alumina. PM100T, PM250. Courtesy: Phoenix System, France[29]

2.2.2.2 Laser Engineering Net Shaping (LENS)

Created in 1997 by Sandia National Laboratories and commercialized by Optomec Design Co., the Laser Engineering Net Shaping (LENS) process is based on laser cladding and has the potential to create complete, dense, ceramic or metal components by fusing powdered substances within the focal zone of a laser beam. The high-powered laser beam is focused on the substrate into which, with the aid of a computer guidance system, the powder is injected. Once this layer is formed, the next step is to raise the deposition head in order to prepare the process for the subsequent layer.

The deposited material cools and solidifies rapidly as the focus point of the laser beam moves on and changes position. Generally speaking the process is conducted within an inert atmosphere to prevent oxidation of the material being deposited. Greater ductility and better part strength is achieved due to the rapid solidification process. Moreover, the powder that is not used in the layer (overspray) can be reused. A graphic describing the process is shown in Figure. 2.13 and 2.14.

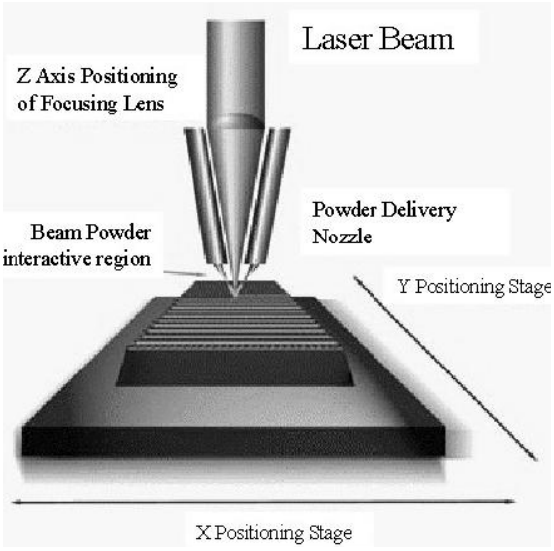

Figure 2.13: LENS process (courtesy of Optomec Design Co) [30]

The LENS process proves quite beneficial as is enables the creation of completely dense parts constructed entirely out of a powder containing just one material. As compared to other Additive Manufacturing processes, the LENS process is unique in requiring no further heat treatment for the production of ceramics.

Parts with multi-materials, cermets and gradient materials can also be produced with this process as it facilitates the use of various mixtures of powders, such as ceramic particles mixed with metal particles. Thus, for the production of parts with specific requirements and applications, such as die cast tooling, this process proves to be quite flexible as components with different materials and properties can be easily created[31].

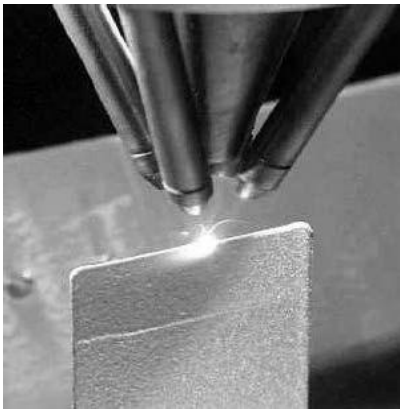

Figure 2.14: LENS process close up (courtesy of Optomec Design Co)[32]

2.2.3 Ink Jet Printing based methods

Basically, there are two methods of using inkjet techniques for AM of ceramics: Three-dimensional printing (3DP) and Direct Ceramic Jet Printing (DCJP). These methods differ from each other in that the first one uses an inkjet-print head to apply a binder to the ceramic powder whilst the second one uses an inkjet-printing nozzle to deposit a ceramic suspension directly.

2.2.3.1 3-Dimensional Printing of Ceramics

In 3D printing, parts with complex shapes are formed by depositing a thin layer of ceramic powder onto a build platform, one layer after another, much like the laser sintering method. However, a binder solution is printed onto the powder surface using an inkjet print head to selectively define the geometry of the part [33, 34].

The binder can be a refractory material, such as colloidal silica, or a temporary polymer binder. A thin layer of the powder can be formed by roll compaction, but more homogeneous particle packing and a higher packing density are obtained by deposition from a well-dispersed suspension (e.g. through a nozzle 100 to 200μm in diameter) followed by drying. After application of the binder solution to fix the powder, the layer is heated to remove excess liquid (water). Once a single layer is complete, a piston lowers the part, the next layer is spread and the binder is printed again. The slurry and binder deposition processes are repeated until the part is completed and it is then removed from the unbound powder. Figure 2.15 shows the basic principles of the 3D printing process for ceramics.

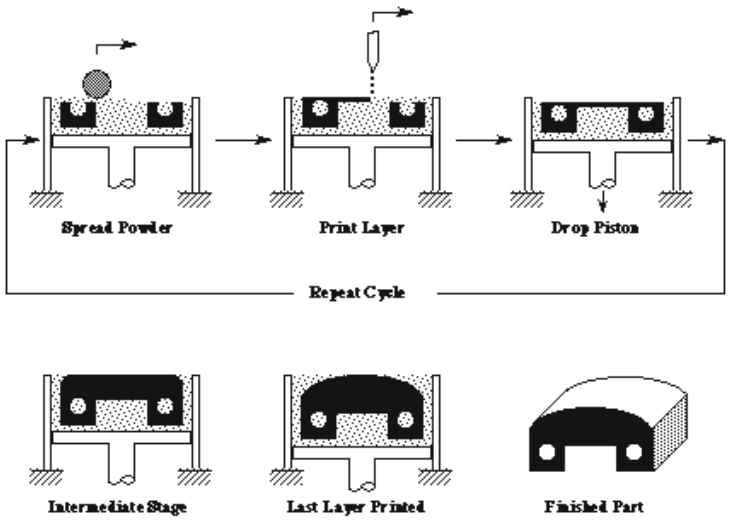

Figure.2.15: 3D Printing Process for Ceramics[33]

When removed, the part has a relatively low density, typically 50% of the theoretical, and the density is increased either by isostatic pressing and sintering or by

infiltration. There are two main considerations for processing ceramics using 3DP printing:

The colloidal properties of the suspension and the drying of the deposited layer, control the structure of the deposited powder layer. The interaction of the binder solution with the powder layer must be optimized to control the shape uniformity of the printed part[33].

Several companies have been established which offer systems and services for the 3D printing of ceramics. The range of applications extends from the production of casting moulds and cores to structural ceramics components (industrial applications), but recently a special interest in the 3D printing of ceramic art-crafts and traditional ceramics applications has been observed. Most of these projects, in the above-mentioned field are still however under research. The following figures show different examples of the application of this process; Figures 2.16 to 2.20 refer to industrial applications. Figures 2.21 to 2.27 refer to art and design applications that have recently presented considerable opportunities for direct manufacturing. Although some technical issues still need to be solved, e.g. ceramic shrinkage, surface finish, and porosity of the material, these methods present a very satisfactory ceramic end piece with possible post- processing by infiltration or glazing. Moreover, the exploration of these technologies has extended to other ceramic materials, such as marmol (Figures 2.28, 2.29). Another ceramic material

being explored, for the production of components and sculptures respectively, is cement (Figures 2.30 to 2.31).

Figure 2.16: Cast metal part (left) produced from a z cast sand mould (right) Courtesy: Z corp U.S.A.[35]

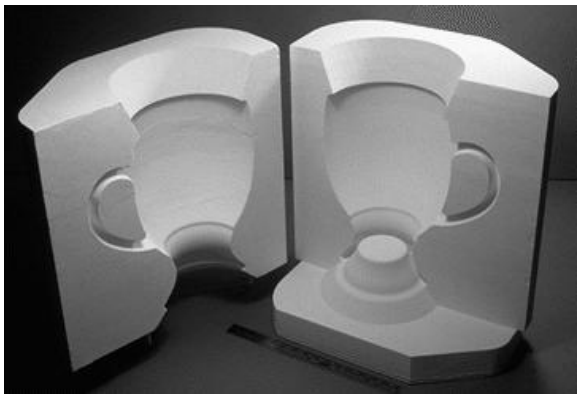

Figure 2.17: Ceramic shell with integral core for slip casting
Courtesy: Soligen[36]

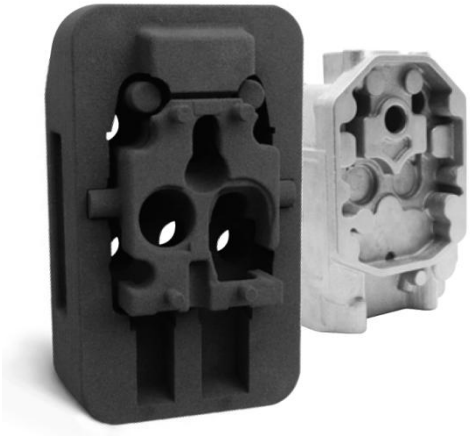

Figure 2.18: Complex 3D printing by sand casting of mould and cores produced by 3D printing.
Courtesy: ProMetal[37]

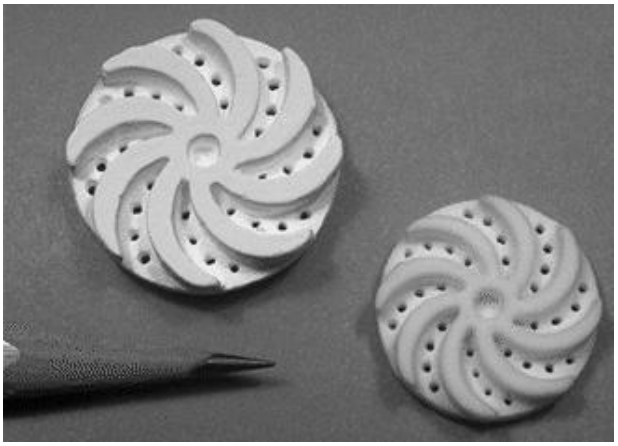

Figure 2.19: Structural Alumina part produced by 3D printing, before and after sintering.
Courtesy: MIT[38]

Figure 2.20: Ceramic filters produced by Specific Surfaces Inc using 3D printing.
Courtesy: MIT[39]

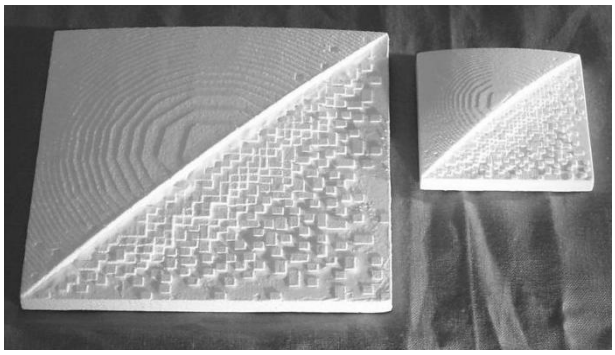

Figure 2.21: Alumina ceramic tiles produced by Specific Surfaces Inc using 3D printing.

Figure 2.22: 3D printing and infiltration, Eco ceramic coating Process.
Courtesy: Mike Eden, Royal College of Art[40]

Figure 2.23: 3D printing of traditional ceramics powder, Bowling Green State University Ohio, USA.

John Balistreri, Courtesy: Johnbalistreri.artist[41]

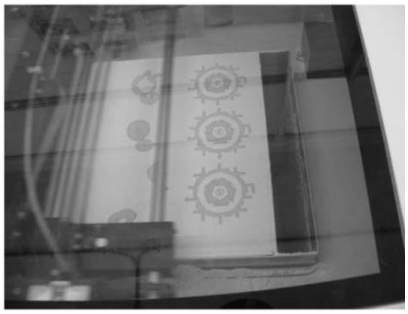

Figure 2.24: Printing Object on ceramic powder, Courtesy: University of the West of England. David Huson.[42]

Figure 2.25: Printing Object on ceramic powder. Courtesy: the Solheim Rapid Manufacturing Laboratory. Mechanical Engineering Department at the University of Washington. Seattle[43]

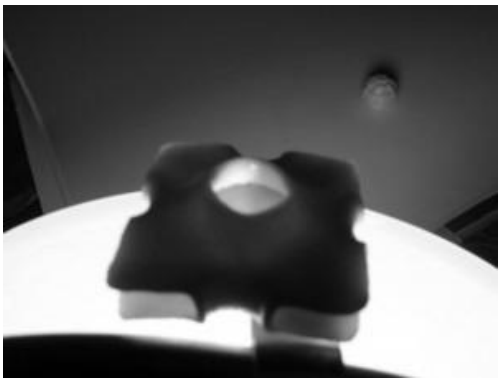

Figure 2.26: Printing Object on translucid porcelain powder, Courtesy: University of California at Berkeley

Figure 2.27: Additive manufacturing glaze part

Courtesy: University of the West of England.

David Huson[44]

Figure 2.28: Hygea Head printed using marble powder. Process ProMetal
Courtesy: IFAM Bremen Institute

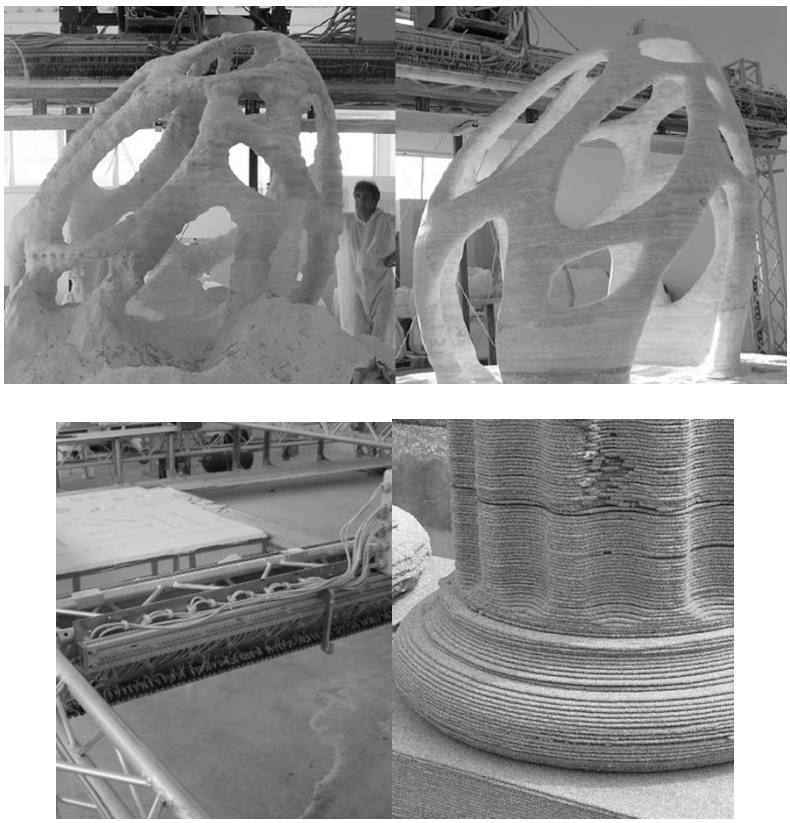

Figure 2.29: Mega scale 3D printing of sandstone.
Courtesy: D-Shape [45]

Figure 2.30: 3D printing of cement composites.
Process: 3D printing of cement
Courtesy: WMG's Rapid Prototyping and tooling Group, University of Warwick [46]

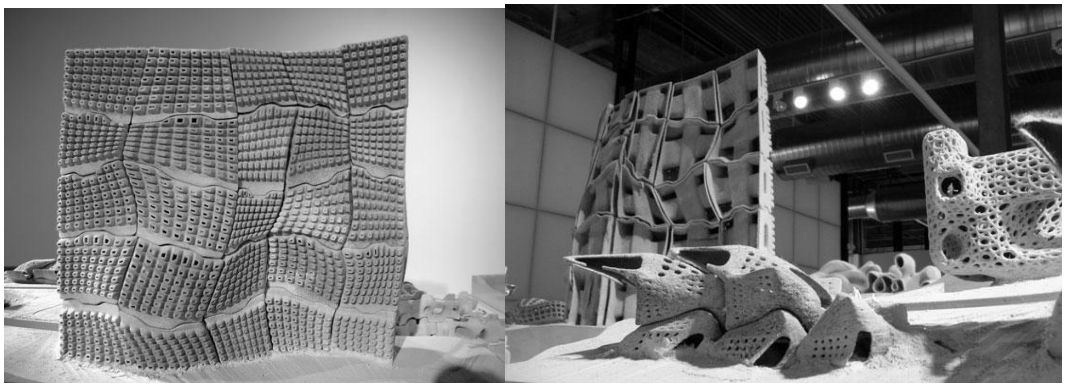

Figure 2.31: 3D printing of cement composites.
Process 3D printing of cement
Courtesy: [Rael San Fratelo , Architects][47]

2.2.3.2 Direct Ceramic Ink-jet Printing (DCIJP)

Rather than printing a binder onto a powder bed, it is also possible to print an entire ceramic object through a print head using an “ink” which is a suspension containing ceramic particles [48, 49].

Typically, the nozzle diameter is around 60µm and leads to droplets with an average diameter of 100µm. Smaller droplets lead to rich details of the part, but require an increased mechanical effort and finer nozzles, which bear a greater risk of wear[13].

An appropriate ceramic ink, which is basically a well-mixed suspension of fine ceramic powder, maintaining 10 to 15 vol% particles, 5 vol% organic additives (dispersant and binder), and 80 to 85% liquid (90) is required to be developed. This suspension should have an adequate quantity of particles to allow the part

construction and at the same time, it should also maintain the proper viscosity and surface tension for constant droplet development.

The ink is prepared by breaking down the agglomerates with the help of a twin-roll mill, ultrasound or high-energy bead-milling or a combination of these techniques. The suspension is stabilized by using the dispersant by absorption on the powdered surface, also the second stage might require the addition of other additives such as the binder or plasticizer which are mixed by ultrasonic agitation where the dispersion phenomena is produced by waves which cause cavitations and deaglomeration of the flocs[50].

In addition, these inks should posses a high drying rate to enhance the printing speed and to enable rapid drying of the finished part to develop enough green strength for subsequent handling (removal of unbonded support powder). All these properties depend on the particle characteristics, the kind and amount of the solvent and organic additives and adequate processing procedures.

The high liquid content in the ink is one of the chief restrictions with the DJCP as the liquid content reduces the forming rate due to the extended drying time required before printing of the next layer can begin.

This process offers a very versatile potential for use in Additive Manufacturing. Components made by this technology exhibit a dense microstructure, well-defined porosity and high shape accuracy[51].

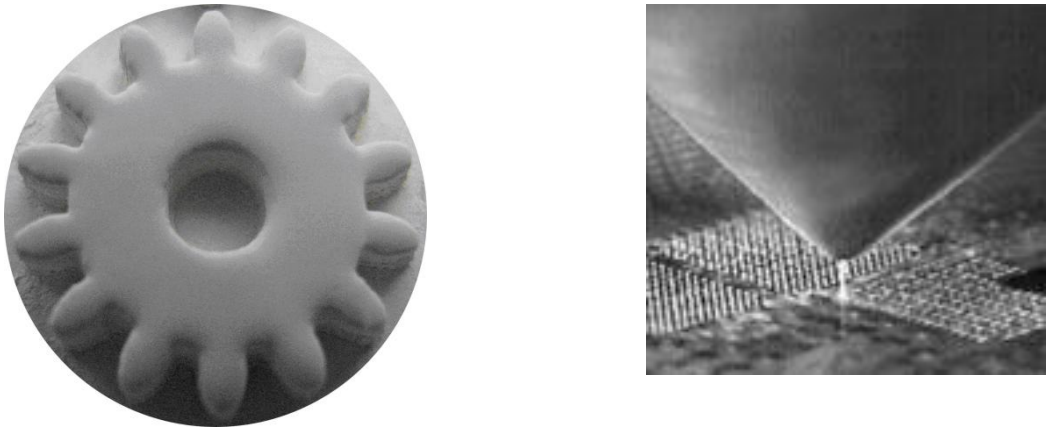

Figure 2.32: Ceramic printed part, Process Direct Ceramic Ink jet Printing. Courtesy: RWTHaachen University left. Electronic Board. Process M3D deposition Mesocalse 1-100 microns, Right.

2.2.4 Laser Cutting of Ceramic Sheets

2.2.4.1 Laminated Object Manufacturing (LOM)

The commercial version of the LOM process was introduced by Helisys Corporation, Torrance, CA to produce models for metal casting patterns.

The patterns are built from adhesive bonding paper, with each layer of the model consisting of a single sheet of paper fed from a roll. Laminated Object Manufacture (LOM) cuts the component slices from thin layers of material using a CO_2 (carbon

dioxide) laser mounted on a 2D plotter; this laser quickly cuts the outline of each layer of the object. Then a heated roller, which activates the adhesive, laminates the sheet to the previous layer.

The outside of the sheet is cut into small blocks by the laser to become the support structure. The process repeats until it generates a solid object enclosed within a support formed by blocks of the excess material. The object can then be removed from the supports (de-cubed). The materials used in LOM include coated paper, tapes of metal, polymer and ceramics[52]. Fig.2.33 shows the basic principles of the LOM process .

Creating ceramic objects by LOM is a relatively easy concept since the paper can be replaced with ceramic green tape. Although it differs in detail, most of this concept is based on the well-known ceramic tape cast process, also sometimes referred to as the doctor-blade process [48].

The mixing of ceramic powder with an appropriate binder creates a ceramic tape, which is used to assemble a physical 3D model of the actual CAD data after the sheets have been stacked together; afterwards, the material has to be removed manually.

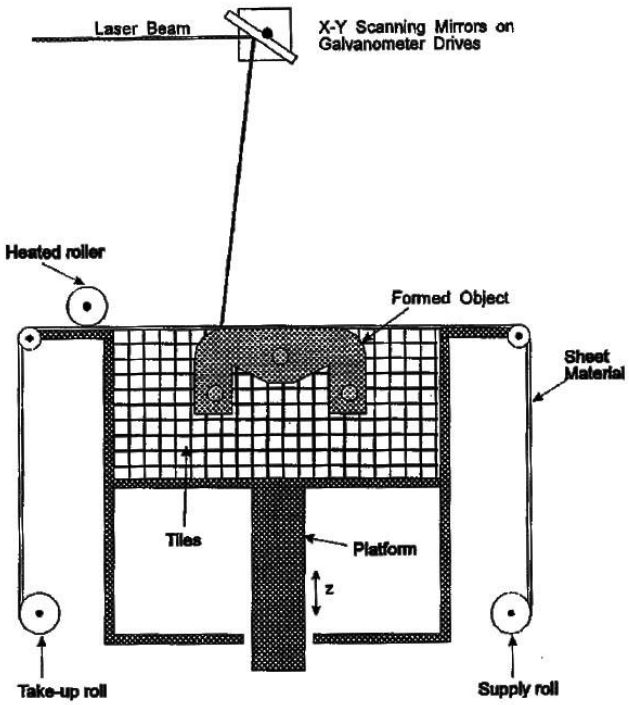

Figure 2.33: Basic principles of the LOM process [12]

2.2.4.2 Computer-Aided Manufacturing of Laminated Engineering (CAM-LEM)

A modified form of the LOM process, referred to as computer-aided manufacturing of laminated engineering (CAM-LEM), has been developed to produce complex shapes directly from the tape-cast ceramics[53]. In CAM-LEM, individual slices are cut from the tape-cast sheet using a laser and assembled to fabricate the computer-aided design. Following lamination of the slices and binder removal, the body is sintered to produce a ceramic component. Computer Aided Manufacturing of Laminated Engineering Materials (CAM-LEM) differs from LOM by using a "cut and

stack" approach rather than the "stack and cut" procedure used in the LOM ceramic process.

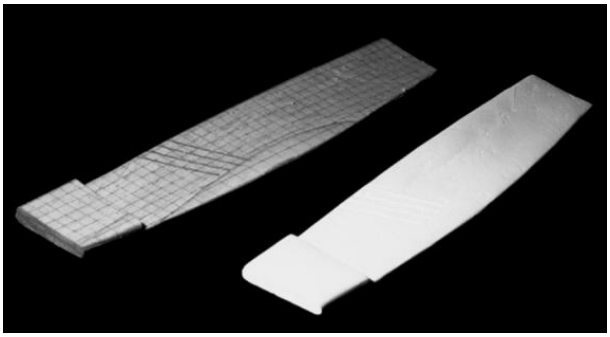

Figure 2.34: Decubing Ceramic Part.CERLAM™ Process Modified LOM process.

Courtesy: Javelin[54]

2.2.5 Extrusion or Printing of slurries

A special section in this chapter is dedicated to the extrusion methods since the direct writing approach adopted in this research is based on the extrusion method; the overall process includes feedstock preparation, deposition through nozzle solidification and post processing. The post-processing phase will be debinding, if required, followed by sintering. Most of the techniques based in this process are still under research, and they have been derived from the well-known FDM method, explained in the followed section.

2.2.5.1. Fused Deposition Modelling (FDM)

This method was developed by Stratasys[55]. These systems extrude a thin bead of thermoplastic, one layer at a time; the build and support materials are extruded from a fine tipped nozzle directed by an x-y positioning device. The material is supplied on spools as a firm filament about 1.8mm thick [56]. The filament is fed from a storage spool into a moving "liquefier head", where it is melted and laid down as "roads" of material with the desired width and thickness. Precise temperature control is needed (±0.5°C) and dimensional accuracy rests on the use of shrinkage compensation factors and deposition strategies[57, 58].

A spindle located at the rear or side of the machine carries the spools whilst a flexible tube, which is generally attached on the back of the extrusion head, is used to feed the filaments.

The extrusion head plays a crucial role in this system; it is split into two different drive blocks which are the located on the backside of the extrusion head, and these are the main raw material feeding mechanisms. The entire system is computer controlled which enables it to load and unload the filaments in a precise manner. This system consists of two parallel wheels connected to small-sized electronic motor gears.

The heating chamber, which is normally a 90^{o} curved elbow wrapped in a heating element, is the next component in the system. It generally serves two main functions. The first is the ability to change directions of the filament flow from a horizontal axis to a vertical axis, and the second, and most crucial, is to provide a melting area for the material. The system is equipped with feedback thermocouples to maintain a stable temperature. The filament passing from the exit of the chamber is usually in a semi-molten state as the heating elements are held at temperatures slightly above the melting point of the material. The extrusion nozzle is located at the end of the heating chamber, which is about four inches long. The extrusion nozzle tips are directly connected to the heating chamber exit.

The extrusion head velocity and the extrusion rate must be coordinated in order to lay down a constant-sized bead. The acceleration of the motion system is not infinite and would lead to excess extrudate at turns within a layer unless the extrusion rate can be slowed down. Cutting of the extrudate bead when a layer is finished or moving to a differing portion of a layer involves simultaneously lowering the piston and stopping the extrusion[59] .

The rheology of the thermoplastic must cause the bead to snap back and prevent the formation of a thread of excess material. Apart from thermoplastics, other materials than have been used by this method are glass and liquid crystal reinforced polymers, wax and new elastomer materials [60] [61].

This method has been extended to accommodate more than one material, and has been called Fused Deposition of Multi-materials (FDMM) [62]. Figures 2.35 and 2.36 show the schematic FDM process.

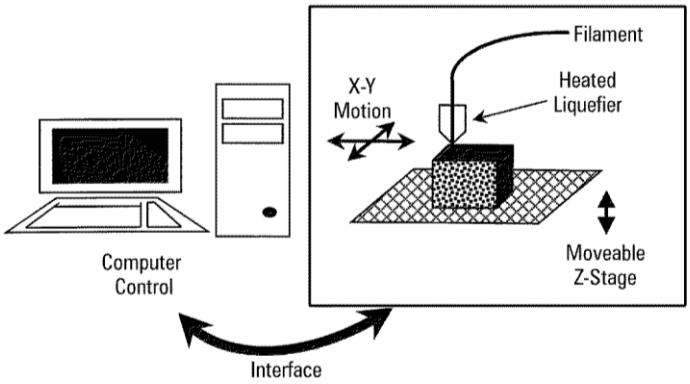

Figure 2.35: Basic principle of the FDM Process

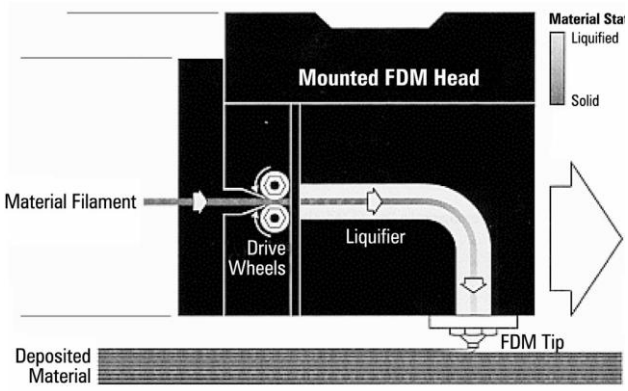

Figure 2.36: Extrusion head FDM process [63]

2.2.5.2 Fused Deposition of Ceramics (FDC)

The same approach, applied to ceramic suspensions in a polymer or wax vehicle, is known as Fused Deposition of Ceramics (FDC)[64]. In this process, ceramic components are fabricated using a commercially-available FDM modeller retrofitted

with a modified extrusion head suitable for extruding ceramic suspensions. This technique uses suspended ceramic particle systems similar to injection moulding. The mixed powder-binder feedstock is extruded into filaments, which are then deposited. Solidification occurs on cooling of the molten material, see Figure 2.37.

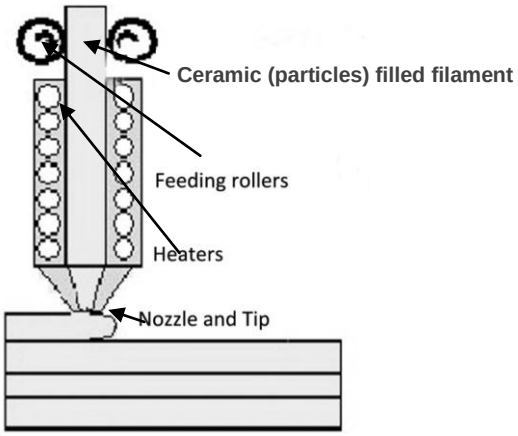

Figure 2.37: FDC process [65]

Numerous monolithic ceramic materials like silicon nitride, alumina and zirconia can be applied using this process. Until now, this process has been basically used to create structural ceramics and piezoelectric ceramics, an intention to use this process for traditional ceramics has been mentioned, but is still under research[66].

The material used in FDC is a ceramic-polymer mixture (50 to 60 vol% particles). This is first extruded to form filaments with a diameter of 0.2 mm, after the spool filaments have been fed into an extrusion head at temperatures of 100 to 150^{o}C. Extrusion of the plastic mixture through a nozzle (diameter 0.25 to 0.64mm)

according to a computer-controlled pattern is used to form the object layer-by-layer. The green body is then subjected to debinding and sintering steps to produce a dense object. Figure 2.38 shows an example of unfired ceramic parts.

The process rapidly creates a green prototype but, because the volume content of the binder is significantly different in comparison to powder injection moulded parts, the burn out may take several days [67].

As in the FDC process, the ceramic-polymer filaments must also have enough flexibility to allow winding and unwinding of the molten material through the fine nozzles. There must be good adhesion between each layer. Removal of the large amount of polymeric binder material as cleanly as possible must be considered. As in any manufacture process, there are a number of variables that determine the success and quality of the fabricated parts e.g. an inadequate processing of the ceramic-polymer feed material and limitations of the deposition process can lead to internal and surface flaws that degrade the strength of the final sintered object. Figure 2.38 shows an example of unfired ceramic parts fabricated by FDC.

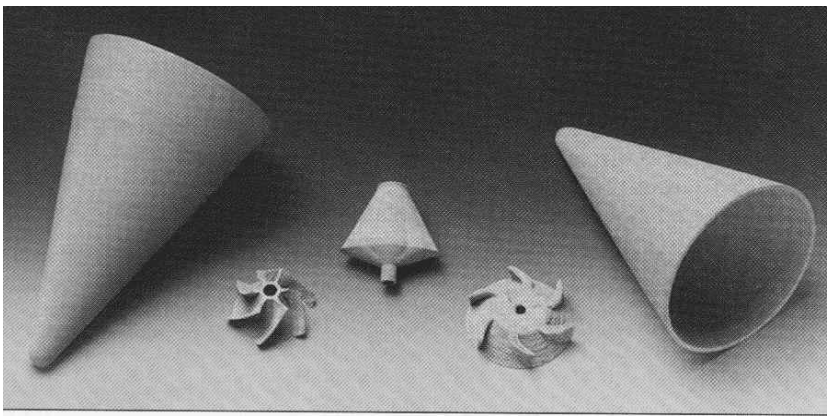

Figure 2.38: FDC green ceramic parts[68]

2.2.5.3 Multiphase Jet Solidification (MJS)

This process developed by Fraunhofer-IFAM [69] uses a thermoplastic powder mix, which is similar to conventional injection moulding material. The process can be used with any injection-mouldable ceramic or metal system. As with most of the Advanced Manufacturing Technologies that are applied to ceramics, the MJS process consists of a robotically-controlled nozzle, which builds parts from small beads of extrudate, followed by binder removal and sintering.

The working principle of the MJS process is shown in Figure 2.39. The material is supplied as a powder-binder mixture (feedstock) and then heated to achieve suitable viscosity, squeezed out of a nozzle by a pumping system and deposited layer-by-layer. The molten binder solidifies when it comes into contact with the platform or previous layer due to the cooler temperature, pressure decrease and heat transfer to the part and the environment. On contact, the liquefied binder material causes a

partial re-melting of the previous layer, resulting in a strong bonding of layers. The extrusion jet is mounted on an x-y-z table that is controlled by a computer system. After one cross-section has been produced in the x-y plane, the extrusion head moves in the z direction and the next layer is manufactured. The part is created layer-by-layer until its full extent is reached[70].

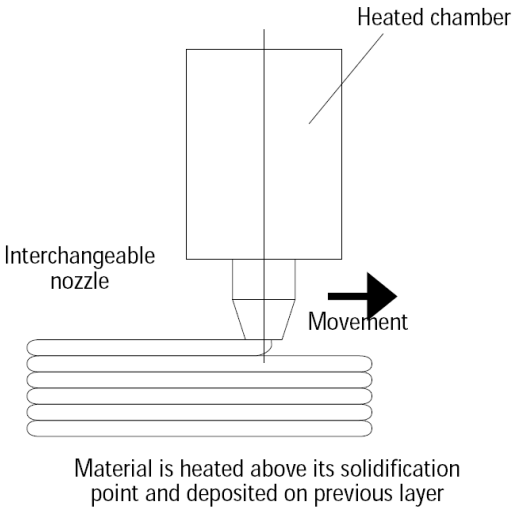

Figure 2.39: Multiphase jet Solidification MJS Process [70].

2.2.5.4 Robocasting

Developed at the Sandia Laboratory, Albuquerque, NM[71], Robocasting is a novel technique for the fabrication of dense ceramics. This FDC system uses a computer controlled, layer-by-layer deposition by extrusion of ceramic suspensions with high solid loads through a fine nozzle. (Figure 2.40) The nozzle diameter may vary. The material formulation contains 50 to 65 vol% particles, 35 to 50 vol% solvent (commonly water) and 1 to 5 vol% organic additives. In the process, the layers are

sequentially deposited one after the other and every individual layer has had sufficient time to dry. In some ways, Robocasting is similar to slip casting or gel casting but without the use of moulds. Proper control of slurry rheology, build parameters and drying conditions are the key to the structural integrity of the component.

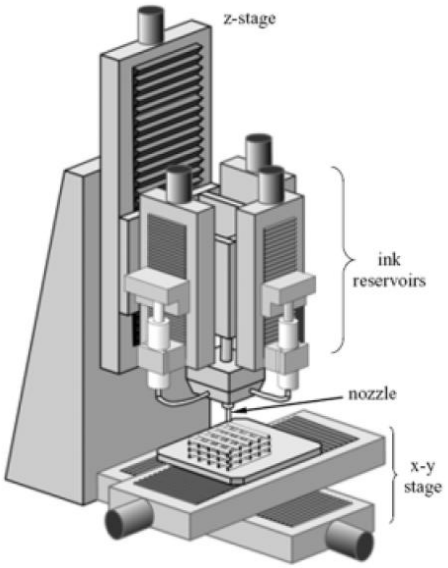

Figure 2.40: Robocasting process [72]

The key to successful robocasting is a thorough understanding of the fluid characteristics of the colloidal ceramic system. The slurry must be sufficiently pseudoplastic to flow through a narrow orifice and yet must transform to a solid-like mass after deposition. If drying is too slow, slumping may occur because the accumulated mass of several layers provides a stress greater than the yield stress of the pseudoplastic layer. On the other hand, too rapid drying may lead to cracking, warping and deformation. To overcome limitations on the shape uniformity of the

deposited material and to reduce macroscopic defects, robocasting of gel casting suspensions has been investigated[73].

Lately Robocasting has demonstrated a wide variety of ceramic materials for different applications, such as aluminium oxide, barium titanate, feldspar, hydroxyapatite, kaolin, mullite, silicon nitride, zirconium oxide etc. Applications include filtration, custom shapes, labware, thermal analysis, catalyst etc. Figure 2.41 below shows alumina ceramic parts produced by robocasting process.

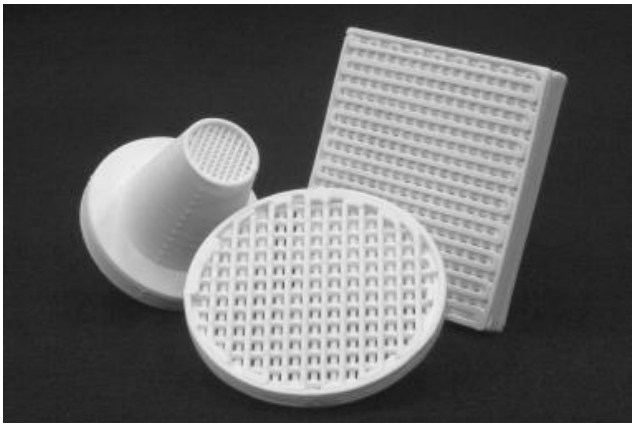

Figure 2.41: Lattice filtration ceramic part (Robocasting)[74]

2.2.5.5 Extrusion Free-Form Fabrication (EFF)

This process is similar to MJS in that it produces parts from a suspension of ceramics or metals using a wax or polymer vehicle which is extruded onto the building platform by a high-pressure extrusion head. The material used in these approaches is a suitable ceramic feedstock, which needs many of the qualities commonly desired in raw materials for ceramic injection moulding[75]. These formulations consist of around 55 vol% ceramic powder dispersed in an organic binder.

The binder is commonly a mixture of polymer, wax and plasticizer and serves as a vehicle for the free-form ceramic powder. The EFF feedstock should also possess a reproducible rheology with a low melt viscosity (extrudable at low pressures) as well as the ability to undergo rapid solidification upon deposition (enabling more rapid, part-build rates). The binder should be easily removable from the free-formed green body under controlled conditions, leaving minimal pyrolysis residue. Finally, it should be possible to sinter the resulting ceramic body into dense ceramic components.

2.2.5.6 Freeze Form Extrusion Fabrication (FEFF)

This process developed at the University of Missouri–Rolla, Rolla, Missouri [76] works with the extrusion of an aqueous ceramic paste. The paste is extruded layer-by-layer into a build chamber which is held below room temperature to cause freezing of the paste. As only water is used as the binding media it is quite an environmentally friendly approach. Solid loading as high as 60 vol % has been achieved with this method using aluminium oxide (Al_20_3). Figure 2.42 shows the schematic FEFF process.

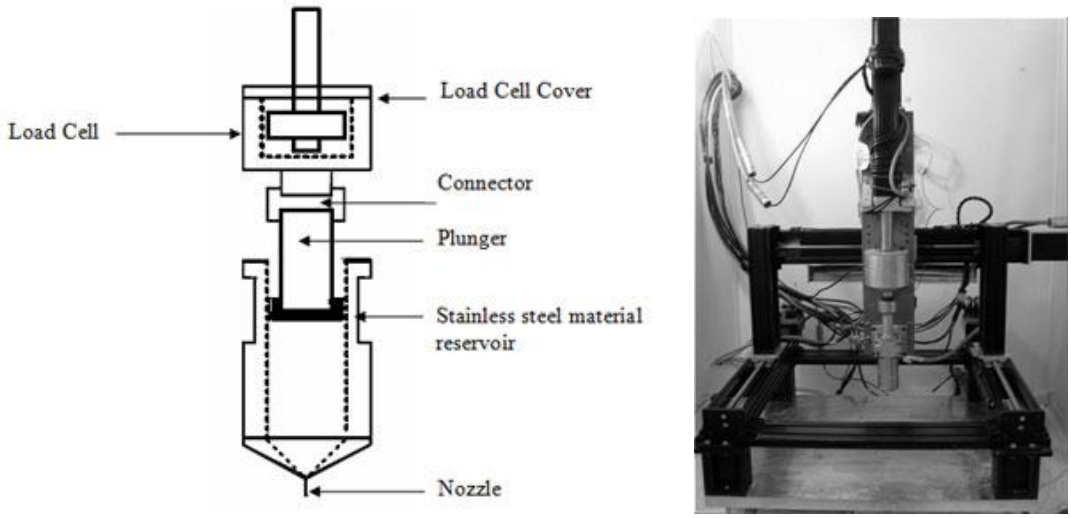

Figure 2.42: Freeze Form Extrusion Fabrication process.

2.2.5.7 Contour Crafting (CC)

Another extrusion method is The Contour Crafting Process (CC)[77] developed by Behrokh Khoshnevis of the University of Southern California. This method is an additive fabrication technology which uses the computer-controlled extrusion of ceramic material to construct large structures with internal features; this system incorporates a blade that flattens the freshly-deposited extruded ceramic material to create a smooth external surface.

The overall process is a combination of an extrusion process for forming the part surfaces and a filling process (pouring or injection) to build the object core. The Figure 2.43 shows a schematic representation of the CC process.

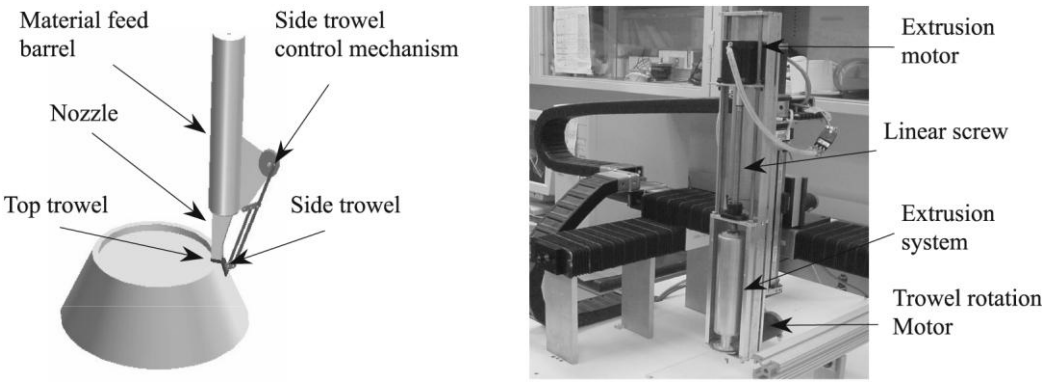

Figure 2.43: CC process

The advantage of this process is the ability to rapidly produce large-scale parts using relatively coarse beads (large nozzle diameters) and yet generate a smooth external surface. This process holds a major potential in the construction sector as large

components with complex geometry can be easily produced with various materials at a rapid speed.

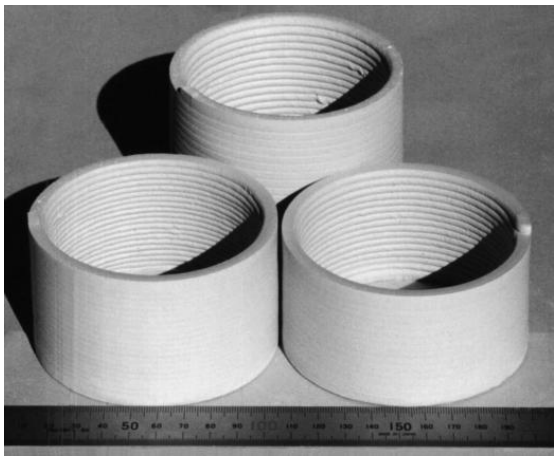

Figure 2.44: CC Ceramic parts[78]

This method uses the material that will be used in the final application, direct manufacturing. Materials explored for this method include various materials for outside surfaces and as fillers between surfaces (clay-based materials and concrete). In addition, multiple materials that react with one another may be fed through the CC nozzle system and mixed in the nozzle barrel immediately before deposition.

2.2.5.8 Slip-jet Printing

This process, developed at DePauw University, USA by David Herrold [79] , produces ceramic objects using a mechanical mechanism which works with a pump to extrude a heavy clay slip ribbon, layer-by-layer through a nozzle, to build the object following the additive manufacturing principles. The slip jet printer works chiefly on rotational

motion as in a potter's wheel. Additionally the system is computer controlled which enables it to create geometric shapes by blending various functions such the twist, offset, extrude and lathe techniques of the potter's wheel. Figures 2.45 shows the Slip Jet process.

Figure 2.45: Slip Jet Process[79]

The paste solidifies by drying, which must be accomplished quickly in order to avoid distortion as the material is in a semi-fluid form (low viscosity) in order to achieve bonding of the layers. In particular, the lower layers should have a fast solidification in order to support the weight of the upper layers while maintaining the structural form. Initially, a solution developed for this function involved a semi-circular-shaped manifold which surrounded the rim of the object being constructed to feed air across

the deposited material and promote drying. Figure 2.46 shows a clear example of the process possibilities.

Figure 2.46: Figurative water towers by David Herrold, Slip-jet Process

2.2.5.9 Ceramic Rep-Rap Process

More recently, a Belgian company, Unfold, in partnership with Bits from Bites, is working on a new project called "L'Artisan Electronique"[80]. The project uses a modified extrusion system base on the low cost, Rap Man [81] technology project initiated by the University of Bath UK, for the extrusion of plastics materials. Figures 2.47 and 2.48 show the printing system and an example of a printed part.

L'Artisan Electronique uses the same extrusion method but with dispenser operated by air pressure and a modified syringe nozzle. The system uses drying as the solidification method. The pressure on the reservoir produces a constant flow of clay paste that can be shifted via an electronic valve. This way, the shape is formed layer-by-layer.

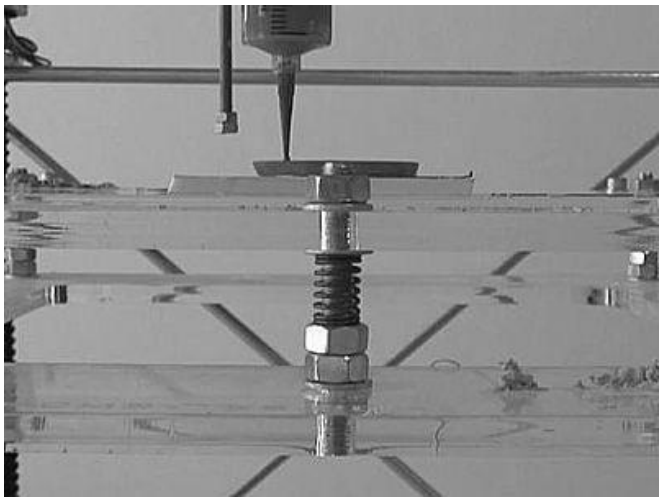

Figure 2.47: Unfold's *L'Artisan Electronique* / REPRAP Process[80]

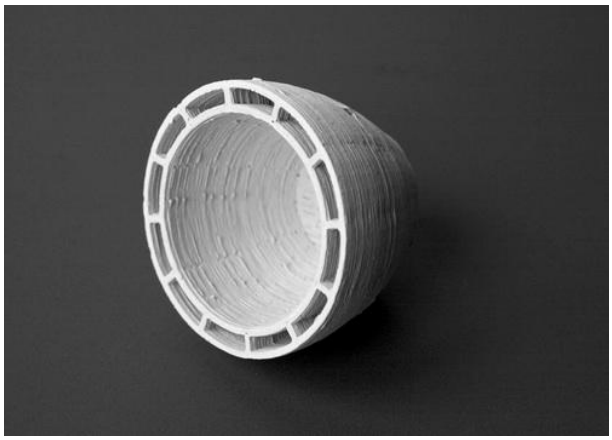

Figure 2.48: Finishing ceramic part Unfold's L'Artisan Electronique.

Table 2.2 shows the most important AM of ceramics that are based on extrusion methods and a brief description of each process.

Additive Manufacturing of Ceramics base on Extrusion Process.			
Method	Description	Deposition Method	Solidification
Fused deposition of ceramics	Ceramic suspensions in a polymer or wax vehicle	High temperature extrusion	Cooling of molten material
Robocasting	Extrusion of high solid loads ceramic suspension	Positive dispensing extrusion	Gel casting Drying
Multiphase Jet Solidification	Thermoplastic powder mix	High temperature extrusion	Cooling of molten material
Extrusion Freeform Fabrication	Thermoplastic powder mix	High temperature extrusion	Cooling of molten material
Freeze Form Extrusion Fabrication	Aqueous base slurry	Positive dispensing extrusion	Freezing of binding media
Contour Crafting	Ceramic slip Concrete	Screw dispensing system	Drying Quick set
Slip Jet 3D printer	Ceramic slip	Air pressure dispensing	Drying system
REPRAP Process	Ceramic slip	Air pressure dispensing	Drying system

Table 2.2: Additive Manufacturing Technologies of Ceramics based on an Extrusion Process

2.3 DESCRIPTION OF THE METHOD

2.3.1 Direct Writing- Freeze-casting (DWFC) system

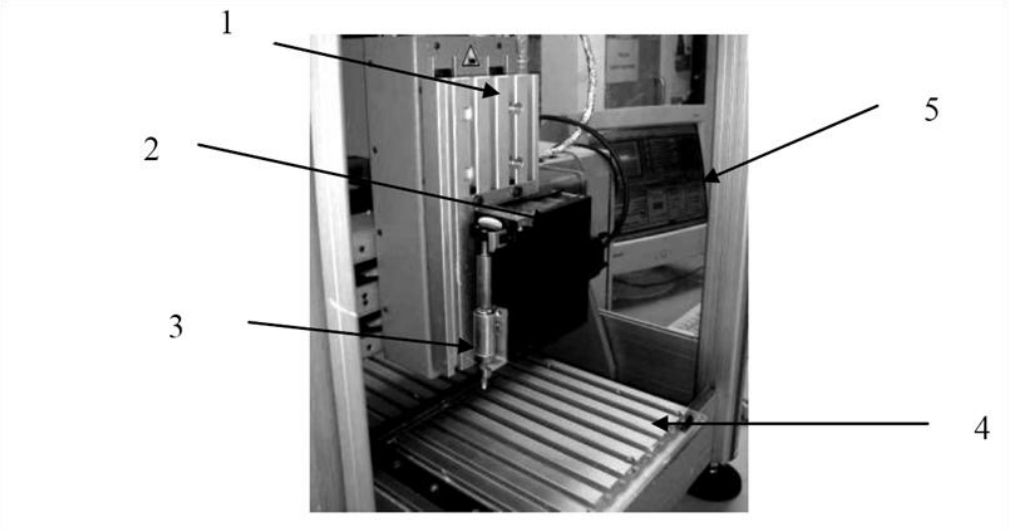

Figure 2.49: ***DWFC*** SYSTEM

The ***DWFC*** extrusion system is composed of five major components (see Figure 2.49): **1)** the actuation system (Isel Multi-K CNC router), the mounting point for the build platform which can be moved in the X-Y direction and a mounting head for the pump which can be moved in the Z direction. **2)** Syringe pump (PVM syringe pump), which extrudes the material using a positive displacement mechanism. **3)** Syringe; plunger, barrel (5ml capacity), and needle (0.9mm diameter orifice). **4)** The build platform, which acts as the substrate for deposition of the extrudate and subsequent freezing. **5)** A computer which runs the software to control the motion of the actuation unit and the syringe pump operation based on data from the required object to be built. The CNC program was written as a text and translated in ISO standard, G&M codes.

The ceramic powder material was prepared as suitable slurry and then extruded via the syringe using a positive displacement system in which the plunger was moved at a constant speed, rather than based on a set pressure. Once the required object was formed, the slurry was rapidly cooled to below -40°C. The layer thickness was typically in the range 0.8mm to 1.2mm.

2.3.2 Freeze-casting Route

Bulk freeze-casting has been known for about 60 years as a complex shape-forming technique mostly for refractory materials. This process is usually employed for the fabrication of technical ceramic parts; such as crucibles and kiln furniture, pouring cups, nozzles, orifice rings and many other components used in the high temperature processing of metal, glass and ceramics. Figure 2.50 shows the bulk freeze casting process, freezing occurs by placing the freeze-casting mould unit in a chilling apparatus with liquid nitrogen or an upright walk freezer temperature controlled bellow -30°C.

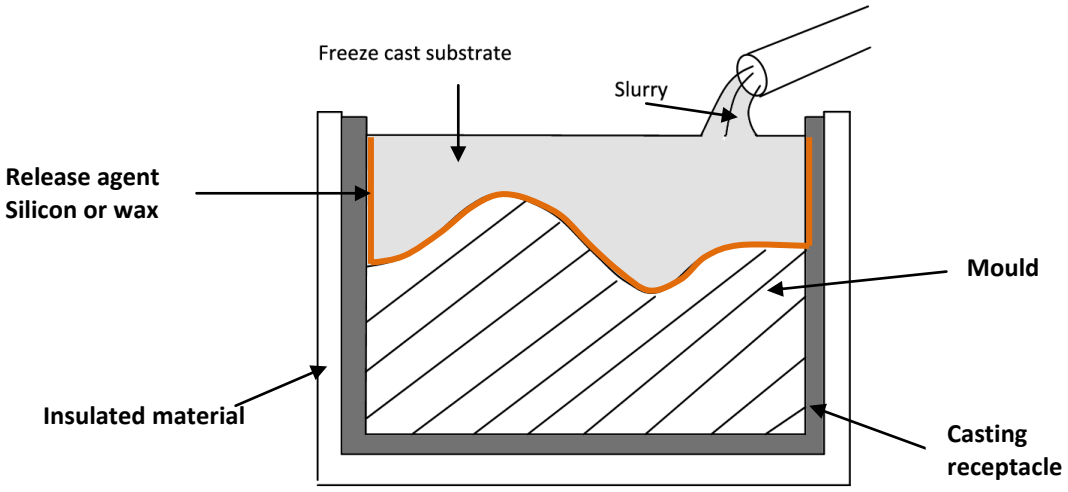

Figure 2.50: Bulk freeze-casting system (Adapted from Roche *et al.*)

At first, the freeze-casting technique was used to fabricate dense ceramic parts, instead of porous ceramics parts, by eliminating porosity through the use of high solid load ceramic suspensions [82]. Thus, the unwanted porosity generated by this method was studied intensely and was found to yield unique microstructures, which are not possible to achieve through other routes. This raises the potential for the use of the freeze-casting method for the fabrication of porous objects. Subsequently, the addition of cryoprotectants* was proposed in order to achieve a high-density green part and better packing of the particles in the freezing stage.

In the bulk Freeze-casting technique, ceramic powders of selected particle size are mixed with a freeze-sensitive sol (a stable suspension of nanoparticles in a liquid medium). The resulting slurries are poured into a nonporous mould, which is frozen, typically at temperatures around -40°C, followed by demoulding and liquid phase removal by sublimation. Figure 2.51 shows the main steps of the process.

The rapid cooling of the slurry causes the solidification mechanism by an irreversible transformation that is based on the physical and chemical reactions at the fluid-solid phase transition of the slurry upon freezing. The demoulded green part has enough strength to be handled for a further firing or sintered stage in order to develop the necessary mechanical properties for the final product.

*Note: A cryoprotectant is a substance that is used to protect biological tissue from freezing (due to ice formation) e.g. Glycerol, PVA and PE.

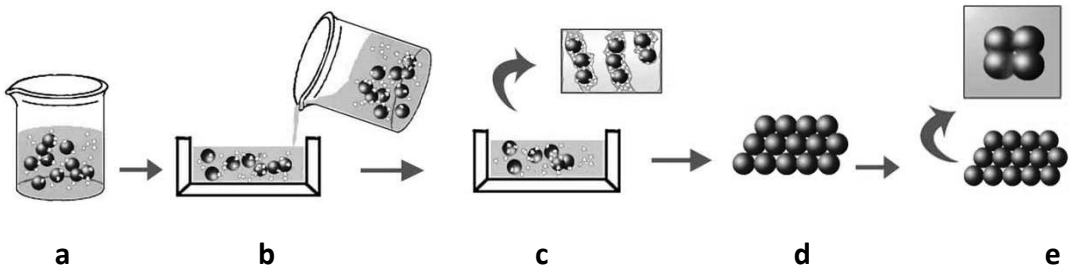

Figure 2.51: Flow chart of the freeze-casting system

a) Slurry preparation, b) Slurry poured into a non porous mould, c) Solidification, the slurry is submitted to lower temperatures (i.e. -40°C), the ceramic particles are entrapped between the ice crystals grow, d) demoulding and drying, sublimation of the ice crystals leading to porosity and e) sintering.

The particles not only interlock irreversibly to form a rigid framework due to the increasing volume of the aqueous solvent during freezing (physical reaction), in addition, in the separation phase between the liquid and the solid particles during freezing, sol nanoparticles and ceramic particles are excluded from the liquid when ice crystals start forming (see Figure 2.52). This enables strong bonds to be produced between the sol nanoparticles (Siloxane bonds), including those adsorbed on the surface of the larger ceramic particles. It is the liquid carrier molecules that separate the sol nanoparticles from each other and stabilize the sol. Once the liquid barrier is removed, the nanoparticles become close enough to enable close attraction through van der Waals forces. An internal uniform pressure is induced and draws all particles together around the ice crystals, as if external pressure had been applied. The

variation of the materials suggest that the mechanism of freeze-casting depends not on the type of material but on the physical interaction rather than the chemical interaction[83].

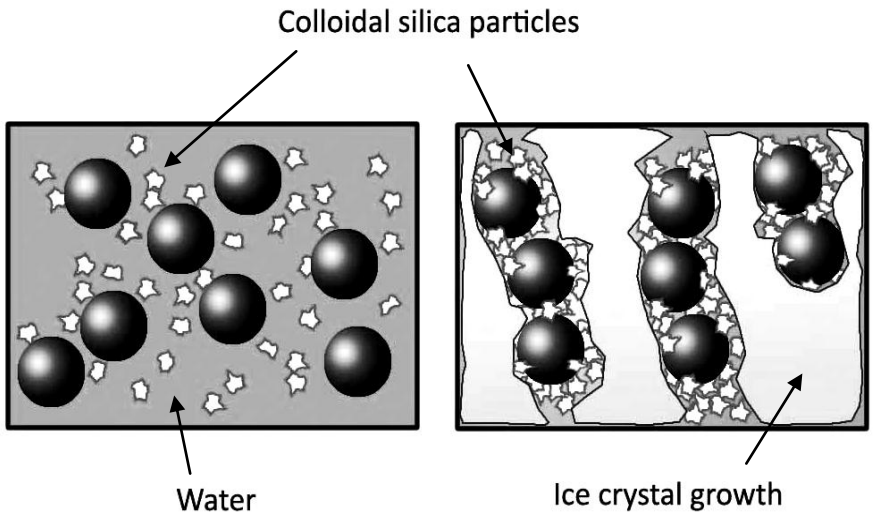

Figure 2.52: Phase separation of water and solid particles during freezing (Adopted from Andresen *et al*.)

Finally, the frozen ice sublimes from the solid phase to the gas phase resulting in a 3D porous network; which is representative of the entwined, dendritic, ice crystals. Thus, the porous structure is primarily defined by the morphology of the growing solvent crystals[84]. Figure 2.53 shows the particle changes throughout the freeze casting process.

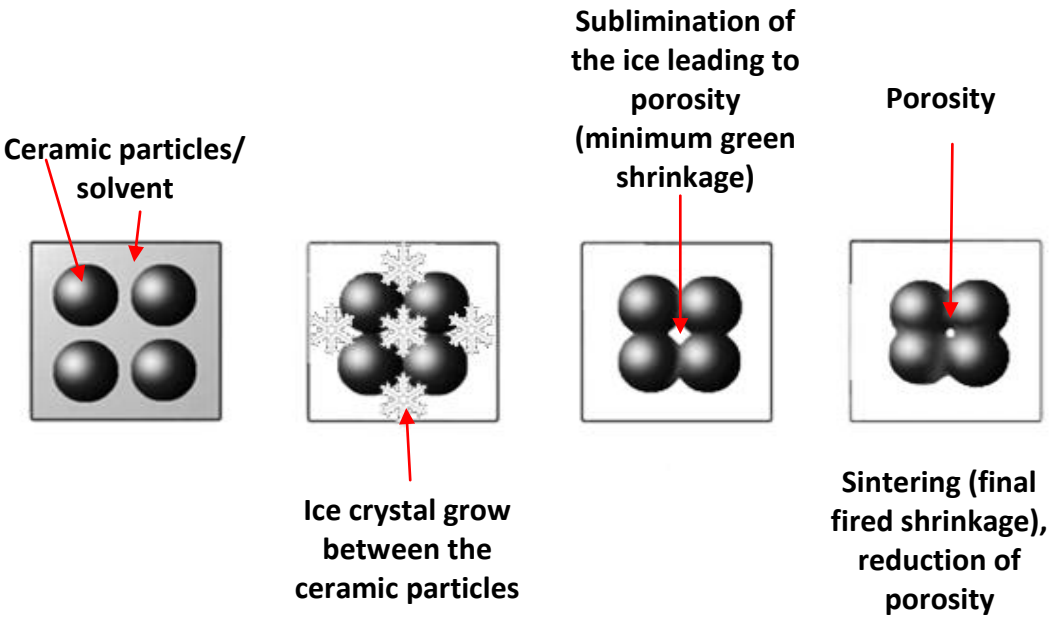

Figure 2.53: The ceramic particle changes throughout the freeze-casting process chain.

2.3.2.1 Control parameters in the freeze-casting method

Four main control parameters have been considered for the freeze-casting method: i) Solid content in the suspension, ii) the temperature and freezing rate, iii) the additives, and iv) the freezing device [85]. The following section presents a brief explanation of these parameters.

i) The solid content in the suspension

The solid content in the suspension is the key parameter in determining the total pore volume and percent porosity in the final ceramic part. The lower the

concentration of the filler particles, the more water by volume is contained in the suspension leading to higher levels of porosity in the final part. On the other hand, a high level of solid particles makes the formation of ice crystal difficult, resulting in a smaller crystal size which in turn leads to smaller pore size when sublimation occurs. The particle size of the filler powder is also an important factor; the porous structure is primarily defined by the morphology of the growing solvent crystals and, secondarily, by the ability of the particles to pack between the crystals, as finer particles will provide a better replica of the solvent crystals.

ii) Temperature and freezing rate

The temperature and freezing rate has a significant influence on the ice-growing stage and the sol nanoparticles separation during the freeze phase, and so on the microstructure formed. A very rapid freezing rate will lead to small ice crystals whereas a slow freezing rate will lead to bigger ice crystals. Nevertheless, the percentage of the total porosity is not affected, as the liquid content is the same[86, 87].

iii) Additives

Dispersant: In the preparation of the freeze-casting slurry, clusters of particles known as 'soft agglomerates' are formed due to the presence of van der Waals forces as the ceramic powder aggregates when it is added to any suspending

medium, such as water. This results in a suspension with higher viscosity, which makes processing more difficult. In addition, the suspension creates high-stress areas, reducing the mechanical properties of the component. Therefore, the prevention of agglomerates formation or their elimination from the suspension before the actual fabrication of the green body becomes crucial. Electrostatic, steric and electrosteric dispersion are the three main ways to achieve this, with the later being the most effective. This method involves the adsorption of either uncharged polymers onto an electrostatically-charged surface or the adsorption of charged polymers, referred to as a polyelectrolyte.

Cryoprotectant: The addition of a cryoprotectant has been proposed in order to control the ice formation and then the microstructure of the final part[88], the cryoprotectant affects the freezing kinetics of solidification morphologies, it binds to the liquid molecules, disrupts the complete crystallization of ice and results in an amorphous structure which has a smaller crystal size. Almost any water-soluble substance is likely to affect the freezing behaviour and crystal morphology. The desired properties of cryoprotectants for freeze-casting ceramics are: low toxicity, solubility in water, low freezing-point depression and cost effectiveness[89]. Several possible cryoprotectants have already been tested, such as ethylene glycol, propylene glycol, glycerol, methanol, ethanol and polyvinyl alcohol (PVA)[90].

Overall, the most commonly use is glycerol, especially for the preparation of a homogenous paste, the glycerol usually decreases the freezing point of glycerol-water mixtures by -1.6°C when 10%, -4.8°C when 20% and -9.5°C when 30%. Furthermore, glycerol reduces the volumetric expansion of water from 9% to 5% by volume at 20wt% glycerol in water[89, 91], thus a more dense green part can be obtained, furthermore, since the overall the defects are reduced, the final density also increases.

iv) Freezing Device

The freezing device gives the total porosity distribution in the final part. In this way, if the sample is subjected to bulk freezing, for example in a close rubber mould, this will lead to a homogeneous microstructure. However, if the suspension is cooled from one direction, the porosity distribution can be aligned to a particular orientation. The freezing device can be configured to produce complex microstructures.

2.3.2.2 Combination of freeze-casting with different ceramic methods

Freeze-casting has been combined with other ceramic processing methods (injection moulding, sol -gel and tape casting) in order to utilise the advantages of each technique. This new hybrid approach is described as follows:

- Injection moulding

Quickset™ is a commercial process based on a combination of freeze-casting and injection moulding[92, 93]. This process represents the most viable technique for the fabrication of complex ceramics shapes. In this process, a powder is mixed with a binder liquid, mostly water, with a specific freezing point. It should be noted that conventional organic binders are not used; the mould is filled and rapidly cooled to freeze the binder fluid. The solid phase is compressed into interdendritic regions to produce a solid body. This is then dried and sintered as required. The advantage of this process is a shorter debinding and drying time.

- Freeze- Gel-casting

Gel casting is widely used in manufacturing advanced ceramics, because high-strength green bodies can be obtained. Freeze-casting has been use in conjunction with gel casting with different gelation routes, such as agar, alginates and finally chemical gelation. In all cases, the freezing phase has taken place after the gelation has occurred[94, 95].

- Freeze-tape-casting

The freeze tape-casting method results from a combination of the freeze-casting and tape casting processes[96]. This method is used to prepare gradient pore structure materials. As with the conventional tape casting process, aqueous ceramic slurry is cast onto a carrier and a doctor blade is used to control the thickness of the slurry. The ceramic slurry is then unidirectionally solidified and freeze dried in a high vacuum. This method has been applied to zirconium ceramic suspensions.

2.3.2.3 Freeze-casting Materials

Due to its applications and its advantages (fabrication of porous materials and controled porosity), the freeze-casting route has been extensively studied for the production of ceramic materials, mostly advanced ceramics and biomaterials such as alumina[89], hydroxyapatite[97], tricalcium phosphate, zirconia, titanium dioxide[98], silicon nitride, mullite[99], glass[87], silica and silicon carbide. Freeze-casting of traditional ceramics, though studied, has been research on a limited scale. Ceramics such as lamponite clay, are used as additives in the freeze -casting process as a rheology modifier or film former due to its colloidal properties and also the use as a filler has been investigated[100] . Furthermore, there has been a lack of investigation of ceramic materials composed of three or more components, as in the case of triaxial porcelain or other similar pastes. Moreover, the potential to exploit this method for porous materials applications opens up interesting research into non-

ceramic materials. The following section describes briefly the state-of-the-art for this process and it uses.

2.3.2.4. Freeze-casting of ceramic suspensions

- Dense ceramic parts

The first trials in freeze-casting were aimed at the production of dense ceramic parts [82]. These trials were undertaken using ceramic powders such as mullite and show that the freeze-casting process is able to yield structures that are more homogenous, have increased mechanical properties and can be sintered at a lower temperature than for conventional ceramic manufacturing processes.

Trials undertaken by Dogan *et al.* [88] resulted in highly-dense, sintered alumina, ceramics with a uniform microstructure because of the increased solid load (up to 60 vol%). The high solid content in the formulation causes the restriction of ice crystals during the solidification of water, which is essential for successful freeze casting. The solid-load content in the suspension and the effect of glycerol (an additive used to obtain a higher density in the final ceramic part) has been also studied [89] .

- Porous ceramic parts

The fabrication of porous ceramic parts by freeze-casting has been particularly studied using alumina and zirconia materials. Trials undertaken by Fukasawa *et al.* [101] resulted in porous alumina ceramics, with aligned macroscopic open pores. The pore structure was substantially affected by the starting slurry concentration and sintering temperature. Similar structures were also obtained by Mortiz *et al.* [102] for hollow ceramic components produced by the freeze-casting technique using ice as a mould material. Moreover, the production of porous ceramics by freeze-casting has been suggested as a route for the fabrication of metal-impregnated, ceramic-metal composites, as described by Roy and Wanner [103, 104].

Other composite materials which have also been explored include aluminosilicates, such as kyanite and SiO_2/mullite. Different morphologies were obtained depending on the freezing rate[105]; a slower rate results in the evolution of the porous structure from irregular to unidirectional columns and dendrites. In addition the suspension concentration determines the apparent macro-porous structure for high concentration levels[106].

Recently, a particular interest has arisen in the freeze-casting of nanoparticle systems[107]. To do this, an understanding of the freeze-casting behaviour of

nanoparticle suspensions is required, especially the interaction between the glycerol and the dispersant chains, such as poly(acrylic acid) (PAA), in order to obtain a properly-dispersed and stable suspension.

The use of nanoparticles of zirconium also has been explored by the freeze-casting route for the fabrication of dental parts, in which the open porosity can be infiltrated with dental materials and the ice-mould technique can be used with a steel core[108].

Porous ytria-stabilized zirconium (YSZ) ceramics were fabricated by freeze-casting using aqueous ceramic slurries. Polyvinyl alcohol (PVA) was added to the slurry with the aim of controlling the microstructures and properties of the porous YSZ ceramics[109]. The same material, yttria-stabilized zirconium oxide (YSZ), was selected as the preliminary material for use in a Freeze–Tape-Casting Process for the production of catalyst supports, biological membranes and fuel cell applications[96].

The structures obtained by this method can also be infiltrated with other materials, for example Gold[110] .

2.3.2.5. Freeze-casting of non-ceramic suspensions

Another use of the freeze-casting technique will be the fabrication of cellular implants with control of pore structure and size in freeze-dried collagen sponges[111]. Freeze-casting has also been use in the development of porous, solid, drug-delivery systems by freezing a mixture of 93 (w/w%) potato starch and 7 (w/w%) theophylline active ingredient to -20^{o}C[112].

Another application which has been explored is the use of the freeze-casting method to create titanium foams with aligned elongated pores[113] and the preparation of NiO-YSZ tubular scaffolds with radially-aligned pore channels.

2.4 WHITEWARE CERAMIC MATERIALS

The most common ceramics are composed of oxides, carbides, nitrides, silicides, borides, phosphides, tellurides and selenides. Ceramic processing generally involves high temperatures and the resulting materials are heat resistant or refractory[114]. Traditional ceramics refers to materials composed of unrefined clay and combinations of refined clay and powdered or granulated non-plastic minerals. They are commonly used as building materials or within the home and industry. Although there is a tendency to equate traditional ceramics produced by manual processes

with poor repeatability and production efficiency, in reality, advanced manufacturing technologies are often used in this industry.

Ceramic whiteware is defined as “fired ware consisting of glazed or unglazed ceramic bodies that is commonly white translucent and of fine texture, designating such product classification as tile, china, porcelain, semi-vitreous ware and earthenware”[115].

These compositions include hard porcelain, for art ware, tableware, vitreous sanitary ware, electrical porcelain, semi-vitreous tableware, hotel china, dental porcelain and others.

A typical composition could be considered as equal parts of clay, feldspar and flint. This composition is called hard porcelain. One of the main advantages of quartz-clay-feldspar bodies is the fact that they are not sensitive to minor changes in composition, fabrication techniques and firing temperature. This adaptability results from the interaction of the phases present to increase continuously the viscosity of the fluid phase as more of it is formed at higher temperatures [116]. A wide range of traditional ceramic compositions are mixtures of clay, feldspar and flint.

Among many classifications, whiteware can be further classified into four categories:

a) Earthenware; is defined as glazed, non-vitreous (medium porosity), clay-based ceramic ware. Applications for earthenware include art ware, kitchenware, ovenware, tableware and tiles. Colours may be red, for bodies with a high iron oxide content, to white, for the talc and triaxial formulas. The body is fired at a comparatively low temperature, producing an opaque product that is not as strong as stoneware or china. The product may be glazed or unglazed.

b) Stoneware; is a vitreous or semi-vitreous ceramic ware of fine texture, made primarily from non-refractory fire clay or some combination of clays, fluxes and silica that when fired, has properties similar to stoneware made from fire clay. Applications include art ware, chemical ware, cookware, drainpipes, kitchenware, tableware and tiles.

c) Chinaware; is a vitreous ceramic ware of zero or low absorption after firing that is used for non-technical applications such as art ware, ovenware, sanitary ware and tableware.

d) Porcelain; is defined as glazed or unglazed vitreous ceramic ware. Applications for porcelain include art ware, tableware and chemical, mechanical, structural, or thermal applications e.g. ball mill balls, ball mill liners, chemical ware and insulators. Porcelain represents the foundation of the ceramics discipline and one of the most complex ceramic materials. Composed primarily of clay, feldspar and quartz, porcelains are heat-treated to form a mixture of glass and crystalline phases. Porcelain is further divided

into high-fired porcelain (hard porcelain) and low-fired porcelain (soft porcelain).

Porcelains typically are a triaxial composition of about 50% clay, 25% flux 25% filler, and fired parts containing these three constituents. Because of its glassy content (~ 70%) and close porosity, hard porcelain has to be fired to very high temperatures, its silica-rich hard glaze is both chemically durable and abrasion resistant, fine translucent china basically consists of kaolin (30–40 wt.%), feldspar (25–40 wt.%) and quartz (30–50 wt.%). The body has low clay content but more feldspar and quartz, which improve the translucency. Fine translucent china is essentially soft porcelain, being biscuit fired at about 1230°C and gloss fired at 1150 °C. Fine translucent china is expected to have lower values of strength and fracture toughness than bone china since it contains more of the glassy phase and it also has an easily scratched glaze similar to bone china. The glaze is then applied and fired on at 1050–1100°C under a different heating cycle. Bone china is a highly crystalline (~70% crystalline) material with the properties of being resistant to edge-chipping. Bone china is also the whitest pottery among the others and prized for its unique appearance. However, it is not very suitable in severe service conditions such as hotels and restaurants because its alkaline-rich glaze is easily scratched. Furthermore, it softens during firing and becomes pyroplastic so that it cannot retain its shape unless it is supported by refractory furniture [7,8].

3. METHODOLOGY

3.1 INTRODUCTION

This chapter summarizes the methodology adopted for the experimental approach used in this research project. In addition to providing the overarching structure for the research, the materials and methods utilised at each stage of the project are also described.

3.2 REVIEW OF PREVIOUS WORK

As can be seen from the literature review, in recent years there has been significant interest in developing an AM method for ceramics, to enable complex ceramic shapes to be formed without the use of mould tools. In particular, extrusion is one of the approaches investigated, where ceramic powder is formed into a viscous, aqueous suspension (slurry). Unfortunately, akin to many conventional ceramic-processing methods, parts produced by extrusion (direct writing) generally suffer from high levels of drying shrinkage (>5%).

More recently, the AM method for ceramics has benefited from techniques based on extrusion combined with conventional ceramic-forming methods. In these so called

direct casting processes[2], (sol-gel techniques, gel casting, starch consolidation, freeze casting etc.), the ceramic slurry is transformed into a solid state without the removal of water. This allows the use of a non-porous mould, which has considerable economic advantages, as well as an improvement in the homogeneity of the green body.

Aim: The aim of this PhD study is to develop a material (based on a triaxial whiteware formulation) which can be successfully processed using the new AM approach of combining direct writing and freeze casting to enable customised ceramic products to be formed.

Objectives of the experimental work;

- Investigate the suitability of conventional triaxial whiteware ceramic formulations for the DWFC process.
- Develop and fine tune a material that can be successfully extruded, freeze cast and fired.
- Investigate the properties of the new material formulation and compare with conventional materials.
- Develop improved processing conditions.

3.3 EXPERIMENTAL APPROACH

The following methodology was used to investigate and develop suitable triaxial porcelain materials for the ***DWFC*** process. The trials were divided into three main stages;

(1) Initial scoping trials based on standard porcelain triaxial system (clay based) to determine the suitability for the freeze casting process and development of a modified system based on non plastic porcelain (**NPP-1**).

(2) Testing and further development of the material in extrusion, freeze casting and firing took place, which led to the developed of a refined formulation (**NPP-2**).

(3) Fine tuning of the formula took place based on extrusion performance and this led to a development of the final formula (**NPP-3**).

3.3.1 Freeze-Casting Trials

As the Freeze Casting route is the proposed method for the solidification of the ***DWFC*** system, the first step of the experimental work was to understand the mechanism involved in freeze casting for the production of whiteware bodies, the experimental work sequences in four main freeze casting tests, as shown in the Figures 3.1, 3.2, 3.3.

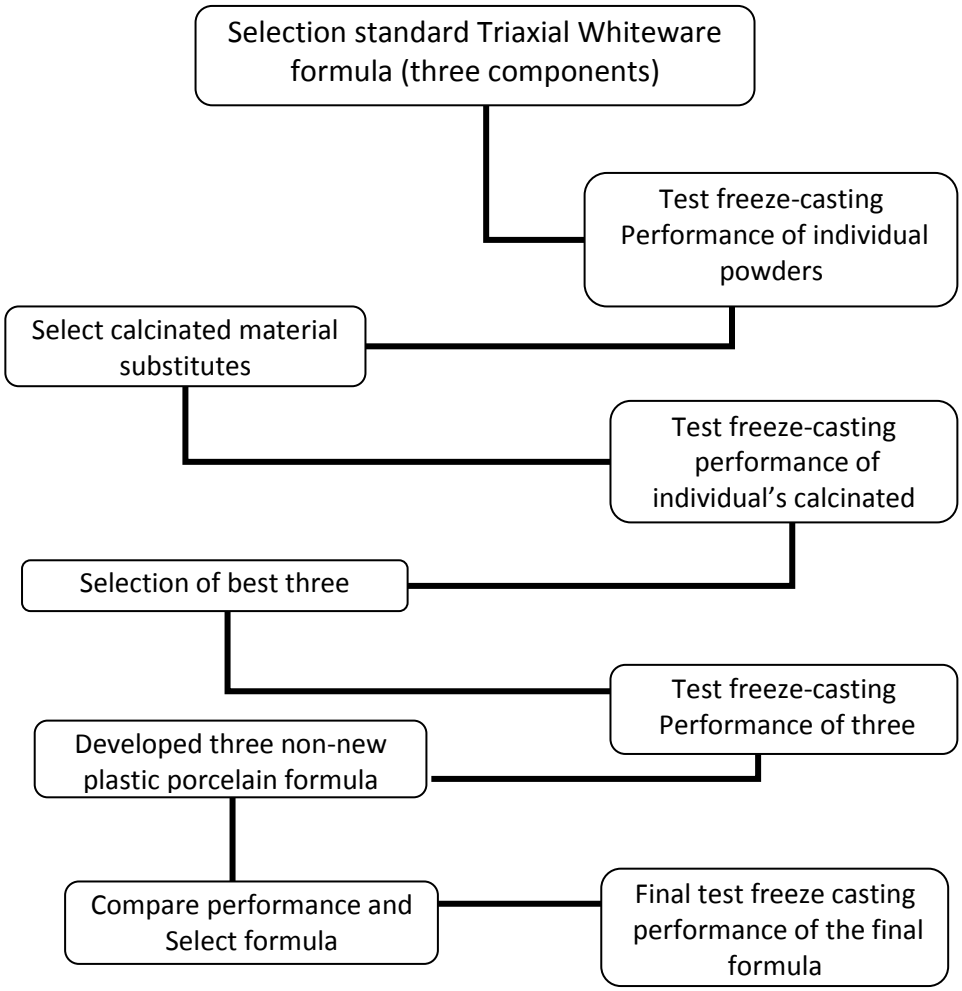

Figure 3.1: Preliminary freeze-casting trials

3.3.2 Extrusion Trials

The Direct Writing trials in this experimental work involve the micro-extrusion of the developed material through fine nozzles, using a positive displacement mechanism. The overall experimental work comprises three main steps

1. Test performance in extrusion.

2. Refine material to improve extrusion (particle size reduction, reduction in water content, addition of additives).
3. Test performance for extrusion parameters, different velocities and different nozzle size.

These stages are shown in more details in Figure 3.2.

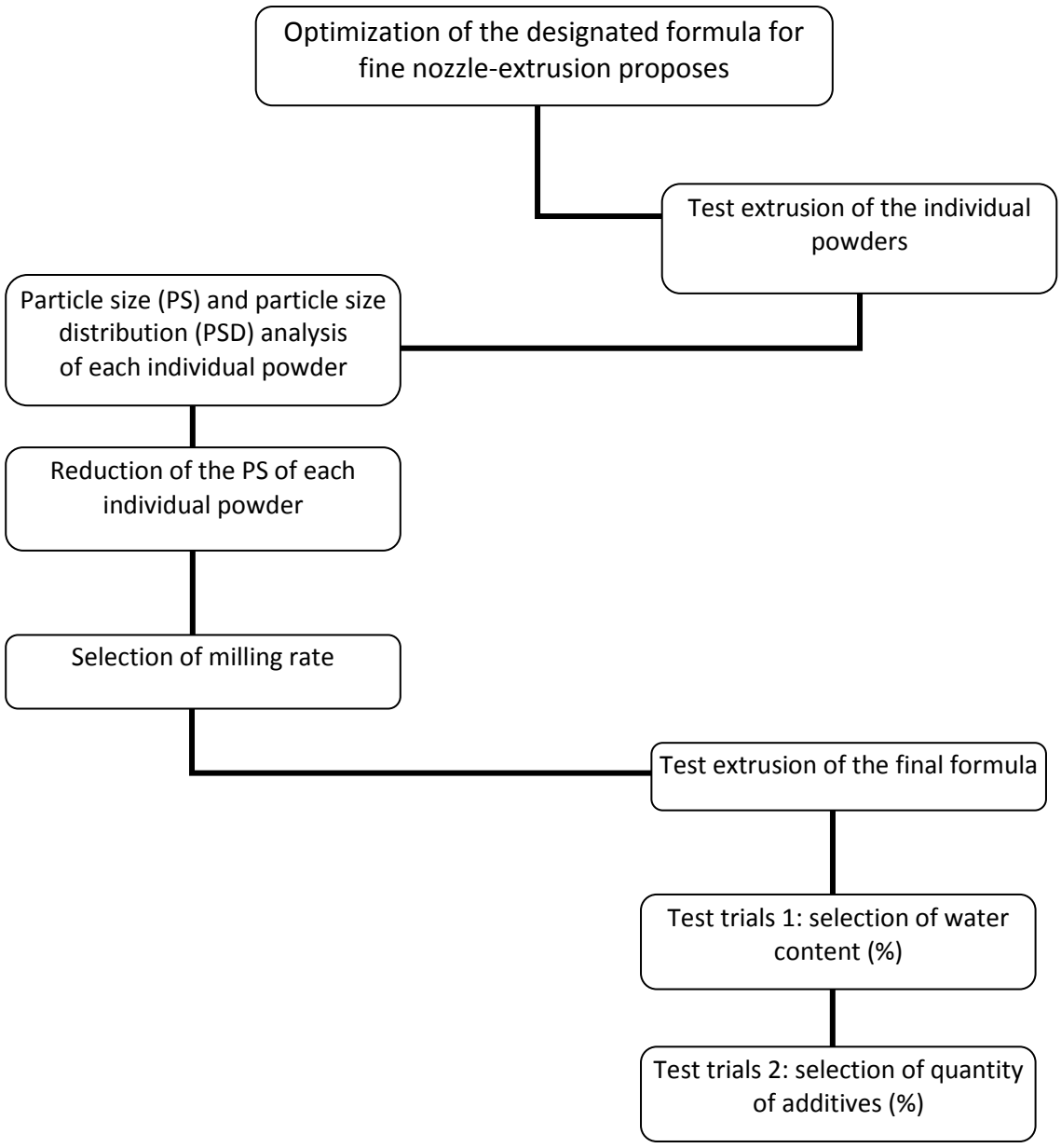

Figure 3.2: Preliminary extrusion tests.

3.3.3 Optimisation of process parameters

After the selection of the final formula, an optimisation of the FC and extrusion parameters was proposed as a set of trials. This procedure is shown in the flow chart below (Figure 3.3):

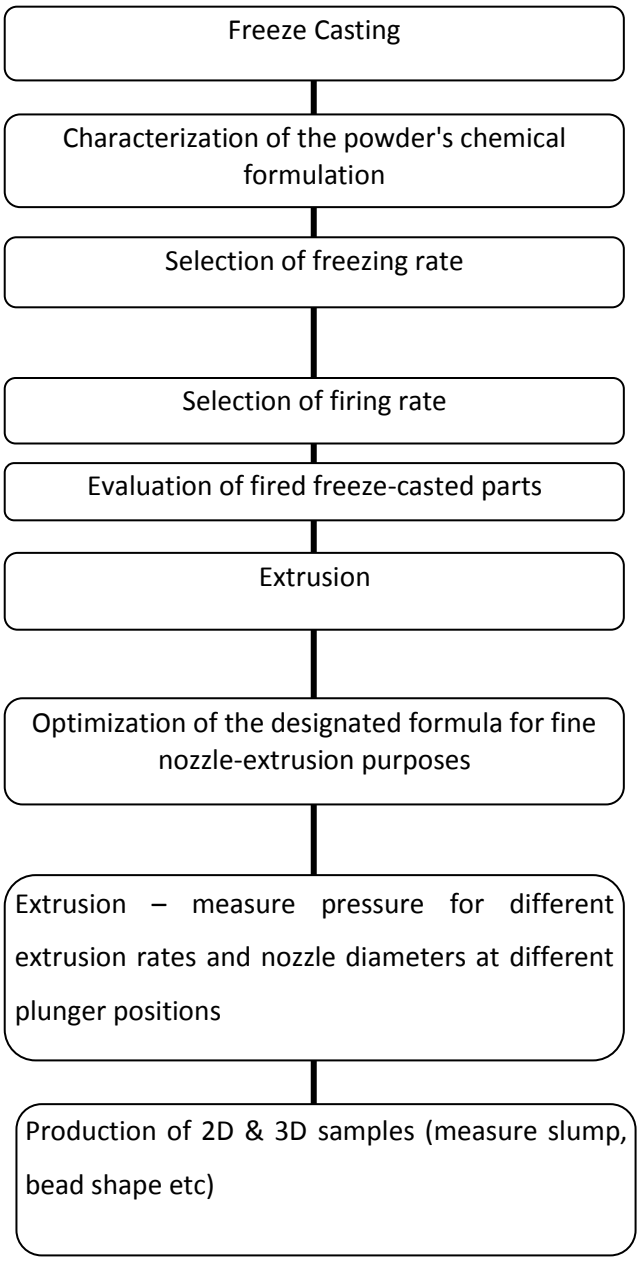

Figure 3.3: Optimisation of the process parameters

3.4 MATERIALS AND METHODS

3.4.1 Materials

Materials are divided into solvent (liquid medium) and fillers (the powders).

3.4.1.1 Solvent

The solvent is comprised mainly of the colloidal silica sol dissolved in water with a small volume of additives (dispersant and cryoprotectant). The quantity of silica sol and additives within the formulation was initially based on the specification given in the literature (freeze cast patent)[117] .

Silica Sol: A sol is a colloidal suspension of solid particles in a liquid. The silica sol is a stable dispersion of submicron size SiO_2 particles in water. The silica sol used in this experimental project was a commercial colloidal silica sol (Morisol AS 2040 from Morrisons, Liverpool, United Kingdom). In this silica sol, the liquid carrier consists essentially of water, stabilised with ammonia with a pH value of 9.0, such a sol usually has a SiO_2 content of 20% to 50%. The main advantages of the use of water as the liquid carrier include the specific morphology of the ice crystals leading to unique porosity characteristics and its compatibility with many functional additives.

Additives (dispersant): The dispersant utilized in this research was Dispex A40 (Ciba Speciality Chemicals Inc.). According to the manufacturer's literature, this is a solution of an ammonium salt of an acrylic polymer in water (ammonium

polyacrylate: NHPA) with 40% active content, a density of 1.16g cm^3, a pH of 8.0 and an average molecular weight of 4000. The structure of NHPA and its dissociation in water separates the particles in the suspension by electrosteric repulsive forces producing negatively-charged poly ions and ammonium counter ions [118]

Additives (Cryoprotectant): The cryoprotectant used in this investigation was glycerol (reagent plus >99.0% grade from Sigma-Aldrich). As mentioned in the literature review, glycerol is well known for its antifreeze (freezing point depressant) properties in other applications. In this research project, glycerol was used to disrupt the morphology of the solidification process and thus produce a more dense structure[89].

3.4.1.2 Filler

Several traditional ceramic powders (fillers) were used in the experimental work. The initial trials focused on the components of conventional triaxial porcelain (quartz, feldspar and clay). In later trials calcined clay substitutes were also used (fired porcelain and Molochite). In the freeze casting process the properties of the starting powders can have a major effect on the characteristics of the final material[119], the interaction between particles is a critical part of the process and a number of parameters can modify these interactions, including the size of the particles, particle size distribution, particle shape, surface roughness and surface tension.

Filler type	Supplier	Product Code	Particle size*
Quartz	Pottery Crafts	P03337-05	<75µ
Feldspar	Pottery Crafts	P03296-01	<75µ
Clay (Kaolin)	Pottery Crafts	P3309-05	<75µ
Molochite (Calcinated Kaolin)	Pottery Crafts	P3311-01	<17µ

*According to the manufacturer information.

Table 3.1: Filler powders used in the trials

3.4.2 Methods

Several test methods were performed for each stages of the project; overall they can be divided into three main steps, i) selection, characterisation and preparation of the powders, ii) forming the ***DWFC*** process and iii) testing the mechanical and physical properties of the final parts. An experimental matrix is shown in Table 3.2 and each method used is explained in detail in the subsequent sections.

Experimental Matrix/ DWFC of Triaxial Porcelain Preparation of the powders, forming and measure of properties			
	Test	Method	Equipment
Selection, Characterization and Preparation of the powders.	Reduction of Particle Size and Mixing	Ball Milling	Planetary Mill, RETSCH PM 100
	PS	Sieving	Analytical sieve shaker AS 200 control RETSCH
	PS, PSD	Laser Diffraction Technique	Masteries 2000 PS analyser Malvern.
	Particle shape agglomeration	Scanning Electro Microscope	Analytical scanning with the simultaneous EDS (Sigma advance Carl Zeis NTS GmbH Germany)
	Phase identification	X-ray Diffraction	Bruker, D8 ADVANCE™ X-ray powder diffraction System
	Elemental composition	X-ray Fluorescence	XRF spectrometer Panalytical AXIOS Advanced
Forming Extrusion/ Freeze Casting	Direct Writing / extrusion parameters	Direct Writing Extrusion parameters device.	Direct Writing test ring
	Freeze Casting/solidification and sintering	Freeze casting Kilns	Freeze casting device
Physical Mechanical Properties of the Slurry and Final Parts Test	Viscosity	Rheology and density of the slurry	Brookfield-type viscometer
	Properties of the fired parts	Bulk Density of the fired part	ASTM testing methods for the characterization of fired whiteware
		Water Absorption	
		Linear shrinkage	
	Open porosity-microstructure	Scanning Electronic Microscope	Analytical scanning with the simultaneous EDS (Sigma advance Carl Zeis NTS GmbH Germany)
	Flexural Test	Three Point Bending	(CRE) testing machine, Instron 4301

Table 3.2: Experimental Matrix DWFC for Triaxial Porcelain.

3.4.2.1 Characterization and Preparation of the powders

- Ball Milling / reduction of the particle size

The first step in the preparation of the powders for extrusion is crushing or milling the raw materials to achieve the required particle size. This was accomplished by dry ball milling the initial powder feedstock using a planetary ball mill (RETSCH PM 100, capable of reducing feed stock of up to 10 mm in diameter down to 1µm). The milling media was zirconia (ZrO_2) balls with a diameter of 10 mm and a density of 6.0 g/cm^3. The ball mill jar was also constructed from zirconia. With dry ball milling, the use of the additives (in this case Polyethylene glycol -PEG-400- due to its compatibly with water) to reduce agglomeration was recommended. Each powder was ball milled separately. 100g of powder and 0.05g of additive (PEG) was the composition of each mix. 300g of spherical alumina milling media (4-10mm) was added. The compositions were milled at 180 rpm. The milling time varied for each powder depending on the particle size and density[120] , long ball milling times were required to achieve the desired particle size, 30 hours for quartz, 24 hours for feldspar, and 22 hours for molochite. The equipment was set up with an interval of stand by 1 minute every 10 minutes to avoid heating.

- Mixing

After individually ball milling the powders to reduce the particle size, the final formula (three powders together) was ball milled (mixed) to generate a homogeneous mixture. In total 100g. of powder mix, with a composition of 50% molochite, 25% quartz and 25% feldspar, the ball milling time was 10 hours, with an interval of 1 minute every 10 minutes to avoid heating.

Figure 3.4: Milling Media, top, Ball Milling Machine bellow.

- Sieving

In early trials, dry sieving was used to characterise the starting powders to be used in subsequent tests and determine the appropriate particle size distribution for successful extrusion. An analytical sieve shaker (AS 200 control RETSCH) using sieve sizes 20, 35, 50 and 100µm was used to separate the particles into fractions with various size ranges.

The powders were deposited individually in a stack of four sieves arranged in a progression of sizes (largest mesh size uppermost). The stack is then vibrated for a fixed time and the residual mass of powder on each sieve was measured. Initially sieving takes place for 20-30 minutes, this gives an idea of the PSD of the powders but problems can occur due to agglomeration of the powders and clogging of the screens during sieving. To separate the powder into true volume fractions of different particle sizes requires a relatively long sieving time. For this reason an accurate PS and PSD of the final formula were determined by laser diffraction techniques and SEM.

Figure 3.5: 20,30,50 micron mesh size sieves.

- Laser Diffraction Technique

The Particle Size (PS) and Particle Size Distribution (PSD) of the individual powders used in the final formula were analysed separately (before and after ball milling) using the laser diffraction method (Mastersizer 2000 particle size analyser from Malvern Instruments). The technique of laser diffraction is based on the principle that particles passing through a laser beam will diffract light at an angle that is directly related to their size: large particles scatter at low angles, whereas small particles scatter at high angles. Powders samples of each material were dispersed in water and isopropanol (concentration of 1 wt %), (0.40 g of powder in 4 ml of liquid).

Figure 3.6: Mastersizer/E, International Manufacturing Centre

University of Warwick.

- X-ray Diffraction (XRD) analysis, X-ray Fluorescence (XRF) analysis

XRD was used to analyse the crystalline phases in the suggested formula. In the XRD trial, the triaxial formulation was mixed for 1 hour in a ball mill before being placed in a sample holder and the diffraction patterns were recorded. This analysis was performed taking the powders of each material into a diffractometer D8 Advance (Bruker AXS Ltd, UK), using the copper *K*α radiation, K 0.9 and λ1.54Å, a range of 2ϑ of $10–70^{o}$, and a scan rate of 2^{o} per minute. Phase identification was determined by comparing the diffraction patterns with the JCPDS standard powder diffraction files. XRD was also used to analyse the phase changes that the samples underwent during sintering.

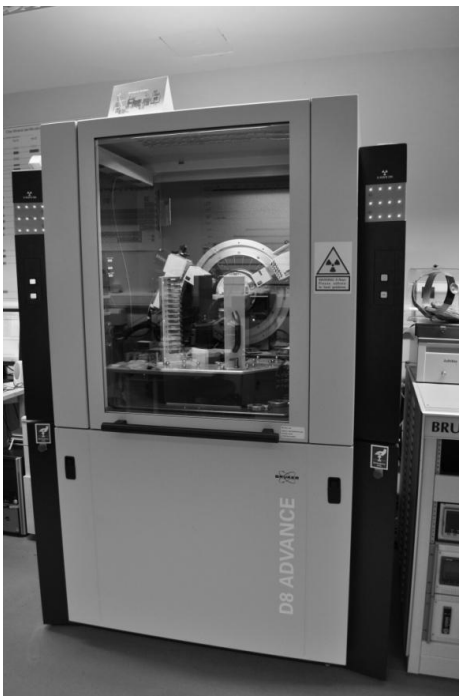

Figure 3.7: X-ray diffraction system/Geology department, University of Leicester.

X-ray Fluorescence (XRF) analysis was used to determine the elemental composition of the powders in the final formula. The test was performed using a simultaneous X-ray spectrometer (Panalytical AXIOS Advanced). The body mix contained 50% china clay, 25% quartz and 25% feldspar. The raw materials were mixed and ground in a ball mill for 10 hours prior to characterization. The fitting limits were 3.994 64.000 and the number of steps 200, R/R0: 5.04, RWP: 14.6, major elements were determinate on fused glass beads prepared from ignited powders, sample ratio 1:5, (80% Lithium Metaborate: 20% Li tetraborate flux).

Figure 3.8: X-ray Fluorescence (XRF), Geology department, University of Leicester.

3.4.2.2 Freeze-Casting Method

- Freezing Medium and Device

Two freezing media were used in this project: liquid Nitrogen (-196^{o}C) and a freezing bath with a mixture of ethanol and dry ice (-75^{o}C). K-Type thermocouples (PTFE insulated) were connected to a Pico data logger TC180 and used to monitor both the temperature of the cooling bath and the specimen.

The samples were generated in a non-porous mould (RTV silicone rubber), which was completely immersed in the freezing bath, resulting in omni-directional freezing (see

literature review) thus producing an isotropic, ice-crystal formation. Figure 3.9 shows the freezing device used in this project.

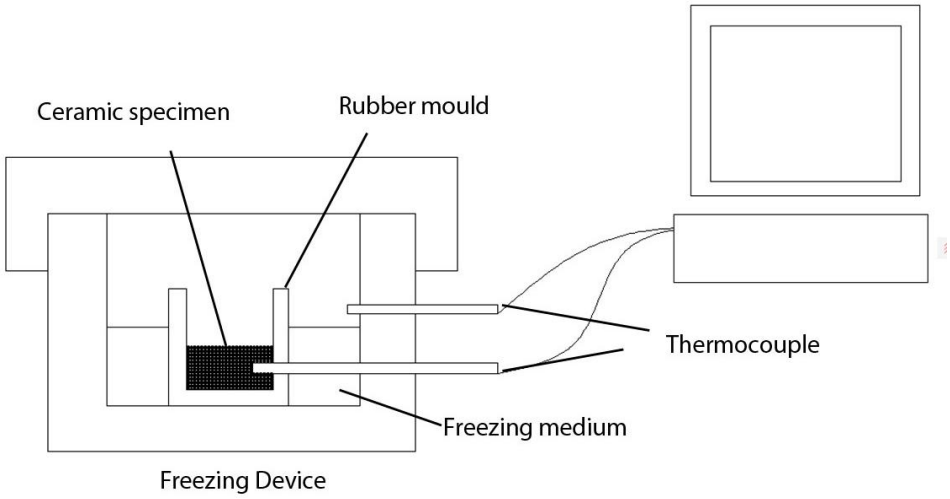

Figure 3.9: Freezing device apparatus.

- Drying and Sintering

Drying: Freeze casting results in drying of the material by sublimation. However, contrary to conventional ceramic processing, where drying is a critical stage because of the tendency for parts to warp or crack, in the freeze casting process, the shrinkage of the green part is relatively small (<1%). In bulk freeze casting once solidification of the parts is achieved the samples are maintained at low temperature to "freeze dry" the sample. However, in this experimental work, the vapour pressure was high enough to allow sublimation at room temperature, so that this step was not

required. The samples were dried under ambient conditions for 24 hours at room temperature until the sample weight was stable.

Sintering: Once the solvent had been totally removed, the resulting green body could be sintered in a kiln (ST314, Stafford instruments). A different level of shrinkage occurred during sintering depending on the firing temperature used and the corresponding level of vitrification accomplished. As with any other ceramic process, the sintering stage can be optimised to control the porosity / density of the final piece[101] . In this project, three different temperatures were utilised in order to select the most appropriate sintering regime depending of the microstructure and properties of the ceramic specimens (this is explained in the next chapter).

Figure 3.10: Kiln / Ceramic Workshop, De Monfort University.

3.4.2.3 Properties of the freeze-cast specimens

The properties of the freeze-cast samples were established by three different techniques, described as follows;

- **Phase changes in the fired samples:** XRD analysis was conducted on the freeze cast and fired sample to analyse the phase change that the samples underwent during sintering. The solid samples, fired at different temperatures, were ground to form fine particle by ball milling for 2 hours. The resulting powders were analysed and the effect of firing temperature on the sintering of the freeze-cast specimens was measured. To analyse porosity evolution during firing, the microstructure of the fired specimens was examined by Scanning Electron Microscopy (SEM).

- **Scanning Electron Microscope and Energy-dispersive Spectroscopy (SEM/ EDS):** A scanning electron microscope (SEM) Sigma advance analytical scanner with simultaneous EDS (Carl Zeis NTS GmbH Germany) was utilized to analyse the powders (particle shape, level of agglomeration) and also the microstructure evolution of the fired samples. The EDS analysis was undertaken simultaneously with the microstructure observations, which supports identification of the phases. EDS quantifies the elemental composition of a sample by measuring the wavelength and intensity of X-rays generated within a Scanning Electron Microscope. The X-rays are generated as a result of interaction of the electron beam with the electronic orbitals of

the atoms. Each element emits a characteristic set of X-rays under electron bombardment, and these are detected to identify the elements in the sample. The final samples were fired to different temperatures and the Microstructure evolution was investigated by scanning electron microscopy, energy-dispersive spectroscopy and x-ray diffraction analysis. At temperatures in the 850-1150°C range.

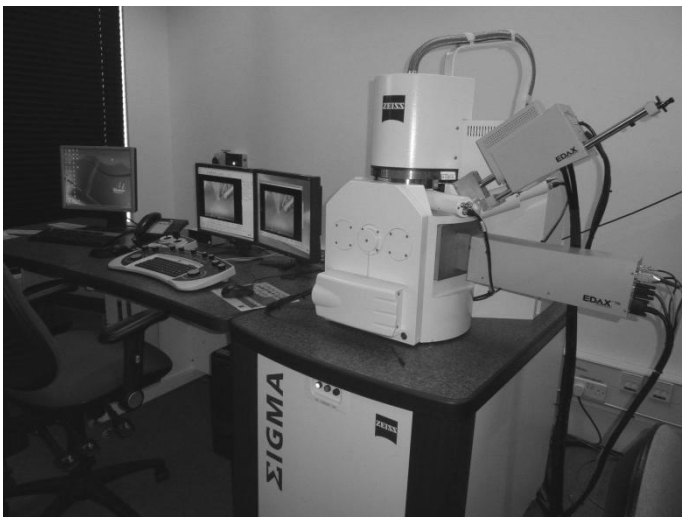

Figure 3.11: SEM/ EDS, Scanning Electron Microscope with an integrating EDS system. Warwick Manufacturing Group, University of Warwick.

The preparation of green bodies for microstructural analysis is more difficult than for dense fired samples, since they are weaker and tend to break up during grinding and polishing. For this reason, the green ceramic specimens were manually broken and a flat ceramic surface was prepared for analysis by manual grinding in order to reduce the amount of crumbling of the surface layers. The samples were then cleaned with an air jet, attached to an

aluminium disc and PVD coated with gold to ensure that their surface was electrically conductive.

The fired ceramic specimens were cut by grinding and mounted in Epo-Set clear epoxy mounting compound (Met Prep Ltd). They were then ground using 340 and 600 grit silicon carbide (25lbs force, 175rpm, contra-rotating, three minutes) and polished for four minutes using one and nine micron polycrystalline diamond (Met Prep). Then they were silver 'dagged' completely covering the top surface (except for the sample) and carbon coated. Unfortunately, this was found to be insufficient to prevent charging so a 30nm gold layer was sputtered on to the samples (this was sufficient to stop charging). All SEM images were taken at 10kV and all EDS results were taken at 20kV.

- **Physical & Mechanical Properties:** The physical and mechanical properties of the samples were tested, following the standard approach commonly utilised in the ceramic industry (for example, porosity, shrinkage, density etc). These test methods were based on the ASTM (American Standard Testing Methods) glass and ceramic whitewares section (ASTM C373 – 88) and are described in detail in the following chapters.

  The flexural properties of the samples were measured using the three-point bend technique. Prior to conducting the experiment, the depth and thickness

of the samples were measured. The sample was placed centrally in the testing rig, with the surface which had been exposed to the coolant during the solidification process uppermost. A universal tensile test machine (Instron 4301) was used to perform the trials, fitted with a bespoke 3-point bend test set up. The maximum load and deflection was recorded and used to calculate the peak stress and strain values (see equation 5.7, Chapter 5). The total number of samples was 15 divided in 3 repetitions of five samples.

3.4.2.4. Extrusion Tests

- **Viscosity:** Basic rheological characterisation of the suspension was performed using a rheometer (Brookfield RS Soft Solids Tester) fitted with 14mm diameter concentric cylinder system operated at a constant temperature of 21 °C +/- 0.2°C .

- **Measurement of Extrusion Parameters:** A test rig was developed to determine the flow of the slurry during extrusion based on an adapted constant rate of extension (CRE) testing machine (Instron 4301). This machine incorporated a highly sensitive electronic weighing system with load cells (25 and 250N) that use strain gauges for detecting and recording tensile loads. The crosshead is moved by two vertical drive screws driven by stepper motors controlled through a PC interface. The magnitude of and load on the crosshead is continually recorded during testing.

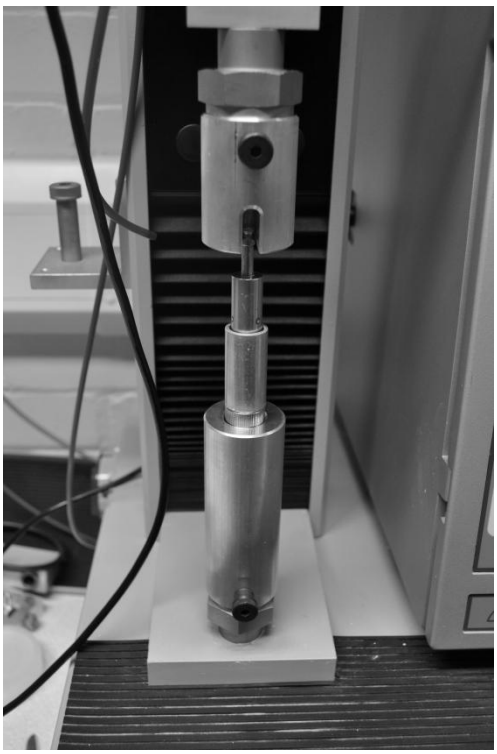

Figure 3.12: Instron 4301 Materials Tensile Strength Machine, extrusion device.

Figure 3.13: Instron 4301 Materials Tensile Strength Machine.

Figures 3.12 and 3.13, shows the test rig designed by the author to enable the axial load on the plunger to be measured over its entire stroke. It involves mounting the syringe used in the ***DWFC*** process directly on to a universal tensile testing machine thus enabling the plunger to be moved at a precise speed whilst simultaneously recording the load required to move it. It consists of four main parts, 1) a barrel of 14.5mm internal diameter by 36.88 mm length. 2) a rigid support housing that allows access to the extruded liquid (**NPP-3**), 3) a series of interchangeable nozzle attachments and 4) a plunger with a diameter of 14.33 mm by 60 mm length fitted with a replaceable PTFE ring. This PTFE material ring is clamped in place with a disc screwed to the end of the plunger. The use of this type of ring helps to stop friction at the barrel surface and avoids the possibility of any paste leakage moving upwards within the apparatus.

Within the setup is a “cup and ball” type bearing that fixes the plunger to the universal test machine and transfers the force from the plunger to the load cell. This setup ensures that the plunger moves smoothly within the barrel. The load cell is typically placed under a maximum force of up to 250 N.

The prepared material paste is placed within the barrel and the plunger mounted in the top of the barrel and the assembly mounted into the supporting housing on the base of the tester. The plunger was then driven down at the pre selected speed. The force generated was then recorded on

the load cell as a function of ram position and the plunger was then placed in contact with the Porcelain paste. The front of the paste surface was then pushed into and along the nozzle. The resulting force data was recorded via software on the attached computer and latter collated.

4. MATERIAL DEVELOPMENT

4.1 INTRODUCTION

Based on the findings of the literature review, this chapter describes the experimental methods used for the preliminary trials and sets the parameters for further studies. This chapter comprises three major aspects: i) development of the material, ii) preliminary freeze casting trials and iii) preliminary extrusion trials. At this stage of the research, these three aspects were studied simultaneously, as the results are directly related. Throughout the development of the material 3 different formulations were developed, **NPP-1, NPP-2, and NPP-3 ,** the first formulation was developed to enable freeze casting to take place and then this formulation was refined to improve extrusion behaviour to formulate **NPP-2** and finally **NPP-3** .

4.2 EXPERIMENTAL WORK: PRELIMINARY FREEZE CASTING TRIALS

4.2.1 Material Selection

Due to it's already known performance in whiteware applications, a standard porcelain triaxial formulation was used as the logical starting point for the research. Triaxial porcelain formulations are generally fabricated using quartz, feldspar and clay minerals such as kaolin. Kaolin, also known as 'china clay' is the purest form of clay, being a hydrated, crystalline, aluminium silicate mineral (it's structural formula

is $Al_2O_3 \cdot 2SiO_2 \cdot 2H_2O$.) which acts as a plastic raw material [121]. Plastic raw materials are normally required in triaxial formulations because they not only provide plasticity, but also transform into glass and crystalline phases during firing. Unfortunately, initial trials using conventional porcelain slurry formulations showed that the solid load content used in traditional ceramic processing methods was too low, leading to insufficient viscosity for controlled extrusion.

Further trials were performed to reduce the water content of the slurry and although this addressed the problem of extrusion, no solidification occurred during the freeze casting process. It was deduced that this was due to the high level of water within the clay component of the slurry and its particle shape (clay's sheet-like crystallography) that is present in a plastic, water-clay system. Kaolin is a complex platelet particle (Figure 4.1, 4.3) with a negative surface charge and a positive edge charge. Unlike other colloidal systems where there is only one type of surface charge at a given condition, fluidity depends on arrangement of the particles and their orientation. A loosely packed card-house structure (Figure 4.2) is typical for aqueous kaolin suspensions[122, 123] Poor results with freeze casting of kaolin, where no solidification occurs, has been mentioned in previous literature [119].

To explain the high level of water within the clay (clay water system), it must be highlighted that the most important characteristic of clay is its capacity to change volume by absorbing water molecules (swelling behaviour), plastic clay minerals have

the properties of water absorption common to all fine grained materials as the clay's mineral grains are below 2µm. In clay systems, the surface charges found on the mineral structure attract and absorb water in layers. Although these layers are arranged in a loose fashion, the water cannot be easily extracted and hence lithostatic pressure is necessary to desorbs water from within the clay[124, 125]. All clays attract water to their surfaces (adsorption), but some of them incorporate it into their structure (absorption). Absorption is the incorporation of molecules into the crystal grain, whereas adsorption is the addition of molecules onto the surface of grains[126]. In the freeze casting route, the liquid content in the formulation must be frozen and the growth of the ice crystals will interlock the solid particles. The layers caused by adsorption of the micro-particles and the swelling of the particles (absorption) do not allow the ice crystals to grow freely. Interlocking of the clay particles does not occur and the material will become liquid again at ambient temperature.

In conclusion, it can be stated that a new approach must be investigated for the freeze casting of triaxial formulations. In this new approach, the clay mineral may be substituted by other ceramic materials that give the same properties when sintered but enable the growth of ice crystals when the liquid component in the formulation is frozen.

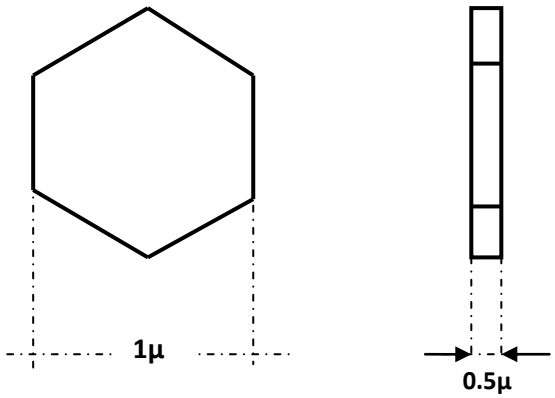

Figure 4.1: Schematic illustration of particle platelet, Kaolin Clay.

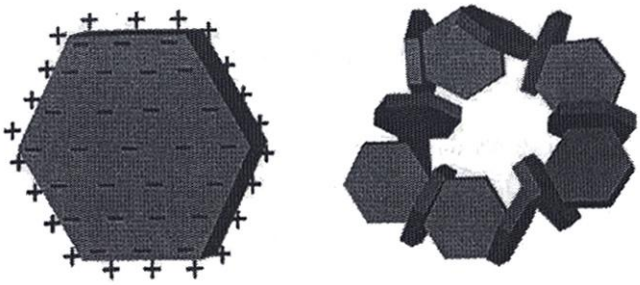

Figure 4.2: Schematic illustration of the clay particles in water; surface charges on individual particle (left) and aggregated particle network formed by the attraction of oppositely charged faces and edges also called house of cards(right)[6].

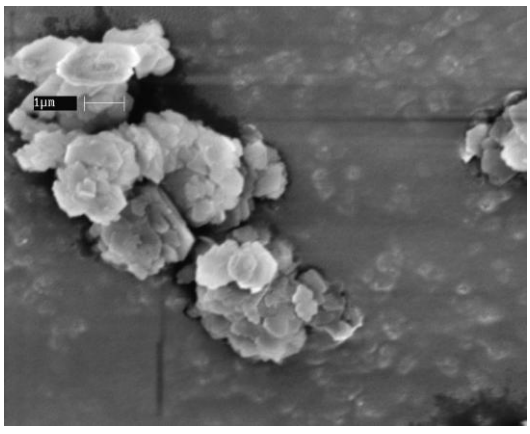

Figure 4.3: SEM micrographs of Clay Kaolin shape like Particles in water.

4.2.2 Substitution of the clay material

To provide a formulation which has more appropriate properties for the ***DWFC*** process, it was decided to replace the clay material, which is the primary source of alumino-silicates and the colloidal constituent in the slurry formulation, with pre-fired bodies (already calcined) (molochite, that is calcined kaolin and fired porcelain). The difference between these "processed" materials and raw materials is that they have been submitted to a heating process, which although below the melting point of the material itself, changes its characteristics and the ability to absorb water. The use of calcined materials as a substitute for the plastic body in the triaxial porcelain formulation for the preparation of non-plastic porcelain has been investigated by different authors[127-129].

The constituent materials used in subsequent trials were Feldspar and Quartz powders, molochite (calcined clay-kaolin) and high-fired (HFP) and low-fired (LFP) porcelain prepared by milling unglazed porcelain in a Retsch PM 100 planetary ball mill (formulation and ball milling process are described in more detail in Chapter 3 Methodology). Polyethylene glycol, (PEG-400) was added as a plasticiser, not only in the ball-milling stage but also in the extrusion phase, to off-set the adverse effects of removing the clay (i.e. to provide "plastic" properties). A colloidal silica sol, Morisol™ 2040 AS, was used as the sol component in the slurry, glycerol was added as cryoprotectant to reduce the formation of large elongated ice crystals during the freezing process[89] and Dispex A40 was used as a dispersant in order to achieve

uniform mixing and avoid agglomeration of the particles or setting of the suspension. The chemical composition and firing temperature of the powders are shown in Table 4.1

Material	Temperature of fired	Composition
Molochite	1550ºC	55% (Al2O32SiO2) 45% (SiO2).
HFP	1280ºC	K2O-AL2O3-SiO2
LFP	1100ºC	K2O-AL2O3-SiO2

Table 4.1 Composition and fired temperature of the calcined powders

Six different slurry formulations were prepared (their composition is shown in Table 4.2). F-1 to F-3, were based on the formulation mentioned above: triaxial porcelain, which varies the composition due to the substitution of the clay component. F4 to F6 are simply the raw materials molochite, low and high fired porcelain.

Composition	Feldspar w%	Quartz w%	Molochite w%	HFP w%	LFP w%
F-1	25	25	50	-	-
F-2	25	25	-	50	-
F-3	25	25	-	-	50
F-4	-	-	100	-	-
F-5	-	-	-	100	-
F-6	-	-	-	-	100

Table 4.2 Material compositions with progressive replacement of clay material (w %)

4.2.3 Sample Preparation

The powders for each formulation were mixed together for 10 hours, along with the PEG-400, utilizing a planetary ball mill with 20mm diameter zirconium media at 180 rpm. The suspension was prepared with 75.6 wt % powder and 24.31 wt % solvent, (silica sol, Dispex and glycerol in percentages of 93.80 wt%, 5.62 wt% and 0.56 wt% respectively) no additional water was added to the formulation. The solvent composition characteristics are described as follows; silica sol suspension (Morrisol AS 2040, Liverpool United Kingdom), based on water containing 40% silica nanoparticles, the particle size of the silica is 20µm and the solution was stabilized with ammonia[117], Dispex, ammonium polyacrylate (NHPA) (CIBA chemicals United Kingdom)[130]**.** Finally, the cryoprotectant glycerol was added within the formulation to act as a freezing point depressant, improving the mechanical properties of the sintered part and achieving dense bodies with uniform microstructure but also increases the viscosity of the slurry[91]. All the components and percentage in the formulation were according to the patent for freeze cast process example six[117].

The solvent was added to the powder in small amounts while stirring. After homogenous slurry was obtained, bubbles were removed from the slurry using a vibrating table (50-100Hz) for two minutes, being careful to avoid segregation.

4.2.4 Freeze Casting Trials

Following the steps in the bulk freeze casting process (see literature review, section 2.3), the slurry was poured into a non-porous rectangular mould, (80mm long x 20mm wide x 5mm deep) and immersed in a dry ice and isopropanol (IPA) bath at -70^{o}C (constant freezing rate) for two hours to completely freeze the mixture and allow the growth of the ice crystals between the particles.

The samples were then removed from the mould and dried at room temperature and the weight was regularly checked until stable. The dried samples were then sintered at 1280°C, the minimum temperature required for high fired porcelain[131]**.** The selection of the minimum temperature was chosen because the substitution of the clay for a pre-fired material may lower the firing temperature of the ceramic body and over-fired parts will lead to a pyroplastic deformation (distortion of the sample compared to the shape of the mould as a function of the vitrification of the ceramic body during its firing)[129]**.** This kind of deformation is related to an excess of liquid phases formed during firing and the reduction of the viscosity of these phases[132].

The samples were then assessed by measuring the linear-firing shrinkage and water absorption. These tests are commonly performed within the Traditional Porcelain (TP) Industry and give an insight to the characteristics of the fired body. Absorption and linear-firing shrinkage are related to other important factors such as density,

vitrification and porosity. In addition to absorption and linear-firing shrinkage, a visual assessment of each sample was undertaken to give an indication of deformation, surface finish and colour. Deformation was assesses by simply measure the deflection arrow of the ceramic specimen, value of *d*, which is the measure of the slump on the ceramic bar, after firing, see Figure 4.4 A. to determinate *d* a metal bar was placed against the ceramic bar on the concave side so that its ends were equidistant from those of the ceramic bar, and d was measured with a calliper. Then 3 different values were given; *low, medium* and *high* according to the deformation level.

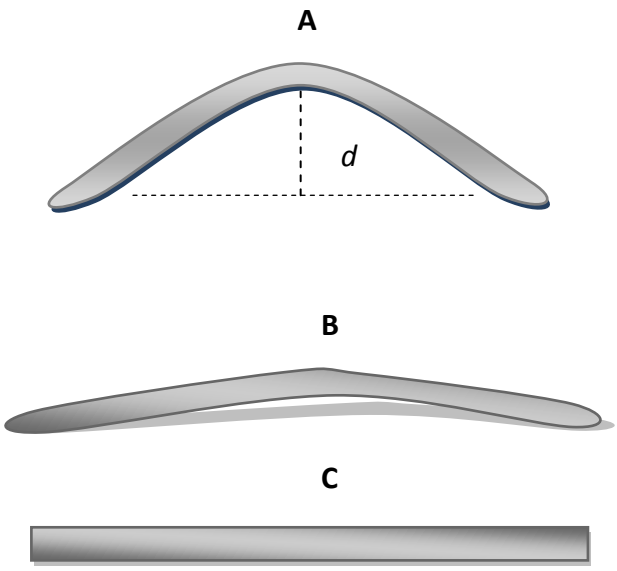

Figure 4.4: Deformation assessment of pyroplastically deformed bars.

The linear-firing shrinkage was assessed by measuring the distance between two reference lines, marked on the surface of the sample, after drying and after firing (as specified in ASTM C326 [133]– see Appendix 1 for full details). The water absorption was measured using the industry standard method (ASTM C373-88[134]). The fired sample was immersed in boiling water for five hours and allowed to cool for 24 hours before removing and weighing the sample. The weight of the sample before and after the absorption test was measured and used to calculate the mass of water absorbed as a percentage of the weight of the fired sample.

Once the samples were assessed the substitute clay material was selected. The chosen final formula was referred to as **NPP-1** (non plastic porcelain formula 1), and was subjected to further analysis to characterise the raw powders used. X-ray Diffraction analysis (XRD) of the clay material substitute (molochite) was undertaken to identify its mineralogical composition. In addition, a further XRD and X-Ray Fluorescence (XRF) analysis of the formula with the three components combined mixed by ball milling (as described in Section 3.5 on methodology, Chapter Three) was performed to establish the chemical and mineralogical composition of the overall formula. Finally, the particle size, particle size distribution and particle shape of the individual powders was determined by a dynamic light-scattering analyser (Malvern Instruments Inc.) and scanning electron microscopy.

4.2.5 Results and Discussions

4.2.5.1 Linear-firing Shrinkage and Water Absorption

The linear-firing shrinkage and water absorption values of the different slurry formulations are shown in Table 3. Formula F-1 not only gave the lowest linear-firing shrinkage in the freezing and firing stage of the process but also less deformation, a good quality surface finish and an off-white colour. Ideally, the material should be white and glossy in appearance to match the current performance of conventional porcelain materials (see literature review Section 2.4). The F-4 formula (only molochite), although suitable for freeze casting, gave relatively low firing shrinkage levels with no deformation. Its mechanical and visual characteristics did not, however, compare favourably with traditional porcelain (TP) in terms of transparency, surface finish or strength. It gave a “chalky” material texture without any visual signs of vitrification. This was because molochite is a refractory material and it does not go through a vitrification phase (there is no chemical transformation during firing).

	Linear-firing shrinkage (%)	Absorption (%)	Deformation	Surface finish	Colour
F-1	1.81	19.50	None	Matte/glossy	Cream/pink
F-2	5.26	13.31	None	Glossy	Grey/pink
F-3	7.27	8.58	Medium	Glossy	White
F-4	1.90	19.27	None	Matte/rough	Cream
F-5	7.27	11.40	None	Glossy	Brown
F-6	12.72	2.03	Medium	Silk	White/grey

Table 4.3 Comparison of the characteristics for samples F-1 to F-6

In a porcelain body, as the firing temperature is increased, a point is reached where major vitrification occurs after this point a series of defects can occur (bloating, deformation, cracks etc.). Porosity in the body is reduced but this leads to higher levels of linear-firing shrinkage. The choice of firing temperature is thus critical, as firing shrinkage can lead to cracks or deformation in the final body and is an important factor in AM if accurate, high-integrity parts are required. The relationship between the linear shrinkage and porosity (as indicated by water absorption) is clearly shown in Figure 4.5.

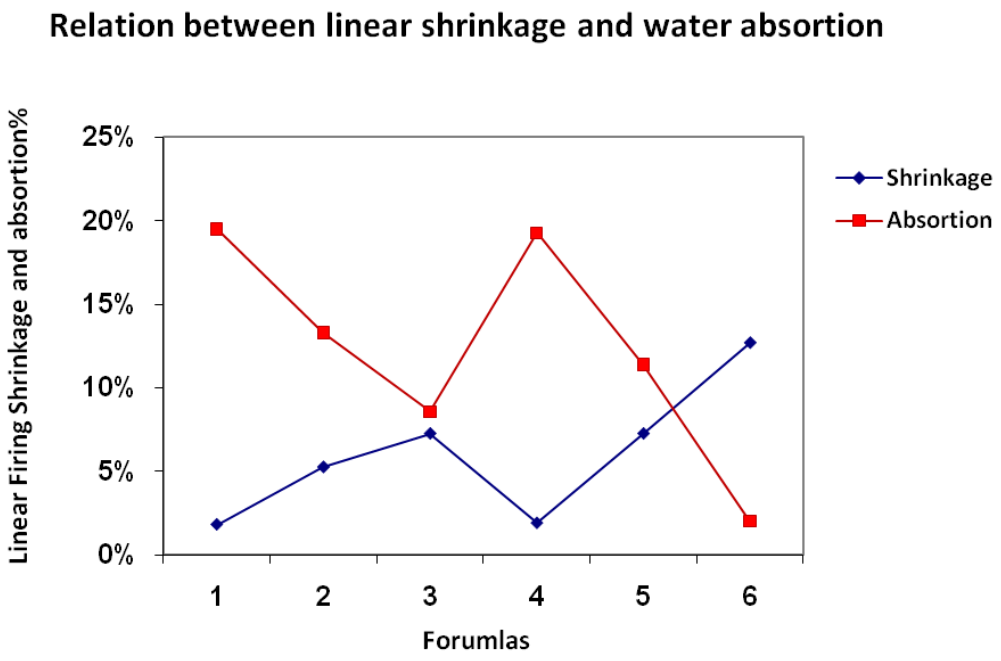

Figure 4.5: Relationship between linear-firing shrinkage and water absorption.

The linear-firing shrinkage of a fully vitrified TP body (fired above 1200°C) processed traditionally by slip casting process, is usually between 13 to 15%, depending on the formula and manufacturer (maximum temperature of firing). It can be seen from Table 4.3 that the levels of linear shrinkage for samples processed by freeze casting are significantly lower. However, the material looses one of the main characteristics of high-fired porcelain, which is ~0.5 water absorption[121], due to total vitrification of the body. Nevertheless, it should be possible to reduce the porosity of the material by changing the firing temperatures and freezing rate.

Finally, based on the previous experimental results; the sample F1 was selected. This formulation will be referred **NPP-1** hereafter, and further analyses will be performed for its optimization.

4.2.6 Criteria for Successful Freeze Casting

One of the critical criteria to assess is the ability of the material to undergo successful freeze casting. Although there is evidence that the clay-based material does not undergo freeze casting and the **NPP-1** material does freeze cast, it is important to provide clear criteria for judging when freeze casting has occurred. Unfortunately, there is no clearly defined single method of assessing the suitability of a material for freeze casting. Assessing if freeze casting has occurred is based on the interpretation of micrographs of samples, together with a physical assessment of the material. For example, it would be easy to confuse freeze casting with samples processed by freeze gellation (in the latter, samples are dried by the freezing process but an irreversible chemical reaction does not occur)[135]. With this in mind, the ceramic specimens produced in the previous experimental work (section 4.2.2) were assessed to find evidence of successful freeze casting. The main points considered as criteria for successful freeze casting were: solidification, dry shrinkage, cracking and pore structure[119] (as discussed in Chapter Two). The characteristics of the new material are listed as follows:

1) **Irreversible Solidification** - after thawing, all the specimens have sufficient strength to be removed from the mould without breaking up. Although removal from the mould is not required for the ***DWFC*** process**,** the parts have sufficient green strength to enable handling and post processing.

2) **Dry Shrinkage** (shrinkage of the unfired part) - the average of the dry shrinkage of the new material specimen is around 1% (must not exceed ~5% which is the maximum shrinkage for unfired freeze cast parts – above this level, parts have not been correctly freeze cast). [85, 119]

3) **Cracking**- there is no visible cracks after drying.

4) **Pore Structure** - finally, the three-dimensional, interconnected, pore network structure replicates the pattern of the ice formed when freezing occurs. In the freeze casting route, the pore structure is a replica of the morphology of the ice crystal growth pattern during the solidification of the solvent [13]. Extensive work has been carried out in order to understand the nature of the pore morphology formed in a freeze cast ceramic specimen[136, 137]**.** When the main component is water, pores are expected to exhibit the shape of water ice crystal growth structure. The interconnected dendritic structure formed in the newly developed material (see Figure 4.6 left) is indicative of water's common structures when freezing under special conditions. The morphology of super cooled water changes with the growth time, from a circular disk to a perturbed disk and finally to a developed dendrite with hexagonal symmetry[138]**.** As the main component in the solvent is water, the

dendritic pore structure found in the freeze casting samples produced in the trials is clear evidence of the ability of the new material to be freeze cast. Figure 4.6 shows an SEM image of the three-dimensional, interconnected, pore network for; (a) ice that show the dendritic structure due to a slow freezing rate and (b) freeze casting slurry material (unfired) which shows a similar structure.

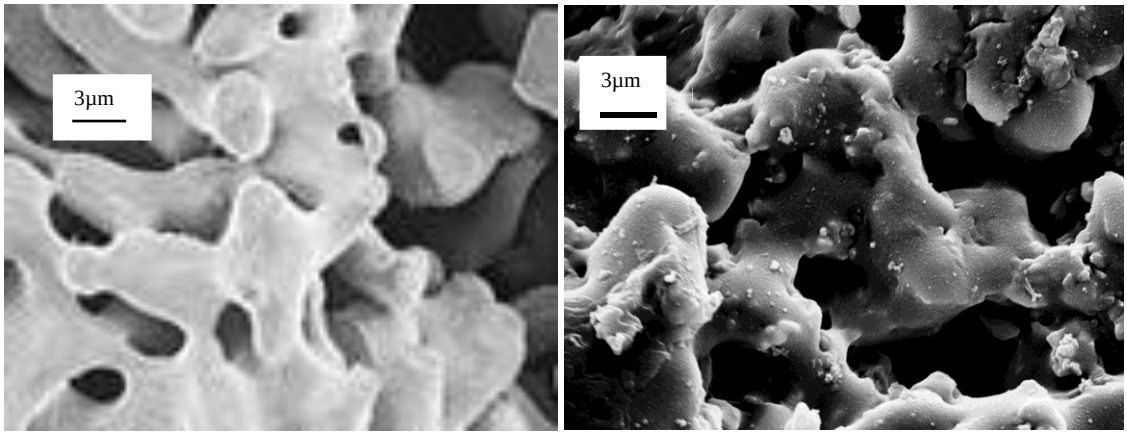

a) **b)**

Figure 4.6: Entwined, dendritic, ice crystal structure of water **(a),** three dimensional interconnected pore network image taken by scanning electron microscope (SEM) of an unfired specimen of the freeze cast new material; this structure is representative of the entwined, dendritic, ice crystals and proves the reaction of the material during the freeze casting process **(b).**

4.2.7 Raw material characterization NPP-1

4.2.7.1 Characterization of substitute material

Further characterization of the raw powders was needed, in order to understand the properties of the newly developed material. As a starting point, a chemical characterization of the selected substitute material was performed. The substitute material, molochite, is a ceramic material commonly used in the traditional ceramic industry as grog (see glossary of terms, Appendix- 2) and can be found commercially as a powder ranging from fine to coarse graded. Molochite is a hard, abrasion resistant, alumino silicate produced by the calcination of a specific type of Kaolin to a peak temperature above 1500°C. In its production, the selected kaolin powder undergoes several processing stages, as follows: preparation of the raw powder, calcination, crushing, ball-milling and, finally, screening. Commercially available molochite can be found with particle sizes ranging from 17 (fine molochite) to 72µm (grog kind molochite). Figure 4.7 shows the SEM picture of the powder used in these experiments. This is molochite (fine) powder with particles below 17µm. It can be seen in the figure that the finer particle size is ~1µm and higher particle size is ~17.62µm.

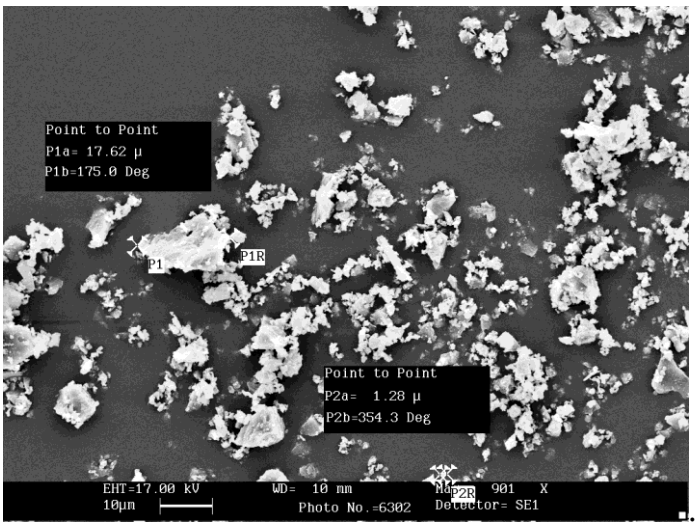

Figure 4.7: Scanning Electron Microscope (SEM) picture of molochite Powder.

At this stage of the research, a chemical characterization of molochite was performed. Figure 4.8 shows the mineralogical composition analysis by XRD**.** The study shows mullite as the main material, as molochite is fired china clay, fired to a temperature of 1500°C. Basically the calcination process converts the kaolin into a mixture of mullite crystals and amorphous material (amorphous silica glass). It can be noted from the analysis that the process of calcination completely avoids the production of crystalline silica, such as cristobilate or quartz. Instead, amorphous silica glass was produced because the molochite used in this project was produced from a particular kaolin component which is low in iron and alkalis and high in alumina, Al_2O_3 (alumina) 30.68 w% and Fe_2O_3 (Iron Oxide) 0.59 w%. See the chemical composition (Table 4.6 page 131).

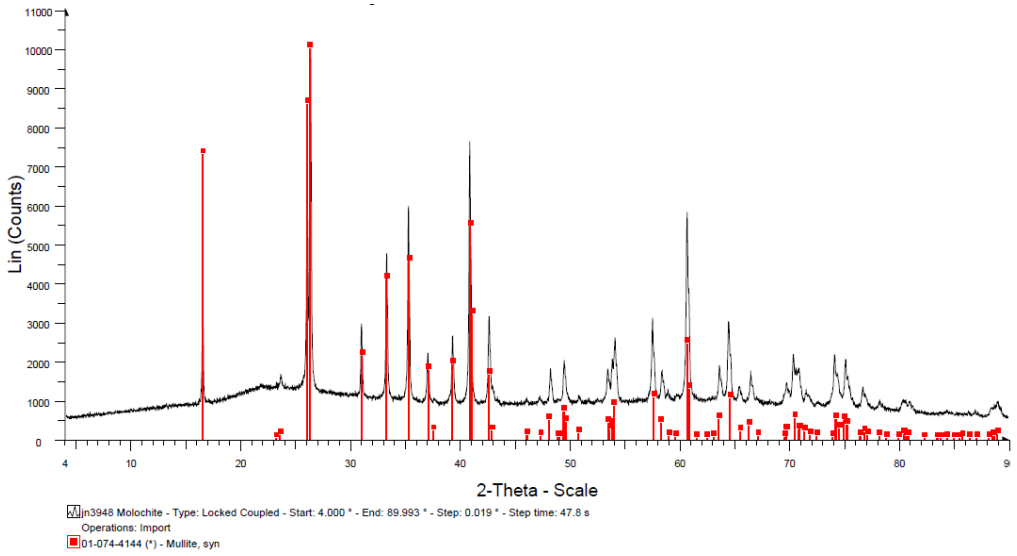

Figure 4.8: XRD analysis of molochite, the red peaks identifies the main component as mullite. The noise in the background, represented by a black line, is the amorphous material (silica).

In the transformation of the kaolin to mullite, the material undergoes three main chemical phases as the firing temperature increases. These three steps are described in Table 4.4 below.

	Phase 1	**Phase2**	**Phase3**
$6Al_2Si_2O_5(OH)_4$ kaolinite	$6Al_2Si_2O_7$ metakaolinite 500°C	$3Al_4Si_3O_{12}$ silicon spinel 925°C	$2Al_6Si_2O_{13}$ primary mullite >1100° C

Table 4.4 Transformation of the Kaolin clay to mullite, chemical phases[131]

In Phase 1, at 500°C, the material kaolin, $6Al_2Si_2O_5(OH)_4$, undergoes dehydroxylation where the water between particles and bound into the mineral lattice is removed. This separation is represented as ($12H_2O$ + $6Al_2Si_2O_7$) and transforms the material to metakaolinite. In Phase 2, at 925°C, the material undergoes further reaction where

the parent crystal is rearranged and silica is rejected in the form of glass, ($3SiO_2$ + $3Al_4Si_3O_{12}$) and spinels form. In Phase 3, over 1100°C, primary mullite forms, to leave primary mullite and amorphous silica.

Identifying the main material as mullite, provides a good opportunity to understand what will happen to the material in subsequent stages of the firing process. Basically, in the freeze-casting route, two main chemical transformations are expected to occur, both of them due to the chemical reaction of the material caused by the temperature change. The first one is freezing, where the solvent transforms from a liquid to solid and when the material returns to room temperature the solvent sublimes from a solid to a gas. The second stage is the vitrification of the ceramic green specimen during firing at an elevated temperature.

In a conventional triaxial porcelain formula, the reaction between the three powders during the firing phase is significant. Table 4.5 shows the different reactions of the material due to the increase in temperature which results in a grain-bonded microstructure consisting of coarse particles (filler) held together by a glassy matrix that contains mullite and dispersed or partially-dissolved quartz particles[139, 140].

Mullite ($3Al_2O_3 .2SiO_2$) plays an important role in this transformation. Mullite forms in vitreous ceramic formulas from the pure clay and its interaction with the other components. The amount of mullite produced is directly related to the amount of alumina in the raw powders and the sintering temperature. Generally, two kinds of

mullite are present in fired porcelain bodies; primary mullite, formed from the decomposition of pure clay, and secondary mullite, formed from the reaction of the three materials together, feldspar and clay, and feldspars, clay and quartz[121].

Phase	Temperature °C	Reactions
1	Up to 100	Loss of moisture.
2	100-200	Removal of absorbed water.
3	450	Dehydroxylation.
4	500	Oxidation of organic matter.
5	573	Quartz inversion to high form, little overall volume damage.
6	925	Spinel forms from clay, start of shrinkage.
7	<1100	Primary mullite forms.
8	1050-1100	Glass forms from feldspar in a glassy phase, secondary mullite forms, shrinkage continues.
9	<1200	More glass, mullite grows and pores close some quartz dissolution.

Table 4.5: Processing history for a conventional triaxial body [131]

As can be seen in Table 4.5, until Phase 7 - the formation of primary mullite - the clay material undergoes the same transformation as in the production of molochite. After this point, the material reacts with the other components to form secondary mullite.

Feldspar is transformed into a viscous glassy liquid and as the temperature increases further, the solid feldspar particles discompose to form more liquid. When Phase 9 is reached, it is found that quartz will partially discompose at these very high temperatures. This phase will be followed by a soaking period at the maximum firing temperature (to enable temperature gradients to even out). The next phase is cooling where the liquid solidifies to a glass which binds together the unmelted particles and crystals (silica quartz particles and mullite). In the new non-plastic

formulation (**NPP-1**), the material replacing the clay is already a pre-fired body, where kaolin has been converted to primary mullite but the reaction with the other components is expected to continue until the glassy phase is reached. Further analysis needs to be performed on the fired specimens in order to determine the exact temperature at which vitrification occurs. Full vitrification is reached when a degree of melting or firing confers a high (>40%) glass content to the fired porcelain bodies. Over-firing will lead to an excess of liquid in the glassy phase and thus to a pyroplastic deformation.

4.2.7.2. Characterization of the formula for the triaxial, non-plastic porcelain NNP-1

As a second stage of the material characterisation, a further examination of the raw powder was performed. In this case, the study was undertaken on the triaxial porcelain formulation **NNP-1**, with the three powders together. It was expected that understanding the mineralogical composition of the formula would help explain the physical and chemical changes occurring during firing. The chemical composition of the unfired powder was determined by XRF. Table 4.6 shows the components in the formula, where it can be seen that silica (SiO_2) and alumina (Al_2O_3) are the dominant oxides (63.59 and 30.68 wt% respectively), the raw materials used were molochite, potash feldspar and quartz. The crystalline phases of the formulation were identified by XRD and are shown in Figure 4.9.

Material	%
SiO_2	63.59
TiO_2	0.051
Al_2O_3	30.68
Fe_2O_3	0.59
MnO	0.009
MgO	0.10
CaO	0.17
Na_2O	0.79
K_2O	3.66
P_2O_5	0.078
SO_3	<0.002
LOI	0.88
Total	**100.61**

Table 4.6: Chemical analysis of the **NNP-1** non-plastic porcelain material (XRF analysis)

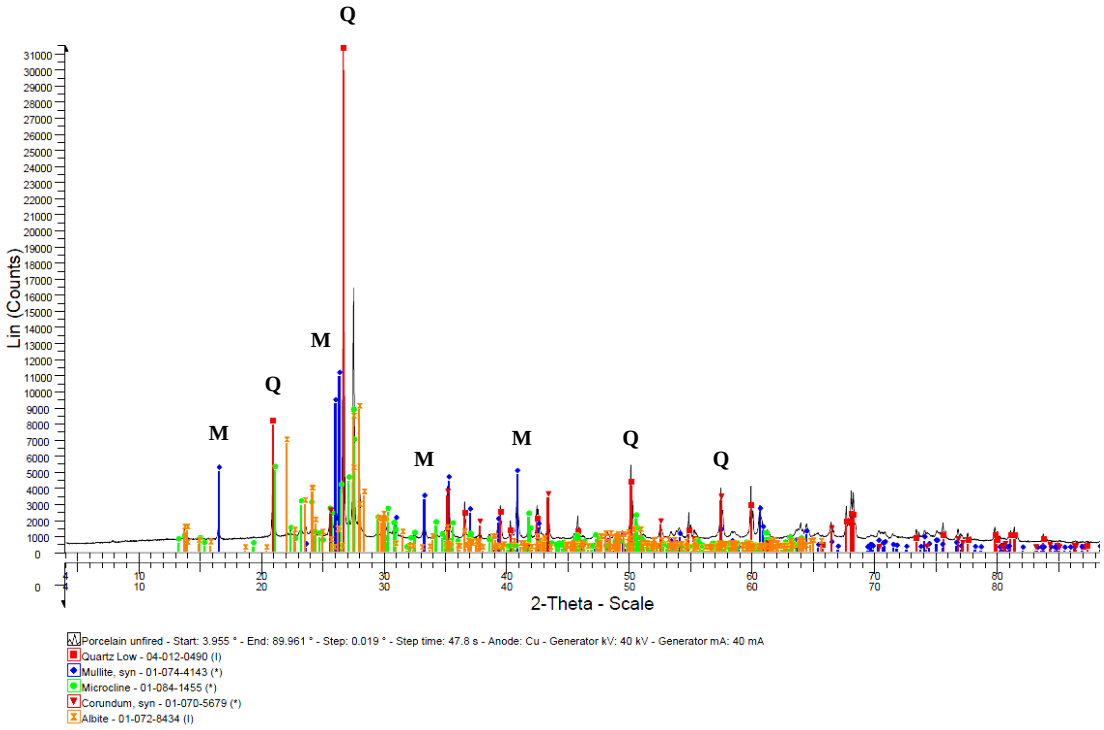

Figure 4.9: Results of XRD analysis **NNP-1** non-plastic porcelain formula

The crystalline phases identified in the triaxial composition were quartz (SiO_2) and mullite ($3Al_2O_3 . 2SiO_2$), being major crystalline phases, and corundum (Al_2O_3), albite ($NaAlSi_3O_8$) and microcline ($KAlSi_3O_8$) as minor crystalline phases. Some amorphous material (amorphous silica) can also be seen in the background of the analysis (black line on graph – Figure 4.9). In Figure 4.9 the quartz corresponds to the quartz itself, mullite corresponds to the molochite and corundum, albite and microcline to the potash feldspar. The overall materials were identified as 36.0% Quartz Low, 25.7% Mullite, 16.6% Microcline, 5.7% Corundum and 16.0% Albite.

4.2.8. Final remarks developed of the NPP-1

The new approach to preparing highly concentrated solid load slurries (75.6 wt% solids) of triaxial porcelain composition suitable for freeze casting (**NPP-1**) has overcome the significant difficulties relating to the freeze casting of kaolin clay by the substitution of clay with pre-fired materials. However, trials must be performed to check if the selected substitute material, molochite, changes the parameters of the sintering process, such as the temperature of firing. Once the solid content in the formulation has been established, the mechanical behaviour of the novel porcelain could be influenced by two other main parameters: freezing rate and temperature of firing, which dictate the level of porosity in the sintered part. The freezing rate will dictate the morphology and size of pores and the temperature of firing will dictate the reduction of porosity due to the quantity of glass formed in the vitrification phase. A deeper understanding of the mineralogy of the materials will lead to a

better comprehension of the physical and chemical changes during processing (after the freeze casting stage) and thus determine the composition and microstructure of the final part. Further work needed to be carried out in order to establish the critical parameters of the process, including the freezing and firing rates (these will be addressed later in this chapter).

In addition to the ***DWFC*** method, the **NPP-1**, material developed could be applied to other processes that involve freeze casting, such as freeze casting-injection moulding, freeze casting-tape casting and freeze casting-gel casting. The advantages of the bulk freeze casting route as a method for traditional ceramic materials have been discussed before[141]. The process allows the use of non-porous, flexible moulds (for example, silicone rubber moulds) for the fabrication of complex parts.

This facilitates the removal from the mould phase, thus allowing the formation of intricate parts, complex surface patterns and the reproduction of extremely fine details. This offers the potential to form ceramic shapes that cannot be formed by plaster moulds and are usually achieved by techniques such as hand carving or hand modelling, severely restricting the rate of production. One example could be the use of flexible moulds that facilitate the fabrication of a complex object in a one-piece mould, as is the case of a cup, thus eliminating the need for a post-process to join the handle with the main body. Thus, freeze casting, as a route for traditional ceramics, also offers less distortion and less cracking or warping.

Having demonstrated that the **NPP-1** material can be successfully freeze cast, the next step was to optimise the formulation for the extrusion process. It was expected that a reduction in particle size, a wider particle size distribution and the use of additives would help to reduce the viscosity to facilitate extrusion through fine nozzles, as will be required in the new ***DWFC*** process. Preliminary extrusion trials were performed to optimise the formula based firstly on the selection of particle size and particle size distribution and then on the solid content and additives used.

4.3 DIRECT WRITING FREEZE CASTING PROCESS

4.3.1 Process Stages

The selected formula **NPP-1** from freeze casting trials was then extruded using the ***DWFC*** system to provide an indication of its suitability for extrusion. The preparation of the raw powders and the formulation was the same as that described in the previous bulk freeze casting trials but this time the material was loaded into a syringe and deposition was achieved by the positive displacement method. After this step the extrudate was subjected to low temperatures (lower than -40°C) layer-by-layer. Further steps include drying by sublimation of the ice crystals and firing. Each of these steps will be explained in more detail later in this section.

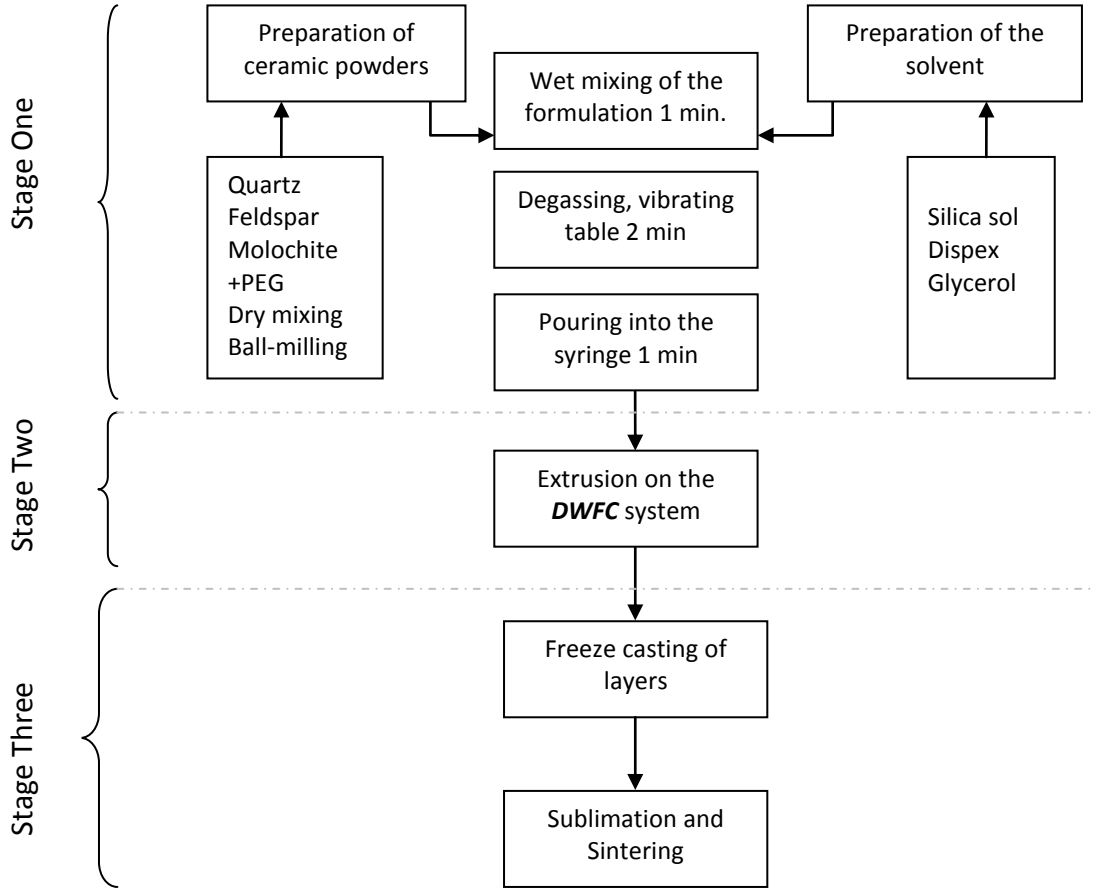

Figure 4.10: Flow chart of the *DWFC* process.

As can been seen in Figure 4.10, the ***DWFC*** process was divided into three basic stages that had been carefully controlled throughout the experimental test; **1) paste preparation** (dry mixing -raw particles-, wet mixing and degassing), **2) forming** (***DWFC***) and **3) finishing** (drying and firing). These stages are explained in detail in the section below:

Paste Preparation:

- **Dry Mixing** – after the selection and weighting of the powders, dry mixing was used to uniformly mix all solid components in the formulation. The powder components were mixed together to give a 100g sample, where 50g

correspond to Molochite, 25g feldspar and 25g quartz, mixing was undertaken by ball-milling these powders in a dry state for a period of 6 hours at a slow milling rate (100rpm). Careful mixing of powders was a critical step to provide a homogenous formula in triaxial compositions.

- **Wet mixing and high-shear mixing** – In this stage of the preparation of the paste the solvent was incorporated into the powder in a uniform way to help promote uniform particle packing and ensure stable extrusion properties. The particles used in the extrusion process can be locked together in the form of agglomerates. For extrusion to be most effective and to avoid perturbations during extrusion, it was necessary to break down any agglomerates to single particles and to ensure that these are fully covered with the liquid phase. The agglomerates found in the formula were soft agglomerates, which are easy to break down and mix with the solvent using high-shear mixing.

- **Degassing** – This stage aimed to reduce the entrapped gas inside the paste. Entrained gas, present in the paste due to mixing, could lead to bubbles and thus to defects in the final part. Gas removal was promoted by increasing the surface area of the paste, for example by shredding. Usually, the application of vacuum conditions is desirable as this can cause the gas to nucleate and form bubbles, which rupture and leave the paste. Unfortunately, in this case, the application of a vacuum could result in significant water loss through

evaporation. The approach employed in these trials was the use of a vibration table; once when initially mixing (1 minute) and again when filling the syringe (1 minute). This allows the bubbles to rise to the surface of the slurry. As the material is loaded into the syringe, vibration was applied to assist with the removal of any entrapped air.

Forming:

- **Extrusion** – In the ***DWFC*** system, extrusion is used to deposit the material using positive (constant) displacement dispensing method, where the linear movement of a stepper motor-driven plunger was employed to push out the paste from a syringe. This enables a precise volume of paste material to be dispensed, which cannot be guaranteed with a constant pressure approach, Details of this method will be discussed later in this chapter. In positive displacement extrusion unless the material is compressible the flow rate of material remains constant for a particular plunger speed, irrespective of all other factors. A schematic drawing of the system is shown in chapter 2 section 2.3.1.

  In the ***DWFC*** system; the positive displacement mechanism includes, a stepper motor and a syringe. The syringe includes a metal barrel and a plunger which is mechanically connected through a series of gears and a belt to the stepper motor. The plunger forms a tight seal with the barrel. The

stepper motor causes the plunger to move up and down by a discrete number of steps. Depending on the selected mode of operation the stepper motor can make 3,000 or 12,000 discrete steps per plunger full stroke. The syringe barrel has a useable capacity of 5ml that the plunger can displace in one full stroke. The plunger travel is 30 mm and its velocity can be varied from 1.5 – 12mm/min.

- **Freeze casting** - After the deposition of the extrudate (all layers), the material was subjected to an extremely low temperature (below -70°C). At this temperature, the solvent solidifies causing an irreversible reaction (hardening) of the extrudate. This step determines the porosity, microstructure and the mechanical properties of the material. After freeze casting, the material is dried by sublimation of the ice crystals and then fired. The microstructure of the freeze cast material reduces the level of drying and firing shrinkage.

Finishing:

- **Drying** -The freeze cast part was stored at ambient temperature (20°C) for 24 hours where sublimation of the ice crystals occurs. At this stage, based on the results of previous freeze casting experiments, drying shrinkage of around 1% occurs. This avoids the deformation of the part associated with normal

whiteware material, which typically exceeds 6%. The final shrinkage will be during the firing stage.

- **Firing** - The firing stage was the final stage of the overall process in which the final part is vitrified and the major shrinkage occurs. This stage can be controlled through varying different parameters, such as the temperature of firing, which leads to different levels of vitrification, porosity and physical and mechanical properties. A further study of these stages will be discussed in the next chapter. Table 4.7 shows the difficulties that can be presented in each stage of the process.

Process stages	**Difficulties**
Dry Mixing	Poorly mixed particles (adhesion to the sides of the ball mill jar)
Wet Mixing and high-shear mixing	Air entrapped Breaking down agglomerates
Degassing	Failure to remove entrapped gas
Extrusion	Uneven extrusion Excessive pressure drop Surface defects Deformation Blocked nozzle
Freeze casting	Microstructure control
Drying	Drying cracks Extrudate handle Initial dry shrinkage
Firing	Shrinkage-deformation

Table 4.7: Process stages and difficulties

4.3.2 Optimization of the formula NPP-1

Having selected the paste formula **NPP-1** extrusion trials were performed using the ***DWFC*** system. It was found that the slurry readily extruded; ideally, the material should shear-thicken and not flow after deposition. It was concluded that the combination of the reduction of the particle size by ball-milling the powder during the dry mixing of the three components and the presence of the additives improved the flow characteristics of the material. Further work would be conducted to optimize the formulation to enable controlled extrusion to take place. Moreover, this may enable the water content in the formulation to be reduced, thus increasing the density of the objects formed. As a quick test to evaluate the extrusion behaviour of the material, the formula was prepared to form a paste and hypodermic syringes with different nozzle sizes were then utilized. Although the positive displacement system (utilised in the ***DWFC*** system) is slightly different to the hypodermic syringe used for these initial trials (material of construction and size) it was concluded that a reduction of particle size and a wider particle size distribution would help the extrusion behaviour of a high solid-load paste.

4.3.3. Reduction of the particle size in the formulation for extrusion proposes

As mentioned in the previous section, preliminary extrusion trials in the ***DWFC*** systems indicated that a further reduction of the particle size could facilitate the deposition of the material through a fine nozzle. The characteristics of the powders in the **NPP-1** formula (as received) were examined. The powders were classified

according to their different particle sizes using a dry sieving method; a sample of each powder was individually placed into several sieves and classified into different particles sizes: below 20, 50 and 100µm. Subsequently, the resulting powder for each particle size was then mixed with the solvent (75.6 wt% solids content) and submitted to a further extrusion test (mixing, degassing, extruding and freeze casting). The resulting mixture with the finest powder of the mesh below 20µm was selected.

The powders were subjected individually to a further reduction in particle size by ball-milling for several hours, followed by a particle size distribution analysis by the light-scattering method, (see methodology chapter for details of this test method). Finally, the three powders were dry-mixed together, according to the required composition, in order to get a homogenous mixture.

4.3.4 Results and Discussion

As mentioned in the previous section, for each raw powder, the particle size and particle size distribution was determined using a dynamic, light-scattering analyzer (Malvern Instruments Inc), before and after ball-milling of each individual powder, Figure 4.11 shows the particle size and particle size distribution of the powders, individually, before and after ball-milling.

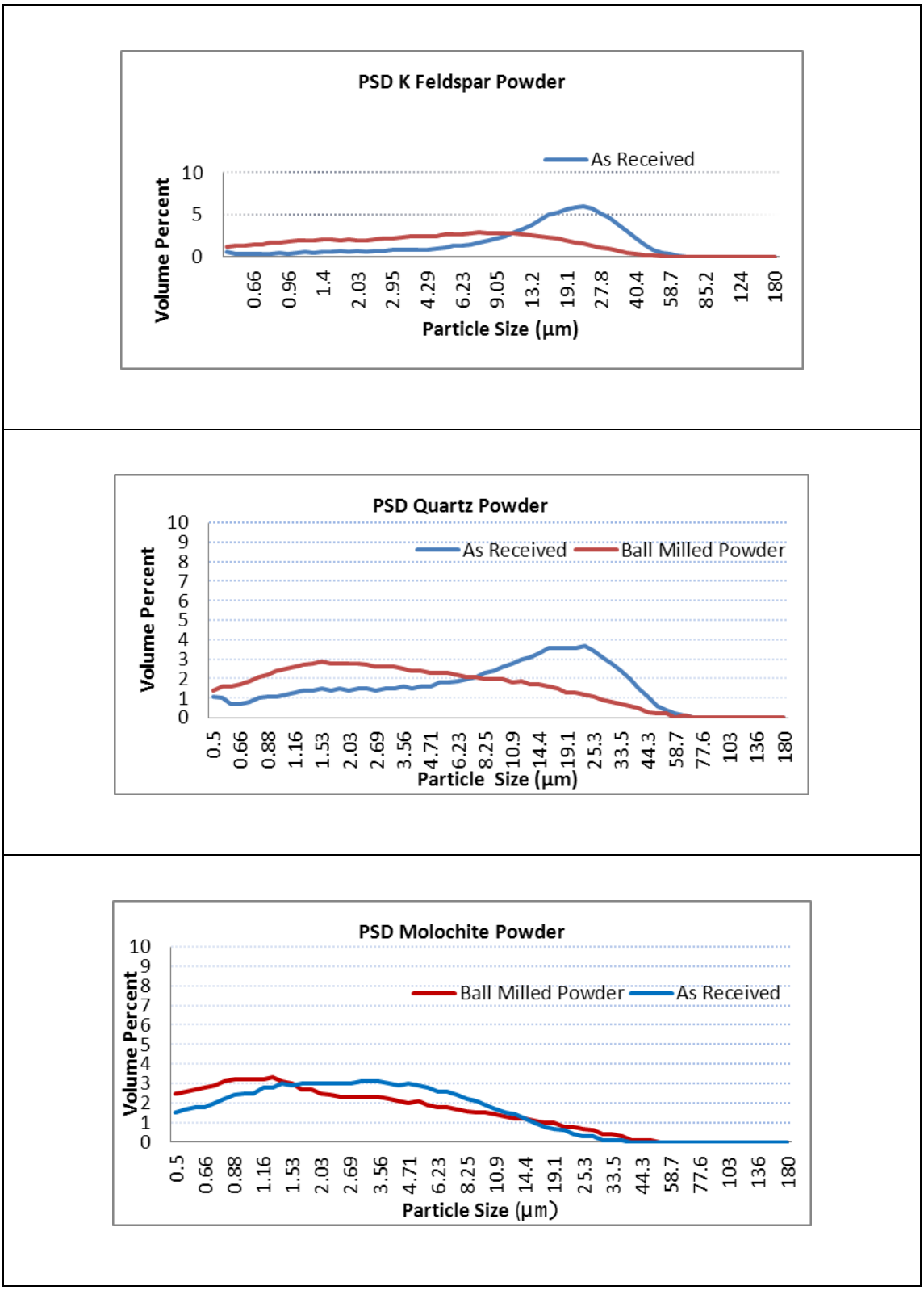

Figure 4.11: Particle size distributions of the powders before and after ball-milling

As can been seen in Figure 4.11, before ball-milling the received powders had a peak at 25µm for the quartz and feldspar and 1.5 and 6µm for the Molochite received as a fine powder. After ball-milling, all particles were below 33µm peaking between 6 to 8µm, for the feldspar particles and between 1.5 to 0.5µm for the quartz and molochite particles. The reduction in the particle size changed some of the basic parameters of the process (e.g. the shrinkage), demonstrating the strong influence of the characteristics of the constituent powders on the processing characteristics and microstructure of the object formed. The new formulation based on reduced particle size will be referred to as **NPP-2** hereafter.

Figure 4.12 shows the final particle size distribution of the **NPP-2** formula; these were the three powders mixed together after the final ball-milling (dry mixing). The reduction of the particle size in the formulation was extremely important, not only for extrusion purposes, but also in the final stages of the freeze casting process (drying and firing). Particle size directly affected the reactions that took place during firing, since particles that were not in contact cannot react. Local arrangements, particle-to particle contacts and compositions were control factors of the firing behaviour in a ceramic body. Thus, packing density, surface area and reactivity of the materials were also affected by particle size distribution and in turn, affected the firing behaviour. These factors will be studied in detail later in this thesis. Additive chemistry and solid content were usually adjusted after the particle size distribution has been selected. In order to obtain desirable suspension properties, the solvent,

solid content and additives must be properly attuned. A set of experiments to adjust the solid content and the additives will be presented later in this chapter.

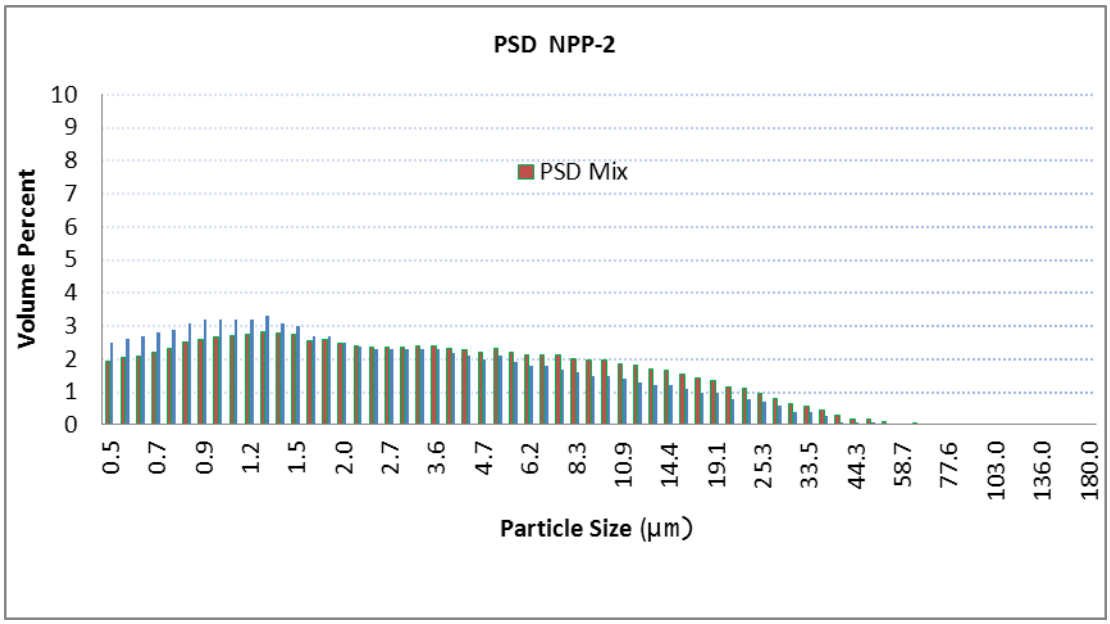

Figure 4.12: Particle size distributions (PSD) of **NPP-2** (three ball-milled powders together)

The particle size of the three powders (50% Molochite, 25% Quartz and 50% Feldspar) after ball-milling was calculated from the particle size of the individual powders (Figure 4.13). The particle size of the powders was below 44.3µm and peaked between 0.9 and 1.5µm. The powder mix showed a broad particle-size distribution, as there was an insignificant difference in the volume percentage of material between 10.9 and 0.7µm in size.

It must be considered that in both formulations, the one with the coarser particles and the one with finer particles have the same solid content. Thus, the main variable

in both formulas was particle size and the number of particles (as a coarser powder will have a lower number of ceramic particles). In wet mixing, when the solvent is added to the powder, the pores between particles must be filled by the carrier fluid (the solvent). When the voids are completely filled, the remaining fluid separates the particles and imparts fluidity to the mix.

In the case of the **NPP-2** formula, because of the high solid content of the formulation, the carrier fluid was limited and can be considered to be insufficient for the coarser particles (that for the smaller particles). In freeze casting, the carrier fluid forms the ice crystals, which will be reflected in the porosity and pore size distribution. Furthermore, the particle size also influences the fluidity of the material. Broad particle size distributions generally give higher packing efficiency, as smaller particles can sit between the large particles and a minimal amount of carrier fluid is required to fill interparticular voids[142].

Another important factor observed to be affected by the particle size reduction of the powders was the state of agglomeration. As the particle size was reduced, the level of soft agglomerates was increased. Agglomerated particles behave like coarser particles, changing the behaviour of the slurry. Thus, the coarser powder formulation was considered more stable and to had a lower dependency on the mixing stage.

In order to understand the effect of the particle size reduction and the change of particle size distribution of the final formula in the freeze casting process, two sets of five ceramic specimens were freeze cast in the same conditions and then fired to 1200°C with the two different particle sizes (coarse powder, as received, and fine powder after ball-milling). As in the previous experiments, the linear-firing shrinkage was assessed; following the ASTM standards (see Appendix 1). The results are shown in Figure 4.13 and Table 4.8.

Sample	Particle Size	Linear-firing shrinkage (%)
A	Coarse	1.52
B	Fine	6.38

Table 4.8: Affect of particle size on linear-firing shrinkage

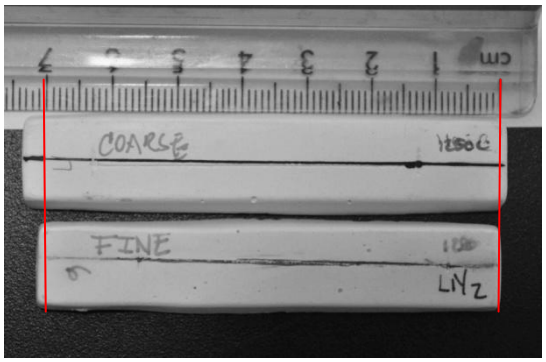

Figure 4.13: Coarse and fine powder samples fired at 1200^{o}C

This experiment confirms that the linear-firing shrinkage is affected by the reduction in the particle size. It was deduced that the finer particle size material undergoes a

higher level of vitrification than the coarse material and this leads to the higher level of shrinkage. [142-144]

Ball-milling the material to reduce the particle size also inevitably influenced the particle size distribution (as shown in Figure 4.11). The particle size will also influence the linear-firing shrinkage in ceramic specimens as, generally speaking, a broader particle size gives higher packing density, lower porosity and lower firing shrinkage (Figure 4.13) [143].

In whiteware, vitrification is the driving force of maturation and to some extent, determines the final properties of the body itself (such as strength, density size and colour). Maturation can be defined by a minimum level of porosity along with maximum shrinkage and density, without pyroplastic deformation. Thus, vitrification is required to accomplish the desired level of densification and part strength.

4.4 ADJUSTMENT OF SOLID CONTENT AND ADDITIVE CHEMISTRY (DISPEX)

The **NPP-2** formulation was subjected to extrusion trials in the ***DWFC*** system. A simple 2D-lattice pattern was deposited (-45°, +45°, 0°and 90°) as shown in Figure 4.14. It was found that the slurry extruded was quite fluid (slightly too low viscosity), due to the particle size reduction that change the flow characteristics of the material.

It can also be noted from Figure. 4.14 that further work needed to be carried out to optimize the formulation (solvent content and amount of dispersant) for extrusion, as the lines, which should have an identical width, were relatively inconsistent.

Three different parameters were found to have an influence in the deposition of the material, i) viscosity, ii) velocity of the pump and iii) nozzle diameter. In the following extrusion experiments, constant nozzle diameter and pump velocities (deposition rate) were used to establish the appropriate liquid content to be used in the formulation. The amount of Dispex and the solvent content were varied (as mentioned in the literature review, the liquid content inside the formulation is also an important parameter for the freeze-casting process).

In the deposition of the material, the velocity of the plunger (stepped motor speed) and the movement of the head in “y” and “x” must be matched in order to deposit the right amount of material. Where too much material is being extruded relative to the velocity of the head this will result in additional material built up. On the other hand if the extrusion rate is too low bead material becomes “stretched” and this may result in breaks in the beam resulting in gaps and missing points in the final shape.

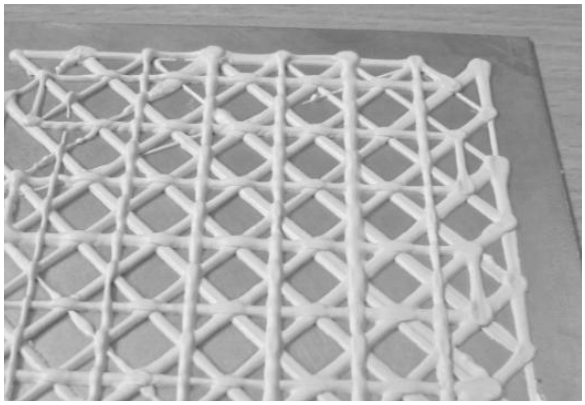

Figure 4.14: 2D-lattice pattern deposited (-45°, +45°, 0° and 90°), relatively too low viscosity

4.4.1 Experimental procedure

Different compositions were prepared where the solid load in the formulation was changed by varying the quantity of solvent and keeping the same amount of powder. The liquid content in the slurry and the amount of dispersant was adjusted (as shown in Table 4.9) to give 20 discrete formulations. Every formulation was extruded using the ***DWFC*** system through a medium nozzle (0.7mm internal diameter); at a velocity of 3.65mm/min. The samples were frozen immediately after extrusion by direct immersion in a bath of liquid nitrogen. The extrudate was deposited on to a ceramic plate (black colour-high fired porcelain). The ceramic plate facilitated the measurement of the extrudate and its handling during subsequent stages (freezing and firing). Ten lines were printed (L-1 to L-10) and their cross section measured in microscope to establish the stability of the formulation. The Table 4.9 shows the combination of the four formulations with different amounts of liquid (sol and

glycerol) and Dispex. This was combined with 8g. of powder by high-shear mixing (as described in Section 4.3.1 dry mixing).

Liquid (g)	**Quantity of Dispex (g)**			
	0.4	**0.3**	**0.2**	**0.15**
2.67	F1-1	F2-1	F3-1	F4-1
2.62	F1-2	F2-2	F3-2	F4-2
2.57	F1-3	F2-3	F3-3	F4-3
2.52	F1-4	F2-4	F3-4	F4-4
2.47	F1-5	F2-5	F3-5	F4-5

Table 4.9: Formulations F1-1 to F4-5 based on different quantities of liquid and Dispex

Four solvent formulations were prepared varying the amount of Dispex. Table 4.10 shows the content of Dispex within each solvent formulation.

Composition	**Silica sol w%**	**glycerol w%**	**Dispex w%**
F1	93.6	5.61	0.7
F2	93.8	5.62	0.56
F3	93.98	5.63	0.37
F4	94.0	5.64	0.28

Table 4.10: Formulations F1 to F4 based on different quantities Dispex (solvent)

Formulations F1 to F4 were prepare individually, each with different amounts of solid content by weight.

4.4.2 Results and Discussions

Extrusion deposition allows some control over the cross sectional shape of the extrudate. The shape of the cross sectional section of the extrudate is not cylindrical as can be seen in the Figure 4.15. The contact angle between the extrudate and the substrate (table) is determined by the wetting behaviour of the paste with the substrate and the viscosity of the material. Good wetting lowers the contact angle and maintains the shape of the extrudate. Depending on the type of surface and liquid content the droplet may take a variety of shapes as illustrated in Figure 4.16 The ideal shape will be the one when the optimum contact angle comes close to 90^{o}, above this level excessive slump occurs and below this level the contact length between beads (built one of top of another) is reduced thus compromising the strength of the part and also the surface finish of the object[145]. A contact angle of near to 90° indicates the most stable formula, as there is less slump of the material.

After the printing and freeze casting of lines L1- L10, it was possible to determine the contact angle of the cross section of the ceramic specimen. This contact angle was measured by a digital optical microscope (Nikon, AZ100 Multizoom, England) with the use of a back light to capture the profile of the extrudate on the solid substrate. The image was also captured by the microscope via an internal camera and software was used to analyse the final contact angle. The lines that were measured from L1 to L10 showed no significant difference between the other lines within the sample and proved that the same line quality was possible and could be created during

replication via extrusion. Seen illustrated in Figure 4.17 a drop starts at point L1 demonstrating the start of the material flow and L10 shows a change in the volume as the material stops flowing.

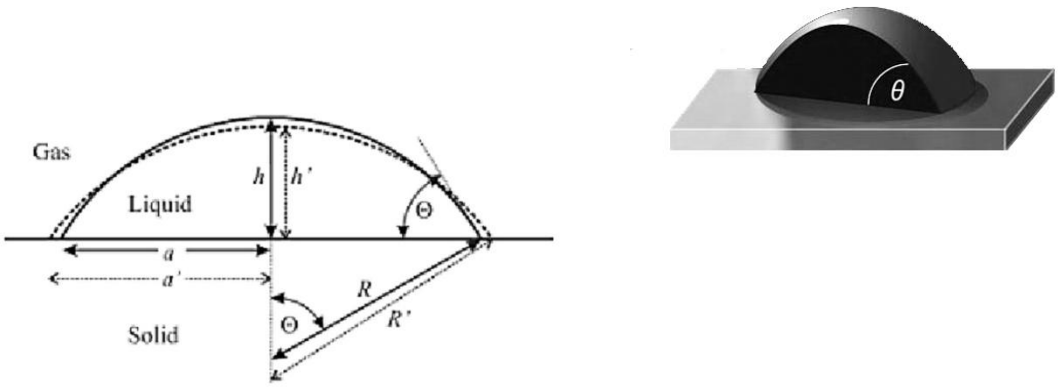

Figure 4.15: Schematic image of cross section through extrudate on substrate (left) and measurement of internal contact angle (right).[146]

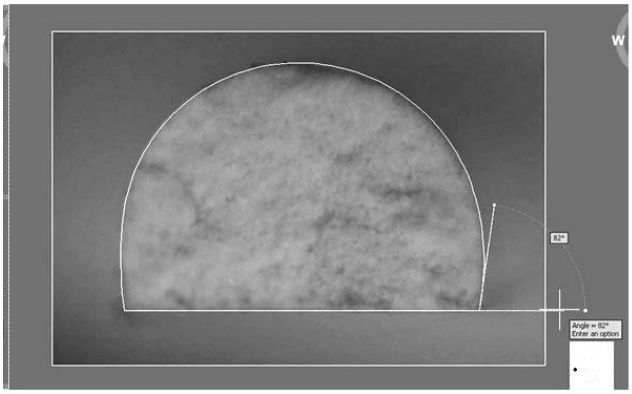

Figure 4.16: Cross section through extruded bead nearest 90° angle.

Formulations with 2.67g of liquid (F1-1, F2-1, F3-1 and F4-1) were found to flow too easily giving an unacceptable level of slump. Formulations with 2.62g of liquid (F1-2, F2-2, F3-2 and F4-2) and 2.57g of liquid (F1-3, F2-3, F3-3 and F4-3) gave more stable formulations with formulas F3-2 and F3-3 (0.2 g of Dispex) being the most stable. However, formulations based on 2.52g of liquid (F1-4, F2-4, F3-4 and F4-4) and 2.47g of liquid (F1-5, F2-5, F3-5 and F4-5) were difficult to extrude, resulting in inconsistent line widths. Formulations F4-4 and F4-5 were too viscous to extrude.

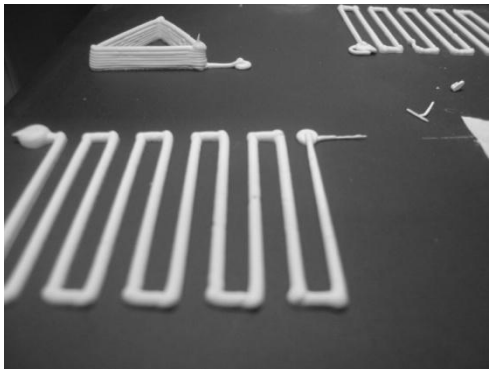

Figure 4.17: Example of printed lines

The printing of a 3D triangular pyramid (sides 30mm long x 10 layers high) was performed for each of the formulas. The amount of solvent influences the ability of the material to form a layer or bead and the amount of Dispex affects the plasticity. Even if the layer was formed the ability of the material to support itself depends on the amount of Dispex. The formulation with a lower Dispex level gave a rough

surface finish and incomplete features. Materials with a high content of Dispex, gave a constant bead but the shape deforms after deposition of the next layer.

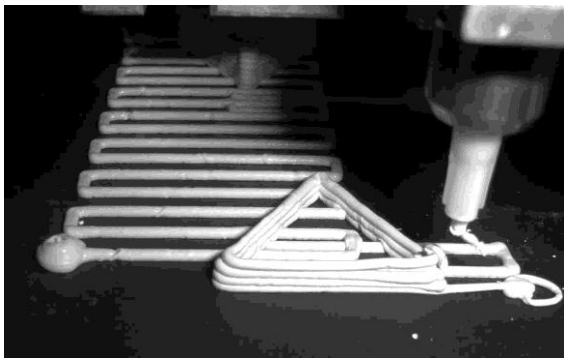

Figure 4.18: Example printing of 3 dimensional shapes

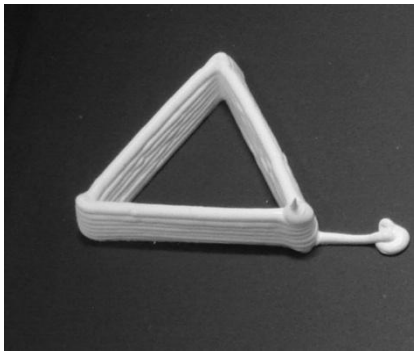

Figure 4.19: Printed layers Formula F3-2 printed layer by layer

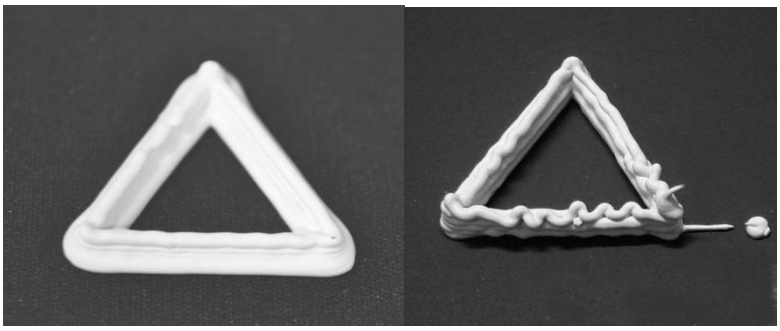

Figure 4.20: Printed layers Formula F4-1 left, Formula F1-5 Right.

4.5 THE EFFECT OF STAND-OFF DISTANT

Having selected an appropriate formula based on the results of the previous trials, further extrusion trials with a medium nozzle (0.9mm internal diameter) were performed. This time, a square-based, 3D pyramid was printed with a self supported geometry. The formulations used were F3-2 and F3-3 and a new formulation based on 2.60g. of liquid was also included, as a middle point for completeness. The selected formula will be called **NPP-3** hereafter and will be the formula utilized for the remainder of the experimental work.

Unfortunately, although material formulations that could be extruded had now been generated, a new problem was identified during the trials. It was found that the stand-off distance between the nozzle tip and the surface of the build platform or previous layer is critical to the success of layer extrusion, Figure 4.21 shows the stand off distance between nozzle tip and plate. If this distance is too small, distortion of the deposited layer (and in extreme circumstances the previously deposited layer) occurs. If the distance is too large, the deposited lines may not be straight (curling occurs). In Figure 4.22, two extruded square pyramids are shown in the left hand image in which the stand-off distance is too small and this results in a flattening of the deposited track (so that the height is smaller than its diameter). In the right hand image the stand-off is too great, resulting in curling of the deposited track.

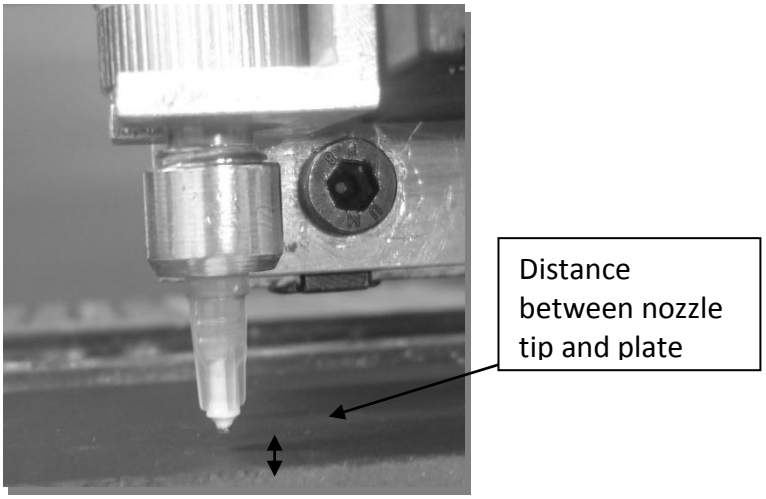

Figure 4.21: Distance between nozzle tip and plate

Figure 4.22 Flattening of layers due to insufficient stand-off (left) and curling of the bead due to excessive stand-off (right).

To establish an optimum stand-off distance (or at least an acceptable range of values), a series of tests were conducted with varying stand-off distances from 1.8mm (twice the nozzle diameter) to 2.5mm (2.77 times the nozzle diameter) – see Table 4.11

Test condition	Stand-off distance (mm)
1	1.8
2	1.9
3	2.0
4	2.1
5	2.2
6	2.3
7	2.4
8	2.5

Table 4.11 Test matrix to assess the effect of stand-off distance

A set of lines with different distances was extruded using the same nozzle diameter and pump velocity as previous trials. The optimum nozzle stand-off was found to be 1.9mm (2.11x the nozzle diameter). Above this level curling occurred and below this level there was a risk of bead flattening (see Figures 4.23 and 4.24).

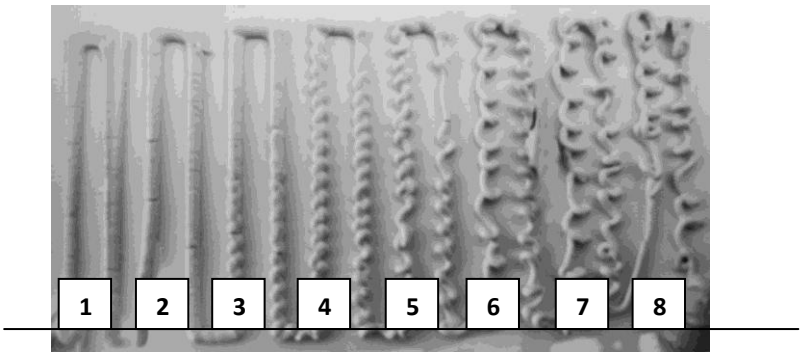

Figure 4.23: A single extrusion line showing different stand-off distances (Test conditions 1-8).

.

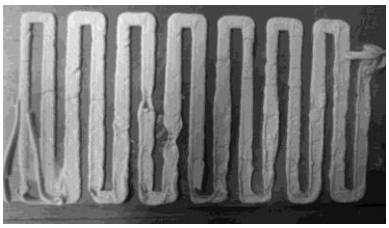

a) Distance 1.8mm (Test condition 1)

b) Distance 1.9mm (Test condition 2)

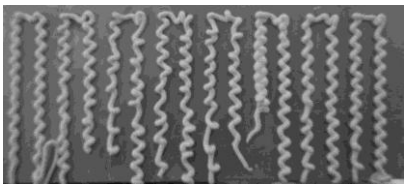

c) Distance 2.0 mm (Test condition 3)

Figure 4.24: Effect of the stand-off distance on the extruded bead

To determine the most suitable distance between the nozzle and the substrate, three main factors should be taken into consideration: extrusion rate, nozzle diameter and nozzle moving speed. The following formula (based on Wang's previous work[147]) illustrates the calculation of the distance between the nozzle tip and the plate;

$$h_c = \frac{\mathrm{Vd}}{\mathrm{Vn.Dn}} \tag{4.1}$$

Where h_c, is the critical nozzle height, that is the necessary distance to extrude a straight line without squeezing it from the top, *Vd* is the extrusion rate (volume of

slurry extruded per unit time cm^3/s), *Vn* is the nozzle moving speed with respect of the extrudate (mm/s), and *Dn* is the nozzle diameter. When the value of height is below the critical nozzle height, ($H<h_C$) the material will be squeezed (test condition 1) and when the value of height is above the critical nozzle height ($H>h_C$) the deposition shows undulation behaviour (test condition 3). This undulation behaviour increases as the stand off distance increases, see Figure 4.25 and 4.26.

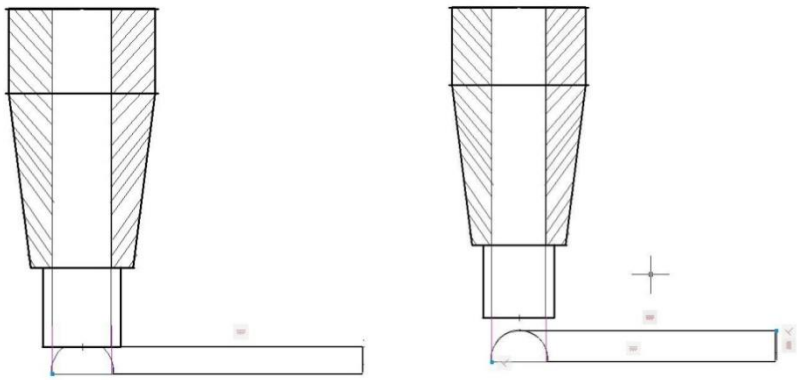

Figure 4.25: Effect of stand-off distance on extrudate, $H<h_c$ (left) and optimum stand-off distance $H>h_c$(right).

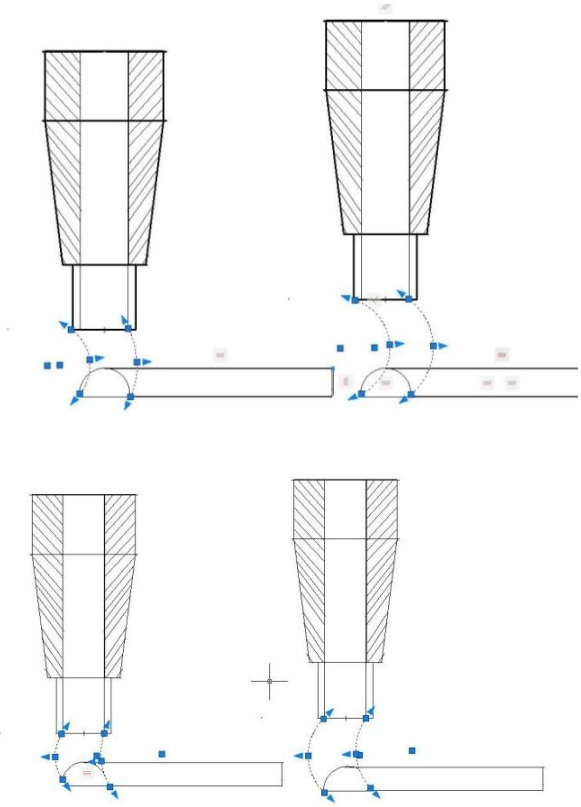

Figure 4.26: Effect of the stand-off distance when the distance is higher than h_c different directions.

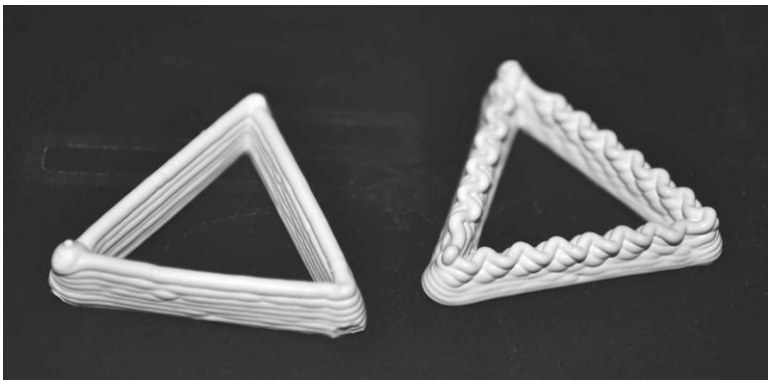

Figure 4.27: Effect of the stand-off distance on the behaviour of the extrudate line $H=h_c$ (left) and $H > h_c$ (right)

From these experiments it was concluded that it is possible to generate beads which are free from distortion (flattening or curling) with the appropriate selection of stand-off distance (See Figure 4.27).

4.6 FINAL REMARKS FOR FORMULATION NPP2 AND NPP3

A suitable ceramic paste for the ***DWFC*** process was developed and demonstrated. A highly-concentrated solid load paste (75.47 wt % solids) of triaxial porcelain composition was found to be suitable for freeze-casting and extrusion processes. This formulation, **NPP-2**, is a modification of the **NPP-1** material. The raw powders and the overall formula were analysed and the particle size was reduced for extrusion purposes. A set of preliminary trials to determine the final particle size were carried out, these preliminary tests consist of two main phases which consist of a simple extrusion with a hypodermic syringe with the intended nozzle size (0.7mm internal diameter) and a freeze casting test with a constant temperature of freezing. In this final test the effect of the reduction of the particle size was measured in terms of linear shrinkage and absorption. The temperature of firing for the **NPP2** formula was reduced based on the particle size reduction. It was found that the shrinkage of the samples produced in this final experiment was directly affected by a combination of the firing temperature and particle size. In addition, the particle size distribution also plays a critical role; a broad particle size distribution allows better packing of particles, and thus results in lower shrinkage. Furthermore, the first extrusion trials

were carried out after the selection of the particle size. Within these trials the additive chemistry and the solid content were selected by experimentation and it was found that 0.2g was the optimum amount of Dispex to be used (in 8g of powder and 2.60 g of solvent). This formulation was called **NPP-3**, and is the final formulation used for the remained experiments. For **NPP-3**, the wetting method and the measurement of the contact angle were selected as a method to select the right amount of solid content and Dispex. Further trials needed to be carried out to determine the optimal freezing rate and firing temperature of the specimens.

The aim of the trials described in the next Chapter was to assess the influence of the freeze casting parameters and firing conditions on the properties of the ceramic samples produced.

In addition, in this chapter the critical extrusion parameters were identified (nozzle moving speed, extrusion rate and nozzle diameter). It was found that the stand-off distance between the nozzle tip and substrate is critical, too small and flattening of the bead occurs, too large and curling occurs. An optimum stand-odd distance can be calculated from the equations developed, depending on the size of the nozzle, extrusion rate and the speed of the extrusion head with respect to the substrate.
Further analysis of the extrusion parameters was undertaken and is presented in Chapter 6.

5. FREEZE CASTING: DETERMINATION OF PARAMETERS AND MATERIAL PROPERTIES

5.1 INTRODUCTION

The work presented in this chapter represents a more extensive investigation into the freeze casting of the **NPP-3** material developed in this study. There were two main objectives behind this work. The first was to establish the effect of the freezing temperature on the microstructure (pore structure, pore size and distribution) of the ceramic specimen and its effect on the physical and mechanical properties. The second objective was to study the effect of substituting the clay material with the calcined component (molochite) in terms of both microstructure evolution during firing and the physical and mechanical properties of the final specimens fired at different temperatures.

From a practical perspective the author decided not to combine the freeze casting step within the direct write process. By separating these two steps it enabled a much simpler test rig to be used (see section 2.3.1 Chapter 2 ***DWFC*** system) several research groups have commented about the difficulty in combining DW and FC in a single unit [148] Moreover, it enabled each trial to be focused specifically on either

direct writing or freeze casting thus helping to achieve robust conclusions from the trials.

It should be noted that trials undertaken within the Technology Strategy Board funded project – *Direct Writing and Freeze casting of Bioceramics implants* have demonstrated the difficulty in sequentially depositing and freeze casting layers. The results show that depositing material onto a layer of material which has already been freeze cast results in very poor bond strength. In this thesis this problem has been overcome by bulk freeze casting of samples once direct writing has been completed.

Since in the previous trials, a slurry formulation was developed which could be extruded, freeze cast and fired. This work provided the foundation for the subsequent experimental trials (presented in this chapter and also in Chapter 6) in which the formulation was fine-tuned and also the optimum processing conditions will be established. The aim of these trials was to determine the appropriate freeze-casting and firing conditions for the **NPP-3** material developed in this project. The samples produced for freeze-casting trials were subsequently fired and the results used to establish the influence of firing conditions. Three factors were assessed in the trials: 1) apparent porosity, 2) linear-firing shrinkage and 3) mechanical properties. Porosity and shrinkage are key factors for ceramic materials and were also measured in the initial trials. However, the mechanical properties of samples were also assessed, as this is another parameter which can be used to determine the effectiveness of the new material.

5.2 INVESTIGATION OF FREEZING PARAMETERS

Based on the findings in the literature review, there were two primary parameters which must be considered in the freeze casting stage of the process: 1) the freezing temperature to which the slurry is exposed and 2) the rate of cooling. Varying these parameters may result in a different microstructure being formed and thus changes to the final properties of the material[83]. In this work, the effect of the freezing temperature on the characteristics of the final material was investigated. In addition, another important parameter, temperature of firing, which may have a significant effect on the microstructure for triaxial formulations, was assessed. Because of the complex interactions between the raw materials, the kinetics of the firing process were expected to be more complicated than for many other ceramic systems[121].

5.2.1 Freezing temperature

Although there is evidence, albeit anecdotal[117], that freeze casting is initiated (i.e. crystal growth commences) once -5^{o}C is reached and that the process is completed at a temperature of -40^{o}C, these findings are not robustly supported by rigorous experimental data and moreover, the specific freeze-casting performance will depend on the precise formulation of the slurry.

5.2.2 Speed of cooling

The literature review highlighted that one of the key parameters for the freeze casting process is the rate of cooling as this can determine the pore size and pore size distribution, which, in turn, affects the shrinkage and properties of the final object.

5.2.3 Freezing Temperature trials

A total of 30 ceramic samples were prepared from a combination of the three powders (75.47 w %) and the solvent (24.52 w %) that make up the **NPP-3** formula (see Table 5.1). The constituent components were mixed vigorously together by hand and by using a pestle and mortar for 2 minutes. This broke up the soft agglomerates and then air bubbles were eliminated using a vibratory table. The prepared slurry was then poured into flexible silicone rubber moulds (RTV 664, General Electric Company) to produce test bars (80.5 mm long x 20mm wide x 3.14mm thick see Figure 5.1).

NPP-3 Powders	Feldspar w%	Quartz w%	Molochite w%
	25	25	50
NPP-3 Solvent	Silica sol w%	Glycerol w%	Dispex w%
	93.98	5.63	0.37

Table 5.1 Material composition

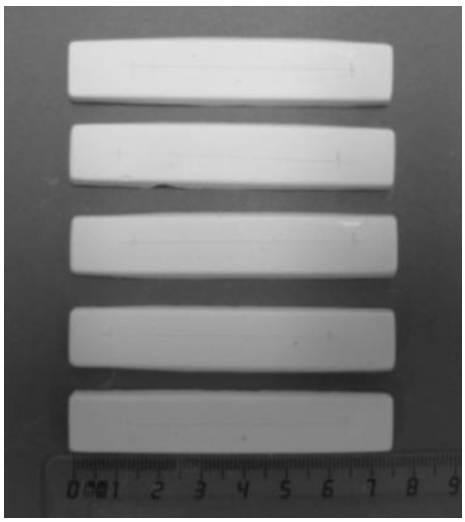

Figure 5.1: Freeze casting test specimen bars before firing (green state)

The specimens were freeze cast at different temperatures using two different methods: 1) immersion in liquid nitrogen and 2) immersion in a mixture of isopropanol (IPA) and dry ice (approximately 50:50 by volume) to give temperatures of approximately -196^{o}C and -72^{o}C respectively. The RTV silicone moulds filled with ceramic slurry were placed in an aluminium tray containing the cooling medium. The tray (freezing bath) was enclosed in an insulating polystyrene box. A non-directional approach to freezing was chosen, (see literature review section 2.3.2 for the freeze-casting parameters), here freeze casting is not initiated from one surface, instead the specimen is bulk cast into a non-porous mould[89, 149]. The test parts were held at the temperature of the freezing bath for two hours. This was carefully monitored using a K-Type thermocouple connected to a data-logging device (Pico Technology limited TC-08, 8-channels). Two channels of the thermocouple were utilized during

the experiment, one within the ceramic material and the other one inside the freezing device (freezing bath), in order to obtain a better understanding of the actual conditions within the sample.

Three sets of five samples were produced for each freeze-casting condition. After completing the freezing process, the samples were removed from the cooling device and exposed to normal room temperature (18-21°C) for 24 hours. Samples were then subjected to different sintering regimes (as described in Section 5.3 below). The properties of the fired samples were then measured following the relevant ASTM standards (see Appendix 1).

5.2.4 Results and conclusions

Figures 5.2 and 5.3 show the temperature of the freezing bath (liquid nitrogen and dry ice/IPA respectively) and the ceramic specimens during the freeze casting process. For the liquid nitrogen bath, the minimum temperature reached was -175°C; however, the temperature of the bath increased to -122°C after the specimen was introduced. The temperature continued to rise until it reached -93°C after ninety minutes. In a similar way, the ceramic specimen also reached a minimum temperature of -175°C but rapidly increased in temperature until a temperature of -100°C was achieved after twenty minutes.

On the other hand, the dry ice/IPA bath reached a minimum temperature of -79°C and the ceramic specimen only reached a minimum temperature of -74°C after 5 minutes. It can be seen from Figure 5.3 that the temperature remained constant for the entire two hour period for the dry ice/IPA bath sample. The cooling rate of the two systems (Liquid nitrogen and dry ice/IPA) was compared for the first (critical) 3 minutes when the sample temperature drops below -40^{o}C and freeze casting is initiated (Figure 5.4). It can be seen from Table 5.2 that the cooling rate for the liquid nitrogen is 3.51 times higher than for dry ice/IPA.

Sample	Cooling media	Temperature after 3 minutes (°C)	Initial cooling rate * (°C/min)
A	Liquid nitrogen (LN)	-175	43
B	Dry ice/IPA (IDI)	-49	12

*Based on an ambient temperature of 20°C

Table 5.2 Initial cooling rates for both liquid freezing media

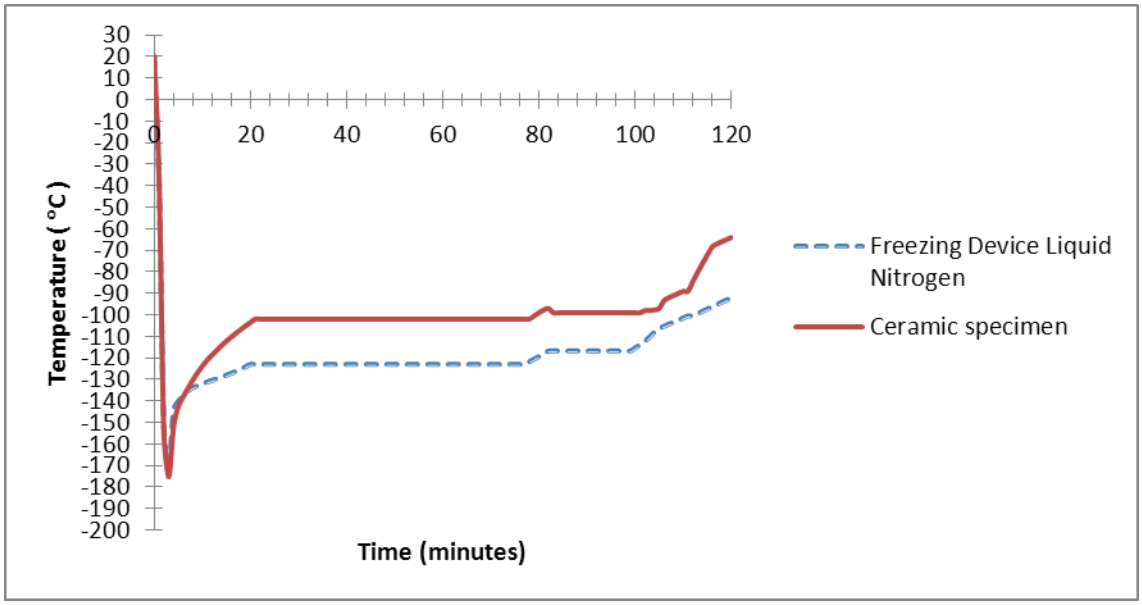

Figure 5.2: Temperature of freezing bath and ceramic sample for liquid nitrogen

`

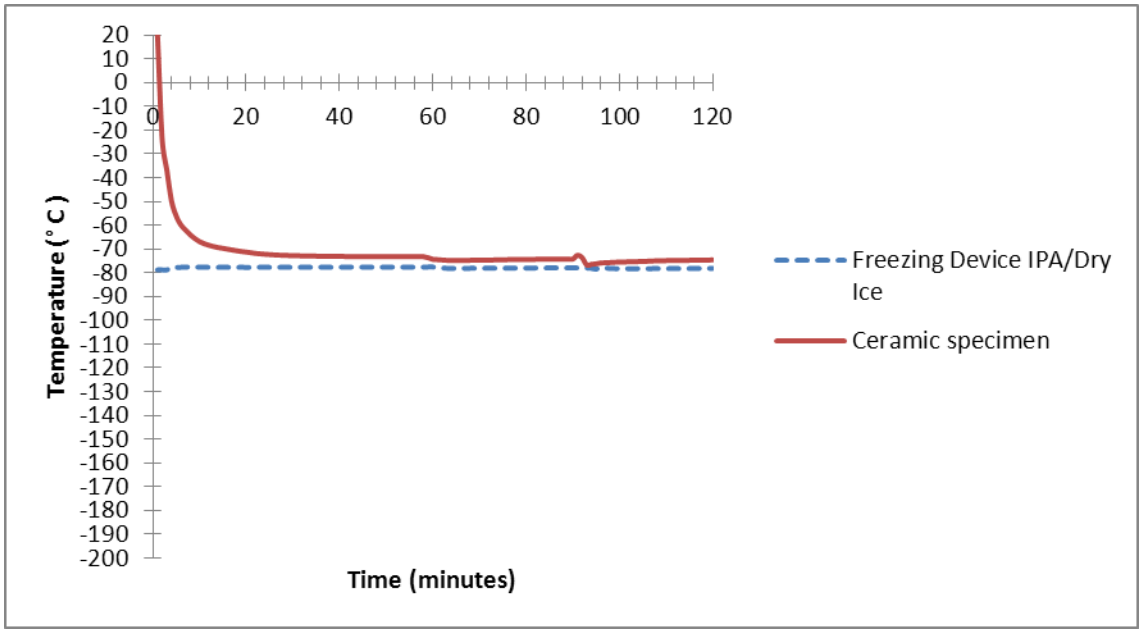

Figure 5.3: Temperature of freezing bath and ceramic sample for dry ice/IPA

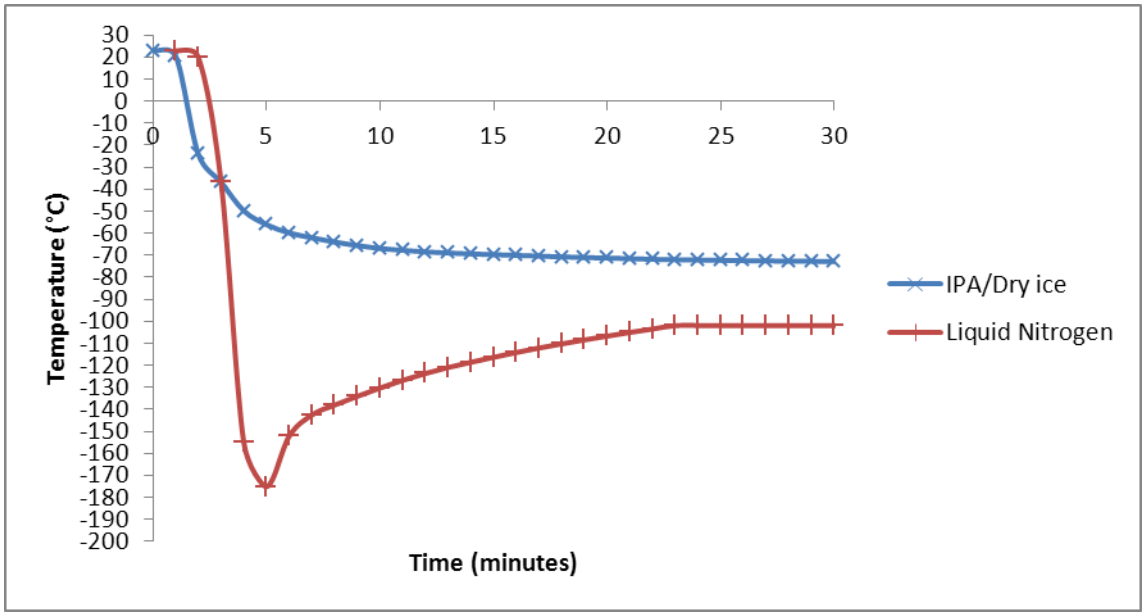

Figure 5.4: Temperature of ceramic specimen processed using liquid nitrogen and dry ice/IPA during the first 30 minutes of freezing

After the samples were removed from the freezing device and dried (24 hours at room temperature), a SEM was used to analyse the microstructure of the dry specimen. Figure 5.5 shows the microstructures of the samples cooled at the two different rates.

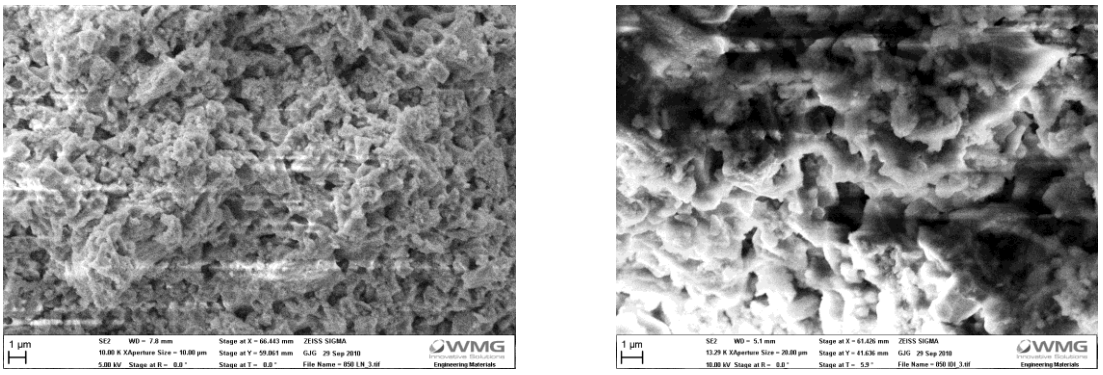

A **B**

Figure 5.5: SEM images of the porous NPP-3 specimens processed with liquid nitrogen **(A)** and dry ice/IPA **(B)**

5.2.4.1 Analysis of the microstructure

SEM images of the fired samples show an even, homogenous macrostructure and porosity. This is to be expected as the freeze-casting method employed was omnidirectional and no clear direction of ice crystal growth can be seen. The method of freezing used had a clear influence on the size of the pores within the fired sample. The rapid cooling from the liquid nitrogen bath resulted in a finer dendritic structure and smaller pores compared to the samples processed using the dry ice/IPA (see Figure 5.5 and Table 5.3).

Sample	Cooling media	Initial cooling rate * (°C/min)	Pore Size (μm)
A	Liquid nitrogen	43	0.5
B	Dry ice /IPA	12	1

Table 5.3 Initial cooling rates for both liquid freezing media

Nevertheless, regardless of the difference in microstructure, because the same amount of liquid is present in the two samples, **A** and **B**, the densities of the parts formed were expected to be the same. The effect of this porosity on the physical and mechanical properties of the fired samples will be described in the following section where a full analysis of the mechanical and physical characteristics with the two temperatures of freezing will be presented.

5.3 INVESTIGATION OF FIRING REGIME

As mentioned in the literature review, triaxial porcelain is a vitreous ceramic material which transforms when subjected to different temperatures. Vitrification means a high degree of melting occurs during firing and the formation of glass which leads to enhanced densification of the ceramic body[140]. In a traditional triaxial porcelain formula, the three components in the formulation undergo different reactions according to the firing regime: when the specimen reaches 100°C, drying is completed; from 300 to 700°C, the organic material additives are burnt off; between 450°C and 500°C, the materials start to decompose and react with each other and at 900°C vitrification occurs (the flux material, in this case feldspar, reacts with the other particles to form a liquid, molten glass). The amount of liquid increases with temperature, the body contracts (shrinks) and it can be seen that the porosity reduces[131]. At this point, new materials may crystallise from the liquid. If the material is over-fired, too much liquid is formed and the ceramic body may suffer from pyroplastic deformation.

After reaching the desired temperature, the firing process is followed by a soaking period at the top most temperature in order to allow the entire object to reach the maximum firing temperature and remove any thermal gradients which may be present. The final stage of the firing regime is cooling, allowing the liquid to solidify

into a glass. This fuses together the unmelted particles and crystals form during heating.

According to information found within the literature review and previous experimental work, the determination of the firing temperature may depend on two primary factors: material composition and particle size.

1) Material composition - as there is no clay within the formulation, the reaction of the materials may occur at a slightly lower temperature[129, 140, 150].
2) Particle size – a reduction in the particle size should result in a drop in the firing temperature[151-154].

Although replacing clay with molochite enables a slurry which can be successfully freeze cast to be formulated, this significant change introduces concerns regarding the ability to fire and generate fully-vitrified porcelain at the end of the process. There has been limited work on the firing of non-plastic porcelain materials[127, 155, 156]. The firing cycle used in the initial trials was based on standard porcelain materials. The ideal firing conditions for the **NPP-3** material used in this project must be determined during the study. It was hoped that it may be possible to use a lower firing temperature for the clay replacement (molochite) as no reaction will take place during the sintering process, which will reduce the level of shrinkage. Based on the

results of previous work[153, 156], the use of smaller diameter particles of Molochite along with quartz fillers should facilitate fusing and vitrification at lower temperatures.

5.3.1 Firing Regime trials – Experimental Procedure

5.3.1.1 Selection of temperatures of firing for the experimental work

The ceramic specimens produced for the freeze-casting parameter trials (described in the previous section) were dried at room temperature (~24 hours until their weight was stable) and then sintered in a laboratory kiln (ST314, Stafford instruments, Germany). In the preliminary trials (described in Chapter 4), all of the specimens were fired to a maximum temperature of 1280^{o}C. However, for this second set of trials, given that the particle size had been reduced for extrusion optimisation, it should be possible to use a lower firing regime. It was predicted, based on information from previous literature, that the firing temperature should be above 1000^{o}C [157] but, to provide a comparison, a lower temperature was also included. For this reason three different firing temperatures of: 900°C, 1100°C and 1200°C, were used

5.3.1.2 Measurement of the temperature of firing

In the traditional ceramic industry, high-temperature kilns can usually lose some heat via the lid covering and a few areas around the walls. This loss, together with natural convection effects, results in a variation in temperature depending on the location within the kiln. To gain a better understanding of the real temperature regime to which the material is exposed, the *Buller's rings* method was used (see Figure 5.6 and Figure 5.7). This is a traditional approach used in the ceramic industry where the shrinkage of circular ceramic rings is used to estimate the actual temperature regime within the kiln. This is important in this experiment because a small variation of the temperature could potentially lead to significant differences in the level of vitrification.

Figure 5.6: *Buller's rings* method

Figure 5.7: Freeze casting specimen bars after being fired at different temperatures

A series of five **A** and **B** samples for each freezing rate (liquid nitrogen and dry ice/IPA) were submitted to the three different temperatures of firing, the resulting samples were used for the evaluation of the physical and mechanical properties of the fired samples by the following test:

i. Water absorption was determined using the Archimedes liquid displacement method (described in Chapter 3) based on ASTM. C326-09 (see Appendix 1)
ii. Linear-firing shrinkage was calculated by comparing the specimen length before and after firing. ASTM C373 – 88 (see chapter 3 and Appendix 1).
iii. Modulus of rupture, of the fired test pieces, was determined using a three-point bending test. ASTM C674-88 (see Appendix 1).

The sintered samples were also characterized by X-ray diffraction (XRD) and the microstructure presented on the fired samples was studied on fracture surfaces using a scanning electron microscope (SEM). The apparent porosity, bulk density and volume, open and total porosity was determined using the following approaches:

Apparent porosity **(AP)** was calculated as the product of bulk density and water absorption. The relationship to determine the parameters mentioned before are expressed below:

The linear-firing shrinkage (%), of the fired samples has been determined by means of the following equation:

$$LFS = \frac{LS - L_C}{L_S} x100 \quad (5.1)$$

L_S and L_C are the length measurements of the green and fired test parts, respectively. The linear shrinkage values obtained were averaged for each firing temperature.

Water absorption, ***WA*** (%), expresses the relationship between the mass of water absorbed into the sample and the mass of the dry specimen as follows:

$$WA = \frac{M - D}{D} X100 \quad (5.2)$$

Where ***D*** is the dry mass of the sample before the impregnation, ***S*** is the mass of the specimen while suspended in water and ***M*** represents the saturated mass after impregnation.

The bulk density, ρ (g/cm^3), was calculated as follows:

$$\rho = \frac{D}{V} \tag{5.3}$$

Where V (cm^3) is the exterior volume including pores **($V = M - S$).**

The open porosity, ε_o (%), expresses the relationship of the volume of open pores to the exterior volume of the specimen, the formula used to assess this matter is represented as follows:

$$\varepsilon_o = \frac{M - D}{V} X100 \tag{5.4}$$

The volume of open pores was expressed by the following relationship:

$$V_{OP} = M - D \tag{5.5}$$

Module of rupture formulation is dictated by the following equation:

$$\sigma = \frac{3PL}{2bd} \tag{5.7}$$

Where, σ is modulus of rupture, Psi (or MPa); ***P*** is the load at rupture, lbf (or N); ***L*** distance between supports, in. (or mm); ***b*** width of specimen, in. (or mm); and ***d*** thickness of specimen, in. (or mm).

5.3.2 Result and conclusions

The *Buller ring* test results for the three different oven (set) temperatures 900°C, 1100°C and 1200°C are shown in Table 5.4. The specimens fired at the highest temperature show some pyroplastic deformation. However, samples fired at the medium temperature did not show any deformation. Figures 5.8 and 5.9 present the ceramic specimens fired at the two different temperatures.

Temperature	Oven Set temperature (°C)	Minimum Temperature* (°C)	Maximum Temperature* (°C)	Average temperature (°C)
Low	900	850	900	875
Medium	1100	1050	1100	1075
High	1200	1100	1200	1150

*indicated by Buller's ring

Table 5.4 Rectification of temperature of firing

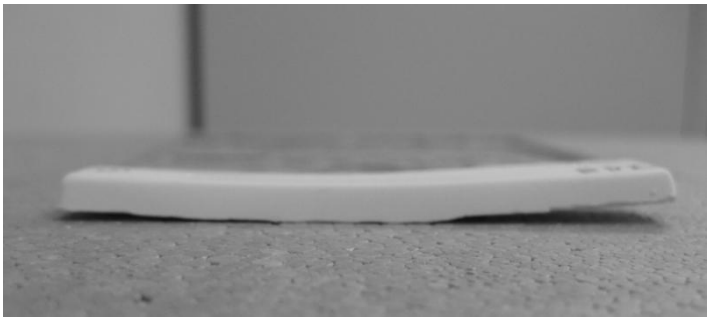

Figure 5.8: Pyroplastic deformation of the freeze-cast ceramic specimen fired at 1150°C

Figure 5.9: Freeze-cast ceramic specimen fired at 1075°C

The results for the three different firing temperatures (average of two runs) were compared with the properties of the triaxial porcelain. Table 5.5 shows the resulting values for the water absorption, linear-firing shrinkage, module of rupture, apparent porosity and bulk density, for the specimens freezing at the faster freezing rate (Liquid nitrogen) whilst Table 5.6 shows the results for the specimens frozen to the slow freezing rate (dry ice/IPA).

Liquid Nitrogen					
°C	**Water Absorption (%)**	**Linear-firing shrinkage (%)**	**Module of rupture (MPa)**	**Bulk density g/cm^3**	**Apparent porosity (%)**
1150	5.19	6.78	24.8	2.26	11.75
1075	12.73	3.92	19.56	1.95	24.89
875	17.84	0.58	17.34	1.73	30.94

Table 5.5 Comparison of properties of the fired ceramics bodies as a function of sintering temperature, with liquid nitrogen as the freezing medium.

Dry ice/IPA					
°C	**Water Absorption (%)**	**Linear-firing shrinkage (%)**	**Module of rupture (MPa)**	**Bulk density g/cm^3**	**Apparent porosity (%)**
1150	6.68	7.04	23.3	2.18	14.60
1075	12.47	3.64	19.69	1.99	24.40
875	17.51	0.54	17.85	1.81	31.75

Table 5.6 Comparison of properties of the fired ceramics bodies as a function of sintering temperature, with the dry ice/IPA bath as the freezing medium.

Water absorption is generally dependent upon the apparent porosity, which in turn is controlled by the temperature of firing. As expected (based on the information from previous literature sources found[158] the lowest water absorption values were observed for the specimens fired at the highest temperature. Comparing the water absorption for the three firing temperatures, the results are broadly linear (see Figure 5.10), with a decrease from 17.85 to 5.19 as the temperature increases from 875 to 1150 °C. The water absorption for the specimens freeze cast using liquid nitrogen and dry ice/IPA is very similar apart from the specimens fired at the highest temperature where the value of water absorption for samples processed using liquid nitrogen is lower than that for dry ice/IPA. This could be expected from the microstructure (see Figure 5.5), which shows that the more rapidly cooled samples have finer pores, which are more likely to close up during firing.

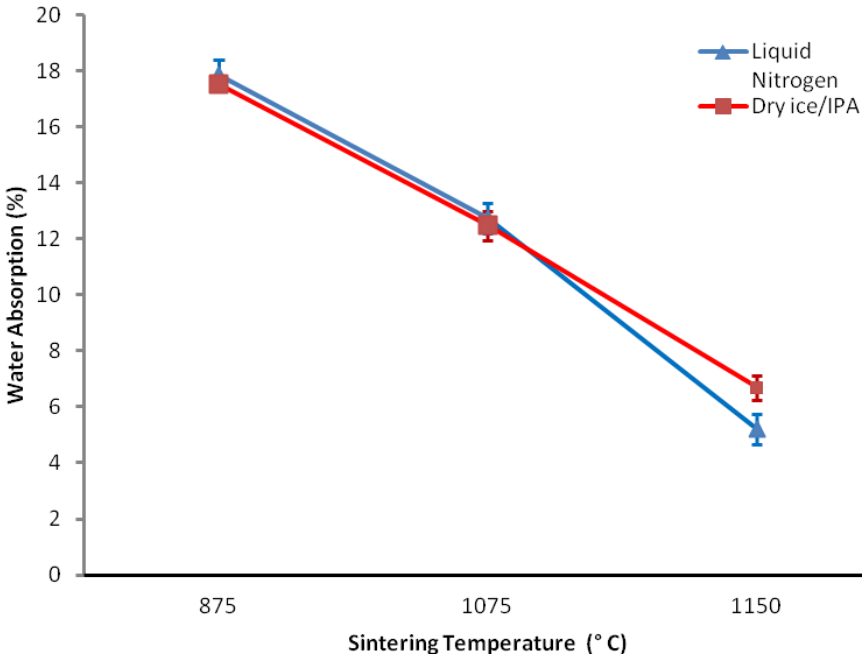

Figure 5.10: Water absorption of liquid nitrogen and dry ice/IPA freeze-cast specimens fired at different temperatures (Tables 5.5 and 5.6).

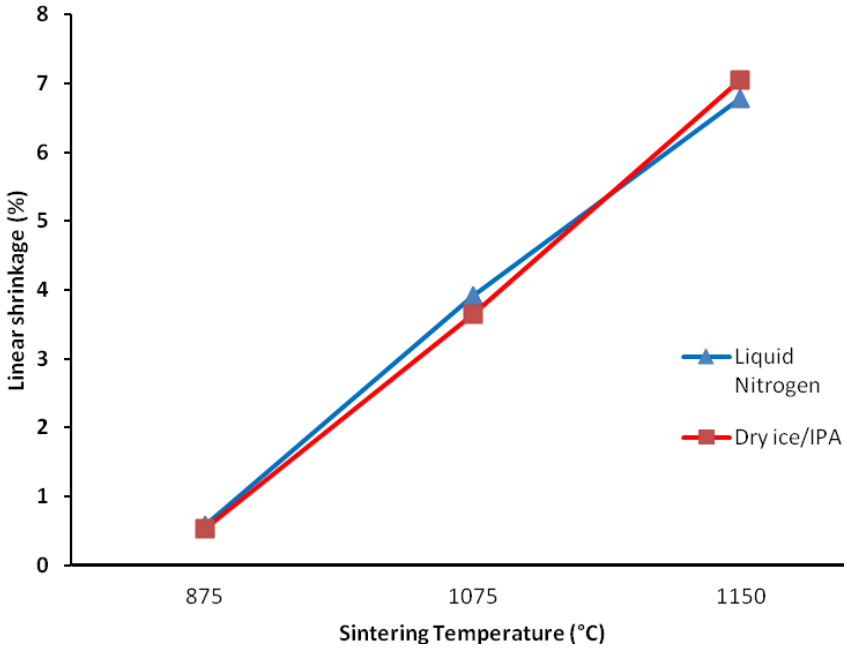

Figure 5.11: Linear-firing shrinkage of liquid nitrogen and dry ice/IPA freeze-cast specimens fired at different temperatures (Tables 5.5 and 5.6).

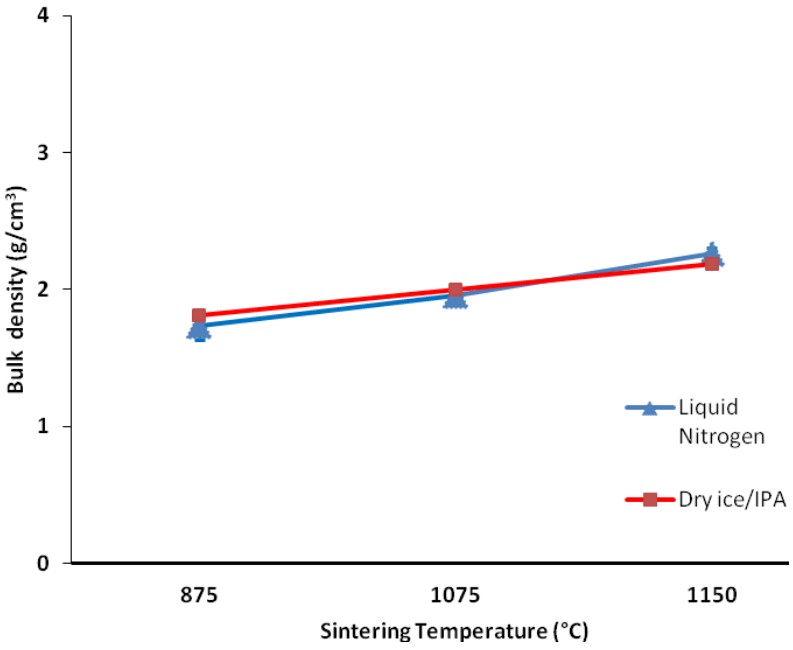

Figure 5.12: Bulk density of liquid nitrogen and dry ice/IPA freeze-cast specimens fired at different temperatures (Tables 5.5 and 5.6).

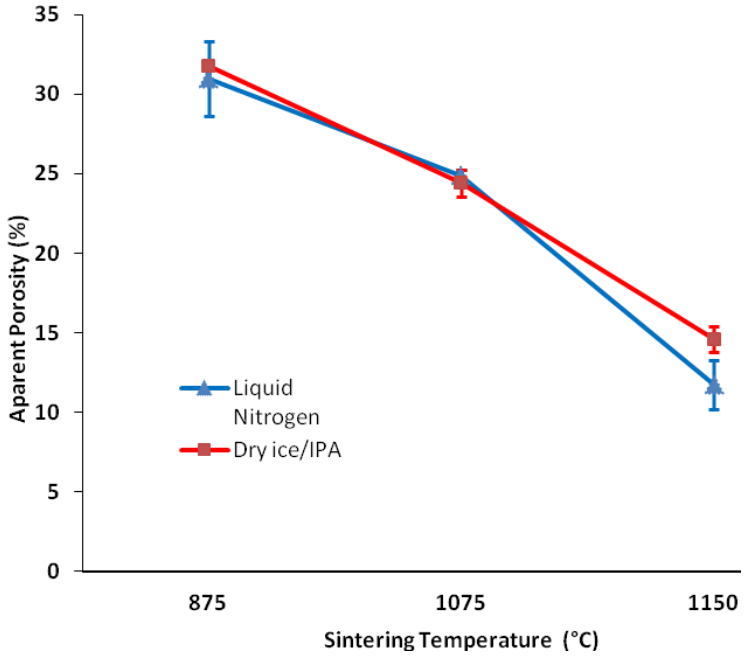

Figure 5.13: Apparent Porosity (%) of liquid nitrogen and dry ice/IPA freeze cast specimens fired at different temperatures (Tables 5.5 and 5.6).

Figures 5.11 and 5.12 show the linear-firing shrinkage and apparent density of the fired bodies respectively. The linear shrinkage values lie within the range of 0.58 to 6.78 % (Liquid nitrogen) and 0.54 to 7.04 % (dry ice/IPA) and the density values range from 1.73 to 2.26 g/cm^3 (Liquid nitrogen) and 1.81 to 2.18 g/cm^3 (dry ice/IPA). In general, shrinkage and density both increase up to the maximum temperature. Dense bodies are expected to have higher mechanical strength than porous bodies. These results are supported by microscopic investigation, which show that as the pores close, the linear shrinkage increases. Figure 5.13 shows the apparent porosity of the ceramic specimens. It can be appreciated that there is not significant variation between the two different freezing rates.

Samples prepared by freeze casting show lower physical (density, porosity etc) and mechanical (flexural, modulus of rupture etc.) properties compared to fired bodies produced using TP compositions[159].This is despite the replacement of the clay material with molochite (mullite), which in theory should yield improved properties. This is also indicated by the decrease in shrinkage values for the freeze-cast material, which indicates lower densification and thus greater porosity. Micro-structural analysis of the specimens reveals that the pores are relatively large and many are interconnected. Nevertheless, this new material is still considered as a whiteware material, due to the level of porosity, density and shrinkages.

5.3.2.1 Microstructure of the fired specimens

The microstructure phases developed in the final fired freeze cast **NPP-3** were study extensively using XRD, SEM and EDS techniques. In SEM images (see Figure 5.14), partially dissolved quartz grains can be observed surrounded by a solution of almost pure silica glass in a finer matrix system. The quartz grains are angular in nature but at the highest firing temperature, extensive dissolution of quartz is evident, as the quartz grains become round in shape. Dissolution of quartz generally depends on the size of particles (coarser quartz grains dissolve at a much slower rate than fine grains).

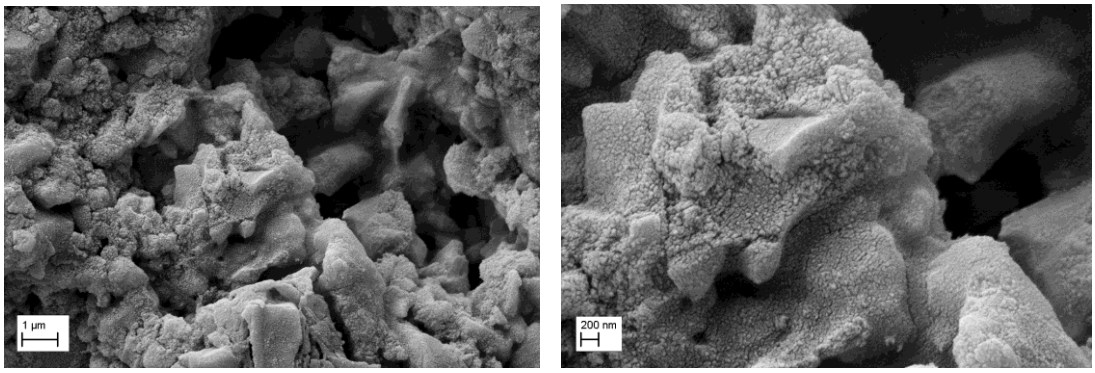

Figure 5.14: SEM photomicrograph, bonding seen as a result of the glassy phase and showing remaining unmelted components, showing micropores ~400nm right.

Additionally the XRD analysis indicates as main components; quartz, corundum, albite and microcline (see glossary of terms), the major phase is quartz, as shown by the Figure 5.15. The quartz phase decreases substantially as the firing temperature increases, giving an amorphous silica phase as indicated by an increase in the background noise levels. At the higher firing temperature the feldspar (albite) was completely dissolved into the glass phase (Figure 5.16).

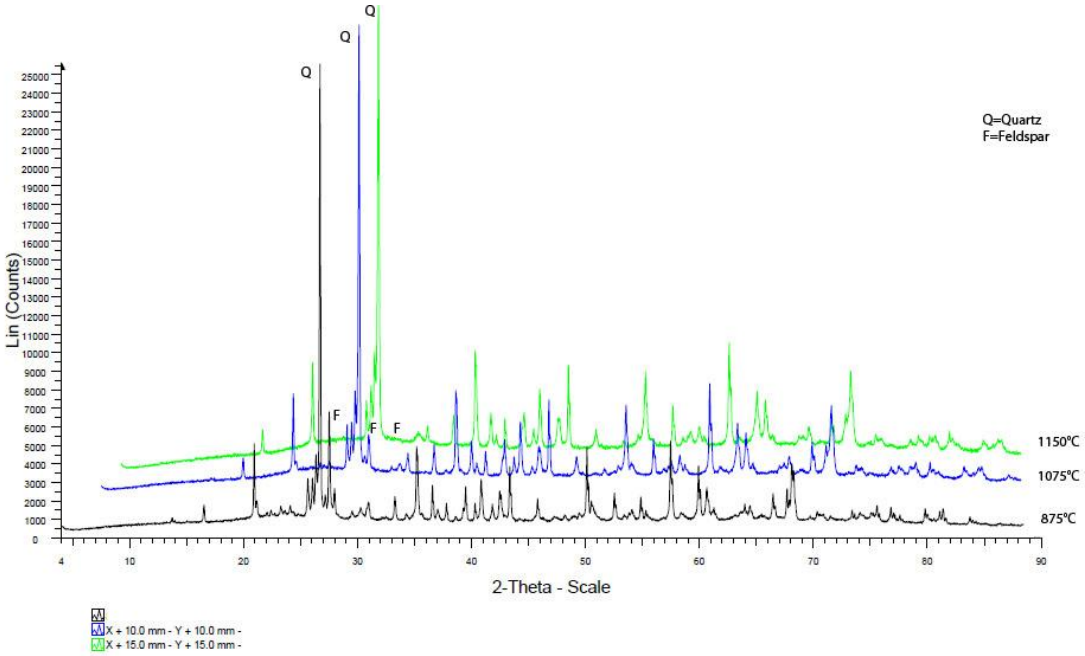

Figure 5.15: Comparison XRD Analysis of NPP-3 fired at different temperatures.

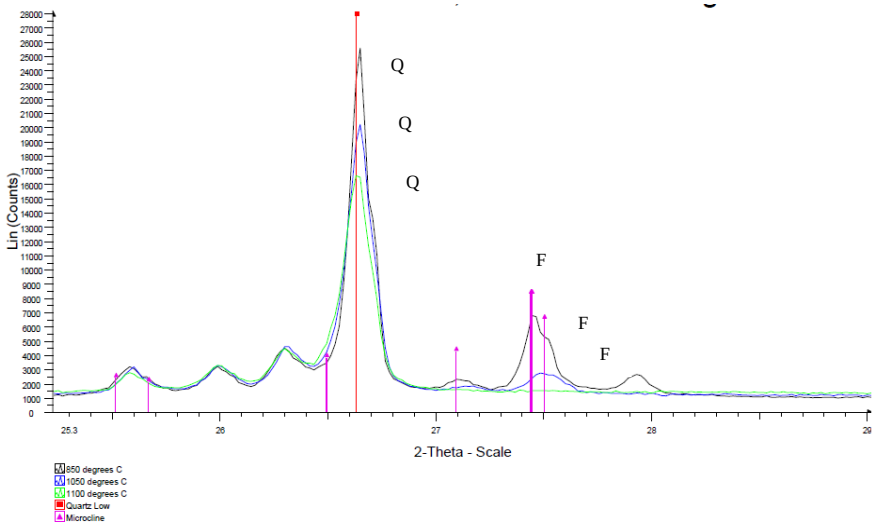

Figure 5.16: Un-normalised XRD data for NPP-3 fired at different temperatures – close up of Quartz and feldspar peaks.

Figures 5.17 to 5.19 show the normalised XRD data for each temperature of firing, it can be seen the increment of the amorphous silica represented as a black line on the background on each graph, apart of the high dissolution of the albite and microline (feldspar), and the quartz (in less proportion).

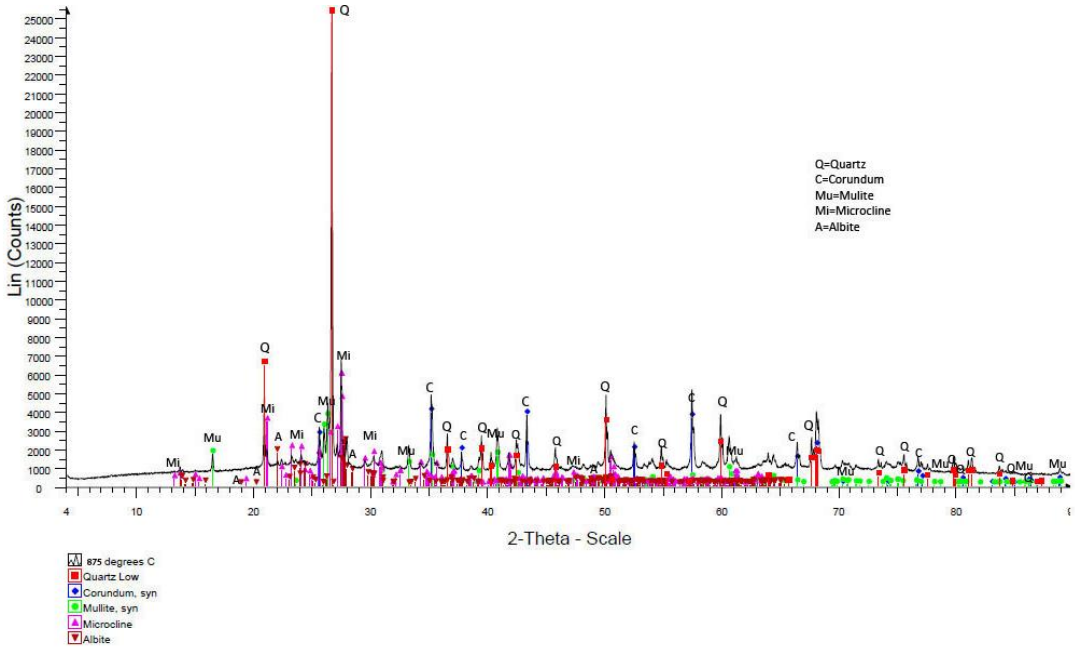

Figure 5.17: XRD Analysis of NPP-3 fired at **875°C.**

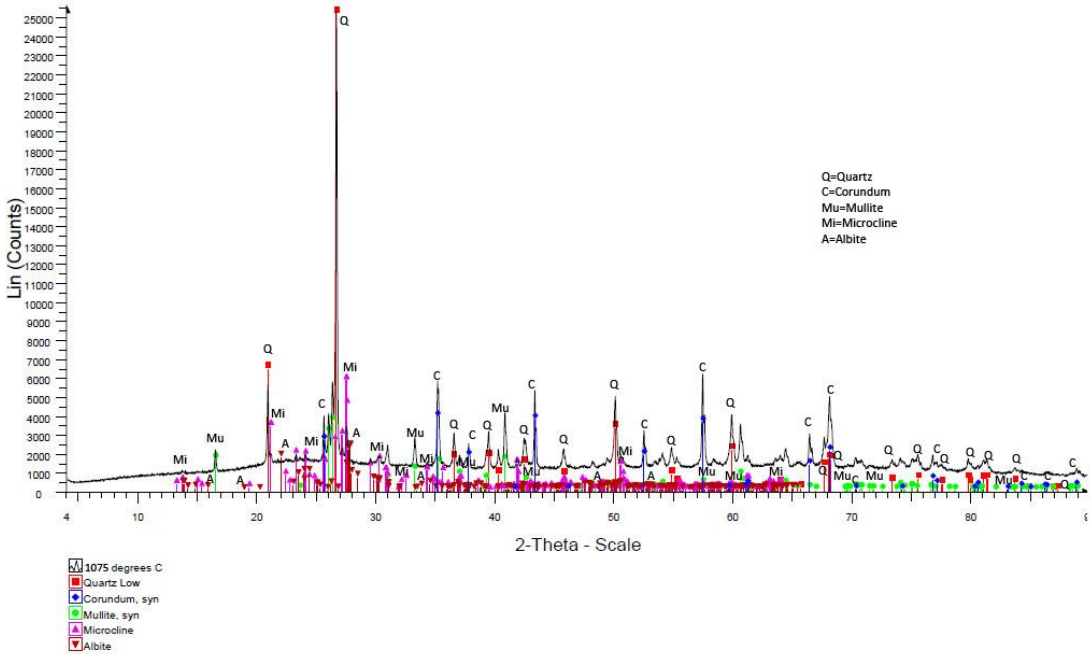

Figure 5.18: XRD Analysis of NPP-3 fired at **1075°C.**

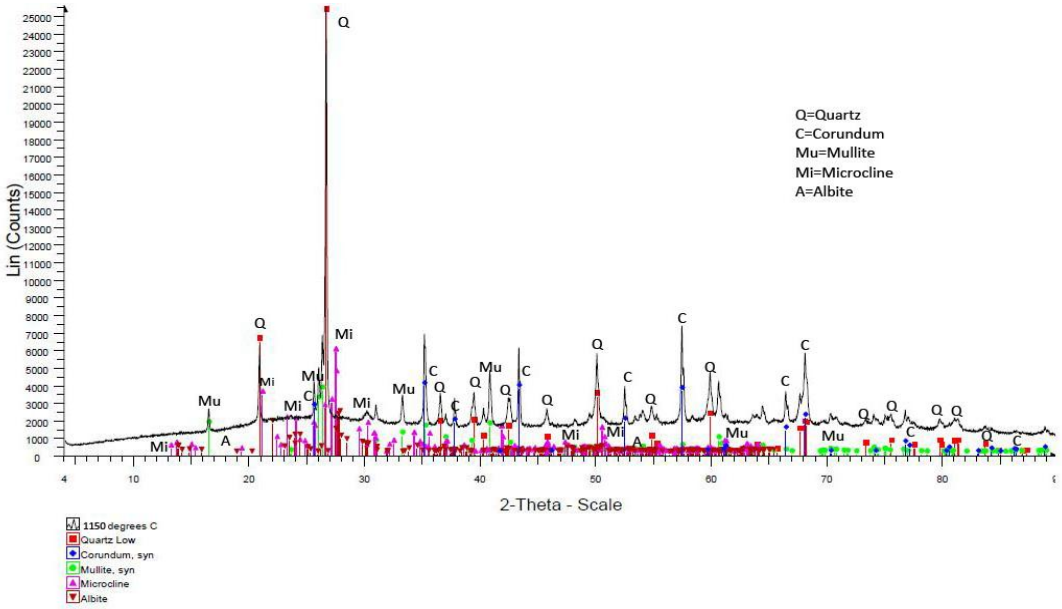

Figure 5.19: XRD Analysis of NPP-3 fired at **1150°C.**

Moreover the SEM analysis of the microstructure shows the evolution of the fired specimens to different temperature (875°C, 1075°C, and 1150°C). **A** Liquid Nitrogen, **B** IPA/Dry Ice (Figure 5.20) during the firing stage. It can be seen there are a significant change according with the vitrification of the material at different temperature.

The difference between **A** and **B** relay on the porous size (see Figure 5.5). From this study it can also be appreciated that **B** comprises a more homogenous microstructure in comparison with **A** each temperature of firing, in B the material dissolve faster due to the temperature of firing, in **A**- 1150°C cracks can also be appreciated. From the figures below it can be deducted that very low temperature of freezing (fast freezing rate), some how represents a more aggressive method of freezing, leaving option **B** as a most appropriate option for this project.

The EDS analysis in Figure 5.21 to 5.23, ceramic specimen's frozed with IPA/Dry Ice (**B**) at different temperatures, confirms the formation anorthite –feldespar- (marker as *f*) and mullite crystal from the addition of the pre-fired material molochite, the presence of Fe confirms that the material is molochite (marked as *m*). It can be seen from Figure 5.23 the amount of K-feldespar is melting and a glassy phase is also appearing.

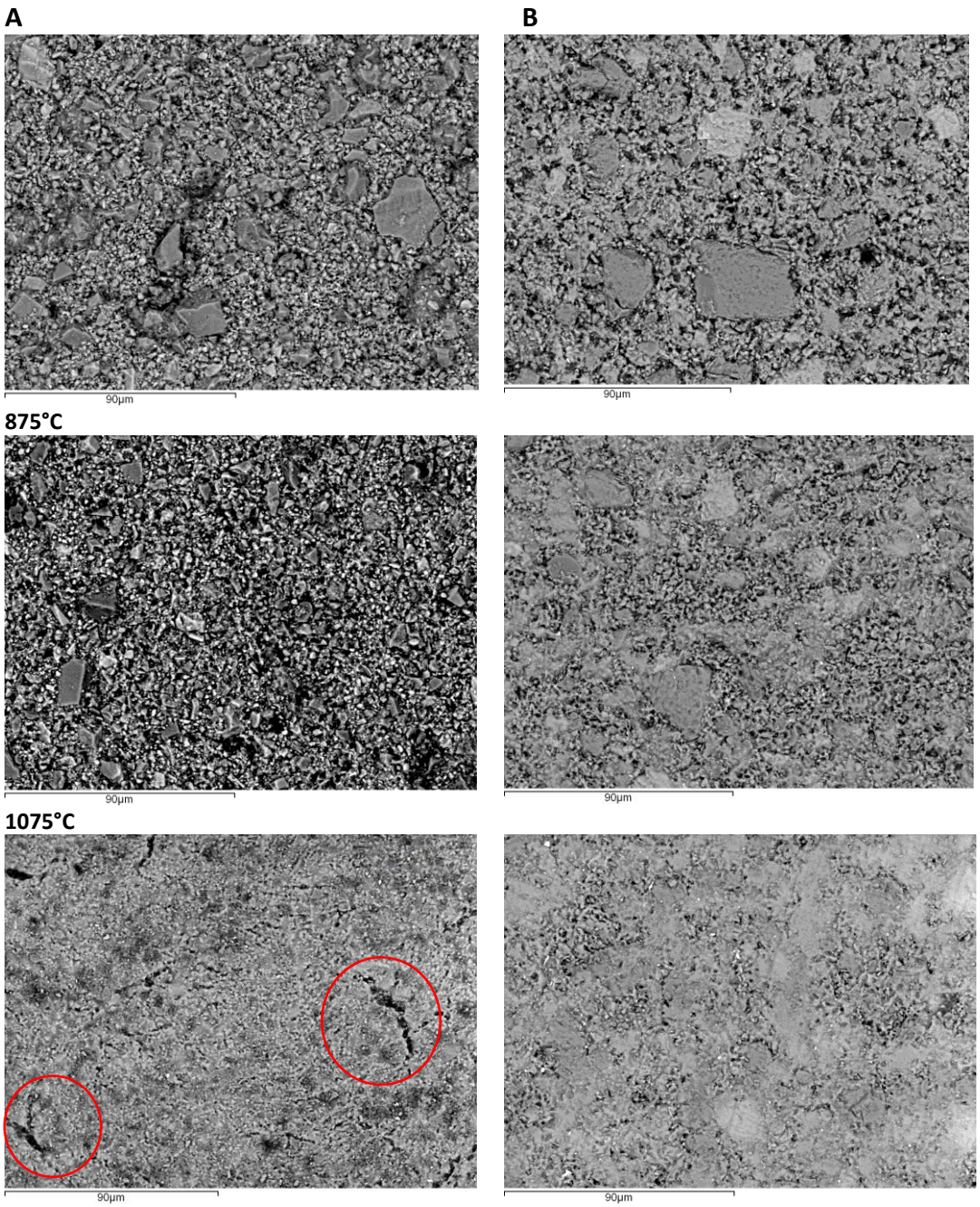

Figure 5.20: SEM micrograph of microstructure, showing the evolution of the microstructure of the fired specimens to different temperature (875°C, 1075°C, and 1150°C). **A** Liquid Nitrogen, **B** IPA/Dry Ice.

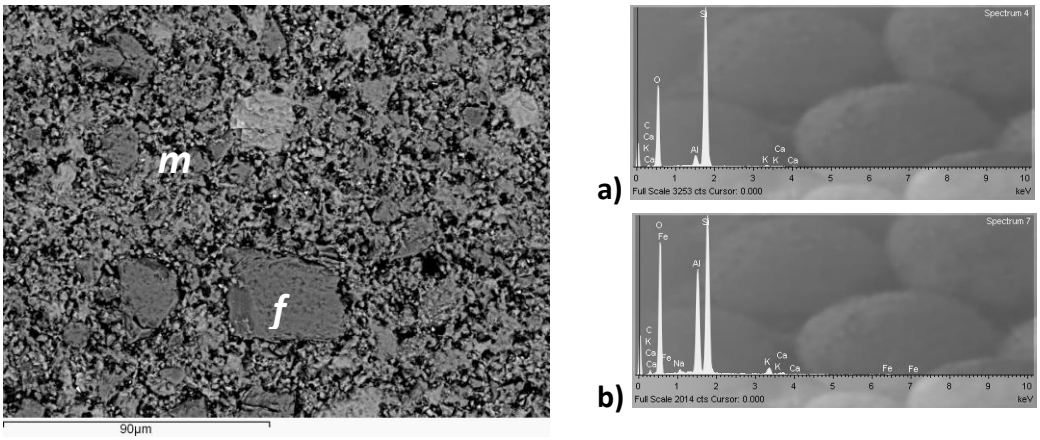

Figure 5.21: SEM micrographs of a ceramic specimen sintered at 875 ◦C showing **(a)** anorthite (feldespar) and **(b)** mullite(molochite) labelled as ***f*** and ***m*** respectively **(left).** EDS spectra obtained from (C) anorthite and (D) mullite crystals**(right)**.

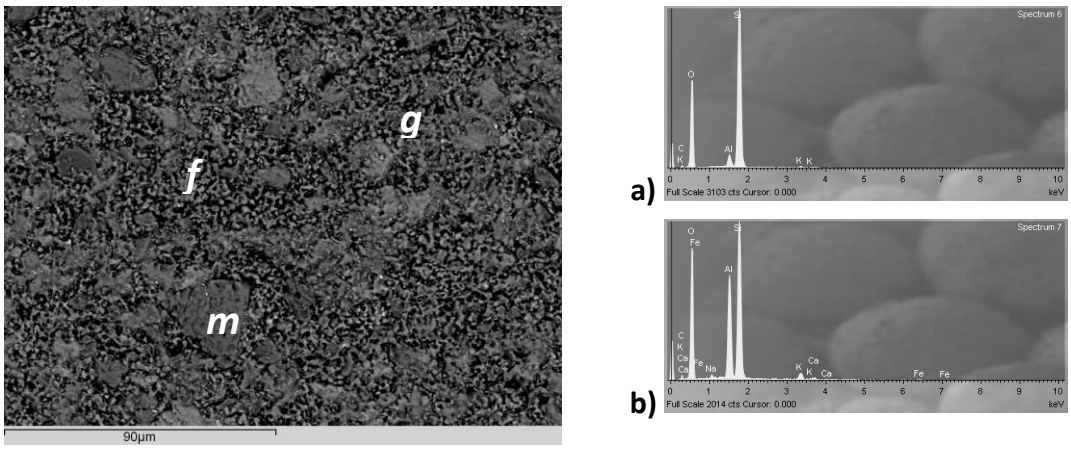

Figure 5.22: SEM micrographs of a ceramic specimen sintered at 1075 ◦C showing **(a)** anorthite (feldespar), **(b)** mullite(molochite) labelled as f and m respectively and g as a glassy phase **(left)** EDS spectra obtained from (C) anorthite and (D) mullite crystals**(right)**.

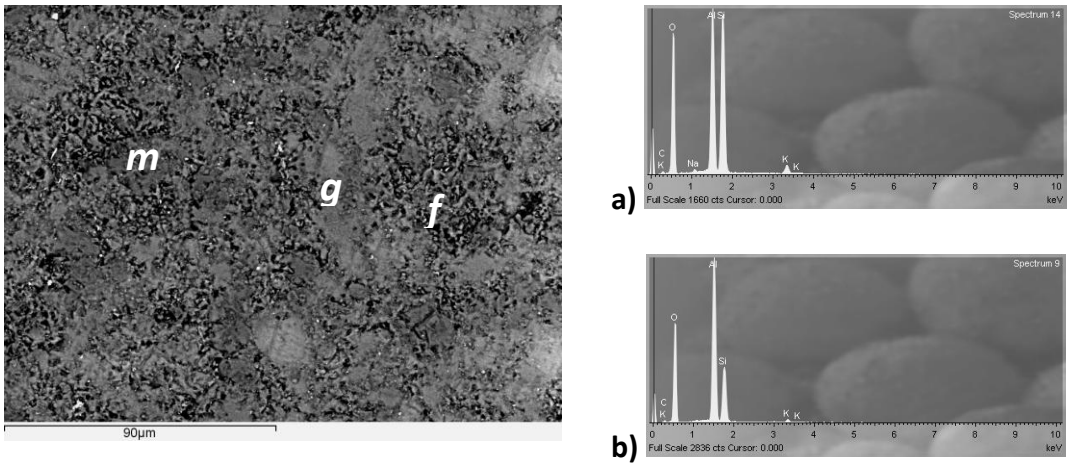

Figure 5.23:SEM micrographs of a ceramic specimen sintered at 1150 ◦C showing **(a)** anorthite (feldespar), **(b)** mullite(molochite) labelled as f and m respectively and g as a glassy phase **(left).** EDS spectra obtained from (C) anorthite and (D) mullite crystals**(right)**.

5.4 SUMMARY OF FINDING FOR CHAPTER 5

The final formula **NPP-3** was tested to assess its behaviour with different freezing rates and different firing temperatures. The samples produced were tested according to the ASTM standards and the results generated were analysed. The linear shrinkage of the **NNP-3** increased from 1.8 % (linear shrinkage of the **NPP-1**) to 6.78 % and 5.4% for the liquid nitrogen and dry ice/IPA respectively. As the linear shrinkage increases, the water absorption and thus the apparent porosity decreases.

It was found that the sublimination of the ice crystal created an open macroporosity with a dendrintic structure. It was found that the faster freezing rate given by liquid nitrogen leads to the formation of smaller pores (1-2µm) whereas the dry ice/IPA resulted in larger pores (0.5-1 µm). The freezing regime made a negligible difference to the apparent porosity, and density of the ceramic specimens.

The effect of the sintering temperature on the porous macrostructure of the ceramic specimens was clearly indicated by the results of the trials. As the firing temperature was increased the apparent porosity of the samples dropped (for both liquid nitrogen and dry ice/IPA processed samples. The mechanisms involved in the formation of porosity during the firing process were presented in Chapter 4 (loss of remaining moisture through the glassy phase of the flux material that bonds together the remaining components). During the sintering process, any microporosity was

removed from the ceramic specimens; however, the macroporosity resulting from the solvent (sol in this study) remained.

As can be seen in XRD test data, the test shows the main reaction of the components to different temperatures on firing ceramic specimens. Basically, the partial or full desolution of the components are observed as a reaction to the temperature change. Among the three components within the formulation, quartz and feldspar had the most notable changes observed, which can be seen clearly in the Figure 5.16: the quartz dissolves partially while the feldspar reaches the fully liquid phase at the highest temperature, causing a pyroplastic deformation.

6. RHEOLOGY & EXTRUSION TRIALS

In this chapter the basic extrusion parameters of the new developed material; **NPP-3,** (pressure, velocity flow rate measure etc) and rheological properties are presented and discussed.

6.1 RHEOLOGY TRIALS

To help understand the rheological behaviour of the material, trials were conducted to see if the material developed in the project conformed to any of the common "models" of rheological behaviour (as shown in Figure 6.1).

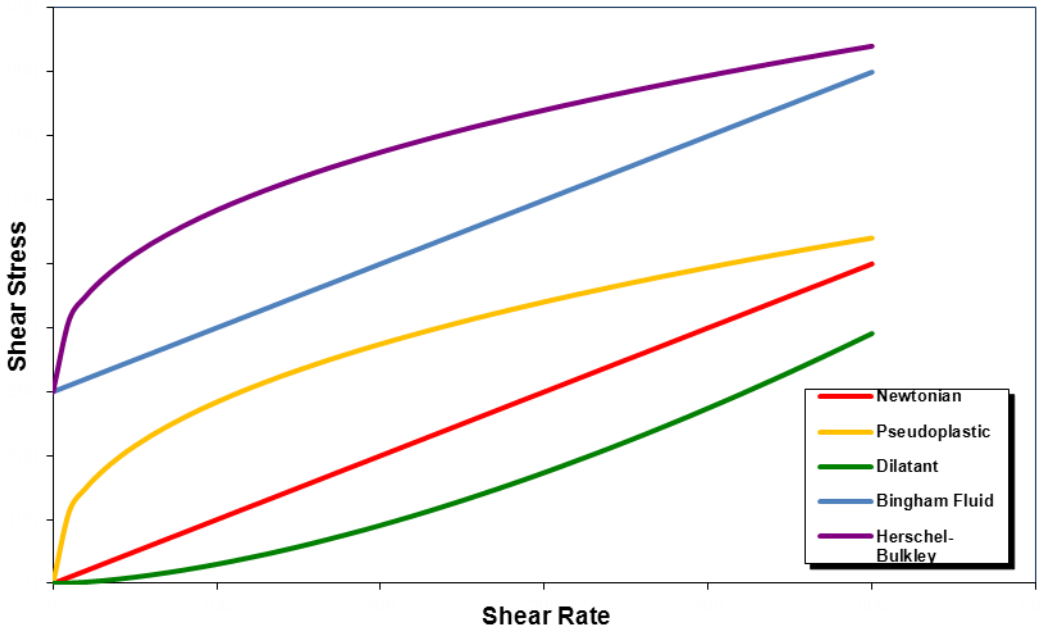

Figure 6.1: Rheogram of ideal shear flow

Viscosity is one of the most important rheology parameters. The viscosity of the suspension is typically obtained by measuring the shear stress at different shear rates. The ratio of these two values (shear stress and shear rate) is defined as viscosity (for Newtonian fluids), when the measurement is applied to non-Newtonian fluids it is described as apparent viscosity. For the direct write process the material must not be too viscous otherwise it will be impossible to extrude, whilst a very low viscosity could make it impossible for the extruded bead to support the next layer of material.

6.1.1 Cone & Plate Trials

In order to understand the rheological properties of the material it was decided to perform a series of experimental trials based on conventional rheological test methods. The first method investigated was the "cone and plate" method. Samples of slurry were placed in a Bolin CVO120 cone & plate rheological unit (see Figure 6.2). This equipment is widely used for the characterization of viscous inks but proved to be entirely unsuitable for the slurry material (influence of relatively coarse particles, very high viscosity and also drying of the slurry occurred).

Figure 6.2: Bohlin CV0120 cone & plate rheometer

6.1.2 Concentric Cylinder Trials

In a second series of trials basic rheological characterisation of the suspension was performed (by Rhealto Ltd) using a rheometer (Brookfield RS) fitted with 14mm diameter concentric cylinder system operated at constant temperature of 21 °C +/- 0.2°C (see Figure 6.3). This apparatus allows the measurement in a control rate mode, (CR mode) that measures the shear stress (τ) imposed on the suspension when the velocity gradient or shear rate (γ) changes. The ratio between both parameters defines the viscosity (η).

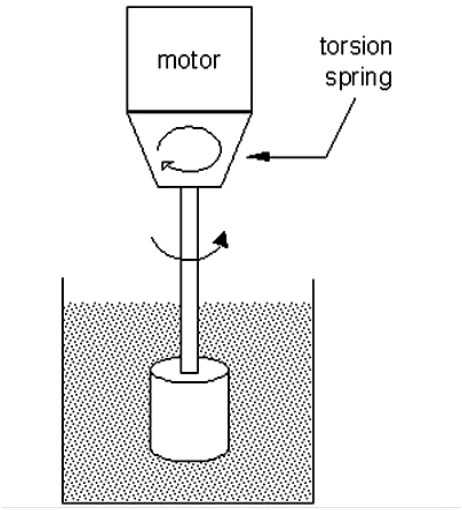

Figure 6.3: Schematic diagram of a Brookfield-type viscometer[160].

The material was subjected to increasing shear rates (5 to 500s^{-1}) and the viscosity was recorded after 600s of shearing at each shear rate. The results of this trial are shown in Table 6.1 and also plotted as graphs in Figure 6.4 and 6.5.

Shear rate (1/s) ($\dot{\gamma}$)	**Shear Stress (Pa)** (τ)	**Viscosity (Pa.s)** (η)
5	53.23	10.645
10	34.00	3.4
20	52.24	2.612
50	117.10	2.342
100	192.50	1.925
200	404.40	2.022
500	1156.00	2.312

Table 6.1 Results of concentric cylinder rheological test on NPP-3

Note: figures highlighted in yellow are in the shear rate range used in the extrusion trials

It can be seen in Table 6.1 that the sample shows a complex combination of shear-thinning and thixotropic behaviour as well as some shear-thickening behaviour in the final stages of the trials. There is significant evidence from the literature [161, 162] that viscous slurry materials exhibit shear thinning behaviour, as observed in these trials. There was some slight evidence of shear thickening towards the end of the trial, although this was rather insignificant compared to the shear thinning through the majority of the trial.

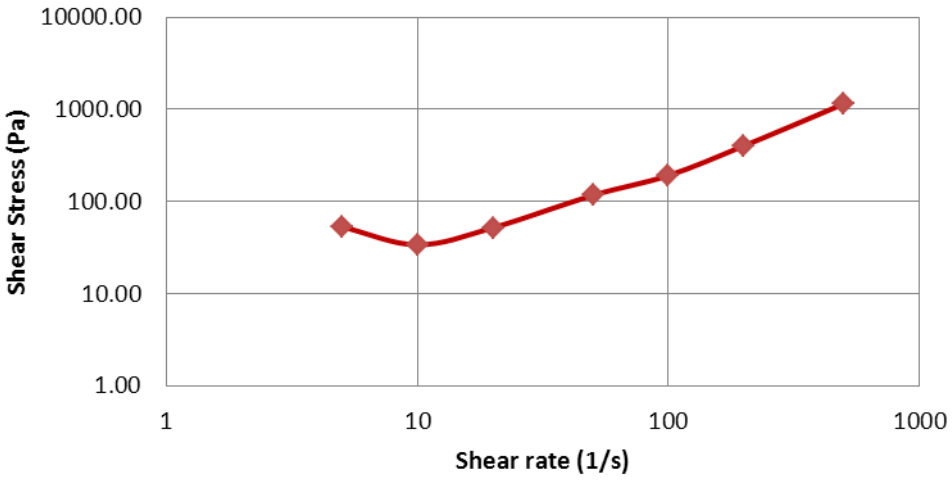

Figure 6.4:Shear rate Vs Shear stress for NPP-3

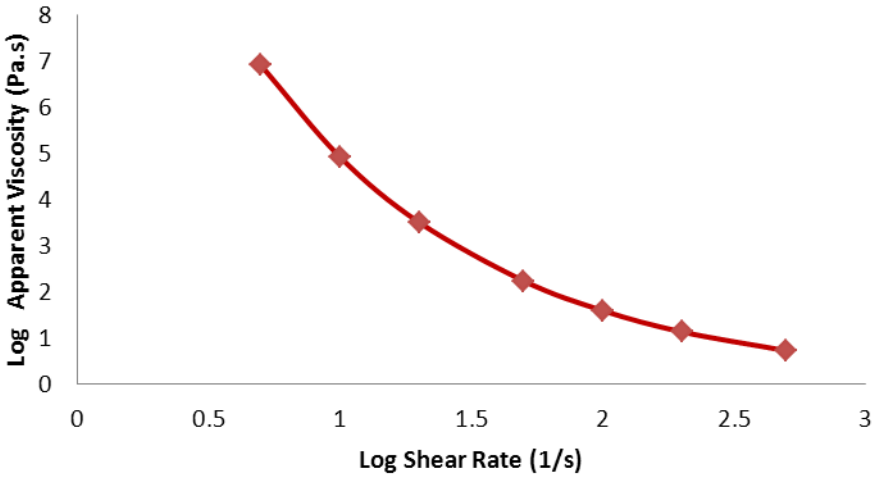

Figure 6.5: Viscosity v.s. shear rate.

From Figure 6.5 it is clear that the material exhibits a non-Newtonian shear flow, complying with the general Herschel–Bulkley fluid model (Figure 6.4), where the shear stress experienced by the fluid is related to the strain in a complex, non-linear way.

Utilising the information from the viscosity test, the following rheology parameters were studied; viscosity, power law index "n", yield stress, and constant number 'K' (also known as the Consistency Index). Each of these parameters is described in the following section.

In general, when ceramic slurry materials have been considered rheologically, they have been found to be shear thinning or pseudoplastic fluids. That is also the case of

this research project, the main characteristic of the pseudoplastic fluid is that the viscosity decreases when the shear rate increases.

A fluid described as a pseudoplastic fluid or a fluid whose viscosity decreases as shear rate increases can fit the power-law mathematical equation. Power-law fluids can be described mathematically as follows:

$$\tau = K(\gamma)^{n} \tag{6.1}$$

Where τ is shear stress, γ is shear rate, n is exponent (flow behaviour index) and K is a constant (consistency index). To calculate the power low index n and the constant K, the log shear rate and log shear stress was calculated with the data given before; when "n" is represented as the slope and "K" and the intercept using a linear regression method. Table 6.3 shows the value of "n" and the value of the constant "K".

Log shear rate (1/s) (γ)	**Log shear stress (Pa)** (τ)	**Viscosity (Pa.s)** (η)
0.699	1.726	6.909
1	1.531	4.922
1.301	1.718	3.507
1.699	2.069	2.239
2	2.284	1.596
2.301	2.607	1.137
2.699	3.063	0.726

Table 6.2 Shear rate, log shear rate, log shear stress and viscosity for NPP-3

Slope n	0.895
Intercept log K	0.571
K	3.725

Table 6.3 n and K values for NPP-3

The n value (0.895) being below unity indicates that the material is non-newtonian and the K value of 3.725 indicates that the material is fundamentally pseudoplastic in nature.

6.1.2.1 Time Dependency

To establish if there was any evidence of time dependency the following trial was performed using the 14mm diameter concentric cylinders fitted to a Brookfield RS rheometer. The material (**NPP-3**) was subjected to constant shearing at 100s-1 for 10 minutes, taking readings of viscosity every 30s and this enabled a viscosity/shearing time profile to be generated (see Figure 6.6).

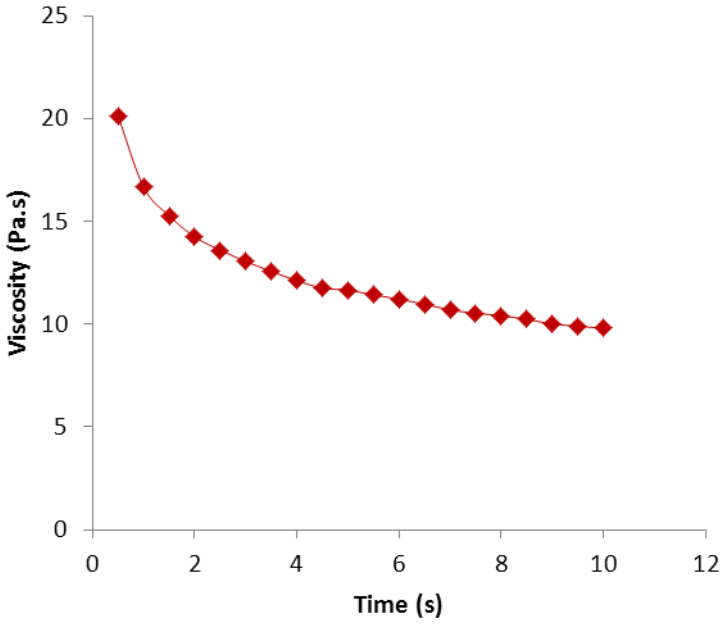

Figure 6.6: Viscosity/Time profile for NPP-3

It is clear that over the course of the trial the viscosity drops with time. This confirms that the material exhibits a time dependant viscosity, thixotropic behaviour. However, we are particularly interested in the increase in viscosity after the material has been extruded, in order that the deposited bead retains its required shape.

Thixotropic behaviour means the reduction in structural strength during the shear load phase and the more or less rapid but complete structural regeneration during the subsequent rest phase[161].

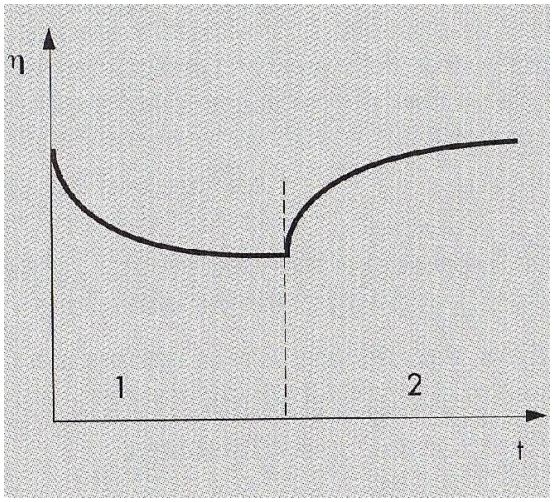

Figure 6.7: Viscosity curve for a thixotropic material (1) time-dependent structural decomposition under constant shear and (2) time-dependent structural regeneration when at rest[161].

Perhaps a more effective test approach, on reflection, would be to allow the material to rest after shearing to establish if the material recovers its original viscosity and over what time period (see Figure 6.6). Ideally a rapid "recovery time" is desirable to maximise the deposition rate of the ***DWFC*** system. However, based on Figure 6.7 it can be deduced that the material will recovers 75% of its original viscosity value within 2 seconds of extrusion. This is discussed in more detail in the Further Work Section of this thesis (see Chapter 7).

6.1.3 Findings – Rheology Trials

Although these trials have shed light onto the rheological properties of the slurry material the behaviour of the material during extrusion may differ significantly due to the fundamental differences between the way in which the material is "worked" in the concentric cylinder and extrusion trials (in the former, for example, all of the material under test is subjected to relatively high levels of shear stress whereas in the later the bulk of the material is subjected to low levels of shear until it passes close to and through the nozzle).

6.2 EXTRUSION TRIALS

The ***DWFC*** system built at De Montfort University to undertaken the extrusion trials, is a micro extrusion machine that works with a positive dispensive (displacement) system to extrude the slurry material through a fine nozzle, in this system the linear motion of a motor-driven plunger is employed to force the fluid out of the needle. Given that the slurry has a solid content of 75.47 w % it is more of a paste than a slurry. To provide a fine extrudate of crowded particles requires an accurate extruder, precise control of the head velocity and extrusion ram velocity, as well as an optimal preparation of the feed material.

The driving mechanism utilised by for AM ceramics extrusion systems (see literature review section 1.1.5); air pressure dispensing (RepRap, Slip jet printer), rotary screw

(FFEF, contour crafting) and positive-displacement (extrusion freeform fabrication robocasting) see Figure 6.8 for descriptions of these mechanisms.

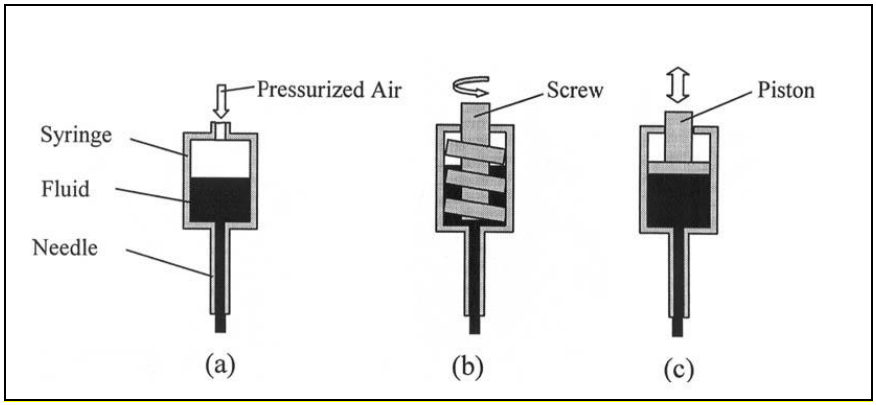

Figure 6.8: Alternative dispensing mechanisms for AM of ceramics

Positive displacement offers clear advantages being a true volumetric dispenser, where the deposition of the extrudate depends only on the linear movement of the plunger and not the properties of the dispensed fluid. However, this is not entirely valid for small volume of fluid [163], this is considered one of the major problems occurring in the positive-displacement dispensing process. Thus different authors states 6 parameters which influence the deposition of the material.

1. Pressure in the syringe.
2. Flow Rate of fluid dispensed.
3. Dispensing time.
4. Fluid level in syringe.
5. Fluid flow behaviour.
6. Fluid compressibility.

*6.2.1 **DWFC** Test Rig*

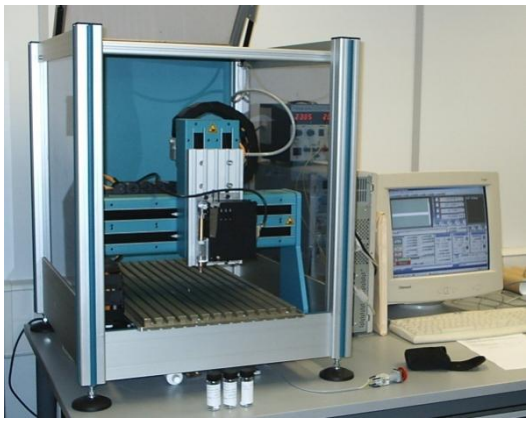

Figure 6.9: ***DWFC*** test rig with close up of DC stepper motor driven syringe pump inset.

The extrusion head consists of a DC Stepper motor-driven syringe pump (see Figure 6.9) fastened to 14mm diameter plunger (PTFE head) sitting inside a 14.5mm diameter stainless steel syringe. Nozzles of different sizes can be attached to the end of the syringe. The extrusion head is mounted onto an actuation unit enabling it to be moved in X,Y and Z. The extruded pattern is defined by the X,Y movement of the head which is moved in Z to enable additional layers to be deposited, to create a 3D structure.

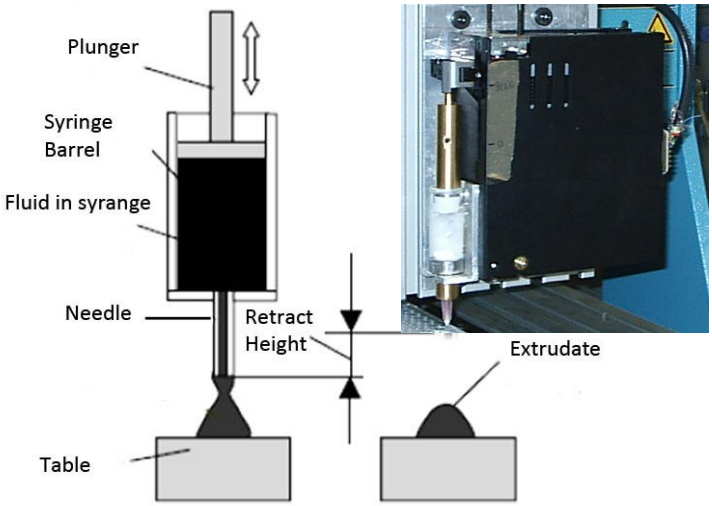

Figure 6.10: Schematic Extrusion Device

6.2.2 Extrusion Parameters

As the plunger is depressed by the syringe pump, pressure is applied to the slurry and a fine bead is extruded which touches the build platform and is subsequently solidified by freeze casting. The speed of the syringe pump determines the rate at which the slurry is extruded, as defined in the Table 6.4.

Plunger Speed		**Deposition Rate (mm^3/s)**
mm/min	**mm/s**	
1.5	0.025	4.1853
1.98	0.033	5.5247
2.46	0.041	6.8640
3.00	0.050	8.3707
3.48	0.058	9.7101

Table 6.4 Deposition rate for different stepper motor speeds

The nozzles used in the trials were standard syringe tips, connected to the syringe using a Luer™ fitting, which were adapted by shortening the length. The three nozzles used in the trials were measured using a digital calliper (0.01mm resolution) and a travelling microscope. Each length and internal diameter was measured 5 times and the results are shown in the appendix. The measured internal diameters were compared with the values quoted by the manufacturers and found to closely correlate. The mean values are shown in Table 6.5.

	Small	Medium	Large
Internal diameter (mm)	0.7	0.9	1.2
Length (mm)	6.54	8.09	5.89

Table 6.5 Nozzle size (internal diameter) and length (mm)

These trials were all conducted using the same material formulation and preparation method (as defined in Chapter 4)

6.2.3 Shear Rate Calculation

For a Newtonian fluid the shear stress and shear rate can be calculated as follows;

$$\sigma = \frac{\Delta P}{2(RL)} \tag{6.2}$$

Where **σ** is the shear stress at the barrel wall; **ΔP** is the pressure drop across the barrel; **L** is the length of the barrel; and **R** is the radius of the capillary. The apparent shear rate will be calculated with the following formula;

$$\gamma_a = \frac{4Q}{\pi r^3} \tag{6.3}$$

Where γ_a is apparent shear rate; **Q** is the volumetric flow rate; **R** is the radius of the capillary. Most ceramic materials are considered non Newtonian fluids, where viscosity is dependent to a greater or lesser extent on the shear rate.

The flow rate (**Q**), apparent shear rate (γ_a) were calculated for each nozzles size and plunger velocity and are shown in Table 6.6.

Plunger velocity v (mm/s)	**Q (mm^3/s)**	**γ_a (1/s) Small**	**γ_a (1/s) Medium**	**γ_a (1/s) Large**
0.025	4.1853	124.2887	58.47876	**24.6920**
0.033	5.5247	164.0641	77.19342	**32.5941**
0.041	6.8640	203.8366	95.90668	**40.4955**
0.050	8.3707	248.5803	116.9589	**49.3846**
0.058	9.7101	288.3558	135.6736	**57.2867**

Table 6.6 plunger velocity and apparent shear rate

6.2.4 Extrusion characteristics of the proposed material

The extrusion parameters were determined based on the results of a series of extrusion trials. These trials were not performed on the ***DWFC*** test rig, instead the syringe was mounted into a universal testing machine (see methodology chapter for details of the machine) using a specially designed fixture (see Figure 6.11). Using this approach it was possible to measure and record the load on the plunger as it is displaced. The same formulation (**NPP-3**) was used throughout these trials but different plunger speeds (1.5, 2, 2.5, 3, 3.5mm/min) and nozzle diameters (small=0.7mm, medium=0.9mm and large=1.2mm) were used.

The equipment set-up consists of four main components;

1. Syringe Barrel, 14.52 mm internal diameter and 30 mm in length.
2. Rigid support housing to allow free access to the extrudate and also easy removal of the syringe.
3. Interchangeable nozzles with different diameters (1.5-3.5mm).
4. Plunger 14.52mm in diameter fitted with a PTFE head to maintain low friction with the internal bore of the syringe.
5. Universal tensile test machine fitted with a 250N load cell.

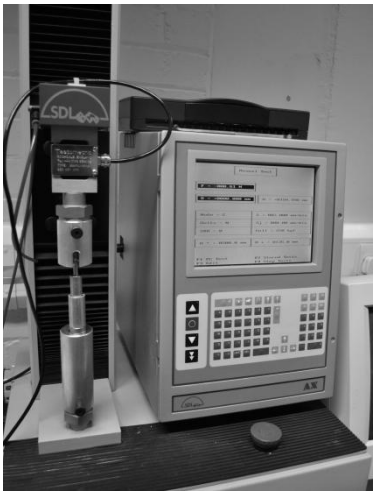

Figure 6.11: Extrusion rheology test rig

The material was prepared with the same formulation and procedure as described in Chapter 5. The prepared paste was placed inside the barrel, the plunger was fitted and the assembly then was positioned in to the support housing which was already mounted onto the tensile testing machine. The plunger was displaced into the syringe at the required velocity and the force on the plunger (N) was recorded over the 30mm of travel. To characterise the slurry, five speeds, corresponding to the range of extrusion rates used on the ***DWFC*** test rig, and three different nozzles diameters were used (see Table 6.8 for the test matrix for the trials). Each trial was repeated three times. In order to correct for friction between the plunger and sidewall of the syringe and the load required to extrude the slurry material through the aperture of the syringe and "dead space" prior to the actual nozzle, a series of trials were performed without the nozzle in place. As with the main extrusion trials

five plunger velocities were used and the same formulation and method of preparation was used.

mm/min	Nozzle diameter	Nozzle diameter	Nozzle diameter
1.5	Small (S-trial 1,2,3)	Medium (M-trial 1,2,3)	Large (L-trial 1,2,3)
2.0	Small (S-trial 1,2,3)	Medium (M-trial 1,2,3)	Large (L-trial 1,2,3)
2.5	Small (S-trial 1,2,3)	Medium (M-trial 1,2,3)	Large (L-trial 1,2,3)
3.0	Small (S-trial 1,2,3)	Medium (M-trial 1,2,3)	Large (L-trial 1,2,3)
3.5	Small (S-trial 1,2,3)	Medium (M-trial 1,2,3)	Large (L-trial 1,2,3)

Table 6.7 Experimental matrix

The total distance of travel for the plunger was 30mm but the first 5mm of travel was disregarded to avoid variation due to “heaping” of the slurry in the syringe. Moreover, the last 5mm of travel was also disregarded as the plunger is very close to the base of the syringe. Therefore all data is shown for 20mm of plunger travel.

A total of 45 experiments were conducted, using five extrusion velocities with three different nozzle size (**S,M,L**) the results are shown in the Table 6.8. For the small nozzle at the two higher velocities it was not possible to successfully extrude the material. It was found that the material as the extrusion force exceeded the safe working load of the syringe pump causing the motor to stall.

Nozzle size	Plunger Speed (mm/min)				
	1.5	2	2.5	3	3.5
Small	Y	Y	Y	N	N
Medium	Y	Y	Y	Y	Y
Large	Y	Y	Y	Y	Y

Y= successful extrusion
N= extrusion not possible

Table 6.8 Result of extrusion experiments different nozzle size at different speed

The force (N) on the plunger was recorded over its entire travel. An example of the original data plotted from the machine is show in Figures 6.12.

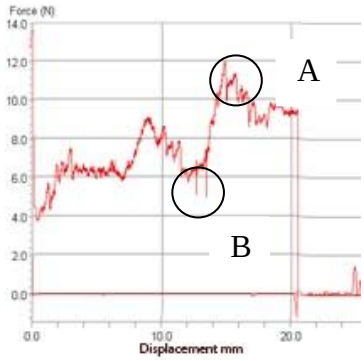

Figure 6.12: Plunger force vs plunger displacement (deflection) for NPP-3 using 0.9mm nozzle at 2.5mm/min plunger velocity.

All of the data collected shows characteristic features to a greater or lesser extent. Firstly, there is evidence of upward spikes (rapid rise and fall) in the pressure, probably due to temporary blockage of the nozzle due to agglomerates (A on Figure 6.12). There are also downward spikes (rapid fall and rise) in the pressure probably due to air bubbles passing through the nozzle (B on Figure 6.12). There was also a

general periodic rise and fall in the pressure, typically over 5-6mm distance (see points A and B in Figure 6.12) which have been due to the formation of slip planes within the material[142, 162]. Finally, there was an overall increase in the force as the plunger moves inside the syringe – this was shown for all tests. These results are discussed in more detail below.

Transient Pressure Rise: These pressure spikes are probably due to temporary blockage of the nozzle by soft agglomerates. Soft agglomerates form in the barrel of the syringe and these block the nozzle but are then broken up as the pressure increases and the material passes through the nozzle[164]. The force breakdown caused by soft agglomerates cannot be predicted as the formation and size of agglomerate is unpredictable size and also their break down occurs in a random fashion.

Transient Pressure Drops: Based on information from the literature the presence of air bubbles is the most likely cause of transient falls in pressure. Although every care was taken to reduce the risk of air inclusions during the mixing of the material and its subsequent transfer to the syringe it is virtually impossible to remove all air bubbles. The use of vibration during the mixing process encourages air bubbles to rise to the surface of the mixture and thus be removed. However, it is much more difficult to avoid “folding” air into the mixture during transfer to the syringe and the application of vibration is far less efficient at removing air under these circumstances. Based on

the literature the air bubbles can congregate and combine as they approach the entrance to the nozzle resulting in a sudden pressure drop [164].

The transient pressure spikes were removed from the original data before taking the mean of the three successive runs at each condition. The results are shown in Figures 6.13, 6.14 and 6.15.

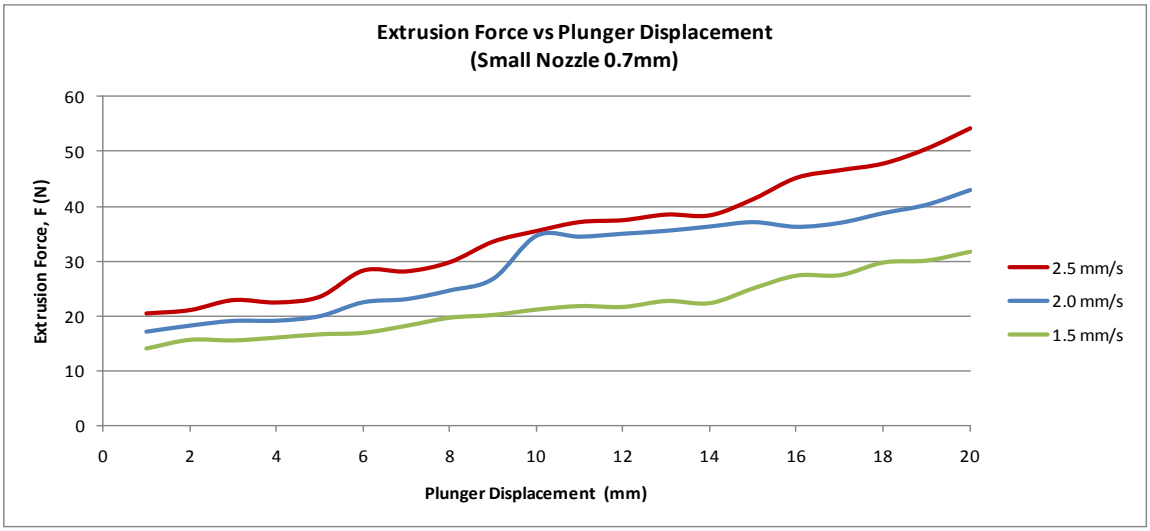

Figure 6.13: Extrusion force Vs Plunger displacement for small nozzle (S-Trials 1,2,3)

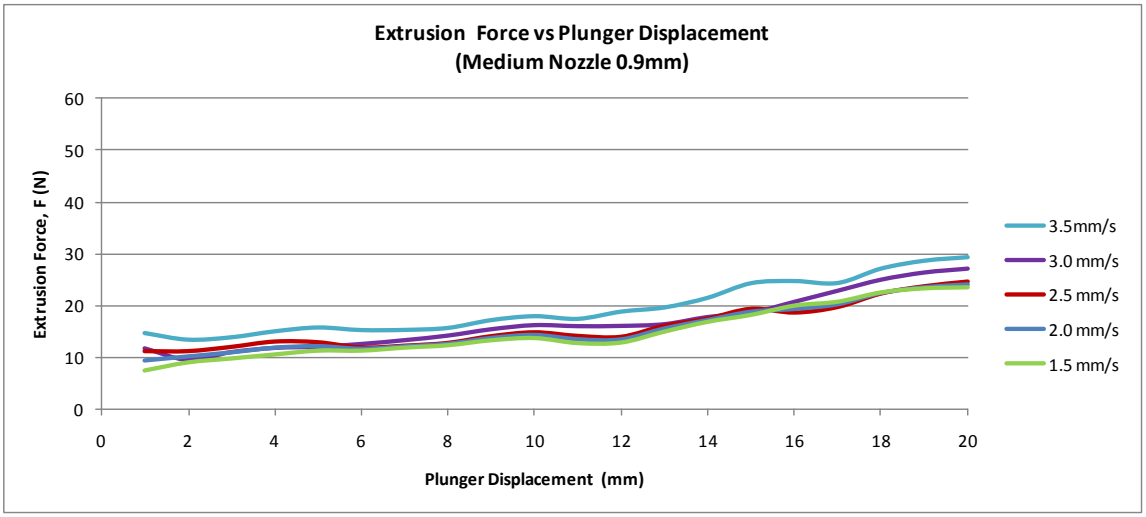

Figure 6.14: Extrusion force Vs Plunger displacement for medium nozzle (M-Trials 1,2,3)

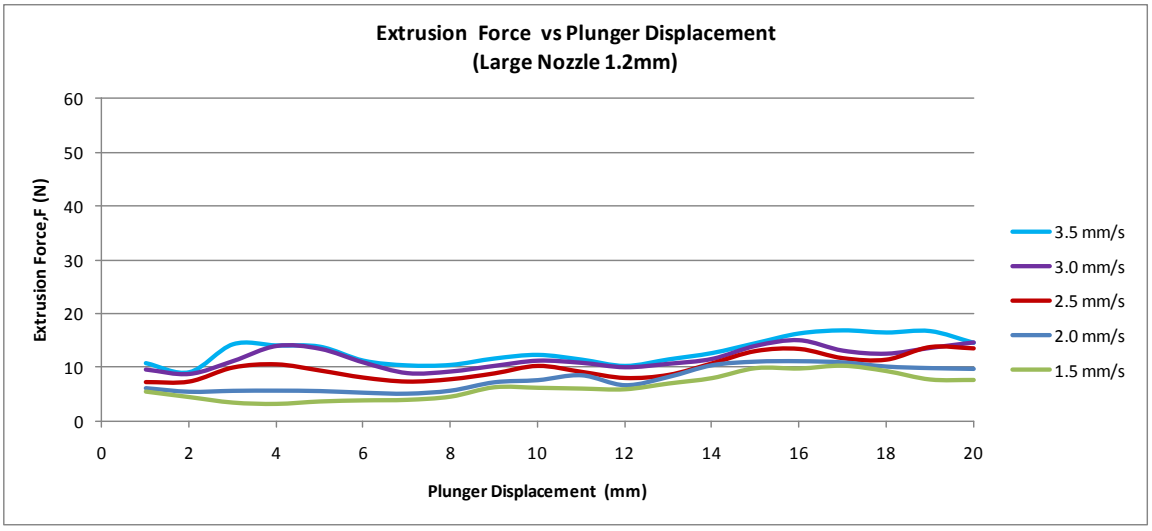

Figure 6.15: Extrusion force Vs Plunger displacement for large nozzle (L-Trials 1,2,3)

Perturbations are more clearly seen in the results for the large nozzle where the overall pressure is low in comparison to the medium and small nozzles thus making the effect more significant in relative terms.

Having obtained the results for the syringe fitted with the different nozzles the trials were repeated with the nozzles removed to provide the extrusion force for the syringe alone. The influence of speed proved to be relatively small and so for simplicity the mean of the force across the different plunger speeds was calculated for each plunger displacement. Using this data the correction factor (load) at each displacement was calculated by linear regression, to remove the influence of perturbations in the system. The correction factor varied between 2 and 5N (see Table 6.9)

Plunger Displacement (mm)	Correction factor (N)
1	2.03
2	2.18
3	2.33
4	2.47
5	2.62
6	2.77
7	2.92
8	3.07
9	3.21
10	3.36
11	3.51
12	3.66
13	3.81
14	3.95
15	4.10
16	4.25
17	4.40
18	4.55
19	4.84
20	4.99

Table 6.9 Correction factor for different plunger displacements

The correction factor was subtracted from the data collected for each nozzle to give the graphs shown in Figures 6.16, 6.17, 6.18. It reduced the offset and slope of the

lines slightly and only makes a significant effect for the large nozzle and slow plunger velocities.

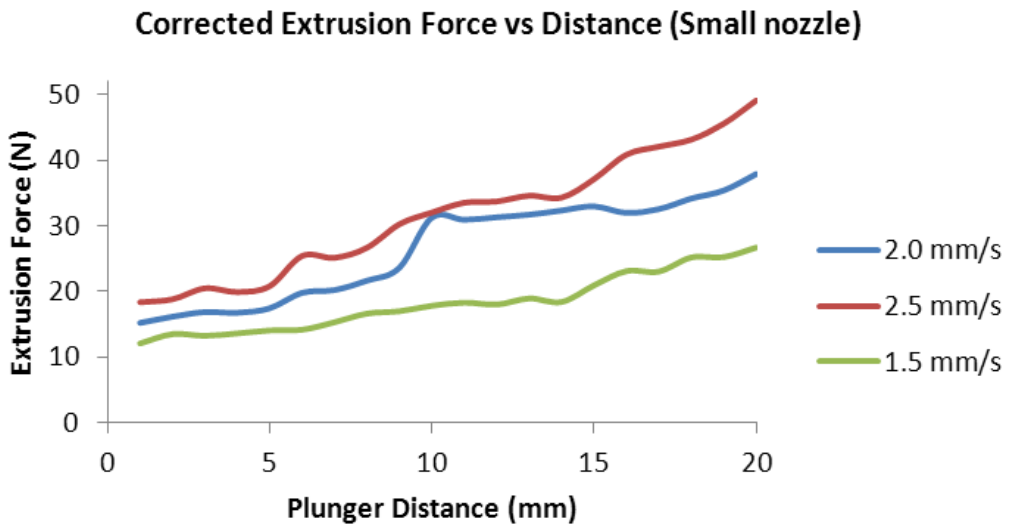

Figure 6.16: Corrected extrusion force Vs Plunger displacement for small nozzle (S-Trials 1,2,3)

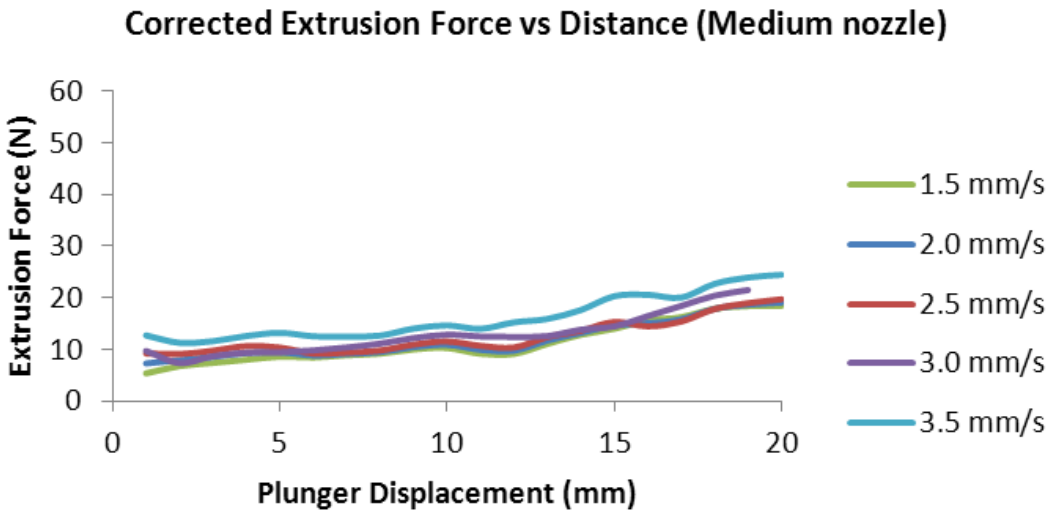

Figure 6.17: Corrected extrusion force Vs Plunger displacement for medium nozzle (M-Trials 1,2,3)

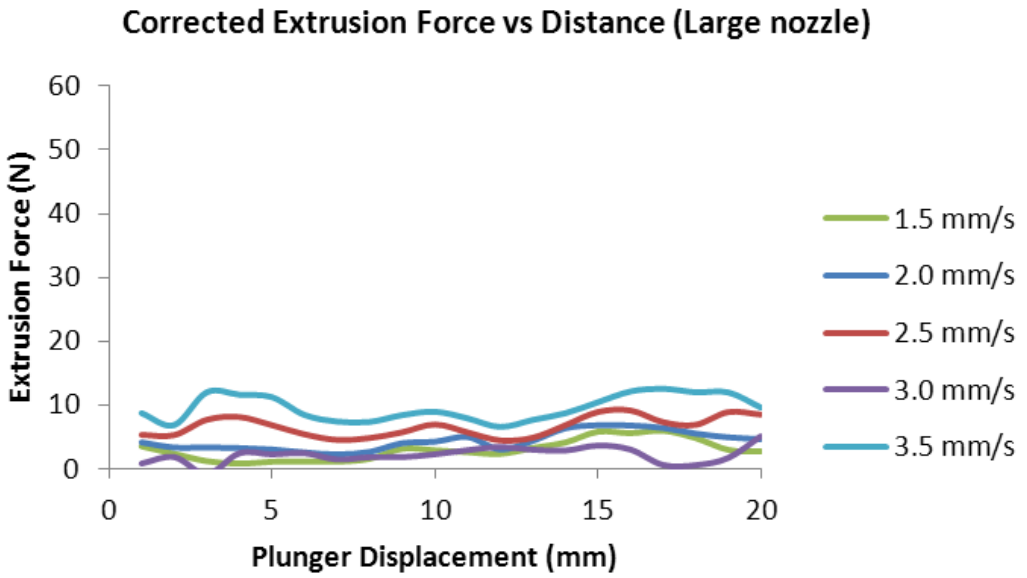

Figure 6.18: Extrusion force Vs Plunger displacement for large nozzle (L-Trials 1,2,3)

The extrusion force was then converted to extrusion pressure and plotted against plunger displacement (as shown in Figures 6.19 to 6.23)

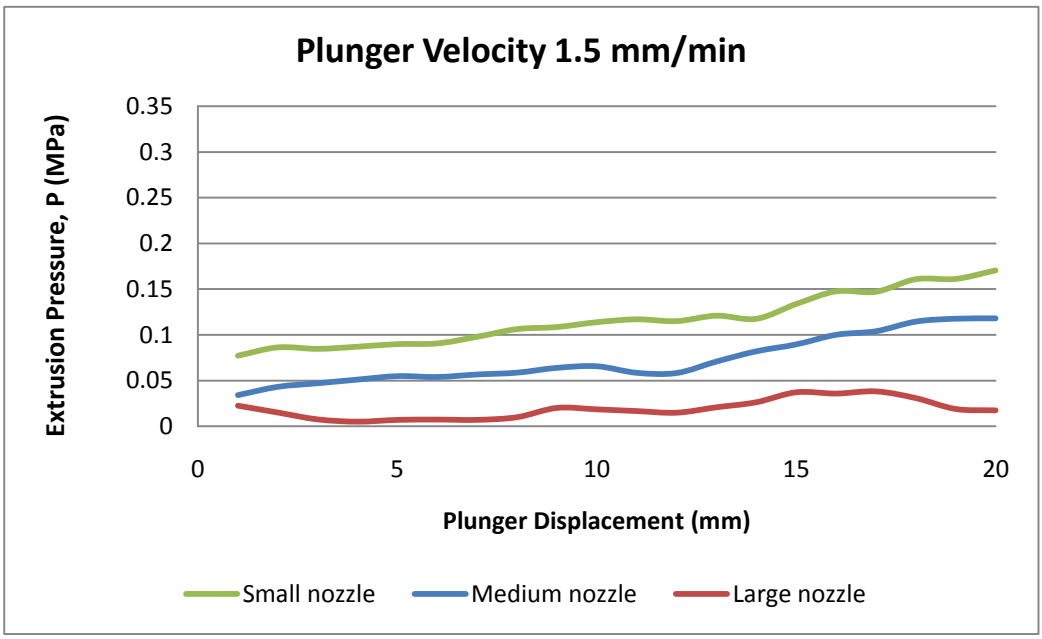

Figure 6.19: Extrusion pressure vs. plunger displacement for small, medium and large nozzles at 1.5mm/min plunger velocity

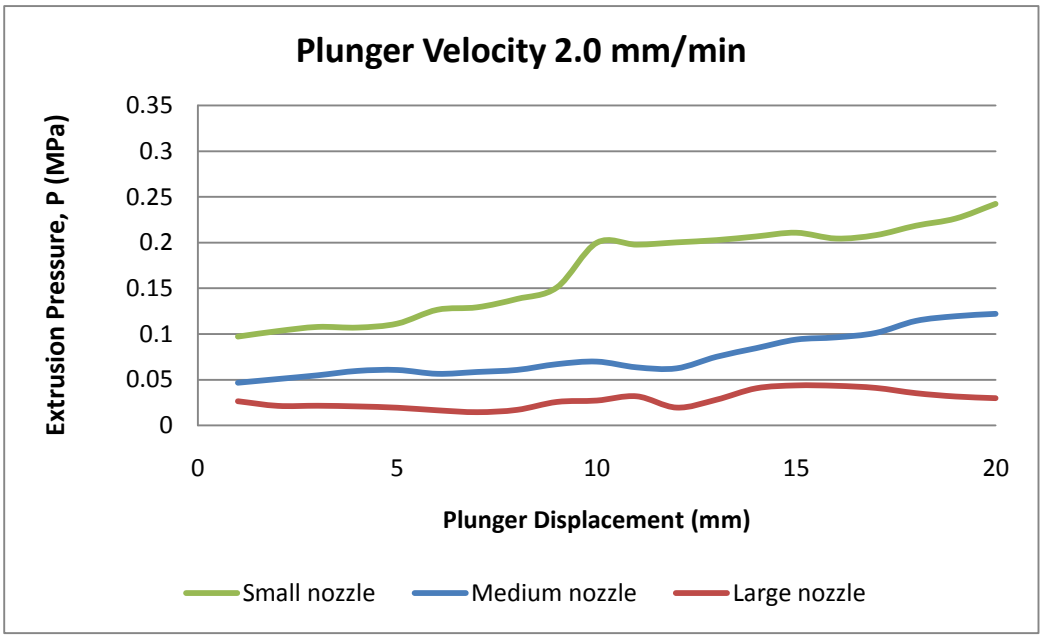

Figure 6.20: Extrusion pressure vs. plunger displacement for small, medium and large nozzles at 2.0mm/min plunger velocity

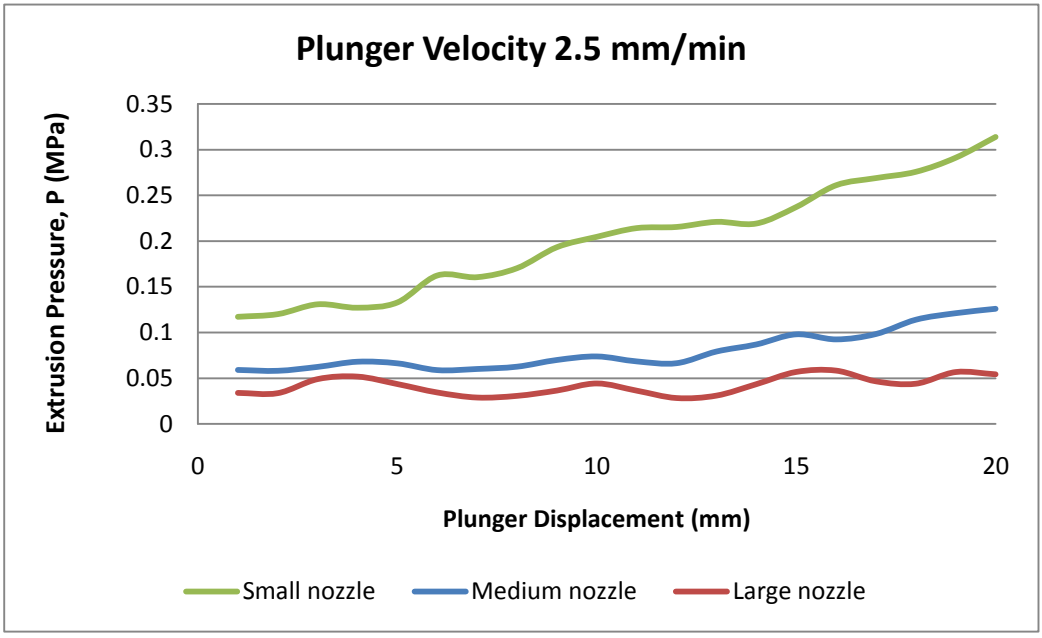

Figure 6.21: Extrusion pressure vs. plunger displacement for small medium and large nozzles at 2.5mm/min plunger velocity

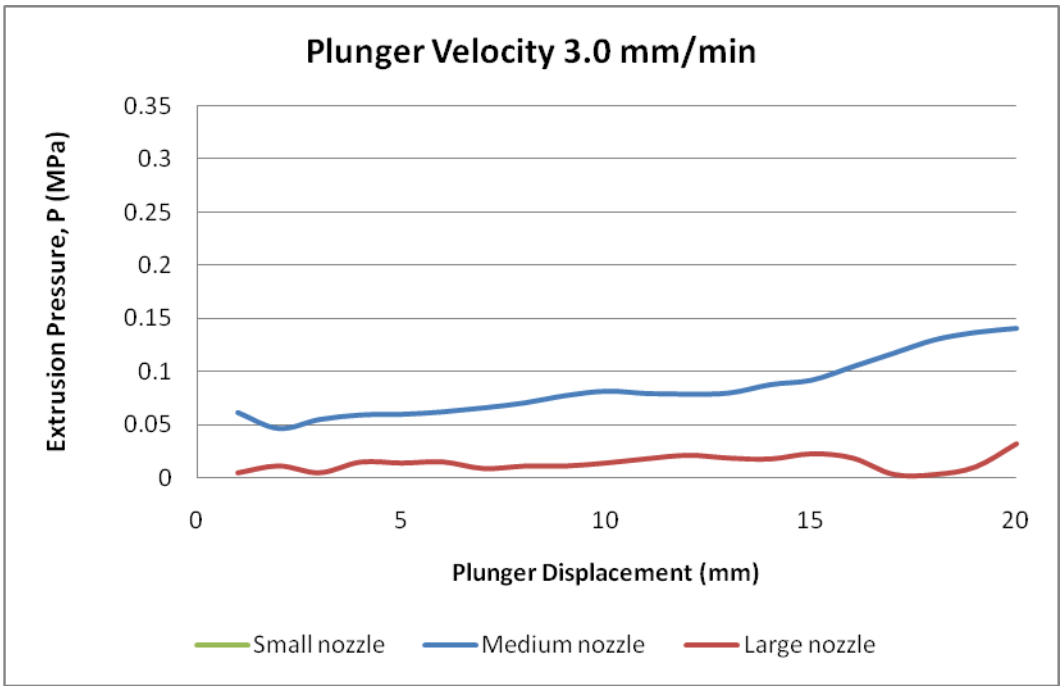

Figure 6.22: Extrusion pressure vs. plunger displacement for small medium and large nozzles at 3.0 mm/min plunger velocity

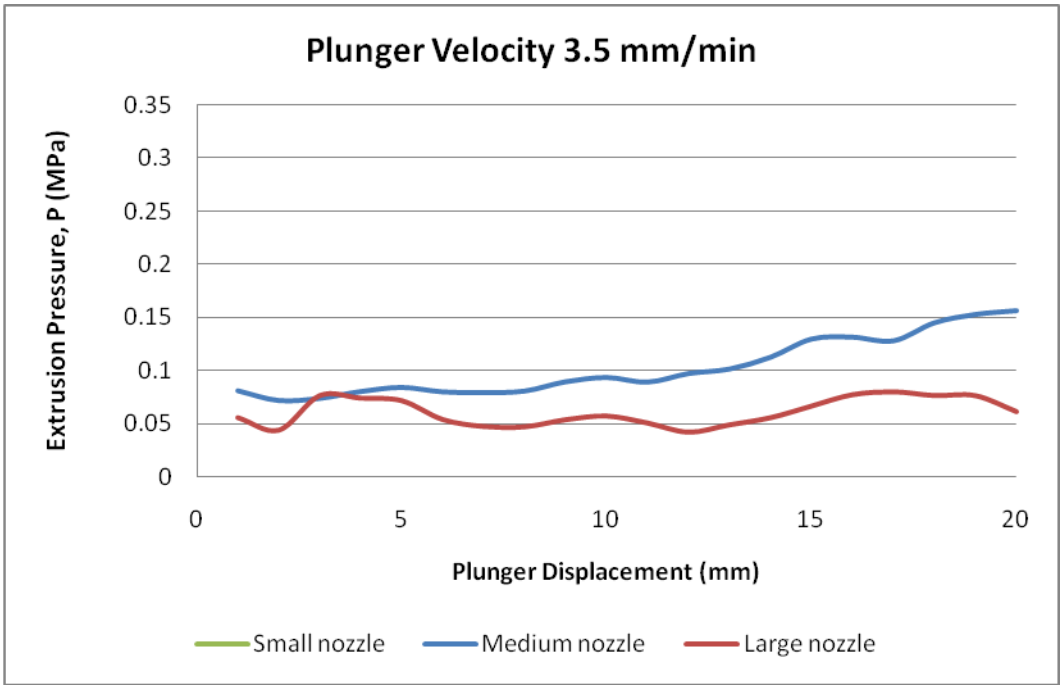

Figure 6.23: Extrusion pressure vs plunger displacement for small medium and large nozzles at 3.5mm/min plunger velocity

As expected from the fundamental equations as the plunger speed increases there is a clear increase in the extrusion pressure. As the size of the nozzle increases there is a corresponding drop in extrusion pressure.

Perhaps the most significant and interesting result, however, is the extrusion pressure increases as the plunger is displaced further into the syringe. This effect is shown across all nozzle sizes and plunger speeds but the magnitude is greatest for the smaller nozzles and the higher plunger speeds. For the majority of the test conditions, there appears to be a linear relationship between plunger displacement and extrusion pressure. There are several potential reasons for this increase;

1. ***Layer of slurry accumulates inside of the nozzle which reduces its effective diameter*** – there is some evidence of a layer of material being accumulated inside the nozzles but the high shear stress within the nozzle should result in a limit to the thickness of this layer being reached. Indeed the periodic rise and fall in extrusion force pressure show in Figure 6.13 indicates the formation of slip planes within the material.

2. ***Water is forced out of the slurry during the early displacement of the syringe thus changing the water content of the remaining slurry*** – there is some evidence (experimental observation) of water loss at the start of the extrusion process for the small nozzle in particular but this appears to cease

after 1-2 seconds and thus could not account for the gradual increase in pressure for the remainder of the plunger travel[165].

3. ***Fine particles of ceramic are extruded more readily leaving an increasing quantity of coarse particles which are more difficult to extrude thus increasing the pressure required*** – As with 2) there is some evidence of fine material being extruded at the start of the extrusion process (along with some water) but given the very viscous, "paste like" nature of the material it seems highly unlikely that the fine particles can exploit their potential to travel faster and be extruded preferentially from the syringe.

4. ***The material is thixotropic and since vigorous mixing is used to prepare the slurry is has relatively low viscosity (due to shear thinning) when it is loaded into the syringe but then the viscosity increases due to the relatively low shear rates experienced by the bulk of the material during the extrusion process*** – although this appears to be an attractive and convincing reason in principle the slower extrusion rates should show a much higher increase in pressure however comparing the results for 1.5mm and 3.5mm for the medium nozzles for example (see Figure 6.19) there is no evidence to support this theory.

5. ***Pressure on the materials results in locking of the particles and thus an increase in apparent viscosity, which in turn increases the pressure required to extrude and leads to a further increase in apparent viscosity*** – there is evidence from the literature that highly loaded material suffer from this effect (lit). This appears to be the most likely cause of the gradually increasing pressure. Although, in principle, the viscosity should rapidly increase due to the positive "gain" in the system (pressure=>locking=>more pressure=>more locking). However an exponential increase in pressure is avoided due to natural damping in the system.

To try to understand the behaviour of the slurry the **shear stress** was calculated and plotted against **shear rate** at five points (0, 5, 10, 15,20mm displacement).

The graphs of shear stress against shear rate for the five plunger position show an approximately linear relationship. This indicates that the material is close to Newtonian behaviour and thus a single viscosity value can be derived at each plunger displacement position. This information can then be used to calculate the effect of plunger displacement of apparent viscosity as shown in Figure 2.24.

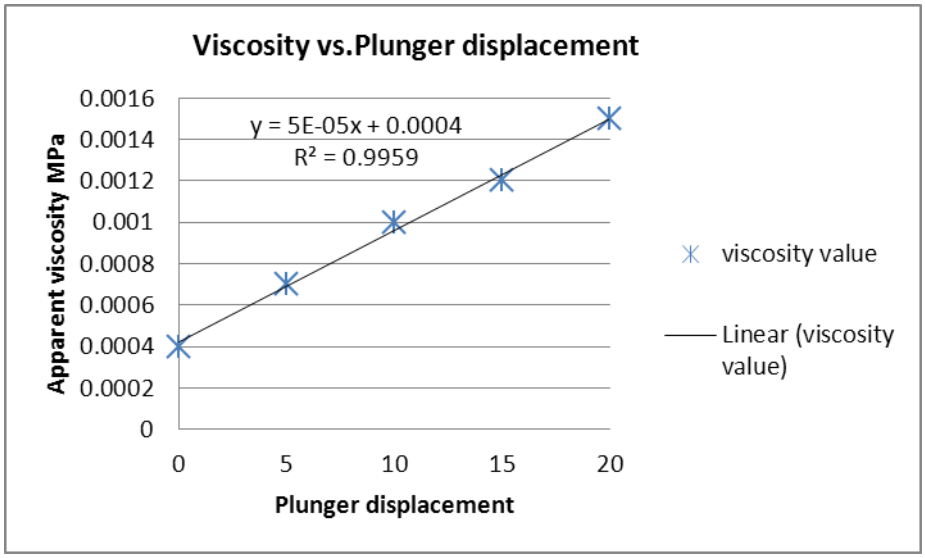

Figure 6.24: Relationship between Viscosity and Plunger displacement

Figure 6.24 shows that the apparent viscosity increases in direct proportion to the plunger displacement (R2 = 0.9959) and enables the viscosity to be readily calculated at any point in the extrusion process. The intercept of the line with the Y axis is at 0.0004 MPa, which indicates the initial viscosity of the material after mixing.

Using the information gathered in the trials it is possible plot the relationship between pressure and apparent viscosity. This is shown for the medium and large nozzles in Figures 2.25 and 2.26 (it was not possible to derive a complete set of results for the small nozzle as the material did not extrude for the 3 and 3.5mm/min plunger velocities).

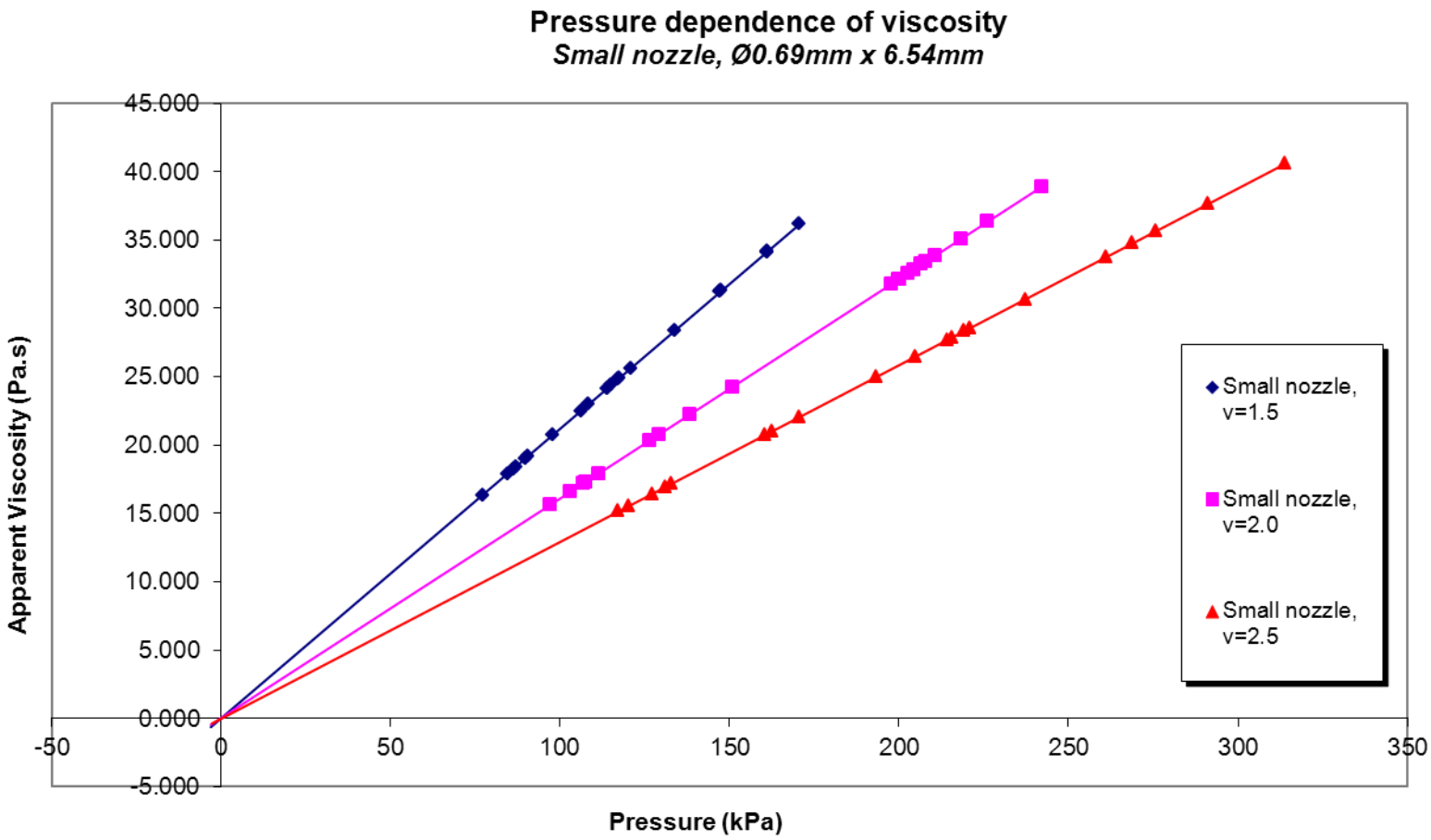

Figure 6.25: Pressure dependence of viscosity, Small nozzle.

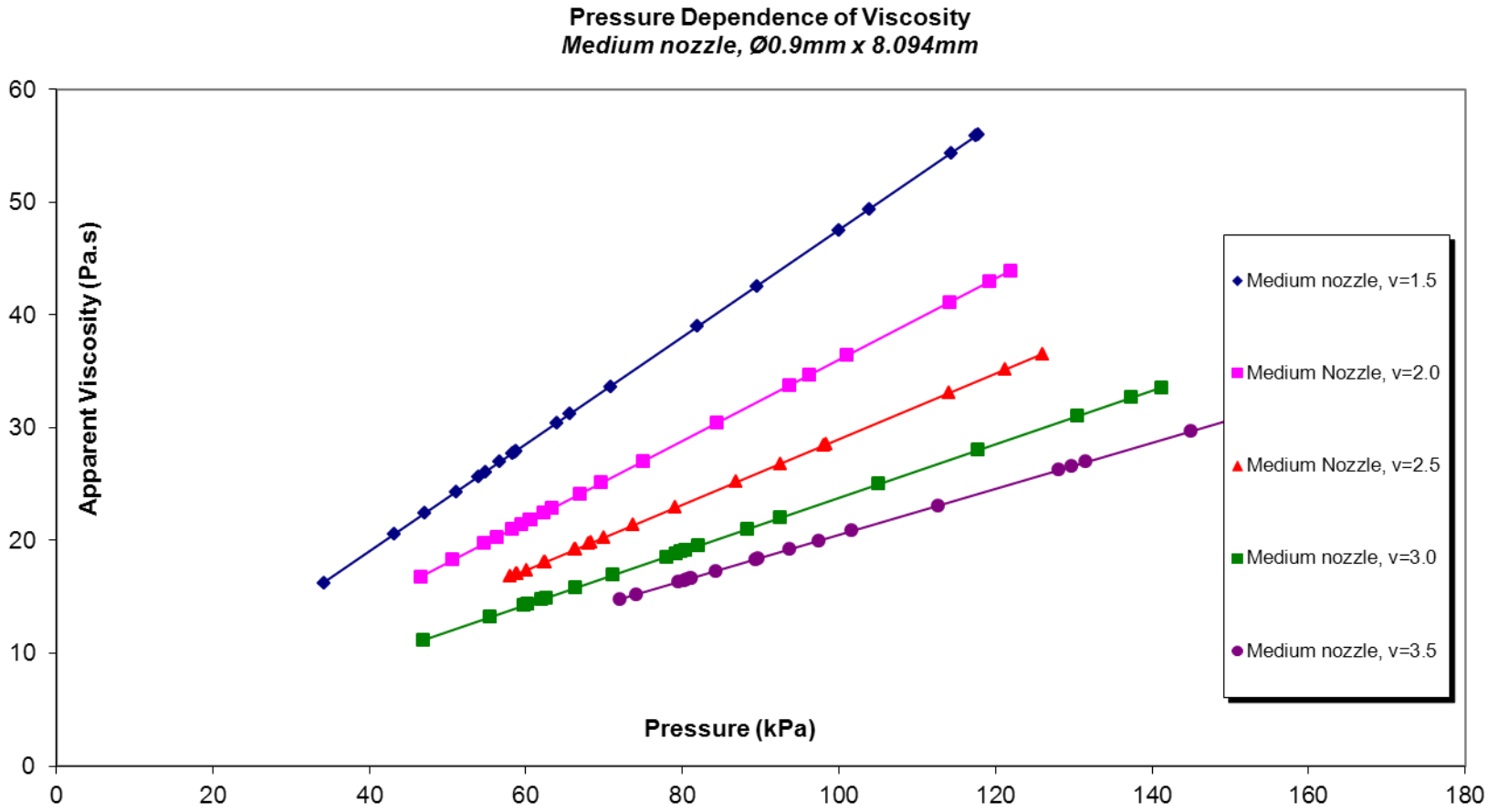

Figure 6.26: Pressure dependence of viscosity, Medium nozzle.

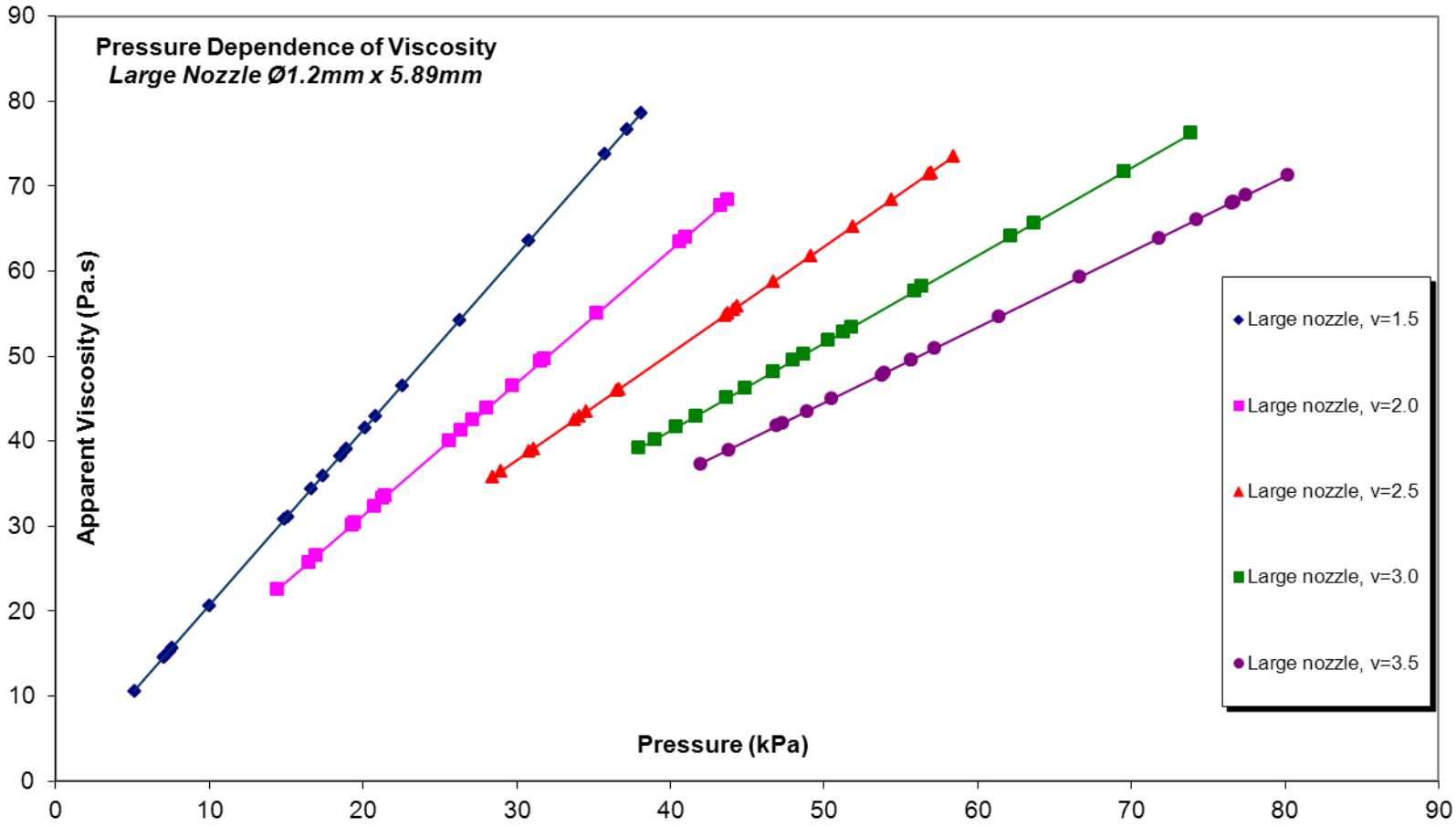

Figure 6.27: Pressure dependence of viscosity, Large nozzle.

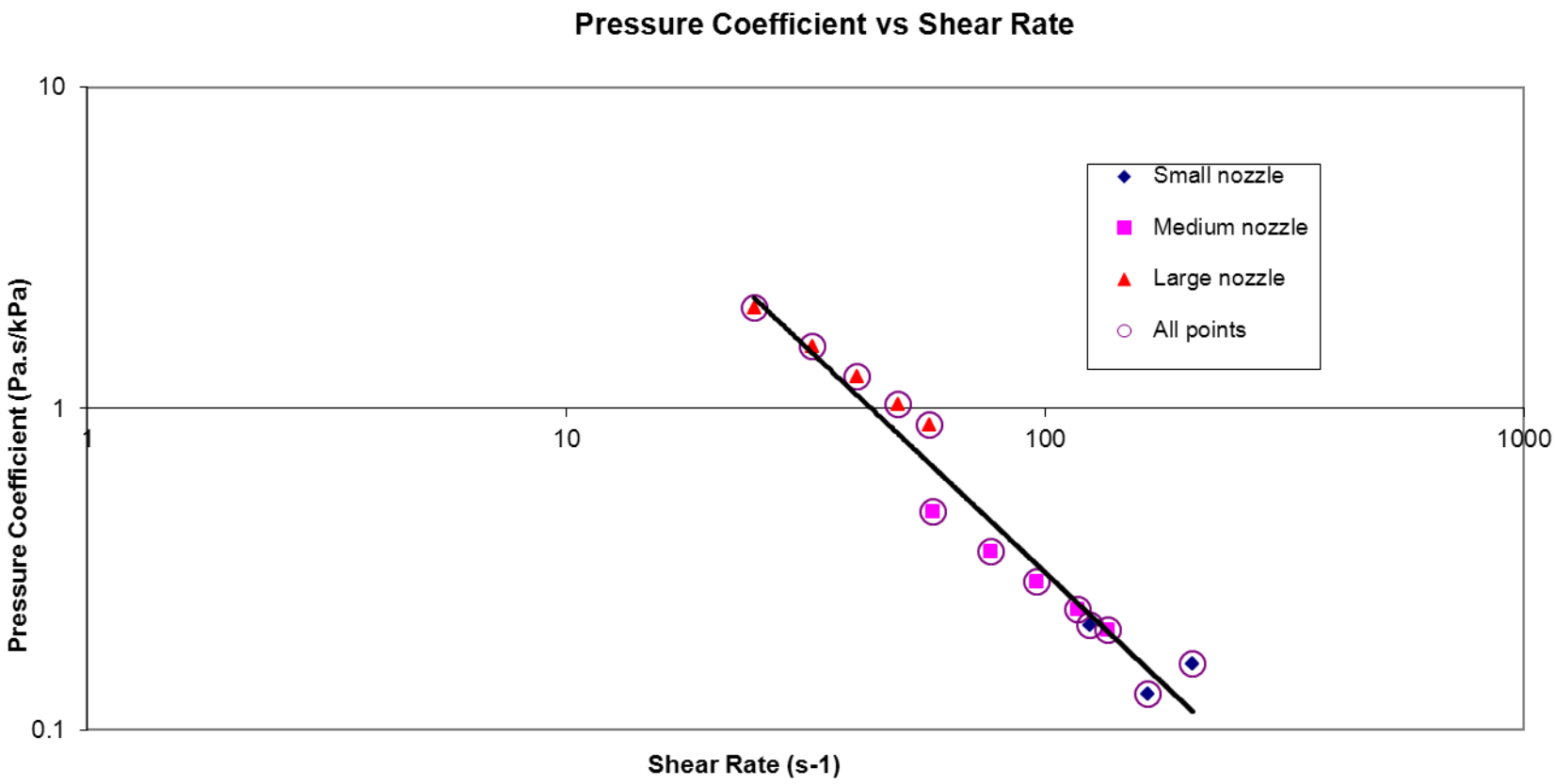

Figure 6.28: Pressure Coeficient vs Shear Rate

These results for both medium and large nozzles show very clearly that the apparent viscosity is dependent on the pressure for a particular plunger velocity (i.e. shear rate).

Interestingly, the increase in apparent viscosity with pressure is greater for the lower plunger speeds. This result indicates that the material is subject to at least two factors; a pressure induced locking of the particles (as described in point 5 above) and a thixotropic behaviour (linking shear thinning and time dependency). This is an important finding demonstrating the complex nature of the material behaviour under actual extrusion conditions.

Ceramic pastes for extrusion behave in a different way from molten polymers, because the mechanics depend fundamentally on the properties and the interaction of both solid and liquid components which act as the filler and carrier system, in traditional ceramic formulations, pastes and slips are extremely complex systems due to the number and diversity of the elements. In this kind of mix when solid and liquid elements are combined the particles immersed in the liquid medium interact with each other and the liquid molecules. The interaction energy depends on two main factors, the amount of liquid and characteristics of the powder (particle size, particle shape, etc, and the nature of the powers), this determines the characteristics of the electrical double layer developed around the particles surface[143]. The fluid

behaviour showed in the suspensions is the result of particle-particle and particle-solvent interaction, as the solid content in the suspension increase particles are forced to be closer to each other[166], in the graphs above the fluid travel at different velocities, as the velocities increase, the fluid velocity and the interaction between the particles and with the flow system itself will also increase, thus the force applied in the plunger also will increase.

Figure 4.12 (PSD of the proposed ceramic formula) show a multimodal particle size distribution; this can easily lead a best packing behaviour between the particles, in case of a high solid suspension, small particles will tend to flow with the fluid, coarser particles will behave independently and flow at different velocity than the fluid. As more independent are the particles with each other having no tendency to unite into clusters which produce thixotropic behaviour. This should depend upon the effectiveness of chemical dispersion.

A further trial was conducted with a paste material (toothpaste – Colgate). The material was extruded through a medium nozzle at 1.5mm/min. The plot of extrusion force against plunger displacement is shown in Figure 6.29.

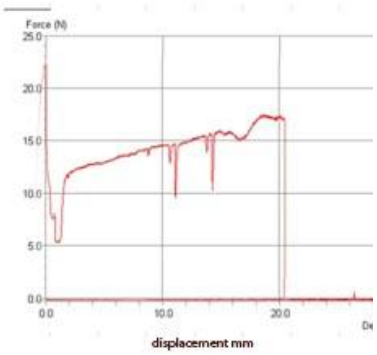

Figure 6.29: Plot extrusion force vs plunger displacement.

There is a clear increase in the extrusion force required as the plunger is displaced, indicating that the behaviour of the NPP-3 material is far from unique.

7. CHAPTER SEVEN – CONCLUSIONS RECOMMENDATIONS AND FURTHER WORK

In this project a non plastic porcelain slurry was proposed for it use in the ***DWFC*** process. The material was modified and fine-tune proving been successfully extruded, freeze cast and fired. Furthermore the mechanical and physical properties of the new material were investigated and compare with conventional materials realising its potential for the fabrication of final ceramics products. The main unexpected process difficulties encountered during the project were finally overcome (described in detail below) such as freeze castability and extrusion of very high solid pastes.

During the first stage of the project it was found that it was not possible to freeze cast (absence of solidification) the conventional clay based triaxial porcelain formulation used in this study. Initials trials also indicated that the structure (plate like morphology) of Kaolin clay prevents effective freeze-casting from occurring when incorporation into a slurry formulation. The replacement of clay (plastic material) by calcined components resulted in a non plastic porcelain formulation which can be successfully freeze cast. The lost of the plasticity in the formulation was overcome with the use of additives. (PEG, Glycerol and Dispex). Thus, it was establish that it is

possible to generate porcelain slurries with a very high solid loading (75.47% by wt.) which can be successfully extruded and freeze cast based on non plastic porcelain, through the addition of additives.

In addition, it was found that compared with TP pastes, the final ceramic specimens generated show higher level of porosity and lower bulk density. However, by changing the temperature of freezing and firing it was possible to achieve a level of porosity and bulk density akin to some whiteware pastes, such as stone ware, or whiteware with talc within the formulation[167]. Moreover, the material was found to be suitable for glassing, or impregnation, thus improving the properties and extending the range of potential applications. Further work will required to adapt the material and processing parameters to enable applications that require higher level of porosity, such as porcelain filters or insulators, to be constructed.

The use of prefired material reduces the temperature of firing compared to conventional Kaolin clay based triaxial porcelains due to the omission of calcination phases that occur when firing clay material. The optimum firing temperature for **NPP-3** was found to be 1075^{o}C. Above this temperature, vitrification results in a dramatic fall in the physical properties leading to excessive deformation. Below this temperature the XRD analysis shows that the material has not yet reached the required (maturation) level of vitrification.

Parallel with the initial findings of the literature review freeze-cast samples, show clear evidence of interconnected microporosity with a dendritic morphology. In addition the microstructure study of the freeze cast specimens shows that the pore structure of fired ceramic specimen was related to the freeze casting conditions used; rapid freezing rates (43^{o}C/min) generate smaller pores (~0.5µm). However, it was established that the freezing rate had a negligible influence on apparent porosity and the bulk density.

Five main parameters were found to have an influence in the deposition of the material; viscosity, extrusion rate, nozzle diameter, deposition head speed and stand-off distance.

The stand-off distance is a critical factor in determining bead quality; if too small the bead is flattened and if too large curling occurs. It is possible to calculate the optimum stand-off distance based on three main variables; extrusion rate, nozzle diameter and deposition head speed across the substrate. The direction and amplitude of the curling which occurs when excessive stand-off distance is used.

From the rheological and extrusion trials it was found that testing of highly viscous slurries which are prone to rapid drying is not feasible using a cone and plate rheometer. Trials undertaken using a concentric cylinder (Brookfield type) rheometer indicate that the material has a complex behaviour which is a combination of shear-thinning and thixotropic and some shear-thickening (during the final stages of the

trials). The material (**NPP-3**) complies with the general Herchel-Bulkley model for a non-Newtonian fluid. However, there are significant concerns with respect to the validity of the trials.The behaviour of the material in extrusion differs from that indicated by the concentric cylinder rheometer. During extrusion transient pressure was measured, it was found that pressure rises (due to agglomeration) and rapid falls (due to air bubbles) occur. Periodic rises and falls in pressure occur (typical wavelength of 5-6mm), indicating the presence of slip planes in the material.

For the **NPP-3** it is not possible to extrude using the small (0.7mm internal diameter) nozzle using the 3 and 3.5mm/min plunger velocity. The extrusion force (and thus pressure) increases with the shear rate (i.e. smaller nozzles and /or higher plunger speeds). The extrusion pressure increases as the plunger is displaced further into the syringe. This effect is shown across all nozzle sizes and plunger speeds but the magnitude is greatest for the smaller nozzles and the higher plunger speeds. The viscosity of the material (NPP-3) during extrusion is directly proportional to the plunger displacement and also the applied pressure.

7.1 TIMELINESS AND SIGNIFICANCE OF THE PROJECT

It is expected that this new AM method will give designers the opportunity to develop high-quality customised ceramics and allow freedom of creation. It may open up previously unimagined possibilities, since manufacturers will realise that they can reproduce any structure created on CAD.

Conventional porcelain or a similar whiteware ceramic material formulation was chosen as the starting material for fabrication using the new system due to its potential for high-impact visual design, including high-quality surface finish, translucent properties and a large range of possible different commercial applications of the material itself. The biggest challenge in this research lay in the optimisation of non-technical porcelain paste in order to formulate not only a freeze-castable material but also one with the qualities necessary for its extrusion through a fine nozzle.

7.2 NOVELTY

Wang [147] has conducted a limited number of trials to extrude dental porcelain materials, however, the material was solidified by a conventional drying approach, and the extrusion behaviour was controlled through control of the pH value of the formulation.

Ceramic materials have been freeze cast using a bulk processing route. Moreover, this work is limited to technical ceramic materials such as alumina, zirconium etc (see literature review section freeze casting of materials). Despite freeze casting of traditional ceramics having been proposed with a number of benefits, there is no evidence that this method has been utilized for the fabrication of bulk, traditional, ceramic formulas.

Moreover, although the potential benefits of a combined direct write and freeze-casting approach has been recognised by researchers to date, there has been no research in this field.

Although research in to the ***DWFC*** process has been conducted in the Technology Strategy Board funded project (TP/4/AMD/6/I/223000) this work focused on the use of bioceramic materials, initially hydroxyapatite[168]. This initial research was followed up by work on alumina for technical ceramic parts. Unfortunately, these trials demonstrated problems with the biocompatibility of the HA slurry due to the addition of the silica sol. The work on alumina is still ongoing as part of a PhD project which is running in parallel with the study presented in this thesis. The research presented in this thesis is linked to but distinctly different from other research conducted. In this study, triaxial porcelain will be processed by direct writing and freeze-casting for the first time. Furthermore, to achieve this overall goal a number of key developments will be required in terms of process and materials development.

7.3 RECOMMENDATIONS AND FURTHER WORK

Adaptation of the formulation to achieve the desired level of porosity

A white, high filler content, non plastic porcelain was developed. The plasticity in the formulation was achieved by the inclusion of additives. The particle size was reduced to improve extrusion, resulting in a broad particle size distribution, which lowered

the firing regime and improving the packing density. However, as freeze casting is a method commonly use for the fabrication of highly porous objects, the resulting material does not meet the (0.5%) porosity level usually found in conventional porcelain (although it was possible to match the level of porosity encountered with whiteware pastes, such as stone ware, or whiteware with talc within the formulation Further work need to be conducted to establish the minimum level of porosity which can be achieved using the freeze-casting route. In addition, further work is required to adapt the material and processing parameters to enable applications that require higher level of porosity, such as porcelain filters or insulators, to be constructed.

Improvement in the method of measuring the extrusion pressure

The trials undertaken to establish the rheological characteristics of the slurry in extrusion were undertaken using a syringe fitted inside an adapted tensile testing machine. This enabled the load on the plunger to be measured during the extrusion process and thus the pressure in the syringe to be calculated. However, although this approach generated some useful results, a more effective and scientifically precise method of undertaking the trials is to measure the pressure directly within the barrel of the syringe using a suitable pressure transducer. Unfortunately, there was insufficient time and resources available to pursue this approach during this study but this method should be investigated in further work.

Production of more complex parts

The material (NPP-3) developed in this project should be used to produce more complex parts. However, to do this will require the development of a suitable support material – potential candidate materials include a waxy polymer which can be removed during the firing of the part by melting or a material (for example polystyrene) which can be removed through immersion in a suitable solvent.

REFERENCES

1. Hopkinson, N., Hague, R. and Dickens, P., *Rapid Manufacturing: An industrial Revolution for the Digital Age*. 2006: John Wiley &Sons,Ltd.

2. Sigmund, W.M., Bell, N. S. and Bergström, L., *Novel Powder-Processing Methods for Advanced Ceramics.* J. Am. Ceram. Soc., 2000. **83**(7): p. 1557–74.

3. Baskaran, S., Maupin, GD., and Graff, G.L., *Freeform fabrication of ceramics.* American Ceramic Society Bulletin, 1998. **77**(7): p. 53-58.

4. Araki, K., Halloran, J., *Ceramic Freeze Casting Technique with Sublimable Vehicles.* J. Am. Ceram. Soc., 2004. **87**(10): p. 1859-1863.

5. Washburn, E.W., Ries, H. and Day, A. L. , *Report of the Comitte on definition of the Term Ceramics.* J. Am. Ceram. Soc., 1920. **3**(7): p. 526-542.

6. Rahaman, M.N., *Ceramic Processing*. 2006, London: Taylor and Francis.

7. ASTM, *Standard Terminology for Additive Manufacturing Technologies*, in *standard F2792*. 2009, P.A.: West Conshohocken.

8. Levy, G.N., Schindel, R. Kruth, J.P., *Rapid Manufacturing and Rapid Tooling with Layer Mabufacturing (LM) Technologies, State of the Art and Future Perspectives*. in *CIRP Annals* 2003.

9. Lewis, J.A., Gratson, G. M., *Direct writing in three dimensions.* Materials Today, 2004. **7**(7-8): p. 32-39.

10. Griffith, M.L., Halloran, J. W., *Freeform Fabrication of Ceramics via Stereolithography.* J. Am. Ceram. Soc., 1996. **79**(10): p. 2601-608.

11. Hull, C.W., *Apparatus for production of three-dimensional objects by stereolithography* 1986, UVP, Inc. (San Gabriel, CA) U.S.A.

12. Henkes, V.E., Onoda, G. Y. and Carty, W. M., *Science of whitewares*, ed. A.C. Society. 1996.

13. Gebhardt, A., *Generative Manufacturing of Ceramic Parts "Vision Rapid Prototyping".Most.* RTejournal, 1993.

14. Brady, G.A., Chu, Tien-Min and Halloran, J. W. , *Curing Behavior of Ceramic Resin for Stereolithography*, The University of Michigan: Materials Science and Engineering Department, College of Engineering, .

15. Chartier, T., Chaput, C., Abouliatim, Y. and Delage, C. , *Rapid Prototyping: Fabrication of Three-Dimensional Complex Ceramic Parts by Stereolithography.* CFI, Ceramic Forum International, 2006. **83**(E102-E108).

16. Steinmann, B., *Nanoparticle-Filled Stereolithographic Resins*. 2000, 3D System Inc. : U.S.A.

17. Alphaform. *dsmsomos,* [Online] Available from: http://www.alphaform.de [cited 2010].

18. Doreau, F., Chaput, C. and Chartier, T., *Stereolithography for Manufacturing Ceramic Parts.* Advanced Enegineering Materials, 2000. **2**(8): p. 493-496.

19. Augsburg, M., Storch, S., Nissen F. and Witt G., *Rapid prototyping with ceramic-filled epoxy resin by optoforming.* Rapid Prototyping Journal, 2004. **10**(4): p. pp.225 - 231.

20. Clarinval, A.M., Carrus, R. and Dormal, T., *Development of the Material for Optoform Process*, in *Proceedings of the 1st International Conference on Advanced Research in Virtual and Rapid Prototyping*. 2003: Leiria, Portugal. p. 279-82.

21. 3DCeram, 2009. [Online] Available from: http://3dceram.com. [cited 2009].

22. Huang, e.a., *Method for Rapid Prototyping by Using Linear Light as Sources*, N.C.K.U. (TW), Editor. 2007: United States.

23. Ventura, S., Narang, S., Lange, F. F., Cohen, E., Twait, D. and Khandelwal, P. *Solid Freeform Fabrication and Design*. in *24th Annual Conference on Composites, Advanced Ceramics, Materials, and Structures: B: Ceramic Engineering and Science Proceedings*. 2008: The American Ceramic Society.

24. ASERM, R.M.A., 2005. [Online], Available from: http://www.aserm.net. [cited 2009].

25. Chu, G.T.M., Brady, G.A., Miao, W., Halloran, J.W., Hollister, S.J., and Brei, D. *Ceramic SFF by direct and Indirect Stereolithography*. in *Solid Freeform and Additive Fabrication MRS Symposium Proceedings*. 1999.

26. Girouard, D. *The SLSTM selective laser sintering process: technology, applications, and materials for advanced rapid prototyping*. in *Proceedings of the IBEC '93*. 1993. Detroit.

27. Tanga, Y., Fuh, J.Y.H., Loh, H.T., Wong,Y.S. and Lub, L. , *Direct Laser Sintering of Silica Sand.* Materials and Design, 2003. **24**: p. 623-629.

28. Karapatis, N.P., Griethuysen, J.P.S. and Glardon, R. , *Direct Rapid Tooling: a review of current research.* Rapid Prototyping Journal, 1998. **4**(2): p. 77-88.

29. Phenix, S., 2009. [Online] Available from: http://www.phenix-systems.com/. [cited 2009].

30. Mudge, P.R., Wald, N.R. , *Laser Engineered Net Shaping Advances Additive Manufacturing and Repair.* Welding Journal, 2007: p. 44- 48

31. Pham, D.T., Dimov, S. S., *Rapid Manufacturing: The Technologies and Applications of Rapid Prototyping and Rapid Tooling*. London 2001: Springer.

32. Hofmeister, W., Wert, M., Smugeresky, J., Philliber, J. A.,Griffith, M. and Ensz, M., *Investigating Solidification with the Laser-Engineered Net Shaping (LENSTM) Process.* TMS JOM, 1999.

33. Sachs, E., Cima, M. and Cornie, J., *Three Dimensional Printing: Rapid Tooling and Prototypes Directly from a CAD Model. .* CIRP Annals- Manufacturing Technology, 1990. **39**(1): p. 201-204.

34. Sachs, E., Cima, M. and Cornie, J. . *Three Dimensional Printing: Ceramic Shells and Cores for Casting and Other Applications*. in *Proceedings of the Second International Conference on Rapid Prototyping, Dayton.* 1991.

35. Solutions, Z. *Metal Casting*., 2011. [Online] Available from: http://www.zsolutions.eu.com/3d_printing_metal_casting_uk.html. [cited 2011].

36. 3DPTM Laboratory, 2000. [Online] Available from: http://www.mit.edu/~tdp/ceramic.html. [cited 2009].

37. Prometal-rct., 2003. [Online] Available from: http://www.prometal-rct.com/en/home.html [cited 2010].

38. 3DPTM Laboratory, M. *Specific Surface, Inc.,* [Online] 2000, Available from: http://www.mit.edu/~tdp/structural.html. [cited 2009].

39. 3DPTM Laboratory, M. *Specific Surface, Inc.,* [Online] 2000, Available from: http://www.mit.edu/~tdp/porousfilters.html. [cited 2009].

40. Eden, M., 2010. [Online] Available from: http://www.edenceramics.co.uk/

[cited 2010].

41. Balistreri, J. *Ceramic Artist*., 2008. [Online] Available from: http://johnbalistreriartist.com/. [cited 2008].

42. Huson, D. *Materials and Process Innovation for 3D Printing of Ceramics*. Centre for Fine Print Research: 3D Laboratory, 2010. [Online] Available from: http://www.uwe.ac.uk/sca/research/cfpr/research/3D/research_projects/2009_symposium/3D%20Symp%20DHuson.pdf [cited 2011].

43. Ganter, M.e.a., *The Printed Pot*, in *Ceramics Monthly*. February 2009: U.S.A.

44. Huson, D., *The Digital Fabrication of Ceramics by 3D Powder Printing* in *Digital Fabrication Conference*. 23 .09.2010: Austin, Texas.

45. Monolite. D-Shape., 2009. [Online] Available from: http://d-shape.com/ [cited 2010].

46. Gibbons, G.J., Williams, R., Purnell, P. and Farahi, E., *3D Printing of cement composites.* Advances in Applied Ceramics,, 2010 **109**(5): p. 287-290.

47. Architects, R.S.F. Rael San Fratello Architects, 2011. [Online] Available from: http://www.rael-sanfratello.com/ [cited 2009].

48. Klosterman, D.A., Richard, P. Chartoff, N.R, Osborne, A., Lightman, A., Han, G. and Rodriges, S. , *Development of of a Curved Layer LOM Process for Monolithic Ceramics and Ceramic Matrix Composites.* Rapid Prototyping Journal, 1999. **5**(2): p. 61-71.

49. Marcus, H.L.e.a., *Solid Freeform Fabrication:Powder Processing.* American Ceramic Society Bulletin, 2007. **57**(2): p. 287-297.

50. Tay, B.Y., Evans, J. R. G. and Edirisinghe, M. J., *Solid Freeform Fabrication of Ceramics.* International Materials Reviews, 2003. **48**(6): p. 341-370.

51. Telle, R., *Direct Inkjet Printing of Ceramics*, in *Rwthaachen University, Departament of Ceramics and Refractory Materials magazine*.

52. Zhang, Y., He, X., Du, S. and Zhang, J. , *Al2O3 Ceramic Preparation by LOM (Laminated Object Manufacturing).* The International Journal of Advanced Manufacturing Technology, 2001. **17**(7): p. 531-534.

53. Cawley, J., *Computer-aided manufacturing of laminated engineering materials.* American Ceramic Society bulletin 1996. **vol. 75**(5): p. 75-79.

54. Griffin, C., Daufenbach, J. and C., Turner., *Laminated Object Manufacturing of an Extremely Tough Layered Ceramic Matrix Composite.* Lone Peak Engineering (DBA Javelin) Final Phase I SBIR report to the U. S. Army, 1994.

55. Prairie, E. 1992, Stratasys, Inc. : MN. US Patent

56. Rangarajan, S., Gang, Q., Venkataraman, N., Safari, A., and Danforth, S.C., *Powder Processing, Rheology, and Mechanical Properties of Feedstock for Fused Deposition of Si3N4 Ceramics.* J. Am. Ceram. Soc., 2000. **83**(7): p. 1663-1669.

57. Dao, Q., Frimodig,J. C. , Le, H. N., Li, X. S., Putnam, B., Golda, K., Foyos, J., Noorani, R. and Fritz, B., *Calculation of Shrinkage Compensation Factors for Rapid Prototyping (FDM).* Computer Applications in Engineering Education, 1999. **7**(3): p. 186-195.

58. Kulkarani, P., Dutta, D. , *Deposition Strategies and Resulting Part Stiffnesses in Fused Deposition Modeling. .* Journal of Manufacturing Science and Engineering-Transactions of the ASME, 1999. **121**(1): p. 93-103.

59. Wales, R., Walters B. , *"Fast, Precise, Safe Prototypes with FDM"*, in *SFF Symposium, University of Texas*. 1991: Austin, TX, p.115.

60. Zhong, W.H.e., *Short Fibre Reinforced Composites for Fused Deposition Modeling.* materials Science and Engineering A- Structural Materials Properties Microestructure and Processing, 2001. **301**: p. 125-130.

61. Gray, R.e.a., *Thermoplastic composites reinforced with long fiber thermotropic liquid crystalline polymers for fused depositon modelling. .* Polymer Composites, 1998. **19**: p. 383-394.

62. Jafari, M.A.e.a., *A novel system for fused deposition of advanced multiple ceramics.* Rapid Prototyping Journal, 2000. **6**(3): p. 161-175.

63. Sung-Hoon, A.e.a., *Anisotropic material properties of fused deposition modeling ABS.* Rapid Prototyping, 2002 **8**(4): p. pp. 248-257.

64. Danforth S.C., e.a., . 1998: US Patent # 5,738,817,.

65. Bellini, A., *Fused deposition of ceramics: A comprehensive experimental, analytical and computational study of material, behavior, fabrication process and equipment design* 2002, Drexel University. p. 297.

66. Guevara, R., Fajardo, J., Matinez, C., Sanabria, D. and Vidal, H., *Prototipado rapido por extrusion de una pasta ceramica en un proceso similar al usado en prototipado por FDM*, in *8 Congreso Iberoamericano de Ingenieria Mecanica*. 2007: Cusco.

67. Agarwala, M.K.e.a., *"FDC, Rapid Fabrication of Structural Components", .* American Ceramic Bulletin, 1996. **75**(11): p. 60-65.

68. *Ceramic Processing*. Lesson CP-4: Forming Technology. [Online] Available from: http://www.worldcyberu.com/samplelessoncp4.htm]. [cited 2008]

69. Greulich M, e.a., *Fast, functional prototypes via multiphase jet solidification.* Rapid Prototyping Journal 1995. **1**(1): p. 20-25.

70. Reinhard, L., *Rapid prototyping of ceramic components.* Advanced Engeenering Materials, 2000. **2**(1-2): p. 40-47.

71. Cesarano, J., *A review of robocasting technology.* materials research sociaty symposium proceedings, 1999. **142**: p. 133-139.

72. Michael Scheffler, P.C., *Cellular ceramics: structure, manufacturing, properties and applications* 2005: Wiley VCH. 670.

73. Morissette, S.L.e.a., *Solid freeform fabrication of aqueous alumina-poly(vinyl alcohol) gelcasting suspensions.* J. Am. Ceram. Soc.,, 2000. **83**(10): p. 2409-2416.

74. Cesarano, J. *Robocasting Enterprises LLC,* 2007. [Online] Available from: http://www.robocasting.net/index.html [cited 2011].

75. Vaidyanathan, R., *The extrusion freeforming of functional ceramic prototypes* JOM Journal of the Minerals, Metals and Materials Society, 2000. **52**(12): p. 34-37.

76. Huang, V., *Fabrication of Ceramic Components Using Freeze–form Extrusion Fabrication,* , in *Ph.D. Dissertation, Department of Materials Science and Engineering*. 2007, University of Missouri–Rolla,: Rolla, Missouri.

77. Khoshnevis, B.e.a., *Automated construction by contour crafting-related robotics and information technologies.* Automation in Construction, 2004. **Vol. 13**: p. 5–19.

78. khoshnevis, B., *Experimental investigation of countour crafting using ceramic materials.* Rapid Prototyping Journal, 2001. **7**(1): p. 32-41.

79. Herrold, D., *Slip jet 3d printer*, in *Chalenging Craft*. 2004: Gray's School of Art Aberdeen.

80. Bowyer, A., 2010, [Online] Available from: http://reprap.org. [cited 2010].

81. Bowyer, A., 2010, [Online] Available from: http://reprap.org. [cited 2010].

82. Kwiatkowski, K.R.a.A.S., *Preparation of Corundum and Steatite Ceramics by the Freeze-Drying Method.* Ceramurgia International, 1980. **6**(2): p. 79-82.

83. Mongkolkachit, C., Wanakitti, S., Wattanapornphan, P. and Srimanosaowapak, S., *Characteristics of Porous Alumina Produced by Freeze Casting.* Journal of the Microscopy Society of Thailand, 2010. **24**(2): p. 126-129.

84. Deville, S., *Freeze-Casting of Porous Biomaterials: Structure, Properties and Opportunities.* Materials, 2010. **3**(3): p. 1913-1927.

85. Tallón, C., *Síntesis de nanopolvos y procesamiento de nanomateriales por liofilización*, Autónoma de Madrid: Madrid.

86. Deville, S.e.a., *Freezing as a path to build complex composites.* Science, 2006. **311**: p. 515–518.

87. Song, J.-H., *Fabrication of a Porous Bioactive Glass–Ceramic Using Room-Temperature Freeze Casting.* J. Am. Ceram. Soc., 2006. **89**(8): p. 2649–2653.

88. Dogan, F., Sofie, S.W., *Microstructural Control of Complex-Shaped Ceramics Processed by Freeze Casting.* CFI. Ceramic forum international 2002. **79**(5): p. E35-E38.

89. Sofie, S.W., Dogan, F., *Freeze Casting of Aqueous Alumina Slurries with Glycerol.* J. Am. Ceram. Soc.,, 2001. **84**(7): p. 1459-1464.

90. Zuo, K.H., Zeng, Y.P. Jiang, D. , *Effect of polyvinyl alcohol additive on the pore structure and morphology of the freeze-cast hydroxyapatite ceramics.* Mater. Sci. Eng.,, 2010. **30**(2): p. 283–287.

91. Zhang, Y., Hu, L., Han, J. and Jiang, Z. , *Freeze casting of aqueous alumina slurries with glycerol for porous ceramics* Ceramics International 2010. **36**(2): p. 617-621

92. Novich, B.E.e.a., *QuicksetTM Injection Moulding of High Performance Ceramics*, in *Ceramic Transactions 26: Ceramic Processing Science III, The Am. Ceram. Soc. Inc,*. 1992: Westerville, OH, Estados Unidos.

93. Adams, R.W.e.a. *Applicability of QuicksetTM Injection Molding to Intelligent Processing of Ceramics*. in *Ceram. Eng. Sci. Proc.,*. 1991.

94. Lee, J.P., Lee, K.H, Song, H.K. , *Manufacture of Biodegradable Packaging Foams From Agar by Freeze-Drying.* J. Mater. Sci., 1997. **32**(21): p. 5825-5832.

95. Chen, R.e.a., *Ceramics with Special Porous Structures Fabricated by Freeze-Gelcasting: Using tert-Butyl Alcohol as a Template.* J. Am. Ceram. Soc., 2007: p. 1-7.

96. Sofie, S.W., *Fabrication of Functionally Graded and Aligned Porosity in Thin Ceramic Substrates with the Novel Freeze-Tape-Casting Process.* J. Am. Ceram. Soc., 2007. **90**(7): p. 2024-2031.

97. Deville, S., *Freeze casting of hydroxyapatite scaffolds for bone tissue engineering.* Biomaterials, 2006. **27**: p. 5480–5489.

98. Ren, L., Zeng,Y.P., Jiang, D., *Preparation of porous TiO2 by a novel freeze casting.* Ceramics International, 2009. **35**(3): p. 1267-1270.

99. Shuqiang, D., *Fabrication of Mullite Ceramics With Ultrahigh Porosity by Gel Freeze Drying.* J. Am. Ceram. Soc., 2007. **90**(7): p. 2276–2279.

100. Hwang, H.J.e.a., *Fabrication of Porous Clay Materials with Aligned Pore Structures by Freeze-Drying.* Materials Science Forum 2006. **510 - 511**: p. 906-909.

101. T. Fukasawa, Z.-Y.D., M. Ando, T. Ohji and Y. Goto, *Pore structure of porous ceramics synthesized from water-based slurry by freeze-dry process* Journal of Materials Science 2001. **36**(10): p. 2523-2527.

102. Moritz, T.a.H.J.R., *Freeze Casting of Ceramic Components Using Ice Cores and Ice Moulds.* Advances in Science and Technology, 2006. **45**: p. 391-396.

103. Wanner, S.R.a.A., *Metal/ceramic composites from freeze-cast ceramic preforms: Domain structure and elastic properties* Composites Science and Technology, 2008. **68**(5): p. 1136-1143.

104. Piat, R.e.a., *Material Parameter Identification of Interpenetrating Metal-Ceramic Composites.* Key Engineering Materials, 2009. **417-418**: p. 53-56.

105. Statham M. J., e.a., *Net-Shape Manufacture of Low-Cost Ceramic Shapes by Freeze-Gelation.* J. Sol-gel Sci. Technol, 1998. **13**: p. 171-175.

106. Laurie, J.e.a., *Colloidal Suspensions for the Preparation of Ceramics by a Freeze Casting Route.* J. Non-Crystal. Sol., 1992. **147-148**: p. 320-325.

107. Lu, K., *Microstructural Evolution of Nanoparticle Aqueous Colloidal Suspensions During Freeze Casting.* J. Am. Ceram. Soc., 2007. **90**(12): p. 3753-3758.

108. Moritz, T., Richter, H. J. , *Ceramic Bodies with Complex Geometries and Ceramic Shells by Freeze Casting Using Ice as Mold Material.* J. Am. Ceram. Soc., 2006. **89**(8): p. 2394-2398.

109. Zuo, K.H.e.a., *Properties of Microstructure-Controllable Porous Yttria-Stabilized Zirconia Ceramics Fabricated by Freeze Casting.* Int. J. Appl. Ceram. Technol., 2008. **5**(2): p. 198-203.

110. Olevsky, E.A.e.a., *Synthesis of Gold Micro-and Nano-Wires by Infiltration and Thermolysis.* Scripta Materalia,, 2007.

111. Schoof, H.e.a., *Control of Pore Structure and Size in Freeze-Dried Collagen Sponges.* J. Biomedical Mater. Res., 2001. **58**(4): p. 352-357.

112. Szepes, A.e.a., *Freeze-casting technique in the development of solid drug delivery systems.* Chemical Engineering and Processing, 2007. **46**: p. 230–238.

113. Chino, Y.a.D.D.C., *Directionally freeze-cast titanium foam with aligned, elongated pores.* Acta Materialia, 2008. **56**: p. 105–113.

114. Loehman, R., *Ceramics, Overview*, ed. I. John Wiley & Sons. 2001.

115. ASTM Designation C 242. Annual Book of ASTM Standards, V.A.S.f.T.a.M., Philadelphia, PA., *Standard Definition of Terms Related to Ceramic Whitewares and Related Products*. I996.

116. Kingery, W., *Introductions to ceramics*, ed. I. John Wiley & Sons. 1967.

117. Jones, R., Todhunter R., *Casting Process*. 2010 Dillon, CO US

118. Rudeerat, S., Pitak, L. and Nisanart, T., *Effects of dispersant concentration and pH on properties of lead zirconate titanate aqueous suspension.* Ceramics International, 2009. **35**(3): p. 1227-1233.

119. Laurie, J., *Freeze Casting A modified Sol-Gel process*. 1994, Bath University.

120. Beddow, J.K., *Particulate Sience and Technology* 1980, New York: Chemical Publishing Co. .

121. Carty, W., Senapati, U. , *Porcelain-Raw Materials, Processing, Phase Evolution, and Mechanical Behavior.* J. Am. Ceram. Soc., 1998. **81**(1): p. 3-20.

122. Teha, E., Leonga, Y.K., Liua, Y., Fourieb, A. and Fahey, M. , *Differences in the rheology and surface chemistry of kaolin clay slurries:The source of the variations.* Chemical EngineeringScience, 2009. **64**(17): p. 3817--3825.

123. Loginova, M., Larueb, O., Lebovka, N., and Vorobiev, E. , *Fluidity of highly concentrated kaolin suspensions: Influence of particle concentration and presence of dispersant* Colloids and Surfaces A: Physicochemical and Engineering Aspects, 2008. **325**(1-2): p. 64-71.

124. Olphen, H., *An Introduction to Clay Colloid Chemestry*. 1967, New York: John Wiley and Sons, Inc.

125. Lagaly, G., *Principles of flow of kaolin and bentonite dispersions* Applied Clay Science, 1989. **4**(2): p. 105-123.

126. Ryan, W., *Properties of Ceramics Raw Materials*. 1987, Bath: Pergamon Press.

127. Tai W., K., K. and Jinnaic, K., *A new approach to anorthite porcelain bodies using nonplastic raw materials.* Journal of the European Ceramic Society, 2002. **22**(4): p. 463–470.

128. Capoglu, A., Messer P.F., *Design and development of a chamotte for use in a low-clay translucent whiteware.* Journal of the European Ceramic Society, 2004. **24**(7): p. 2067–2072.

129. Olhero, S.M., Tarì, G. and Ferreira, J. M. F., *Feedstock Formulations for Direct Consolidation of Porcelains with Polysaccharides.* J. Am. Ceram. Soc., 2001. **84**(4): p. 719-25.

130. Davies, J., Binner, J. G. P. , *The role of ammonium polyacrylate in dispersing concentrated alumina suspensions. .* Journal of the European Ceramic Society, 2000. **20**: p. 1539-1553.

131. Singer, F., Singer, S., *Industrial Ceramics*. 1971, Chapman and Hall: London.

132. Bernardin, A.M., Medeiros, D.S. and Riella, H. G., *Pyroplasticity in porcelain tiles* Materials Science and Engineering A- Structural Materials Properties Microestructure and Processing, 2006. **427**(1-2): p. 316-319.

133. (ASTM), A.S.f.T.a.M., *Glass Standards and Ceramic Standards Volume 15.02 Glass; Ceramic Whitewares*, in *ASTM C326-09 Standard Test Method for Drying and Firing Shrinkages of Ceramic Whiteware Clays*. 2007.

134. (ASTM), A.S.f.T.a.M., *glass standards and ceramic standards Volume 15.02 Glass; Ceramic Whitewares*, in *ASTM C373 - 88(2006) Standard Test Method for Water Absorption, Bulk Density, Apparent Porosity, and Apparent Specific Gravity of Fired Whiteware Products*. 2006.

135. Al-Irimi, I., *Freeze Gelation of ceramics*. 2001, University of Nottingham.

136. Furukawa, Y., Shimada, W. , *Three dimensional pattern formation during growth of ice dentrites, its relation to universal law of dentric growth.* journal of crystal growth, 1993. **128**(1-4): p. 234 239.

137. Shanti, N.O., Araki, K. and Halloran, J. W., *Particle redistribution during dendritic solidification of particle suspensions.* J. Am. Ceram. Soc., 2006. **89**(8): p. 2444-2447.

138. Langer, J.S., Krumbhaar, M.J., *Stability effects in dendritic crystal growth.* Journal of the Crystal Growth, 1977. **42**: p. 11-14.

139. Márquez, J.M., Rincón, J. M. and Romero, M. , *Mullite development on firing in porcelain stoneware bodies.* Journal of European Ceramic Society, 2010. **30**(7): p. 1599-1607.

140. Iqbal, Y., Lee, W. E. , *Microstructural Evolution in Triaxial Porcelain.* J. Am. Ceram. Soc., 2000. **83**(12): p. 3121- 3127.

141. Bollman, H., *Unique new forming technique* Ceramic age 1957. **791**: p. 36-38.

142. Funk, J.E., Dinger, D.R., *Predictive Process Control of Crowded Particulate Suspensions: Applied to Ceramic Manufacturing*. 1993, Boston: Kluwer Academic Publishers. 824.

143. Dinger, D.R., *Influence of Particle Size Distribution on Whitewares Properties and Processing.*, in *Science of Whitewares*, W.M. Carty, Editor. 1996, The American Ceramic Society: OH. p. 105-115.

144. Coble, R.L., *Effects of Particle-Size Distribution in Initial-Stage Sintering.* J. Am. Ceram. Soc., 1973. **56**(9).

145. Yildirim, E.H., *Surface Chemistry of Solid and Liquid Interfaces* ed. W.B. edition. 2006, Oxford UK. 368

146. Butt, H.J., Graf, K. and Kappl, M., *Physics and Chemistry of Interfaces*. Second edition ed. 2003, Berlin: Wiley-VCH Verlag GmbH.

147. Wang, J., *Solid Freeform Fabrication of Biological Materials*. 2006, University of connecticut, USA.

148. Munch, E.e.a., *Porous ceramic scaffolds with complex architectures*, Materials Sciences Dvision, Lawrence Berkeley National Laboratory, Berkeley CA 94720.

149. Lu, K., Kessler, C.S., *Optimization of a Nanoparticle Suspension for Freeze Casting.* J. Am. Ceram. Soc., 2006. **8**(89): p. 2459–2465.

150. Karamanova, A., Emilia, K., Ferrari, A.M., Ferrante, F. and Pelino, M. , *The effect of fired scrap addition on the sintering behaviour of hard porcelain.* Ceramics International 2006. **32**(7): p. 727-732.

151. Moertel, H., *Porcelain for fast firing* Ceramurgia International 2003. **3**(2): p. 65-69

152. Tarì, G., Ferreira, J. M. and Fonseca, A. T. , *Influence of particle size and particle size distribution on drying-shrinkage behaviour of alumina slip cast bodies.* Ceramics International, 1998. **25**(6): p. 577-580.

153. Braganca, S.R., Bergmann, C.P. and Hübner, H. , *Effect of quartz particle size on the strength of triaxial porcelain* Journal of European Ceramic Society, 2006. **26**(16): p. 3761-3768.

154. Stathis, G., Ekonomakou,A., Stournaras C. J. and Ftikos, C. , *Effect of firing conditions, filler grain size and quartz content on bending strength and physical properties of sanitaryware porcelain* Journal of European Ceramic Society, 2003. **24**(8): p. 2357-2366.

155. Karamanov, A., Emilia, K., Ferrari, A.M., Ferrante, F. and Pelino, M. , *The effect of fired scrap addition on the sintering behaviour of hard porcelain.* Ceramics International 2006. **32**(7): p. 727-732.

156. Andreev, D.V., *Ceramic item deformation during firing effects of composition and microstructure (review).* Refractories and Industrial Ceramics, 2009. **50**(4): p. 45-52.

157. Lee, W.E., Rainforth, M., *Ceramic microestructures*. 1994, London: Chapman & Hall.

158. Davidge, R.W., *Mechanical Behaviour of Ceramics*. 1979, Cambridge: University Press.

159. Braganca, S.R., Bergmann, C.P. , *A view of whitewares mechanical strength and microstructure.* Ceramics International 2003. **29** p. 801-806.

160. Hackley, V.A.a.F.C.F., *Guide to Rheological Nomenclature:Measurements in Ceramic Particulate Systems*, U.S.D.o. Commerce, Editor. 2001, NIST National Institute of Standards and TechnologySpecial Publication 946: Gaithersburg.

161. Mezger, T.G., *The Rheology Handbook*, ed. Vincentz. 2006. 400 pages.

162. Goodwin, J.W., *Rheology of Ceramic Materials.* Ceramic Bulletin, 1990. **69**(10): p. 1694-1698.

163. Chen, X., Kai, J., *Modeling of Positive-Displacement Fluid Dispensing Processes.* Transaction on Electronics Packaging Manufacturing. , 2004. **7**(3): p. 157-163.

164. Mason, M.S., Huang,T., Landers, R. G., Leu, M. C. and Hilmas, G. E., *Aqueous-based extrusion of high solids loading ceramic pastes: Process modeling and control* Journal of Materials Processing Technology, 2009. **209**(6): p. 2946-2957

165. Liu, H.L., Ming C., *Liquid Phase Migration in Extrusion of Aqueous Alumina Paste for Freeze-Form Extrusion Fabrication.* International Journal of Modern Physics, 2009. **23**(06-07): p. 1861-1866.

166. Quemada, D., *Models for Rheological Behavior of Concentrated Disperse Media under Shear* Advances in Rheology, Universidad Nacional Autonoma de Mexico, 1984. **2**: p. 571-582.

167. Geller, R.F.e.a., *Talc in whiteware.* J. Am. Ceram. Soc.,, 2007. **20**(1-12): p. 137, 147.

168. Tallis, A.e.a., *Rapid manufacturing of bioceramic implants by direct writing*, in *The 2nd International Conference on Additive Technologies* 2008: Ptuj, Slovenia.

Designation: C 373 – 88 (Reapproved 2006)

Standard Test Method for Water Absorption, Bulk Density, Apparent Porosity, and Apparent Specific Gravity of Fired Whiteware Products[1]

This standard is issued under the fixed designation C 373; the number immediately following the designation indicates the year of original adoption or, in the case of revision, the year of last revision. A number in parentheses indicates the year of last reapproval. A superscript epsilon (ε) indicates an editorial change since the last revision or reapproval.

1. Scope

1.1 This test method covers procedures for determining water absorption, bulk density, apparent porosity, and apparent specific gravity of fired unglazed whiteware products.

1.2 *This standard does not purport to address all of the safety concerns, if any, associated with its use. It is the responsibility of the user of this standard to establish appropriate safety and health practices and determine the applicability of regulatory limitations prior to use.*

2. Significance and Use

2.1 Measurement of density, porosity, and specific gravity is a tool for determining the degree of maturation of a ceramic body, or for determining structural properties that may be required for a given application.

3. Apparatus and Materials

3.1 *Balance*, of adequate capacity, suitable to weigh accurately to 0.01 g.

3.2 *Oven*, capable of maintaining a temperature of 150 ± 5°C (302 ± 9°F).

3.3 *Wire Loop, Halter, or Basket*, capable of supporting specimens under water for making suspended mass measurements.

3.4 *Container*—A glass beaker or similar container of such size and shape that the sample, when suspended from the balance by the wire loop, specified in 3.3, is completely immersed in water with the sample and the wire loop being completely free of contact with any part of the container.

3.5 *Pan*, in which the specimens may be boiled.

3.6 *Distilled Water*.

4. Test Specimens

4.1 At least five representative test specimens shall be selected. The specimens shall be unglazed and shall have as much of the surface freshly fractured as is practical. Sharp edges or corners shall be removed. The specimens shall contain no cracks. The individual test specimens shall weigh at least 50 g.

5. Procedure

5.1 Dry the test specimens to constant mass (Note 1) by heating in an oven at 150°C (302°F), followed by cooling in a desiccator. Determine the dry mass, *D*, to the nearest 0.01 g.

NOTE 1—The drying of the specimens to constant mass and the determination of their masses may be done either before or after the specimens have been impregnated with water. Usually the dry mass is determined before impregnation. However, if the specimens are friable or evidence indicates that particles have broken loose during the impregnation, the specimens shall be dried and weighed after the suspended mass and the saturated mass have been determined, in accordance with 5.3 and 5.4. In this case, the second dry mass shall be used in all appropriate calculations.

5.2 Place the specimens in a pan of distilled water and boil for 5 h, taking care that the specimens are covered with water at all times. Use setter pins or some similar device to separate the specimens from the bottom and sides of the pan and from each other. After the 5-h boil, allow the specimens to soak for an additional 24 h.

5.3 After impregnation of the test specimens, determine to the nearest 0.01 g the mass, *S*, of each specimen while suspended in water. Perform the weighing by placing the specimen in a wire loop, halter, or basket that is suspended from one arm of the balance. Before actually weighing, counterbalance the scale with the loop, halter, or basket in place and immerse in water to the same depth as is used when the specimens are in place. If it is desired to determine only the percentage of water absorption, omit the suspended mass operation.

5.4 After the determination of the suspended mass or after impregnation, if the suspended mass is not determined, blot each specimen lightly with a moistened, lint-free linen or cotton cloth to remove all excess water from the surface, and determine the saturated mass, *M*, to the nearest 0.01 g. Perform the blotting operation by rolling the specimen lightly on the wet cloth, which shall previously have been saturated with water and then pressed only enough to remove such water as will drip from the cloth. Excessive blotting will introduce error by withdrawing water from the pores of the specimen. Make the weighing immediately after blotting, the whole operation being completed as quickly as possible to minimize errors caused by evaporation of water from the specimen.

6. Calculation

6.1 In the following calculations, the assumption is made that 1 cm^3 of water weighs 1 g. This is true within about 3 parts in 1000 for water at room temperature.

6.1.1 Calculate the exterior volume, *V*, in cubic centimetres, as follows:

$$V = M - S \quad (1)$$

6.1.2 Calculate the volumes of open pores V_{OP} and impervious portions V_{IP} in cubic centimetres as follows:

$$V_{OP} = M - D \quad (2)$$

$$V_{IP} = D - S \quad (3)$$

6.1.3 The apparent porosity, *P*, expresses, as a percent, the relationship of the volume of the open pores of the specimen to its exterior volume. Calculate the apparent porosity as follows:

$$P = [(M - D)/V] \times 100 \quad (4)$$

6.1.4 The water absorption, *A*, expresses as a percent, the relationship of the mass of water absorbed to the mass of the dry specimen. Calculate the water absorption as follows:

$$A = [(M - D)/D] \times 100 \quad (5)$$

6.1.5 Calculate the apparent specific gravity, *T*, of that portion of the test specimen that is impervious to water, as follows:

$$T = D/(D - S) \quad (6)$$

6.1.6 The bulk density, *B*, in grams per cubic centimetre, of a specimen is the quotient of its dry mass divided by the exterior volume, including pores. Calculate the bulk density as follows:

$$B = D/V \quad (7)$$

7. Report

7.1 For each property, report the average of the values obtained with at least five specimens, and also the individual values. Where there are pronounced differences among the individual values, test another lot of five specimens and, in addition to individual values, report the average of all ten determinations.

8. Precision and Bias

8.1 This test method is accurate to ±0.2 % water absorption in interlaboratory testing when the average value recorded by all laboratories is assumed to be the true water absorption. The precision is approximately ±0.1 % water absorption on measurements made by a single experienced operator.

9. Keywords

9.1 apparent porosity; apparent specific gravity; bulk density; fired whiteware products; water absorption

[1] This test method is under the jurisdiction of ASTM Committee C21 on Ceramic Whitewares and Related Products and is the direct responsibility of Subcommittee C21.03 on Methods for Whitewares and Environmental Concerns.

Current edition approved Feb. 15, 2006. Published February 2006. Originally approved in 1955. Last previous edition approved in 1999 as C 373 – 88 (1994).

Designation: C674 – 88 (Reapproved 2006)

Standard Test Methods for Flexural Properties of Ceramic Whiteware Materials[1]

This standard is issued under the fixed designation C674; the number immediately following the designation indicates the year of original adoption or, in the case of revision, the year of last revision. A number in parentheses indicates the year of last reapproval. A superscript epsilon (ε) indicates an editorial change since the last revision or reapproval.

1. Scope

1.1 These test methods cover determination of the modulus of rupture and the modulus of elasticity of fired ceramic whitewares bodies, formed by any fabrication method, and are applicable to both glazed and unglazed test specimens.

1.2 The values stated in inch-pound units are to be regarded as the standard. The metric equivalents of inch-pound units may be approximate.

1.3 *This standard does not purport to address all of the safety concerns, if any, associated with its use. It is the responsibility of the user of this standard to establish appropriate safety and health practices and determine the applicability of regulatory limitations prior to use.*

2. Summary of Test Methods

2.1 The specimens, either cylindrical, or rectangular, are supported on knife edges over a suitable span and a direct load is applied at the midpoint between the supports at a uniform rate until breakage occurs. The modulus of elasticity may be determined by halting the applied load at definite intervals and measuring the deflection of the specimen at the midpoint to the nearest 0.001 in. (0.025 mm).

3. Significance and Use

3.1 These test methods provide a means for determining the modulus of rupture and the modulus of elasticity, which may be required in product specifications.

4. Apparatus

4.1 *Testing Machine*—Any suitable testing machine may be used, provided uniform rates of direct loading can be maintained.

4.1.1 For all specimens the loading rate should be such that the specimen should fail in approximately 1 min. Table 1 lists loading rates that shall be used for each size specimen. For strengths of specimens intermediate of those specified, interpolation can be used to obtain the equivalent loading rate.

4.1.2 For the prescribed rectangular specimens the loading rate shall be 1000 ± 150 lbs (454 ± 68 kg)/min.

4.2 *Bearing Edges*—For the support of the test specimen, two steel (or high-strength ceramic) knife edges rounded to a radius of 0.125 in. (3.18 mm) shall be provided. The load shall be applied by means of a third steel knife edge rounded to a radius of 0.125 in. When testing rectangular specimens, the supporting members for the bearing edges shall be constructed to provide a means for alignment of the bearing surfaces with the surfaces of the test specimen (it being possible that the rectangular specimen may be wedge-shaped or twisted). The apparatus shown in Figs. 1 and 2 are suggested as suitable devices for ensuring proper spacing and alignment of the bearing edges for rectangular test specimens.

5. Test Specimens

5.1 *Preparation of Specimens*—Form, fire, and finish the specimens by the appropriate methods, following practices used in actual production.

5.2 *Dimensions*—The specimens shall be approximately 1.125 in. (28.6 mm), 0.750 in. (19.2 mm), 0.500 in. (12.7 mm), or 0.250 in. (6.4 mm) in diameter, whichever diameter is most comparable to that of the finished product. The length shall be 6 ± 0.50 in. (153 ± 12.7 mm) to permit an overhang of at least 0.25 in. (6.4 mm) at each end when mounted on the supports. Note that the 0.25-in. specimens may be 3.75 ± 0.25 in. (95 ± 7 mm) long.

5.2.1 The dry-pressed specimens shall be rectangular bars approximately 1 in. (25.4 mm) by 0.50 in. (12.7 mm) in cross section and at least 4.50 in. (114 mm) in length to permit an overhang of at least 0.25 in. at each end when mounted on the supports.

5.3 *Handling*—Observe all due precautions in the forming, drying, and firing to produce straight test specimens of uniform cross section.

5.4 *Storage*—Cool test specimens taken warm from the kiln in a desiccator. If the testing must be delayed, store the bars in the desiccator, or in an electric oven at 110°C, and then cool in

[1] These test methods are under the jurisdiction of ASTM Committee C21 on Ceramic Whitewares and Related Products and are the direct responsibility of Subcommittee C 21.03 on Methods for Whitewares and Environmental Concerns.

Current edition approved Feb. 15, 2006. Published Febraury 2006. Originally approved in 1971. Last previous edition approved in 1999 as C674 – 88 (1999). DOI: 10.1520/C0674-88R06.

TABLE 1 Loading Rates for Specimens

Specimen Size, in. (mm)	Span, in. (mm)	Nominal MOR, ksi (MPa)		
		10 (69)	30 (207)	50 (345)
		Loading Rate, lb/min (kg/s)		
1.125 (28.6) diameter	5 (127)	1100 (8.32)	3400 (25.70)	5600 (42.34)
0.750 (19.2) "	5 (127)	300 (2.27)	1000 (7.56)	1700 (12.85)
0.500 (12.7) "	5 (127)	100 (0.76)	300 (2.27)	500 (3.76)
0.250 (6.4) "	3 (76)	20 (0.15)	60 (0.45)	100 (0.76)
1 by 0.50 (25.4 by 12.7)	4 (102)	400 (3.02)	1250 (9.45)	2100 (15.88)

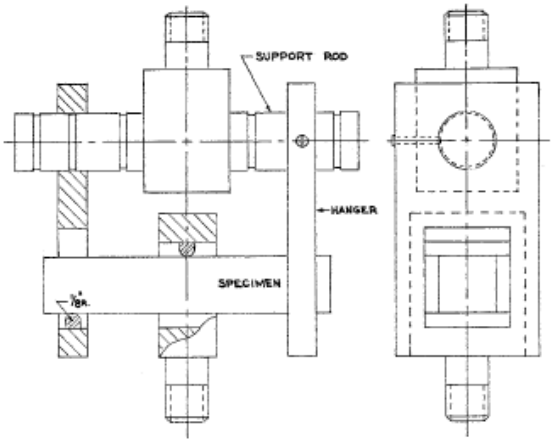

FIG. 1 Suggested Bearing Edge and Specimen Support

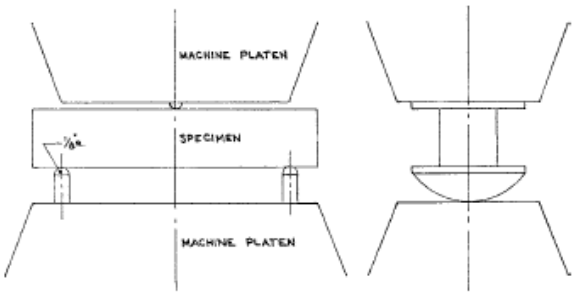

FIG. 2 Alternative Suggested Bearing Edge and Specimen Support

a desiccator before testing. When removing specimens from a hot kiln, take care to avoid thermal shock which will lead to erroneous results.

MODULUS OF RUPTURE

6. Procedure

6.1 Test at least ten dry specimens at room temperature.

NOTE 1—The modulus of elasticity may be determined as described in Sections 10-11 on the same type specimens used for the modulus of rupture test.

6.2 Place the cylindrical specimen on the bearing edges, spaced 5 in. (127 mm) ± 2 % between centers, with the specimen overhanging each end by at least 0.25 in. (6.4 mm). Apply the load at a right angle to the specimen and midway (±2 %) between the supporting edges. Apply the load uniformly at the appropriate rate for the specimen size (see 4.1.1) until failure occurs. Measure the diameter at four approximately equidistant points at the break and take the average to the nearest 0.001 in. (0.0254 mm) for calculation purposes. Break the 0.25-in. diameter rods between 3-in. (76-mm) centers and note this in the report.

6.2.1 Place the rectangular test specimen on the bearing edges, spaced 4.0 in. (102 mm) between centers, with the specimen overhanging at each end by at least 0.25 in. (6.4 mm). Apply the load at a right angle to the 1-in. (25.4-mm) surface of the specimen and midway between the supporting edges. Break specimens glazed on only one of the 1-in. surfaces with the glazed surface either up or down, but break all of the specimens from any one lot in the same position and record this position. Apply the load uniformly at the rate of 1000 ± 150 lbs (454 ± 68 kg)/min, until failure occurs. Measure the width and thickness at the break to the nearest 0.001 in. (0.0254 mm).

7. Calculation

7.1 Calculate the modulus of rupture of each circular cross section specimen as follows:

$$M = 8PL/\pi d^3 \quad (1)$$

where:
M = modulus of rupture, psi (or MPa);
P = load at rupture, lbf (or N);
L = distance between supports, in. (or mm);
d = diameter of specimen, in. (or mm).

7.1.1 Calculate the modulus of rupture of each rectangular specimen as follows:

$$M = 3\ PL/2bd^2 \quad (2)$$

where:
M = modulus of rupture, psi (or MPa);
P = load at rupture, lbf (or N);
L = distance between supports, in. (or mm);
b = width of specimen, in. (or mm); and
d = thickness of specimen, in. (or mm).

8. Report

8.1 Report the following information:

8.1.1 Identification of the material tested,

8.1.2 Data and computed modulus of rupture for each specimen,

8.1.3 The adjusted average of the computed modulus of rupture values (discarding those values from the bars which, upon inspection, show obvious defect), and

8.1.4 In the case of glazed specimens, the position of the glazed surface or surfaces, with respect to the applied load.

8.2 The report may also include:

8.2.1 A description of type of fracture and the behavior of each specimen under load,

8.2.2 Name and rating of the machine used to make the test, and

8.2.3 A graph showing the individual values of modulus of rupture arranged in ascending order.

9. Precision and Bias

9.1 *Precision*:

9.1.1 *Interlaboratory Test Data*—An interlaboratory test was run in 1978 in which randomly drawn samples of five materials were tested in each of four laboratories. One operator in each laboratory tested ten specimens of each material. The components of variance for flexural strength results expressed as coefficients of variation were calculated as follows:

Single-operator component	2.42 % of the average
Between-laboratory component	18.79 % of the average

9.1.2 *Critical Differences*—For the components of variance reported in 9.1.1, two averages of observed values should be considered significantly different at the 95 % probability level if the difference equals or exceeds the following critical differences listed below:

Number of Observations in Each Average	Critical Difference, % of Grand Average[A]: Single-Operator Precision	Between-Laboratory Precision
10	6.72	52.10

[A] The critical differences were calculated using $t = 1.960$ which is based on infinite degrees of freedom.

9.1.3 *Confidence Limits*—For the components of variance noted in 9.1.1, single averages of observed values have the following 95 % confidence limits:

Number of Observations in Each Average	Width of 95 % Confidence Limits, Percent of the Grand Average[A]: Single-Operator Precision	Between-Laboratory Precision
10	±4.75	±36.84

[A] The confidence limits were calculated using $t = 1.960$ which is based on infinite degrees of freedom.

9.2 *Bias*—No justifiable statement on bias is possible since the true value of flexural strength of ceramic whiteware materials cannot be established and will be different for each specific material.

MODULUS OF ELASTICITY

10. Procedure

10.1 Support the specimen in the same way as for the modulus of rupture determination. Set any type of deflectometer capable of indicating to 0.001 in. (0.0254 mm) to measure deflection at mid-span relative to the ends of the span. Apply the load uniformly (see either 4.1.1 or 4.1.2) in accordance with the shape of the specimen. Stop the loading at 15 % increments of the expected total breaking load, as may previously have been determined in the modulus of rupture tests, and record the corresponding deflections.

11. Calculation

11.1 Plot the load-deflection readings to a convenient scale and draw a straight (stress-strain) line to represent, as nearly as possible, the average of the plotted points below the elastic limit. (In some materials, increasing departures from a straight line may be noted at the higher stress. Such evidence of plastic flow, or of non-recoverable strain, indicates that the elastic limit has been exceeded.) If the line does not pass through the zero point, draw a corrected line through this point parallel to the stress-strain line.

APPENDIX 2

Glossary

Agglomerate. - A jumbled mass o collection of two or more particles or aggregates or a combination of thereof, held together by relatively weak cohesive forces caused by weak chemical bonding or an electrostatic surface charge generated by handling or processing.

Albite.- A colourless, milky-white, yellow, pink, green, or black mineral of the feldspar group and plagioclase series, found in igneous sedimentary and metamorphic rocks. It is used in the manufacture of glass and ceramics. Composition: sodium aluminium silicate. Formula: $NaALSi_3O_8$.

Anorthite.- A white to greyish-white or reddish-white mineral of the feldspar group and plagioclase series, found chiefly in igneous rocks and more rarely in metamorphic rocks. It is used in the manufacture of glass and ceramics. Composition: calcium aluminium silicate. Formula: $CaAl_2Si_2O_8$.

Corundum. - A naturally occurring form of aluminium oxide that sometimes contains small amounts of iron and silicon oxide.

Crystallization. - The process of forming crystals. When a substance cools from the gaseous or liquid state to the solid state, crystallization occurs. Crystals will also form from a solution saturated with a solute.

Deagglomeration .- The process of breaking down, usually by physical means, the masses of particles that are held together by relatively weak cohesive forces resulting in a final system of aggregates or primary particles, or both.

Deairing .- The process of removing entrapping air, or absorbed air from a mass or slurry.

Deformation .- Movement of parts or particles of a material body relative to one another such that the continuity of the body is not destroyed, resulting in a change of shape or volume or both.

Dilatant. - A property often associated with suspensions of irregularly shaped particles, in which the liquid exhibits an increase in volume while being sheared. The term is also used in common practice to mean shear-thickening, the increasing resistance to shear with increasing shear rate. It is possible for either of these two effects to exist in the absence of the other.

Drying. - Removal by evaporation, of uncombined water or other volatile substance from a ceramic raw material or product, usually expedited by low-temperature heating.

Feldespar. - A mineral aggregate consisting mainly of microcline, albite or anorthite or combination thereof.

Firing. - The controlled heat treatment of ceramic ware in a kiln or furnace, during the process of manufacture, to develop desired properties.

Firing curve.- A diagram or table showing the time temperature planned or experienced by ware going the a firing operation.

Firing cycle. - The time required for one complete operation (cold-to-cold).

Firing range. - The range of firing temperature within ceramic composition develops properties which renew commercially useful.

Flocculate. - A grouping of primary particles, aggregates, or agglomerates having weaker bonding than either the aggregate or agglomerate structures.

Flow.- Continuously increasing deformation of a material body under the action of finite forces. When the force is removed, if the strain does not eventually return to zero, then flow has occurred.

Flow curve. - A graphical representation of the behaviour of flowing materials in which shear stress is related to shear rate.

Forming. - The shaping or moulding of the ceramic shape.

Free moisture. - That water, which is not chemically bound, and that is loosely bound to a material, but which can be removed by drying

Friction. - The resistance developed between the physical contacting, but otherwise unconstrained, surfaces of two bodies when there is movement or tendency for movement of one body relative to the other parallel to the plane of contact.

Grog.- Fired clay ground to various mesh sizes.

Mullite whiteware.- Any ceramic whiteware in which mullite ($3Al_2O_32SiO_2$)is the essential crystalline phase

Newtonian Flow.- Model of fluids in which a linear relationship exists between shear stress and shear rate, where the coefficient of viscosity is the constant of proportionality.

Non-Newtonian.- Any laminar flow that is not characterized by a linear relationship between shear stress and shear rate .

Nonplastic ceramics.- No clay ceramic materials that when mixed with water do not exhibit the rheological property plasticity.

Microcline.- A white, creamy yellow, red, or green mineral of the feldspar group, found in igneous, sedimentary, and metamorphic rocks: used in the manufacture of glass and ceramics. Composition: potassium aluminium silicate. Formula: $KAlSi_3O_8$.

Quartz.- A natural crystalline form of silica (SiO_2)

Rheology.- The science of the deformation and flow of matter.

Rheopexy An effect by which a material recovers some of its pre-sheared viscosity at a faster rate when it is gently sheared compared to when it is allowed to stand.

Semi-porcelain.- A trade term designating semi vitreous dinner ware.

Semi vitreous (semivitrified).- that degree of vitrification endenced by a moderate or intermediate water absorption. *in porcelain the term semivitreos generally signifies 0.5 to 12.0

Shear.- The relative movement of parallel adjacent layers.

Shear rate [rate of shear strain], The rate of change of shear strain with time for liquids, the shear rate, rather than strain, is generally used in describing flow.

Shear stress.- The component of stress that causes successive parallel layers of a material body to move, in their own planes (i.e., the plane of shear), relative to each other.

Shear-thickening.- An increase in viscosity with increasing shear rate during steady shear flow. The term dilatant is commonly used in practice to indicate shear thickening, although this usage is strictly incorrect.

Shear-thinning.- [pseudoplastic] A decrease in viscosity with increasing shear rate during steady shear flow.

Sublimination. - The conversion of a solid into vapour without the solid first melting. For instance (at standard pressure) iodine, solid carbon dioxide, and ammonium chloride sublime. At certain conditions of external pressure and temperature and temperature equilibrium can be establish between the solid phase and the vapour phase.

Thixotropy.- A reversible time-dependent decrease in viscosity at a particular *shear rate*. Shearing causes a gradual breakdown in *structure* over time.